

**Phase-Specific Studies of the Evolution of
Microstructure and Mechanics in
Elastomer-Containing Blends**

Dissertation

zur Erlangung des Doktorgrades der Naturwissenschaften
(Dr. rer. nat.)

der

Naturwissenschaftlichen Fakultät II
Chemie, Physik und Mathematik

der Martin-Luther-Universität
Halle-Wittenberg

vorgelegt von

Herrn Akshay Karekar
geboren am 8. Oktober 1987 in Shimoga, Indien

Gutachter:

1. Prof. Dr. Kay Saalwächter (Martin-Luther-Universität Halle-Wittenberg)
2. Prof. Dr.-Ing. Katrin Reincke (Polymer Service GmbH Merseburg)
3. Prof. Dr.-Ing. Manfred Wagner (Technische Universität Berlin)

Tag der öffentlichen Verteidigung: 29.01.2024

Contents

1	Introduction and Motivation	1
1.1	Outline	3
2	Scientific and Technological Background — Polymer Blends	5
2.1	Rubbers and rubber/rubber blends	5
2.1.1	Role of fillers	7
2.1.2	Aging of rubber	10
2.2	Reinforcement in rubber/plastic blends	12
2.3	Measurements of cross-link density in blends	14
2.3.1	Phase-specific NMR measurements	15
2.4	Aim and research elements	17
3	Polymer Basics	19
3.1	Physical account of linear polymer chains	20
3.1.1	Ideal chain conformations and entropy	21
3.2	Miscibility of rubber-containing blends	22
3.3	Rubber networks	25
3.3.1	Origin of rubber elasticity	26
3.3.2	Unentangled network models	27
3.3.3	Entangled network models	29
3.4	Polymer reinforcement by fillers	32
3.4.1	The microscopic picture	32
3.4.2	The macroscopic observations	36
3.5	Semi-crystalline thermoplastics	37
4	NMR Spectroscopy	40
4.1	The NMR experiment	40
4.2	Anisotropic spin interactions	42
4.2.1	Chemical shift and anisotropy	42
4.2.2	Dipole–dipole coupling	43
4.3	Distinction of polymer fractions based on spin–spin relaxation	45
4.3.1	Single-pulse free induction decay (FID)	46
4.3.2	Spin–echo	46
4.3.3	Pulsed magic-sandwich echo (MSE)	47
4.3.4	Distinction of polymer fractions	47

4.4	Measurement of cross-link density by NMR	48
4.4.1	Connecting polymer chain dynamics and NMR observables . . .	48
4.4.2	Proton multiple-quantum NMR spectroscopy	50
4.4.3	Enhancement of spectral resolution for phase-resolved measure- ments	52
5	NMR Studies on the Phase-Resolved Evolution of Cross-Link Densi- ties in Thermo-Oxidatively Aged Elastomer Blends	55
6	Effects of Artificial Weathering in NR/SBR Elastomer Blends	68
7	NMR-Based Cross-Link Densities in EPDM and EPDM/ULDPE Blend Materials and Correlation with Mechanical Properties	85
8	Microstructure of Silica-Filled NR/SBR Blends	101
8.1	Materials, preparation, and exposure	101
8.2	Results and discussion	102
8.2.1	Curing kinetics	102
8.2.2	Phase-resolved cross-link densities	103
9	Summary and Outlook	105
	Bibliography	109
	Acknowledgements	125
	Curriculum Vitae	127
	List of publications	129
	Erklärung	131

1. Introduction and Motivation

Since the introduction of the word *polymer* by Jöns Jakob Berzelius in 1833 [1], it took about 75 years for the invention of the first synthetic polymer: a thermoset named phenol formaldehyde (Bakelite™) in 1907 by Leo Baekeland. Innumerable polymers have been invented hence. Where initially the scope of the polymer was defined after its creation, polymers were later produced with the end-use in focus. Many of these have since been innovated to meet very specific demands.

Alternatively, the blending of two or more polymers has been considered a robust option for achieving optimum property-to-cost value. This saves time and resources associated with new monomer development or polymerization routes. A wide range of material properties by just adjusting the blend composition can thus be achieved [2]. In this dissertation, blends of elastomer with another elastomer, and with plastic are considered.

Elastomers (or rubbers) are a class of polymers that are inherently flexible at room temperature due to their sub-zero glass transition temperature. Cross-linking imparts dimensional rigidity to these materials. This allows usage in high load-bearing applications. Rubbers are also suited for compounding with plasticizers, reinforcing fillers, antiaging additives, etc. to facilitate processing and improve their durability, among others. In elastomer blends, the mixing procedure, polymer component ratio, rheology of the constituent polymers, phase morphology, and interfacial adhesion/cross-linking dictate the morphology of the blend, and hence, its properties. These factors also control the distribution of compounding ingredients such as fillers, plasticizers, and cross-linkers across the blend phases [3–6]. The curatives prefer to locate within the continuous phase and the lower viscosity component [7]. Curative reactivity is determined by polymer features like unsaturation and polarity, along with solubility [8]. The most widely used cross-linker, i.e., sulfur, is found to be more soluble in unsaturated rubbers and those containing a styrene group [9, 10], whereas curing accelerators have an affinity to polar rubbers [11]. The blending of elastomers having such different natures can lead to a preferential distribution of additives in the blend phases, and thus to dissimilar cross-link properties. A phase-specific study of the blends is, hence, crucial.

The most important and common objective across all the research themes of this thesis is to distinguish the cross-link densities between the phases of a blend, quantitatively. Popular experimental approaches for the determination of cross-link densities of rubber-containing blends include equilibrium swelling of the vulcanizate (based on the Flory–Rehner equation) [12, 13], rubber elasticity theory (based on the Mooney–Rivlin

equation) [14], rheometry [15], differential scanning calorimetry (DSC) [16], and atomic force microscopy (AFM) [17]. However, a phase-resolved quantification of cross-link densities from these methods has not been achieved. The first three approaches lack resolution as they cannot distinguish between the cross-link densities across the blend phases but give an average value [18], whereas AFM gives qualitative information based on image contrasts in the phases.

The highlight of the studies presented in this thesis is a nuclear magnetic resonance (NMR) spectroscopy approach that overcomes the limitations of the methods listed above. In this NMR technique, a polymer blend sample is spun at a moderately high frequency on an axis at a defined angle with respect to the external magnetic field. This *magic-angle spinning* (MAS) approach gives resolved peaks that make a chemical distinction of the blend phases possible. In combination with a suitable pulse sequence, the measured quantity can be correlated to the average molecular weight between cross-links and hence, the cross-link density. The measured quantity is called the *residual dipolar coupling constant* (D_{res}), which arises due to molecular motional constraints such as cross-links.

As mentioned earlier, the blend phases can possess different cross-link densities when a product is manufactured. As a result, it can be expected that the constituent phases of the blend will evolve differently over the product's lifetime, thus affecting its performance. This is especially evident if the product is exposed to high temperatures, continuous mechanical loading/unloading, oxygen, ozone, etc., such as in the case of a tire. Cases like these require an accurate measurement tool that helps in the modeling and optimum designing of the material composition so that blend as a whole is long-lasting. To address this issue, this thesis also explores avenues of thermo-oxidative aging and accelerated weathering to monitor how the phases evolve over the exposure duration. The motivation here is to establish the NMR experiment as a predictive tool for failure analysis.

The aspect of phase-specific properties can also be extended to rubber/plastic blends. In such materials, the thermoplastic behaves like a reinforcing component of the blend. When a semi-crystalline thermoplastic is considered, the non-trivial synergism of the crystalline and the amorphous regions with the cross-linked rubber phase helps develop interesting properties, the basis for which is still not completely understood. Apart from measuring the D_{res} of these materials, an additional molecular property that can be probed is the *spin-spin relaxation time* (T_2) of the spins. Here, the relaxation time of spins belonging to polymer regions associated with different motional timescales can be obtained, such that the crystalline fractions can be distinguished from the amorphous fractions and so on. With a low-field NMR approach to

the measurement of cross-link density and the identification of the various molecular fractions based on their T_2 times, a detailed microscopic picture can be gleaned.

1.1 Outline

The next chapter (Chapter 2) briefly introduces the blend categories that constitute this research; rubber/rubber and rubber/plastic blends. This extends into a comprehensive survey of the literature to mainly understand the role of aging and the presence of fillers on the performance of rubber/rubber blend phases. The synergism and possible miscibility provided by a semi-crystalline thermoplastic when used as a reinforcing component for rubbers are also surveyed. These discussions revolve around the role of cross-links and other molecular aspects relevant to appreciating blend behavior. The common methodologies in measuring these facets, their limitations, and how NMR techniques can be employed for the quantification of properties on a molecular level are introduced. Based on this background, the aim and research elements of this report are outlined.

In Chapter 3, the theoretical backgrounds for understanding the functioning of elastomeric materials and semi-crystalline thermoplastics are discussed upon establishing the physical features of polymer chains. Sections are also dedicated to introducing phenomena of blend formation, cross-linking, and filler reinforcement. Chapter 4 makes the connection between the material property with quantities observable by NMR. The chapter builds on a basic introduction to the functioning of NMR spectroscopy and into discussing various experiments that probe specific molecular information such as relaxation times and constraints to molecular motions. This includes the MAS-based experimental approach that makes phase-resolved measurements of the blends possible.

Results of applications of these methodologies (in combination with others) for the elucidation of different blend materials are already published in journals as research articles, which are included here as three separate chapters from Chapter 5 to 7. Chapter 5 delves into distinguishing cross-link densities in blends of natural rubber (NR) with styrene-butadiene rubber (SBR) and the individual vulcanizates of the constituent polymers subjected to thermo-oxidative aging [19]. Here, aging-induced changes in cross-link densities, their distribution, and T_2 times as measured by a low-field spectrometer are discussed. This is followed by a first-ever demonstration of the proposed MAS-based experiment for the successful measurement of cross-link densities in the NR and SBR phases of a 50/50 blend. This chapter sets a precedent for the following chapter (Chapter 6) which explores the effects of artificial weathering in NR/SBR

blend [20]. Here, the previously established MAS-based experiment is used in combination with the low-field experiment to assess the depth-specific cross-link density in the weathered specimens. In addition to NMR, IR spectroscopy is employed for chemical analyses of different regions within the specimens, and DMTA and AFM are used to correlate the molecular understanding with the macroscopic stiffness of the materials. T_2 -based results are also discussed.

The theme of this thesis is diversified in Chapter 7 [21]. Here, sulfur-cross-linked blends of ethylene-propylene-diene rubber (EPDM) with ultralow-density PE (ULDPE) are studied to analyze the source of reinforcement in these blends. The reasons for the enhanced mechanical properties of the blends, as observed by tensile tests, are understood by analyzing the crystalline, amorphous, and crystalline-amorphous interface regions by T_2 measurements and by measuring the cross-link density of the EPDM phase.

The penultimate chapter (Chapter 8) builds on the understandings of Chapters 5 and 6. Here, unpublished results on the effects of silica filler and its role in how the cross-link densities across the phases of NR/SBR blends are distributed are briefly presented. The effects of thermo-oxidative aging on the materials in the presence of an antioxidant are excluded from the discussion here.

Chapter 9 comprises an overall summary of the results that make up this thesis. Some open questions and opportunities for continued research in line with this research are also discussed.

2. Scientific and Technological Background — Polymer Blends

Polymer blends can be broadly categorized into those of plastic/plastic, rubber/rubber, and rubber/plastic [22]. Due to their long chain lengths, polymers have a low entropy of mixing and hence are not easily miscible, unlike many organic liquids that are partially or fully miscible at room temperature. As a result, these blends manifest into phase-separated morphologies. For maintaining their significance, it is prudent that the blends do not undergo spontaneous demixing on a macroscopic level, but be miscible to an extent that aids dispersion [23]. This thesis deals with such polymer blends of rubber/rubber and rubber/plastic systems.

2.1 Rubbers and rubber/rubber blends

Etymologically, the term *rubber* was assigned by Joseph Priestly, an English chemist, to a natural product of the *Hevea brasiliensis* tree which ‘rubbed’ pencil marks [24]. This, hence, is historically ubiquitous with natural rubber, which is majorly made up of the polymer cis-1,4-polyisoprene. The word *caoutchouc* is also used which acknowledges its origin in South America, which translates to ‘weeping wood’ in the native language, referring to the latex of the tree from which natural rubber (NR) is produced [24].

Charles Goodyear, who after purchasing a patent for combining NR with sulfur from Nathaniel Hayward, accidentally discovered in 1839 that sulfur forms cross-links with NR when heated to a very high temperature. This process, patented in 1844 [25], overcame the low and high-temperature limitations where it had rendered NR stiff and sticky, respectively. This was thus a method to increase the strength and resiliency of rubber [26]. This heat-induced curing was termed *vulcanization* by William Brockedon who was a friend of Thomas Hancock [27], the recipient of a similar patent that he was independently working on and granted a few weeks before Goodyear’s. Though the term vulcanization relates specifically to curing by sulfur, the more general terms cross-linking and curing are also used interchangeably. Nowadays, synthetic polymers exhibiting elastic behavior are also termed rubbers, interchangeably with the general term *elastomers*. A list of terminologies and their definitions relevant to rubber technology has been summarized in ASTM D 1566.

The first patented polymer blend was that of cross-linked natural rubber and gutta-percha, developed by Alexander Parkes in 1846 [28]. By varying the composition, the rigidity of the blend was controlled. Rubber blends can be prepared by various meth-

ods: Corish classifies them as latex blending, solution blending, combined sol–latex blending, and mechanical mixing of solid rubbers (including particulate or powdered forms) on open two-roll mills, in internal batch mixer or in continuous extruders [29–31]. The mechanochemical route, where interpolymerization of the constituent rubbers can occur, such as by combination due to radicals, is also known. Another process offering good dispersion and cross-linking is dynamic vulcanization, which is performed in the molten state [32].

As summarized in the previous chapter, various factors affect the distribution of additives in the rubber phases, thus causing possible inconsistencies in the curing extents. However, it has been noted that better properties are generally obtained when the blend components have similar curative reactivity [29, 33, 34]. In the case of blend components having contrasting cross-link rates, consumption of curatives in the faster-curing phase can promote migration of curatives from the other phase across the blend interfaces [35–37]. A consequence of this can be appreciated in a multi-curative ply of butyl rubber (isoprene–isobutylene rubber, IIR) and natural rubber in Figure 2.1. The figure demonstrates the diffusion of curatives, which depends on their respective diffusion coefficients and solubilities, on either side of the interface. A result of such differences in cure rate, solubility, and diffusion of curatives is a possible overcure and undercure of the phases in the final vulcanizate along with altered glass transition temperatures of the respective components [29, 38, 39]. This disparity in curative distribution is of course lost when miscible rubbers are employed. Nevertheless, it has also been recognized that the immiscibility of incompatible rubber components brings a diverse set of properties in the blends they are a part of [6]. Such blends of natural rubber are a theme of study in the compilation by Tinker and Jones [3]. Many other blends have been surveyed by Mangaraj [40].

Another aspect of cross-linking in blends is the possibility of co-cross-linking at the interface due to chain interactions of the polymer components [30]. In the references therein, it has been reported that when polymers have similar cure rates, co-cross-linking is possible. The sulfur bond length at the interface has also been debated. In blends of somewhat similar polymers, the characteristic dynamic mechanical loss peaks of the constituent polymers have been observed to merge due to interfacial cross-linking [41, 42]. The criteria for interface cross-linking to occur is the presence of a low interfacial tension between the components [3].

NR and styrene–butadiene rubber (SBR) are two diene rubbers that contribute majorly to worldwide rubber usage. As of 2017, NR constituted approximately 47 % of total rubber produced. Of the remaining 53 %, which is made up of synthetic rubbers, SBR is the most widely produced. NR benefits from very good low-temperature

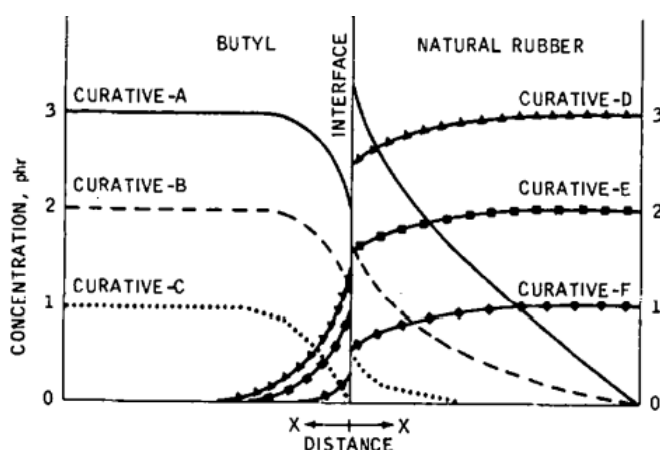


Figure 2.1: Gradients of multicurative diffusion [11]. Reprinted with permission from Curative Diffusion between Dissimilar Elastomers and its Influence on Adhesion. Copyright © (1968), Rubber Division, American Chemical Society, Inc.

flexibility, high rebound, excellent abrasion resistance, very low heat build-up and hysteresis, and unique strain-induced crystallization properties that aid in tensile and tear resistance [43]. SBR exhibits good dynamic fatigue resistance, excellent abrasion resistance, and relatively good heat resistance. As a result, blends of NR with SBR are used in technically demanding applications such as in tires and conveyor belts. In tires, their blends offer high abrasion resistance, wet-skid resistance, and lower rolling resistance [44]. It has been recognized that NR and SBR exhibit low interfacial tension due to their similar solubility parameters [3]. This leads to a smaller phase size. Figure 2.2 demonstrates the diffusion of sulfur measured by microinterferometry at the polymer/polymer interface. Substantial diffusion of sulfur from the NR phase to the SBR phase occurs in a very short time. It has been observed that depending on the conditions and composition, the curatives can achieve equilibrium concentrations in the rubber phases even before the start of cross-linking [11]. In doing so, the interface is cured to a different extent compared to the regions away from it. In an unfilled system of covalcanized SBR and NR, NMR imaging has shown the formation of an interfacial region associated with a modulus higher than that of both SBR and NR [45, 46], thus highlighting possible consequences during cross-linking of two or more polymers.

NR, SBR, and their blends constitute a major part of this thesis and hence are treated preferentially in the sections to follow.

2.1.1 Role of fillers

In the rubber industry, fillers are used not only to reinforce rubbers for improved and longer physical and mechanical performance, but also to modify electrical and thermal

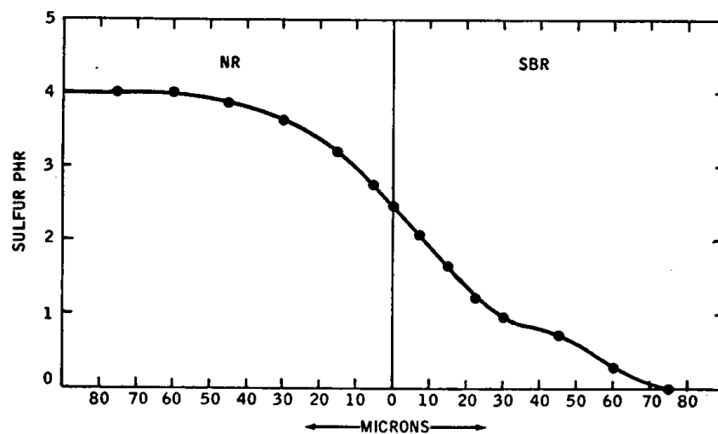


Figure 2.2: Gradient of diffusion of sulfur from NR to SBR measured up to 9 s using a microinterferometer at 150 °C[47]. Reprinted with permission from Measurement of Curative Diffusion Between Rubbers by Microinterferometry. Copyright © (1969), Rubber Division, American Chemical Society, Inc.

conductivity, modify processing, magnetic, optical, and surface characteristics, and reduce product costs. When used adequately, improved abrasion and fatigue resistance, modulus, and tear strength can be directly achieved. The tensile strength, which is probably the most important criterion of amorphous rubber reinforcement by fillers, is a function of filler concentration, size, and structure [48, 49]. Fillers with smaller particle sizes (larger surface areas) have been reported to increase the maximum tensile strength [50]. The flow properties alone are greatly influenced by these *reinforcing* fillers due to the manifesting strong rubber–filler interactions, in addition to their hydrodynamic effects [43, 51]. The fraction of rubber bound to such fillers in solvent-extracted samples has been studied by nuclear magnetic resonance (NMR) T_2 measurements, which yield regions corresponding to different T_2 relaxation times [52–57]. Increasing filler content induces a non-linearity of the Newtonian plateau at small strain rates [58]. Additionally, fillers lead to wall slippage, low extrudate swell, and anisotropic flow during processing.

To achieve adequate mechanical properties, the need for fillers is somewhat lesser in NR due to its ability to undergo strain-induced crystallization. Synthetic rubbers like SBR lack this ‘self-reinforcement’ property, and hence, need fillers [43]. Carbon black with its various grades is the most widely used type of filler for rubber product manufacturing (mainly tires) [49], its early usage dating back several millennia as a pigment [59]. General trends of variations of different properties with the amount of carbon black loading are represented in Figure 2.3 and can be extended to other fillers.

Similar to the distribution of additives discussed earlier, filler dispersion and distribution in the blend phases affect the overall material properties. For example, an inhomogeneous distribution can indirectly affect the phase morphology due to the effect

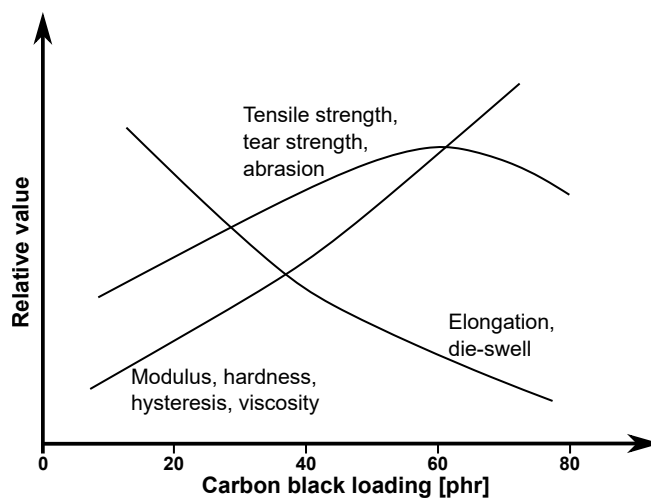


Figure 2.3: Effect of carbon black loading. Redrawn from reference [49].

filler concentration has on the melt viscosity [6]. These filler aspects are controlled by the nature of the polymers, their level of molecular weights, rubber–filler interactions, and mixing method and parameters [30, 60]. In NR/SBR blends containing carbon black, results from gas chromatography have shown that change in polymer weight and the activity of carbon black has no bearing on the distribution of the filler in the two phases [61]. However, using carbon blacks having a higher surface area, or prolonged mixing resulted in a migration of the filler from the NR phase to the SBR phase.

Through the analysis of rubber–filler gel, irrespective of its viscosity, NR has been observed to have a significantly higher wetting rate to carbon black than SBR [62]. The role of carbon black distribution on mechanical properties of NR/butadiene rubber (BR) and NR/SBR blends has been reported by Hess [63], with tear and fatigue resistance showing the highest filler-localization dependence. Electron micrographs showed the localization of carbon black in the NR and SBR phases of the two blends, respectively. The role of carbon black in the mechanical and electrical performance of various blends is further reviewed by Hess [8], with a survey on detection techniques and methods to regulate filler distribution.

An alternative to carbon black is the silica family of fillers. Since its invention in the late 1940s and the introduction of silane as a coupling agent, silica filler systems have evolved into a better alternative to carbon black as a reinforcing filler [64]. The innovation gained huge momentum after Michelin introduced the “green tire” concept for tire treads based on silica. Currently, silica finds major use in passenger car tires where, compared to carbon black, it provides lower rolling resistance, thus leading to a reduction in fuel consumption. Additionally, an enhanced wet grip and a marginally

reduced abrasion are also obtained [59]. It has been reported early on that rubber chains physically adsorb on the active surfaces of carbon black, whereas they combine chemically with silanized silica through the silanization process [48, 65–68].

A tricky aspect of processing using silica is its ability to adsorb accelerator and antiaging agents, thus partially deactivating them [69]. Thus, additional amounts of these chemicals have to be considered while mixing. Study of vulcanization chemistry by solid-state ^{13}C NMR studies on sulfur-cured synthetic high-cis-1,4-polyisoprene (isoprene rubber, IR) showed that inclusion of unsilanized silica as a filler led to enhancement of reversion reactions (chain scission and *cis-trans* isomerism) [70]. More importantly, the proportion of intramolecular structures (cyclic sulfides and pendant side groups) increased, while the intermolecular crosslinks decreased, leading to a reduction in cross-link density with the addition of silica. A solution to this was found in the inclusion of a silane coupling agent or polyethylene glycol (PEG) [71], where the polymer–filler interaction facilitated by silane eliminated adsorption sites on the filler, and PEG formed a coating over the filler surface, both approaches showing no negative influence on cross-linking.

In blends, unsilanized silica has been found to preferentially localize in the phase of acrylonitrile–butadiene rubber (NBR) in NBR/BR blends, but prefers the BR phase after silanization [72]. The former situation arises due to the affinity of silanol groups towards a polar NBR. In line with the wetting concept used for carbon black earlier, compared to SBR, NR demonstrated a higher wetting with silica, too [60]. However, subsequent mixing leads to a transfer of loosely bonded silica to the SBR phase due to a higher SBR–silica affinity. Further study has been carried out to detect filler localization in blends of emulsion and solution SBR [73]. The branches of emulsion SBR appear to occupy the pores of unsilanized silica particles preferentially over the linear solution SBR chains upon initial mixing, while prolonged mixing and silanization favor the linear chains of solution SBR. Scanning electron microscopy (SEM) [74], transmission electron microscopy (TEM), and AFM [17] are the popular methods to detect filler localization in blends of which, results from AFM are discussed in this thesis.

2.1.2 Aging of rubber

As prefaced, this thesis partly includes an evaluation of NR/SBR blends subjected to two aging approaches that are popularly employed in academia and industrial research of polymer degradation: the first of them is high-temperature thermo-oxidative aging. The other, more realistic approach involves studying the effects of weathering

elements (solar radiation, oxygen, ozone, water, and temperature) in an accelerated weatherometer setup wherein polymers can undergo chain scission, oxidation, discoloration, erosion, surface roughening, cracking, embrittlement, etc. [75]. This section is mainly adapted from the book Rubber Technology Handbook by Werner Hofmann [43]. Other references are cited accordingly.

Unsaturated bonds are the boon and bane in diene rubbers. While the unsaturated bonds make cross-linking possible, they also pose a site for attack by oxygen, ozone, radiation, and other chemicals. Higher temperatures act as a catalyst for these agents. The unreacted double bonds in a cross-linked rubber can also undergo post-curing with sulfur to harden the rubber. Depending on the type of rubber, the structural changes that take place can be either predominantly chain softening due to scission reactions or hardening by cross-linking reactions. In the presence of heat alone, modification of sulfur bonds by decomposition of cross-links, formation of inter or intramolecular cross-links, and shifting of cross-links without change in their density can occur.

Rubber reacts with oxygen present in the atmosphere to produce active radicals that promote chain reactions. On the other hand, ozone is known to promote crack growth in rubber that is under static extension, while under dynamic loading (*fatigue*) cracks grow perpendicular to the direction of stress. An unstressed rubber develops a network of small unoriented cracks (*crazing*) when exposed to irradiation, which upon prolongation renders the surface brittle in light-colored materials. Thus, over their storage and service life, polymers undergo integral changes.

One of the earliest studies on the role of oxygen and ozone in rubber aging was reported by Kohman [76]. Various parameters like surface area, the effect of curing, the presence of anti-aging agents, etc. in a simulated environment were considered to mimic and predict natural aging. Compared to raw rubber, the rate and amount of oxygen absorption are found to increase for a cross-linked NR. The rate of oxygen absorption increases with cross-link density and is dependent on the surface area when the surface area is too small. It has been reported that the rate of ozone uptake is rapid initially and then reduces drastically, making the rubber–ozone reaction non-autocatalytic, whereas the rubber–oxygen reaction is autocatalytic and can demonstrate, at the least, decomposition and addition reactions. The presence of fillers itself greatly affects the reactivity of the material towards the free radicals produced by polymer scission during oxidative aging. While these are quenched by carbon black radicals, this property is inherently absent in silica fillers and, hence, mandates the inclusion of additional amounts of antioxidants [69]. Further important studies on the role of oxygen can be found in the references cited herewith [77–90].

Crabtree [91] demonstrated that among the natural weathering agents like air (oxy-

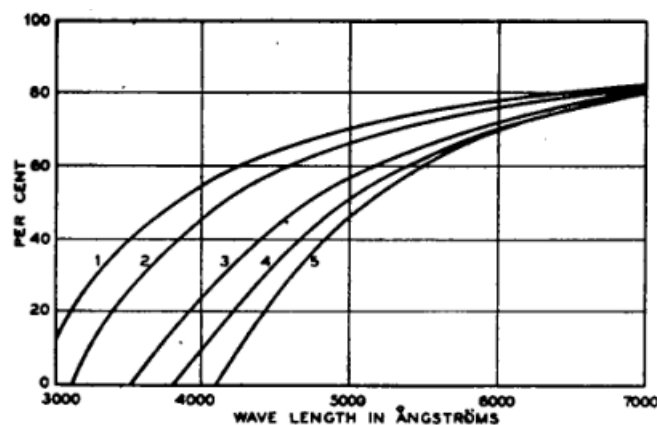


Figure 2.4: Spectral transmission of 0.1 mm thick natural rubber samples [91]. (1) Smoked sheets, (2) Base compound unvulcanized, (3) Vulcanized 5 min at 60 lb/sq.in, (4) 15 min, and (5) 60 min. Reprinted with permission from *Weathering of Soft Vulcanized Rubber*. Copyright © (1946), Rubber Division, American Chemical Society, Inc.

gen and ozone), heat, water, and sunlight, only oxygen, ozone, and light are of major importance. From a point of view of the influence of light, Figure 2.4 shows the spectral uptake in the UV range by various types of NR. It has been concluded that the extent of weathering depends on the relative magnitude of the three components, the exposure temperature, and the nature of the rubber compound.

In polymers relevant to the present study, Brown *et al.* have compared NR and SBR, among other polymers, aged naturally for 40 years with accelerated heat aging for a series of times and temperatures [92–94]. Comparisons have also been made with artificial weathering and exposure to ozone. It has been observed that wetting and drying create local stresses, which together with degradation due to temperature and UV lead to a pattern of cracks in NR. Filled NR compounds also showed evidence of cracks due to UV and water, not witnessed in heat-aging tests. On average, heat aging leads to only a gradual decrease in tensile strength and elongation at break in SBR compared to a faster drop in NR. On a molecular level, NR undergoes chain decomposition due to aging, whereas SBR undergoes intramolecular cross-linking [95, 96]. Noting these distinct aging characteristics, their microheterogeneous blends can be expected to exhibit these specific behaviors in the respective phases, and thus contribute differently to the overall blend properties.

2.2 Reinforcement in rubber/plastic blends

Blends of rubber and other plastics combine the low-temperature applicability of rubbers with the high-temperature performance of thermoplastics. The proportion of the

constituent polymers can be tuned to obtain blends that are resistant to deformation and abrasion, and that can provide good dimensional stability. These materials also exhibit high tensile strength, elongation at break, and impact strength. The combinations of these polymer types thus offer a much wider range of property profiles. These *thermoplastic elastomers* can be further enhanced by cross-linking the rubber phase with a suitable cross-linker, which can produce semi-interpenetrating networks (SIPN) [97].

Rubber/plastic blends draw similarities with block copolymers as both maintain distinct phases. Analogous to the amount of styrene in a styrene–butadiene block copolymer, by carefully controlling the proportion of plastic and rubber, a rubber/plastic blend can be tuned to be anything from a soft-elastic to a hard-ductile material [22, 30]. In addition, based on their viscosities, either or both can be the continuous phase. Although some level of miscibility of the phases is necessary, it is desirable that rubber and plastic maintain synergism in the blend they are a part of to exploit their low and high-temperature characteristics, respectively [22]. A reduction in hysteresis and improvement in hardness by blending plastics of polystyrene (PS), polyethylene (PE), polypropylene (PP), and polyvinyl chloride (PVC) into IR and BR has been previously observed by J. C. Blondel, as described in the chapter by Corish [30]. Improved tear resistance is also gained by PE [29, 30]. Finely divided PS as a filler in SBR vulcanizates increases the viscous component of the network that contributes to an increment in the tensile properties [98].

Blends of polyolefins such as PE and PP with ethylene–propylene–diene rubber (EPDM) constitute a technologically compatible group of materials and have been used extensively [22], especially in the automotive industry [99]. The thermoplastic constituent, in addition to being inexpensive, is semi-crystalline and processable at moderately lower temperatures than other commodity thermoplastics. EPDM belongs to a class of rubbers that contains a saturated backbone. This makes EPDM strongly resistant to ozone, light, and heat and finds use in sealants, solar panels, electrical insulation, transmission belts, etc. By increasing the ethylene content, these amorphous elastomers can be varied from being rubbery to semi-plastic, which can possess low levels of crystallinity [100]. In this regard, EPDM/PP blends have enjoyed tremendous interest over the past six decades [99, 101–104].

In comparison, polyolefin blends of EPDM/PE have been somewhat sparse. The first patent was issued in 1962 to Prillieux *et al.* at Esso [105]. Semi-crystalline PE is especially highly impermeable to fluids and inert to most chemicals. EPDM/PE blends show improved mechanical and electrical properties [30]. These blends benefit from the reduced degree of interfacial tension due to identical monomers in the two constituent

polymers.

The reinforcement in blends of low-density PE (LDPE) with partially crystallized and amorphous EPDM were compared by Lindsay *et al.* [[106]]. In the former blends, a synergistic effect was observed where the tensile strengths of the blends were higher than those of the individual components. However, this was not observed in blends with the latter EPDM type. The reason for the higher tensile strength was attributed to the presence of a high ethylene fraction in the EPDM, the long segments of which crystallized on the nucleates of LDPE. A depression in the differential scanning calorimetry (DSC) melting temperature of the blends was also observed, which was remarked as a result of the partial miscibility of the blend. Starkweather gave evidence for the miscibility of uncross-linked 1,4-hexadiene EPDM with the amorphous and crystalline regions of LDPE by studying dynamic mechanical thermal analysis (DMTA) loss peaks and established co-crystallization of the phases by DSC [100].

In ternary blends of isotactic PP, high-density PE (HDPE), and EPDM, the crystallite melting temperature (T_m) of HDPE decreased in the presence of EPDM, where composite particles of HDPE and EPDM formed due to mixing led to faster nucleation rate and formation of smaller and more number of spherulites [107]. EPDM was observed to reduce the overall crystallinity of the HDPE/PP blends. Through wide-angle X-ray scattering (WAXS) studies, the same team reported that EPDM led to an increase in the percentage crystallinity of HDPE in a related study [108]. This demonstrated enhanced mechanical properties. On the contrary, in blends of LDPE and EPDM-type terpolymer [109], the elastomer fraction showed a reduction in crystalline percentage and the melting temperature, among others. Cross-linking using dicumyl peroxide reduced these properties further.

As can be seen, blends of EPDM and PE offer fascinating characteristics depending on the type of polyethylene, ethylene-propylene-diene terpolymer, and the ratio of components within the terpolymer. Additionally, the proportion of the blend components and the presence of a cross-linker affect the crystallization behavior and thus the bulk properties.

2.3 Measurements of cross-link density in blends

Phase properties of polymer blends can be studied by various physical and chemical characterization techniques like microscopy, thermal and thermomechanical analysis, dielectric relaxation, infrared spectroscopy, NMR spectroscopy, X-ray analysis, neutron scattering, gas chromatography, etc., and by analyzing the solubility differences and

optical properties [10, 29].

Perhaps the most relevant molecular quantity for determining the properties of cross-linked rubbers and their blends is the *cross-link density* (Figure 2.5). The cross-link density, expressed as the number of cross-links per mole or per unit volume, is an empirical quantity that can be used to correlate to different macromolecular properties, as shown in the figure. Its analysis is thus useful in establishing the structure–property relationship, which further helps as a predictive tool in better material designing.

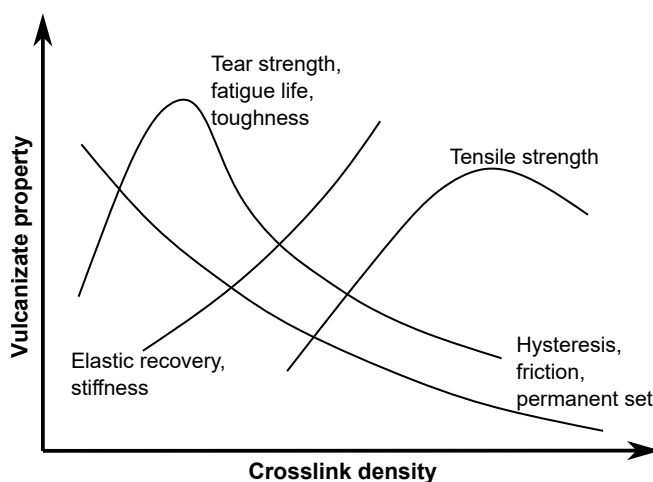


Figure 2.5: Vulcanizate properties as a function of the extent of vulcanization. Redrawn from reference [110].

Various methods for measuring cross-link density in blends were already introduced in the previous chapter. The works by Tinker [5, 111] contain a summary of all possible techniques for cross-link density determination. To abide by the motivation for this work, NMR approaches for phase-specific studies are surveyed next.

2.3.1 Phase-specific NMR measurements

Probably the most versatile characterization technique in academic and industrial use is NMR spectroscopy. It has been widely used in the elucidation of molecular structure and calculation of dynamics. Phase-resolved studies in the NMR context refer to measuring the resonance frequencies of all molecules in different bonding environments in the blend (except, of course, other than magnetic resonance imaging which is based on large-scale spatial resolution studies). Such spectral measurements come with their own limitation in a static setup. The spectrum of a solid sample is a broad featureless line due to the presence of strong dipole–dipole couplings and shielding interactions between nuclear spins in polymers (refer Chapter 4) [112, 113]. One way of overcoming

this is by swelling the blend in a suitable solvent to provide some degree of motional freedom to the polymer chains, which leads to somewhat resolved NMR peaks. Earliest studies were performed using ^1H NMR spectroscopy on slivers of solvent-swollen rubber samples [114–116]. The resulting spectra are resolved to a good degree with additional solvent-related peaks. Cross-link densities were deduced by proton line-width analysis, the idea being that the line-width increases with the extent of cross-linking. Although distinctive peaks are obtained, the approach is somewhat qualitative in terms of measuring the cross-link density. Additionally, the possible effects of mobile defects on the resolved peaks cannot be eliminated. Similar studies exist for blends containing fillers where carbon black has been observed to cause peak-broadening and affect their positions [117, 118].

Other methods of improving resolution include using high-power decoupling and magic-angle spinning (MAS) of the sample. The former involves applying a continuous radio frequency pulse to remove the effects of coupling between the spins of the different nuclei (*heteronuclear* decoupling) or between those of the same nucleus (*homonuclear* decoupling) [112]. The latter method requires spinning the sample at a sufficiently high frequency at the magic angle, which averages the effects of the anisotropic interactions to zero. This approach is pivotal to the present research and is discussed in some detail in Section 4.4.3.

In studying blends, different MAS-based experiments have already been employed to various degrees for studying miscibility. The review chapters by Abolhasani [119] and Asano [120, 121] contain a detailed summary of these experiments used over the years. The studies pertaining to cross-link density, however, have been both rare and only qualitative [122, 123]. In this work, a homonuclear double-quantum (DQ) recoupling pulse sequence (known as BaBa-xy16) [124] is successfully applied to NR/SBR blends for quantitative analysis of the cross-link density [19, 20]. The experiment utilizes the anisotropy of chain fluctuations, which is prevalent when topological constraints such as entanglements and cross-links deter isotropic averaging of motions. The magnitude of this anisotropy is given by the D_{res} , a quantity that is a direct measure of the cross-link density. This experimental approach has its origin in a static multiple-quantum (MQ) analog developed by Baum and Pines [125] that has found very many successful applications in the past couple of decades in the investigation of a variety of polymer material types. This includes different blends [126, 127] including those that constitute this thesis [19–21].

2.4 Aim and research elements

As summarized until now, owing to their still incomplete understanding, rubber/rubber and rubber/plastic blends offer huge scope for improved technical applications. Considering the paramount need for efficient usage of non-renewable resources in today's scenario, a better understanding of the materials is required for optimal product design and longevity. Owing to this, this thesis aims to establish NMR-based approaches for the quantitative evaluation of phase-specific properties in such blends.

The primary research element of this thesis is to demonstrate and establish an NMR approach based on the BaBa-xy16 pulse sequence for quantitatively measuring the cross-link density and their distribution in the phases of sulfur-cross-linked NR/SBR blends. This is achieved by subjecting the blends and their single vulcanizates to thermo-oxidative aging and comparing between the phase-specific cross-link densities before and after prolonged aging. Time-wise evolution in cross-link densities upon thermo-oxidative aging is investigated by solid-state ^1H MQ low-field NMR spectroscopy using the Baum-Pines pulse sequence introduced earlier. This also provides the percentage of chain defects in the samples after aging. The presence of strongly coupled fractions such as proteins in NR or the oxidized fractions formed by aging can have a rigid limit static dipolar coupling value of about 30 kHz and are associated with a T_2 in the range of about 20 μs . These components are measured by free-induction decay (FID) in conjunction with a pulsed magic-sandwich echo (MSE)-FID. Where slowly relaxing components such as defects are present, the FID is extended by combining it with a Hahn-echo experiment.

As a follow-up study, learnings from the studies on thermo-oxidative aging are utilized to understand the role of accelerated weathering in the evolution of the NR and SBR phases in their blend. Apart from the NMR experiments used before, the scope of methodology will be diversified into also studying chemical and mechanical changes by using complementary techniques like IR spectroscopy, DMTA, and AFM.

To broaden the application of the static NMR methodology to other types of blends, the origin of reinforcement in rubber/plastic blends of EPDM with ultralow-density PE (ULDPE) blends is studied. In addition to the static MQ and T_2 experiments, complementary methods like tensile testing, DSC, and AFM are employed for getting additional insights into the blend behavior.

A small portion of this thesis is an extension of the NR/SBR blends to somewhat industrially relevant variants that are composed of silica filler and the antioxidant N-isopropyl-N'-phenyl-1,4-phenylenediamine (IPPD). Here, the (possible) preferential

distribution of silica filler in either of the blend phases is analyzed through microscopic studies using AFM. The consequences of filler distribution on the activity of the curing system are measured by the NMR techniques that are part of the studies on unfilled rubber blends. The effects of thermo-oxidative aging are excluded here.

3. Polymer Basics

This chapter introduces the basic concepts required for understanding polymers from the point of view of their blends, networks, and nanocomposites. The content is mainly based on the books by Rubinstein and Colby [128], Treloar [129], Sperling [130], and Strobl [131].

Polymers or *macromolecules*, as the name suggests, are long chains composed of many repetitive units. A single repetitive unit, known as the *monomer*, can be bonded to thousands of other monomers to make a macromolecular chain. Thus, the molecular weight (M) of a polymer chain is a product of the number (N) of the repetitive units (or monomers) and the molecular weight of the monomer (M_0): $M = NM_0$. N is also often regarded as the *degree of polymerization*.

In a realistic polymerization process, it is technically challenging to polymerize all polymer chains to the same length. Hence, to describe all polymer chain lengths, the polymeric molecular weight is described as weighted averages with different considerations: number-average molecular weight (\overline{M}_n), weight-average molecular weight (\overline{M}_w), sedimentation-average molecular weight (\overline{M}_z), and viscosity-average molecular weight (\overline{M}_v). The most relevant of these, \overline{M}_n and \overline{M}_w , are represented as,

$$\overline{M}_n = \frac{\sum N_i M_i}{\sum N_i} \quad (3.1)$$

and

$$\overline{M}_w = \frac{\sum N_i M_i^2}{\sum N_i M_i} \quad (3.2)$$

respectively.

The distribution of the chain lengths can be represented by the quantity known as the *polydispersity* (PD), which is a ratio of \overline{M}_w to \overline{M}_n . A PD value of 1 indicates the narrowest distribution achievable. In practicality, the narrowest distribution can be achieved by anionic polymerization (PD = 1.02). The other types of polymerization processes such as free-radical polymerization, step-growth polymerization, and coordination and insertion polymerization yield PD in the ranges of 1.5 – 5.0, 1.5 – 2.0, and 2.0 – 20.0, respectively.

Carothers, at the Faraday Society Meeting in 1935, presented his studies on polymerization and demonstrated the validity of Paul Flory's polycondensation theory, which postulated the formation of linear macromolecules by sequential addition of monomers. This also gave more recognition to the concept of covalently bonded macro-

molecules presented by Hermann Staudinger in 1920.

Following these developments, different approaches for classifying polymers have been taken by the scientific community. These are distinguished on the basis of chain constitution, chain configuration, chain conformation, etc. In this thesis, polymers well above their glass transition temperature (T_g) possessing unsaturated bonds that cross-link (*rubbers*), and those with a saturated backbone used usually below their glass transition temperature (*thermoplastics*) are explored later.

3.1 Physical account of linear polymer chains

Actual polymers can be modeled using the *ideal*- and *real*-chain descriptions. The basis for an ideal chain is that monomers that are far apart along the chain show no interactions with each other. The ideal chain follows the *random walk* statistics where, in a two-dimensional representation, the polymer chain can be intersected at a site. On the contrary, the real chain description follows the *self-avoiding walk* where a site occupied by a chain segment cannot be occupied by another. Thus, the real-chain model can be attributed more correctly to an actual chain. Nevertheless, the ideal-chain model can relate to many flexible polymer systems such as concentrated solutions, melts, glasses, and dilute solutions with theta solvents [132]. In this section, polymers from an ideal-chain perspective are discussed.

A polymer chain can take up innumerable conformations depending on the bond angle (θ) and torsion angle (ϕ). The torsion angle assumes the three most energetically stable states and dictates the chain flexibility. These are the trans ($\phi_t = 0^\circ$), gauche+ ($\phi_{g+} = +120^\circ$) and gauche- ($\phi_{g-} = -120^\circ$). The gauche states are responsible for chain turns and bends. Trans conformation is often the most stable wherein the energy (E) is zero. Consecutive trans states lead to an extension of a chain segment into a zig-zag conformation. The *end-to-end* distance of the chain is the largest (R_{max}) when all torsion angles of a polymer chain are only in the trans-state. R_{max} is referred to as the *contour length* and is described by the equation:

$$R_{max} = nl \cos\left(\frac{\theta}{2}\right) \quad (3.3)$$

Here ‘ n ’ is the number of bonds and $l \cos(\theta/2)$ is the projection of the bonds of the same length ‘ l ’.

The size of a polymer chain can be studied by knowing the distance between its start and end points, denoted by the end-to-end vector (\vec{R}), which is an arithmetic

sum over all the bond vectors. An unconstrained chain has no orientational preference and thus yields a zero value for the ensemble average of R : $\langle R \rangle = 0$. The same analogy can be extended to a system with many chains. It is hence appropriate to express it as a mean-square value of l_i and l_j , which takes the general form:

$$\langle R^2 \rangle = \langle \vec{R}^2 \rangle = \sum_{i=1}^n \sum_{j=1}^n \langle l_i l_j \rangle = l_i l_j \sum_{i=1}^n \sum_{j=1}^n \langle \cos \theta_{ij} \rangle \quad (3.4)$$

Here, $\cos \theta_{ij}$ gives a correlation between the bond vectors. With the absence of interactions between distant monomers along the chain, the directional correlations between the different bond vectors are lost. When the bond lengths are constant, the above equation reduces to:

$$\langle R^2 \rangle = C_\infty n l^2 \quad (3.5)$$

C_∞ is the asymptotic value of Flory's *characteristic ratio* (C_n) and arises due to very long chains ($n \rightarrow \infty$). C_∞ is thus a measure of the stiffness of the polymer chain. A rubber like PI has a C_∞ of 4.6 and a thermoplastic like PE has a value of 7.7. Higher values are obtained for sterically hindered polymers. $C_\infty = 1$ gives the **equivalent freely jointed chain**. The equivalency comes from further simplification by replacing the bond length l with that of a statistical monomer called the *Kuhn monomer* (N_K). Kuhn monomers are rigid links of length l_K (*Kuhn length*) and have no restrictions to bond and torsion angles between successive bonds and can be used in the end-to-end arguments as below:

$$R_{max} = N_K l_K = n l \cos \left(\frac{\theta}{2} \right) \quad (3.6)$$

and

$$\langle R^2 \rangle = C_\infty n l^2 = N_K l_K^2 = R_{max} l_K \quad (3.7)$$

Thus,

$$N_K = \frac{R_{max}^2}{C_\infty n l^2} \quad \text{and} \quad l_K = \frac{C_\infty n l^2}{R_{max}} \quad (3.8)$$

A summary of characteristic ratios and Kuhn lengths for some polymers can be found in the books by Flory, and Rubinstein and Colby [128, 133].

3.1.1 Ideal chain conformations and entropy

The diversity in statistical conformations of a polymer chain is central to rubber-like elasticity. At rest, polymer chains take up innumerable conformations, making

them liquid-like due to the weak secondary forces between the molecules. Cross-links and other topological constraints like entanglements, however, render them solid. A polyethylene chain containing 1000 links, characteristic valence angle, and six equally spaced torsion angles that are randomly chosen can produce 6^{998} different conformations in a three-dimensional space [129]. A three-dimensional probability distribution of the conformations, which is derived from random walk statistics where the torsion angles are independent of each other, can be described by a Gaussian approximation:

$$P(N_K, \vec{R}) = \left(\frac{3}{2} \frac{1}{\pi N_K l_K^2} \right)^{3/2} \exp \left(-\frac{3}{2} \frac{\vec{R}^2}{N_K l_K^2} \right) \quad (3.9)$$

This probability distribution function is a product of three independent distribution functions, one for each of the Cartesian components for the chain end-to-end vector. It necessarily explains the probable spatial arrangements of Kuhn monomers within a chain. The number of conformations ($\Omega(N_K, \vec{R})$) for an end-to-end vector at distances R and $R+dR$, circumscribed as the two radii of a spherical shell with the chain starting at the origin, is proportional to a probability distribution function as:

$$P(N_K, \vec{R}) = \frac{\Omega(N_K, \vec{R})}{\int \Omega(N_K, \vec{R}) d\vec{R}} \quad (3.10)$$

The denominator is a normalization factor where the infinity limit actually extends to a maximum value that is achieved by a rod-like conformation. The directional constraints in Equation 3.10 can be removed by multiplying it with the area of a sphere ($4\pi R^2$), while the vector forms are replaced by the end-to-end distance (R).

The number of conformational states has an energetic origin where it is related to the entropy (S) through the Boltzmann constant (k) for a chain with N_K number of Kuhn monomers with end-to-end vector as:

$$S(N_K, \vec{R}) = k \ln \Omega(N_K, \vec{R}) \quad (3.11)$$

Equations 3.10 and 3.11 provide a relation for the entropy whose second part is composed of terms affected by N_K only and is thus a constant for all practical purposes:

$$S(N_K, \vec{R}) = -\frac{3}{2} k \frac{\vec{R}^2}{N_K l_K^2} + S(N_K, 0) \quad (3.12)$$

3.2 Miscibility of rubber-containing blends

Technologically relevant blends are those that are homogeneous on a macroscopic level but are phase-separated on a microscopic level. Cross-linking these macroscopically

compatible blends helps create a network that works synergistically. A truly miscible blend has polymer components that have a segmental level homogeneity. A short overview of entropy (S) and enthalpy (H) in this regard, mainly adapted from the books of Rubinstein and Colby[128], and Strobl [131] follows.

The mixing of two components can be understood by a lattice model, in which individual sites are occupied by monomers for a polymer (or molecules for a solvent). Thus, a polymer chain is represented by multiple connected lattice sites. The entropy is then a product of the natural logarithm of the number of the ways (Ω) in which the molecules arrange themselves on the lattice times the Boltzmann constant, k :

$$S = k\ln\Omega \quad (3.13)$$

The entropy change of mixing for a single molecule of the kind A is:

$$\Delta S_A = k\ln\Omega_{AB} - k\ln\Omega_A = -k\ln\phi_A \quad (3.14)$$

A similar equation can be derived for the entropy change of a single molecule of the kind B. The above equation always yields a positive value for the entropy change as the volume fraction ϕ_A is less than unity. Ω_{AB} corresponds to the case of a homogeneous mixture of A with B. The entropy of mixing per lattice site can be generalized for the two polymers as:

$$\Delta S_{mix} = -k \left[\frac{\phi_A}{N_A} \ln\phi_A + \frac{\phi_B}{N_B} \ln\phi_B \right] \quad (3.15)$$

The number of lattice sites occupied by each molecule are given by N_A and N_B , respectively. The possibility that mixing would indeed occur is governed by the change in Gibbs free energy upon mixing, ΔG_{mix} :

$$\Delta G_{mix} = \Delta G_{AB} - (G_A + G_B) \quad (3.16)$$

The Gibbs free energies of the two components and their blend are given by G_A , G_B , and G_{AB} , respectively. The mixing process can be associated with a volume change where reduction in blend volume due to mixing reduces the number of ways of packing polymer segments and increases the free energy [134]. Using Gibbs energies permits accounting for this change in volume in an environment with constant pressure. Nevertheless, it has been reported that this change is always negligible [131].

A crucial component of the miscibility description is the enthalpic contribution to free energy. Both entropy and enthalpy are related to ΔG_{mix} by the equation:

$$\Delta G_{mix} = \Delta H_{mix} - T\Delta S_{mix} \quad (3.17)$$

where, ΔH_{mix} and T are the enthalpy change and temperature, respectively. The enthalpy term is composed of contributions from monomer–monomer pair interactions and motions, and these factors determine the enthalpic term being favorable (or not) for mixing, whereas mixing is always favored by entropy. The completely miscible blends have a negative value for the change in free energy. From an entropic standpoint, due to their very high molecular weights, the change in entropy of mixing, which depends on the number of molecules, is low for the polymers. More importantly, from an enthalpic standpoint, since the van der Waals attractive interaction energies for the like monomers are more than the unlike, $\Delta H_{mix} > 0$ in most cases and hence wins out over entropy. This inhibits mixing, resulting in polymer blends often possessing a phase-separated morphology. Most compatible blends are a result of increased entropy due to the positional disorder arising due to mixing [23]. This entropy is regarded as translational entropy.

A general form for the Flory–Huggins equation can be derived, with $\Delta H = \chi_{AB}\phi_A\phi_B$ we have:

$$\Delta G_{mix} = kT \left[\frac{\phi_A}{N_A} \ln \phi_A + \frac{\phi_B}{N_B} \ln \phi_B + \chi_{AB} \phi_A \phi_B \right] \quad (3.18)$$

ΔH_{mix} for each interacting segment or molecule is characterized by the dimensionless quantity χ_{AB} , known as the *interaction parameter*. It depends on the temperature, and the composition and molecular weights of the components.

Phase separation in blends occurs either through a nucleation and growth process from a metastable state or via spinodal decomposition for larger quench depths. As to the former, a change in the temperature can lead to minor instability in the blends, which causes the separation of the blend into domains of different compositions [23]. This is different from crystallization but has a similar activation barrier. Phase separation by nucleation and growth yields a final structure of the droplet–matrix type. Phase separation by spinodal decomposition occurs at higher undercooling where the compositional fluctuations in the system of any size become energetically favorable. Spinodal decomposition structures exhibit a high degree of co-continuity, at least in the initial stages of spinodal decomposition. The apparent diffusion coefficient for spinodal decomposition is negative, whereas it is positive for nucleation and growth [135]. From the point of view of NR/SBR blends, curing requires going up to temperatures as high as 160 °C. At such temperatures, these blends undergo phase separation and are hence categorized by the *lower critical solution temperature* [136, 137]. Through AFM studies, Klat *et al.* [138] have observed that higher vinyl-containing SBR usually offer smaller domain size and thus better miscibility compared to grades of SBR having

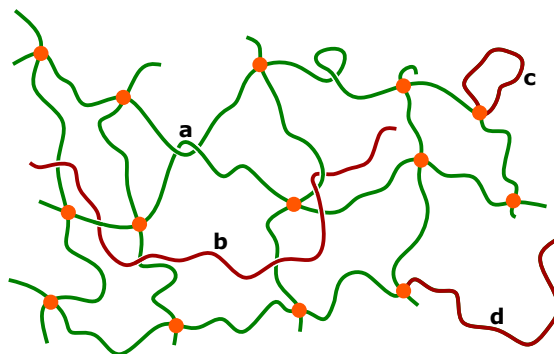


Figure 3.1: Schematic of a real network consisting of an entanglement (a), and the defects composed of sol molecules (b), loops (c), and dangling chain ends (d)

lower vinyl content.

3.3 Rubber networks

Rubbers are synonymous with elasticity due to their complete geometrical recovery from very large compressive and tensile deformations under suitable circumstances. They are also recognized for toughness under static and dynamic stresses, resistance to abrasion, impermeability to air and water, and resistance to many chemicals in favorable conditions. Their tack enables adherence to fibers and metals [43]. Gough in 1805 observed that under a constant load stretched rubber contracts on heating, and when stretched, the rubber gives out heat. These reversible processes were confirmed by Joule in 1859 with his work on vulcanized rubber. The initial observations of Gough are summarized in the book by Sperling [130].

Cross-linking freezes an entangled melt to form a three-dimensional network where all chains are connected to each other to effectively form a single molecule. Cross-linking restricts the irreversible flow of the polymer chains, thus providing dimensional stability. In an ideal network, the three-dimensional cage is made up of cross-links that are separated by polymer strands, all having the same molecular weight. However, a real network is made up of strands that all have different lengths. Figure 3.1 depicts a two-dimensional schematic of a real network.

In addition to the heterogeneity in cross-linking, real networks are also composed of chain **defects** that are formed due to imperfect cross-linking. These consist of chains that cross-link onto themselves (*loops*), chains with only one end connected to the network (*dangling chain ends*), and chains that do not participate in cross-linking and are not chemically bound to the continuous network (*sol molecules*). The latter can be extracted by extraction with a suitable solvent, whereas the network

resists dissolution due to the presence of chemical cross-links. Characteristically, defects reduce the modulus in many different ways.

For a rubber at equilibrium that is undergoing reversible changes (e.g., elastic deformations), a relation between variables like force (f), length (L), temperature (T), hydrostatic pressure (p), and thermodynamic quantities of internal energy (U) and entropy (S) can be developed by combining the first and second laws of thermodynamics to obtain the change in its internal energy as:

$$dU = TdS - pdV + fdL \quad (3.19)$$

where, TdS refers to the heat added to the system, $-pdV$ is the work done to change the network volume, and fdL is the work done in a small displacement. With certain thermodynamic considerations [129], one arrives at the force required to deform a network. The force in rubber is a sum of energetic (f_E) and entropic (f_S) contributions.

$$f = f_E + f_S = \left(\frac{\partial U}{\partial L} \right)_{T,V} - T \left(\frac{\partial S}{\partial L} \right)_{T,V} \quad (3.20)$$

More than 90 % of the total force is accounted for by the entropic component in real networks, whereas the energetic term is zero for ideal networks. A consequence of this entropic domination is the loss of conformational entropy of chains upon heating under constant extension [128]. This results in an increase in the total force with increasing temperature as $\partial S/\partial L < 0$. This behavior is in contrast to simple steel springs or also semi-crystalline polymers where the force decreases weakly with increasing temperature.

3.3.1 Origin of rubber elasticity

The characteristic elasticity of a cross-linked elastomer can be described by the entropy of the chain, as described by Equation 3.12. The deformation of a chain leads to a change in entropy:

$$\Delta S = S(N_K, \vec{R}) - S(N_K, \vec{R}_0) = -\frac{3}{2}k \frac{R_x^2 + R_y^2 + R_z^2}{N_K l_K^2} + \frac{3}{2}k \frac{R_{x0}^2 + R_{y0}^2 + R_{z0}^2}{N_K l_K^2} \quad (3.21)$$

Here the end-to-end vector has been resolved into its three Cartesian coordinate components. The subscript zero represents the initial entropic state. The ratio of the final to the initial end-to-end distance (R and R_0 , respectively) is the deformation λ by which the end-to-end distance along a direction has changed.

For a network, the entropy change encompasses all the ‘ n ’ strands and their corresponding entropy changes as a summation (ΔS_{sum}). It can be deduced that the sum of the square of the initial coordinate components is all same and equal to $nN_K l_K^2/3$. An equation for the entropy change can thus be derived as:

$$\Delta S_{sum} = -\frac{nk}{2}(\lambda_x^2 + \lambda_y^2 + \lambda_z^2 - 3) \quad (3.22)$$

An equation for the elastic force (\vec{f}) within a chain can be derived by deducing an equation for the Helmholtz free energy, A ($A = U - TS$), on the lines of chain end-to-end vector and entropy relation in Equation 3.12. The energy (U) is zero for an ideal chain due to the absence of long-range interactions between the monomers. The entropic part of the equation reduces as the number of possible chain conformations reduces with an increase in \vec{R} . The force can be derived as a partial derivative of A as:

$$\vec{f} = \frac{3kT}{N_K l_K^2} \vec{R} \quad (3.23)$$

A key takeaway from this relation is that with rising polymer temperature the stretching of the chain becomes difficult. At a fixed experimental temperature, a uniaxial stretching produces a similar effect in the force while the end-to-end distance increases. The linear dependency of the Hookean behavior of the ideal chain, valid for $|\vec{R}| \ll R_{max}$ is lost as \vec{R} approaches R_{max} : $|\vec{R}| \leq R_{max}$. The condition when $|\vec{R}| = R_{max}$ causes the force to diverge from linearity due to the *finite extensibility* of the chains.

In the following sections, select models for unentangled and entangled networks to describe the mechanical properties of cross-linked materials are discussed.

3.3.2 Unentangled network models

Affine network model

The simplest of models that are based on non-interacting chains is the **affine model**. Kuhn based this model on the assumption that cross-links are fixed in space and that their positions transform *affinely* with the macroscopic deformation [139]. This implies that the macroscopic and any chain’s relative deformations are the same in any given direction. The chains between the junctions are free to pass through each other but not allowed to interact with each other to contribute towards the elasticity of the network. Thus, the dimensional changes (L) after deformation (λ) are related to the

initial dimensions (L_0) in the x , y and z dimensions as:

$$L_{x,y,z} = \lambda_{x,y,z} L_{x_0,y_0,z_0} \quad (3.24)$$

Likewise, the projections of an unstrained end-to-end vector \vec{R}_0 after deformation changes as:

$$R_{x,y,z} = \lambda_{x,y,z} R_{x_0,y_0,z_0} \quad (3.25)$$

Dry networks are regarded as incompressible materials whose volumes are accepted to be almost constant, which results in a unity value of the product of deformations in the three dimensions: $\lambda_x \lambda_y \lambda_z = 1$. The following equation relates the observed value of the shear modulus (G) and the value predicted by the statistical theory.

$$G = \nu kT = \frac{\rho RT}{M_c} \quad (3.26)$$

where, ν is the number of network strands in a unit volume, k is the Boltzmann constant, T is the temperature, ρ is the network density, R is the gas constant, and M_c is the number average molecular weight of the cross-linked chains. The modulus is related to the corresponding engineering stress (σ_{engg}) and the true stress (σ_{true}) as:

$$\sigma_{engg} = \frac{\sigma_{true}}{\lambda} = \frac{\rho RT}{M_c} \left(\lambda - \frac{1}{\lambda^2} \right) \quad (3.27)$$

Here, the engineering stress and true stress take the original cross-section and the instantaneous cross-section of the deformed specimen into the calculation, respectively. In a typical network, a cross-link junction is a point where four chains are connected (\implies tetrafunctional). Thus, ν is related to the cross-link density (number of cross-links per unit volume, μ) as $\nu = 2\mu$, and owing to the statistical theory, the chemical nature of these network chains has no bearing on the elastic properties.

When the effect of dangling chain ends is considered, the modulus is modified according to Flory [140] as:

$$G = \frac{\rho RT}{M_c} \left(1 - \frac{2M_c}{M} \right) \quad (3.28)$$

where, M is the molecular weight of the primary chain.

Phantom network model

The main limitation of the affine model is the assumption that cross-links are fixed in space, which makes the lengths of the network strands the only source of freedom of

movement for the system. To overcome this, James and Guth proposed that the ends of ideal network strands are attached to cross-link junctions that are assumed to move and hence fluctuate by performing a restricted Brownian motion around their average position. This results in a net lowering of the free energy of the system. The chain ends at the surface are fixed in position and transform affinely. This eventually came to be known as the **phantom network model** where the network strain and average value of cross-link fluctuation are assumed to be independent of each other.

For a phantom network, the shear modulus is modified by adding a prefactor to that of the affine network modulus.

$$G = \left(\frac{f - 2}{f} \right) \frac{\rho RT}{M_c} \quad (3.29)$$

The functionality, f , corresponds to the number of network strands emanating from each cross-link site. Due to the possibility of fluctuation of junctions in a phantom network, the obtained modulus is lower than that in an affine network. Thus, when four strands connect at a junction ($f = 4$), typically in sulfur and divinyl benzene cross-linked systems, the modulus of a phantom network is half that of an affine network. However, at higher f values, the cross-links behave affinely.

The phantom modulus can be alternatively represented in a form similar to that of Equation 3.26 as:

$$G = (\nu - \mu)kT \quad (3.30)$$

where, μ is now a ratio of ν to $f/2$, as the latter represents the number of strands per junction site.

3.3.3 Entangled network models

Tube model and reptation of chains

In real networks, the measured modulus is in large contrast to the predictions of the models discussed above. The affine and the phantom network models present the two extreme cases for the prediction of network modulus: the limits set by the fixed junctions in the affine, and the fluctuating junctions in the phantom models imply that a real network should possess a magnitude of modulus that is intermediate to these cases. However, in practice, the modulus is larger than these predictions. The reason for this is the entangling of chains. These entanglements act as topological constraints and can disentangle over a certain time (*disentanglement time*) in a polymer



Figure 3.2: Chain segment AB in a dense rubber. Points A and B denote the cross-linked points, and the dots represent other chains which, in this drawing, are assumed to be perpendicular to the paper. Due to entanglements, the chain is confined to the tube-like region denoted by the dashed line. The bold line shows the primitive path. Reproduced from Ref. [141] with permission from the Royal Society of Chemistry.

melt or solution, but are trapped if their ends are cross-linked. The resulting addition to modulus due to entanglements in Equation 3.26 can be approximated as:

$$G \approx \rho RT \left(\frac{1}{M_e} + \frac{1}{M_c} \right) \quad (3.31)$$

where, M_e is the entanglement molecular weight. Doi and Edwards proposed a **tube model** that explains the entanglement effects [141]. In this model, a polymer chain is envisaged to be contained within a hypothetical tube created by those of the surrounding chains, thus preventing lateral motion. The tube model for a cross-linked chain can be appreciated in Figure 3.2.

The *primitive path* in the figure corresponds to the average of the rapid fluctuations of the chain within the limit of the cross-section of the tube and is the shortest path between the ends of the chain along the averaged contour. In the case of linear chains, the tube diameter due to the entanglements is about 5 nm. As the chain in Figure 3.2 is cross-linked at points A and B, there is no diffusion of the chain along the length of the tube. However, in the absence of cross-links, such as in a polymer melt, the chain can diffuse along the imaginary tube out of the tube ends. The diffusion itself is akin to a snake or an earthworm moving slowly through a bunch of many others through such a motion called *reptation*. The reptation model proposed by de Gennes [142] explains the disentanglement of a chain, which moves out of its tube but forms new sections of the tube as it reptates along it.

The tube diameter in linear chains allows reptation through the tube ends but does not account for the sideways translational motion that is necessary for branched chains.

In branched chains (Figure 3.3), the motion of a side branch along the main-chain tube is characterized by a decrease in entropy. An energetically favorable process is that the chain changes its conformation such that the branch retracts and shifts with the main chain before extending itself into a random conformation [143]. Such motions are relevant for defects in networks, see Figure 3.1

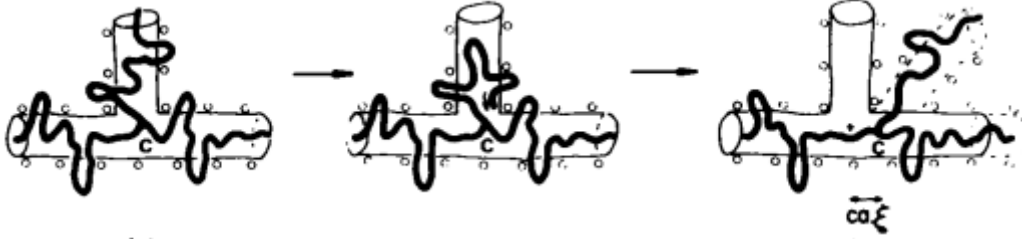


Figure 3.3: Motion of a branched chain. The junction ‘c’ remains stationary while the branch retracts into the main tube (second image). The junction shifts to a new position (third image) and the branch extends, forming a new side-tube, while the main chain reorients itself. Reprinted with permission from [143]. Copyright 1986 American Chemical Society.

Mooney-Rivlin equation

The Mooney-Rivlin approach serves as a phenomenological model of elasticity. It involves plotting reduced stress (σ_{red}) against inverse deformation. A fit to the curve in the linear region using Equation 3.32 gives values for the cross-link density ($2C_1$) and the entanglement density ($2C_2$).

$$\sigma_{red} = \frac{\sigma_{engg}}{\lambda - 1/\lambda^2} = \frac{\sigma_{true}}{\lambda^2 - 1/\lambda} = 2C_1 + \frac{2C_2}{\lambda} \quad (3.32)$$

Due to the difficulty in measuring true stress, engineering stress is used. For a series of networks with increasing cross-linker, C_1 increases whereas C_2 remains almost constant. An example of this can be seen in Figure 3.4 by Mullins [144] where data for NR containing increasing amounts of peroxide are plotted and fitted according to the equation. A special case of this formulation is that $C_2 = 0$ corresponds to a horizontal line and satisfies the conditions laid down by the affine, phantom, and tube models.

The finite extensibility-related divergence mentioned in section 3.3.1 shows up in Figure 3.4 as an upturn in the lower $1/\lambda$ limit. Further non-linearity in the inverse deformation curve occurs, as $1/\lambda$ approaches unity, due to uncontrolled effects such as from specimen clamping. This curve can be linearized by a correction to λ in the form of $\lambda \pm \Delta\lambda$, which gives a corrected reduced stress ($\sigma_{red,corr}$). This procedure is represented in the chapter on EPDM/ULDPE blends (Chapter 7).

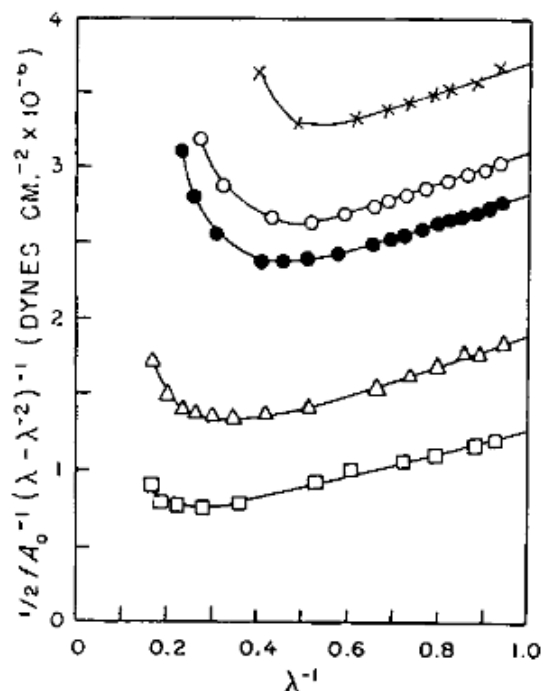


Figure 3.4: Mooney-Rivlin fits to the reduced stress (y -axis) vs. inverse deformation plots of NR cross-linked by peroxide from 1 phr (lowest curve) to 5 phr (highest curve). Reprinted with permission from [144]. Copyright 1959 John Wiley and Sons.

3.4 Polymer reinforcement by fillers

3.4.1 The microscopic picture

The rubber filler market is dominated by different grades of carbon black. These differ mainly based on the size of the primary particle. The size ranges from tens to a few hundred nanometers. A cluster of many primary particles fused together is called an *aggregate* and is $< 1 \mu\text{m}$. The size and specific surface area of the aggregates are responsible for reinforcement. The spatial complexity of the aggregates which is known as its *structure*, determined by the number and arrangement of particles within them, also contributes to reinforcement. Gruber [145] has classified the aggregate shapes as spheroidal, ellipsoidal, linear, and branched which can coexist in a system. Further larger structures composed of aggregates form into a loose *agglomerate*. A similar picture exists for silica fillers (Figure 3.5). The elementary particles form into aggregates akin to a ‘string of pearls’, which have dimensions in the 50–500 nm range [145].

The surface of CB is composed of more than 90 % carbon bonded with oxygen and hydrogen complexes to form carboxylic, quinonic, phenolic, ketonic, lactonic, and

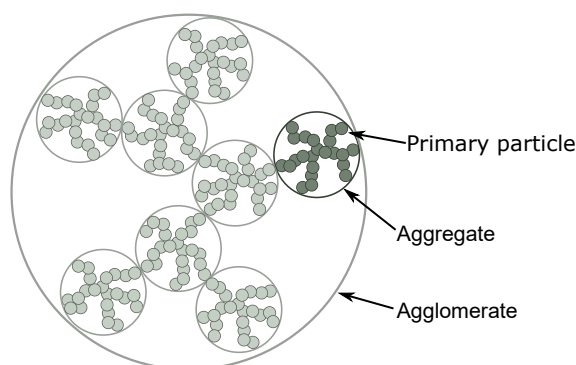


Figure 3.5: Scheme of the hierarchical structure in silica-filled SBR compounds. Adapted from reference [146].

other groups formed into imperfect graphitic layers [59, 147]. These functional groups make reactions with rubber molecules possible. Silica, having a similar surface area and structure, exhibits lower rubber–filler interaction due to the absence of non-polar groups on the filler surface. It forms a filler network due to its tendency to agglomerate by hydrogen bonding aided by the silanol groups present on the filler surface, which also cause moisture adsorption. Silica fillers have a non-permanent structure of these agglomerates that can be destroyed by energy-intensive compounding to improve dispersion. The strain energy (product of stress and strain) associated with this is in the range of 2–4 kJ/m³ for both, silica and carbon black [148].

To overcome the flocculation and develop polymer–filler interactions, silica is treated with silane coupling agents like bis(triethoxysilylpropyl)disulfide (TESPD) before mixing with rubber. The *silanization* process adequately couples a silica surface with a silane agent and markedly improves the silica performance by lowering filler–filler interactions and making it available for reaction with rubber chains [69].

Hydrodynamic effect

The hydrodynamic effect refers to the transfer of strain to polymer chains by inextensible particles such as fillers. An increase in the polymer viscosity due to fillers is a common observation during processing. Einstein [149, 150] derived an equation to describe the increase in shear viscosity (η) of a dilute suspension containing rigid, spherical, disperse inclusions in an incompressible matrix:

$$\eta = \eta_0(1 + 2.5\phi) \quad (3.33)$$

where, η_0 is the viscosity of a gum (unfilled) system. The equation is suitable for the volume fraction of inclusions (ϕ) of up to 0.03. Later, Smallwood [151] obtained a

similar equation to account for the increase in shear modulus (G) of rubber due to fillers as:

$$G = G_0(1 + 2.5\phi) \quad (3.34)$$

Here, G_0 is the modulus of an incompressible rubber matrix. In its form presented here, G is independent of the size of the filler particles and the equation is suitable for small deformations. At larger volume fractions of the filler, particle–particle interactions become relevant and hence cannot be ignored. To account for this, the quantity in the brackets in Equations 3.33 and 3.34 get a quadratic term in ϕ in the form:

$$f = 1 + 2.5\phi + b\phi^2 \quad (3.35)$$

where, f is the *hydrodynamic amplification factor* and is a ratio of G to G_0 or η to η_0 [152, 153]. The above equations are suited for spherical particles only. For non-spherical particles, the equations need to be modified such as the one proposed by White and Crowder [154]. Further, the inclusion of fillers that lead to strong rubber–filler interactions (see next section) requires modifying ϕ to an effective volume fraction, ϕ_{eff} .

Guth [155] presented a theory for the quadratic term of the above series expansion to address concentrated systems and inter-particle disturbances therein, thus modifying f in the equations above. A common value of $b = 14.1$ was devised for both, modulus and viscosity equations. The corresponding equations came to be known as the Guth–Gold equations (the relevant paper was already published in 1938 by Guth and O. Gold). Despite their popularity, the quadratic terms are found to be inconsistent in accurately including the effects of fillers. It has been acknowledged that the value of b depends on factors like the type of matrix (fluid or solid) and on the deformation [153]. Values of about 7.6 [156] for elongational flow and 6.2 for the shear flow of Newtonian fluid, and about 5.0 [156, 157] for shear deformation of an elastic solid have been calculated.

A reformed approach to the hydrodynamic contribution of the fillers to viscosity has been presented by Domurath *et al.* [158], where the hydrodynamic amplification factor has been broken down into components relating to strain amplification and stress amplification.

Rubber–filler interaction

For active (\implies reinforcing) fillers, the volume fraction consideration loses its dependence and is hence modified to an effective volume fraction, ϕ_{eff} [51, 159]. These fillers

are those having a particle size between 10 and 40 nm, which corresponds to a surface area between 250 and 125 m²/g, respectively. In such fillers, the interstices within the aggregates act as sites for rubber to get occluded. Hence, the *occluded rubber* is not deformed and thus leads to a significant increase in the hydrodynamic effect. However, it should be noted that the conformational freedom of the occluded rubber is not lost. The extent of rubber–filler interaction can be roughly understood by measuring the *bound rubber* content of an unvulcanized rubber. This method involves measuring the amount of rubber that is not extracted by a good solvent. Thus, this is a measure of the amount of polymer chains adsorbed on a filler surface and correlates with the occluded rubber. It has been noted that high molecular weight polymers bind preferentially, thus causing a reduction in the molecular weight of free rubber [69, 160]. Carbon black yields a higher amount of bound rubber than silica due to chemisorption and sometimes chemical bonding, in addition to physical interactions.

The thickness of the adsorbed polymer layer has been classified based on the magnitude of constraints developed due to adsorption. A thin layer of tightly bound rubber, wherein chains are immobilized on the filler surface, is measured to be between 0.4 and 1.3 nm and functions effectively like an aggregate [51]. Determined by the surface area and the structure, the immobilized layer is associated with a somewhat higher T_g than that of the bulk. Another layer of rubber, called the loosely bound rubber, is connected to the filler through the immobilized rubber layer and shows the ability to deform. This has a thickness between 3 and 6.6 nm. This layer also forms the connection between the rubber–filler aggregates. The remaining region corresponds to the rubber that forms the majority of the bulk that can be extracted by suitable solvents.

The activity of any filler towards rubber can be understood by knowing its surface energy (γ_s) [51]. This is given as:

$$\gamma_s = \gamma_s^d + \gamma_s^p \quad (3.36)$$

where, γ_s^d and γ_s^p are the dispersive and polar components of the surface energy, respectively. Carbon blacks possess a low polar component and a relatively high dispersive component. This leads to strong rubber–filler and weak filler–filler interactions in carbon blacks. In silica fillers, the opposite is observed. The high polar component leads to dominant filler–filler interactions and weak rubber–silica interactions [64]. Hence, silanization is essential for good rubber–filler bonding in silica-filled systems.

3.4.2 The macroscopic observations

Payne effect

Beyond a critical volume fraction of the fillers (*percolation threshold*), depending on their type, the hydrodynamic prediction fails and the dynamic modulus increases abruptly. The filler forms a percolated network that lends a high modulus to the filled rubber system [161]. Upon deformation of the sample, the capability to store energy decreases as the filler network is destroyed, causing a substantial drop in the modulus already at small strain amplitudes (Figure 3.6). Removal of strain leads to restoration of the filler network. This strain-dependent disruption and restoration of the filler network are popularly known as the Payne effect [162, 163], but early observations were already made by Fletcher and Gent [164]. As shown in the comparison between carbon black and silica-filled compounds, silica demonstrates a higher loss in modulus due to the larger filler network. Thus, silanization acts as a means to reduce the tendency of the formation of a filler network to enhance dispersion.

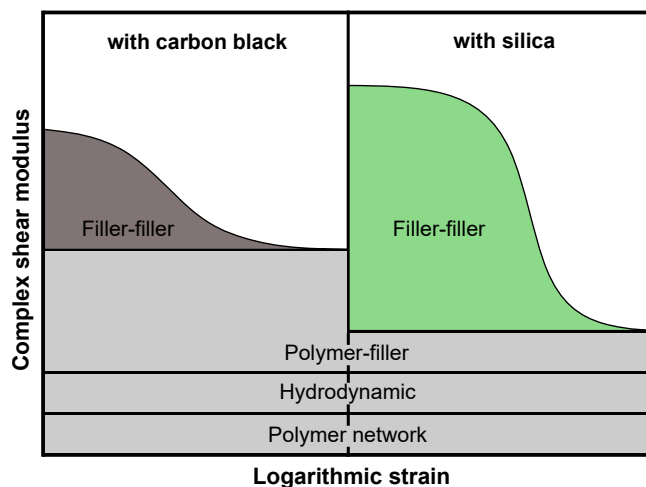


Figure 3.6: Effects contributing to the complex shear modulus. Adapted from reference [161].

The low-strain limit experiment also gives information on the extent of rubber–filler interactions, which is considerably higher in carbon black-filled systems due to the reasons discussed above. Considerable desorption and adsorption of chains on filler make polymer flow possible [51]. It is inferred that the dynamics of the rubber–filler mesophase approach an equilibrium of desorption–adsorption of polymer on the particle surfaces at a given temperature when the sample is at rest.

The next modulus classification is a consequence of the hydrodynamic effects of the fillers along with the occluded rubber argument for which an equation with the

effective volume fractions is suitable. The polymer network forms the softest fraction contributing to the modulus of the composite.

Mullins effect

The Mullins effect is a phenomenon observed in a quasi-static stress–strain experiment wherein the force required for stretching a rubber specimen is lowered in subsequent stretching to the same strain [48, 165, 166]. The instantaneous and irreversible viscoelastic softening achieves a steady state after a few loading–unloading cycles, while the majority of the softening occurs during the first stretch leading to a residual strain (*permanent set*). Nevertheless, a complete recovery of the strain is still possible at high temperatures. The phenomenon is observed in both, unfilled and filled elastomers. In the former, the effect occurs due to cavitation, disentanglement, chain scission, and change in the number of cross-links [167].

In the presence of fillers, the strain experienced by the rubber network is amplified, which causes an increase in hysteresis as the system departs sharply from an ideal network behavior [66]. The process is somewhat complex in filled systems: fracture of aggregates and agglomerates and breakdown of the filler network, and modification of the polymer–filler interface due to desorption/adsorption of polymer chains, molecule slippages, and breakage of bonds at the surface of the filler [167]. The stretching is also detrimental to the overall mechanical properties since the changes are permanent.

3.5 Semi-crystalline thermoplastics

Thermoplastics are a class of polymers that flow upon heating beyond their softening temperature and solidify upon approaching their T_g . They consist of the amorphous and the semi-crystalline polymers and have a T_g that ranges from near-room temperature up to in excess of 200 °C (except some polyolefinic polymers that have a T_g below 0 °C). Thermoplastics, especially semi-crystalline, can complement elastomers to act as reinforcement due to their relative stiffness at service temperatures.

Crystallinity is a virtue of stereo-regular or symmetrical polymers that can undergo three-dimensional long-range ordering. Their crystallizability further depends on the chemical nature of the polymer, and molecular weight and distribution of the molecular weight. Unless grown as single crystals, all crystallizable technical polymers are semi-crystalline.

In addition to the glass transition temperature of the purely-amorphous polymers, semi-crystalline polymers also possess a melting temperature (T_m) of the crystalline

regions (or *crystallites*) and an associated crystallization temperature (T_c). Factors such as ease of molecular packing, and the presence of hydrogen bonding and polarity affect the melting temperature.

Crystallization is a first-order phase transition, which demonstrates sudden volume change due to the change of state of the polymer, while glass transition is characterized by a gradual volume change due to softening of the polymer and constitutes a second-order phase transition. Crystallization in polymers occurs by various mechanisms: solidification through cooling from the melt, separation from solution, by stretching, and due to confinement. Among these, the crystallization of polymer melt by cooling is important on a larger scale as it influences articles formed by various polymer processing techniques. Upon cooling a polymer melt from its state of disorder of interpenetrating random coils, *nuclei* (sites for crystal growth) are formed by aggregation of volume elements of chain segments induced by molecular fluctuations (*homogeneous nucleation*) or by impurities present in the system (*heterogeneous nucleation*). Chain segments from the melt diffuse onto these nuclei to form ordered crystalline regions. This process is associated with a decrease in the free energy, which further drives the diffusion of more chain segments into the crystallite [168].

With further cooling of the melt, the diffusion reduces due to an increase in viscosity. As the T_c approaches, the viscosity becomes extremely high, which significantly restricts chain diffusion. Kinetically, with cooling, the *rate of crystallization* increases, passes a maximum and decreases as the process becomes diffusion controlled. As a consequence of the decrease in molecular mobility, some chains are part of the ordered regions while others are still in the disordered phase.

Chain entanglements are one of the factors that affect the free diffusion of the chain during crystallization. Due to a build-up of stress in segments strained between a region of entanglement and a growing crystallite, an opposite work is necessary to overcome the lowering of free energy. Strong entanglements would hence demand a higher work, which would disfavor crystallization [169]. Another scenario where crystallization is limited is when one or more crystallites grow by simultaneous diffusion of segments from regions that are part of the same chain but far from each other. Like in the previous case, chain segments lying between those diffusing into the crystallites get strained and inhibit diffusion. The result is a chain composed of some regions that have crystallized while others remain disordered.

During crystallization, the alignment of chain segments requires extra free energy, which leads to *supercooling* to variable extents. As a consequence, $T_c < T_m$ by up to a few tens of Kelvin [130]. The ordering associated with crystallization occurs by the formation of *lamellae* that have a thickness of about 10 nm. This transpires by

the folding of chain segments onto themselves into closely packed ordered structures. The lamellae, interspersed by amorphous regions, further proceed to grow radially into superstructures called *spherulites*, which can be as big as a few hundred micrometers.

Further details on the process of formation of crystallites are skipped from this discourse, and readers are invited to refer to the texts cited in this section. At this point, it suffices to state that crystallization causes various changes in the properties of the thermoplastic polymer. The basic distinction comes from the crystalline regions having a relatively higher density in comparison to the amorphous regions. From a macroscopic standpoint, crystallization improves mechanical and thermal resistance. It also improves the impermeability of polymers to liquids and gases. The optical properties can also be tweaked by the use of nucleating agents. In blends of rubber and a semi-crystalline thermoplastic, the phase-separated crystallites can act as load-bearing elements that distribute energy into the softer phase.

4. NMR Spectroscopy

This section on NMR spectroscopy is mainly adapted from the books of Friebolin [170], Keeler [171], Duer [112], Apperley [113], and Levitt [172]. Other sources are cited at their occurrences.

4.1 The NMR experiment

The nuclear angular momentum (L) is an intrinsic property that most nuclei possess and is quantized as:

$$L = \sqrt{I(I+1)}\hbar \quad (4.1)$$

I is known as the angular momentum quantum number or the nuclear *spin*. It takes values of 0, 1/2, 1, 3/2, 2,...6. The most widely studied nuclei (^1H and ^{13}C) have an I value of 1/2. \hbar is the reduced Planck's constant (h) where $\hbar = h/2\pi$. The angular momentum is proportional to its magnetic moment μ through the magnetogyric ratio γ .

$$\vec{\mu} = \gamma\vec{L} \quad (4.2)$$

The magnetogyric ratio is nuclide specific and dictates its sensitivity to detection by NMR, where nuclides with a larger γ are easily observed by NMR. A consequence of the two equations above is that nuclides whose spin is 0 cannot be detected by NMR. These include ^{12}C and ^{16}O , a couple of the most abundant organic elements.

In the presence of a static magnetic field (\vec{B}_0) the z -component of \vec{L} , L_z , in the direction of the magnetic field is quantized, such that:

$$L_z = m\hbar \quad (4.3)$$

The interaction a nuclear spin has with the external magnetic field is known as the *Zeeman* interaction. The directional or magnetic quantum number, m , permits $2I+1$ number of orientations of \vec{L} and $\vec{\mu}$, where m ranges from $-I, I+1, \dots, I-1, I$. A spin-1/2 nucleus can thus have only two orientations corresponding to $m = +1/2$ and $m = -1/2$. Combining Equations 4.2 and 4.3, we get:

$$\mu_z = \gamma m\hbar \quad (4.4)$$

The energy associated with these orientations can be determined by the equation:

$$E = -\gamma m \hbar B_0 \quad (4.5)$$

A spin is in the lower energy (E_α) state when $m = +1/2$. This is also known as the α state and is achieved when μ_z is, for example, parallel to the external magnetic field (assuming $\gamma > 0$). The higher energy (E_β) state, known as the β state, occurs under the condition of $m = -1/2$, with μ_z being anti-parallel to B_0 . The distribution of spins in either energy level follows the Boltzmann statistics. Due to a very small difference in energies between the two states, the populations on both levels are similar, with only a slight excess in the α state.

In reality, the moments do not demonstrate a perfect alignment along the field axis (z -direction), but a distribution of preferential alignments. This is due to the random thermal motions of molecules, which are much larger than the interaction energy of a nuclear magnetic moment with B_0 . Nevertheless, a complete cancellation of moments is prevented as the system marginally favors the lower energy state. This results in the build-up of a net magnetization (\vec{M} , equivalent to the bulk magnetic moment), and is thus a vectorial sum of the individual moments:

$$\vec{M} = \sum_i \vec{\mu}_{z,i} \quad (4.6)$$

where, i represents the i^{th} nuclei. The magnetization, once fully attained, is time-invariant. In an NMR experiment, a radio frequency (RF) pulse from the transverse (x - y) plane tips this magnetization vector away from the z -axis by an angle β . The magnetization then precesses about \vec{B}_0 at this *flip* angle. The frequency associated with the precession is called the *Larmor* frequency (ω_0):

$$\omega_0 = -\gamma B_0 \quad (4.7)$$

The Larmor frequency attains a precessional direction that is dependent on the sign of the magnetogyric ratio of a spin. An RF pulse, although weaker compared to the static magnetic field, oscillating at or near the Larmor frequency (\implies resonance condition) has the ability to tip the magnetization towards the transverse plane where it can be detected. The oscillating magnetic field associated with an RF pulse is given by the time-dependent field B_1 and its frequency can be expressed in the same fashion as Equation 4.7.

4.2 Anisotropic spin interactions

The spins' interaction with the static magnetic field and the oscillating RF field constitute to magnetic fields *external* to the sample. There also exist magnetic fields *internal* to the sample that are created by spins of electrons or other nuclei. The interactions of a nucleus with these fields mainly depend on its chemical environment. These interactions also depend on the orientation of the molecule or the molecular segment with the external magnetic field and are hence, intrinsically *anisotropic* [173].

In liquids, these anisotropic interactions are averaged out by fast isotropic molecular tumbling, which leads to high-resolution spectra but also to a loss of information on structure and dynamics. In soft materials such as polymers, anisotropic interactions are only partially averaged due to restricted molecular motions. This results in line-broadening and thus a loss of resolution. In the following, such interactions affecting the spectral quality in polymers are briefly introduced. Indirect (J) coupling, which leads to the splitting of peaks but is overshadowed by dipole–dipole coupling, and quadrupolar coupling, which is irrelevant to the polymer materials considered in this thesis, are excluded from the discussion.

4.2.1 Chemical shift and anisotropy

The electrons present around a nucleus react with B_0 to produce a small local secondary field (B_{loc}) that reduces the total field experienced by the nucleus compared to a hypothetical 'bare' nucleus as $B_{loc} = \sigma B_0$. The interaction of the secondary field with the nucleus is called the *shielding interaction*. The interaction is anisotropic since electrons are not distributed spherically around a nucleus. This condition can be described by a shielding tensor (σ) for every site, which yields the orientation-dependent values for the local symmetry axis with respect to B_0 .

Shielding interaction can change the Larmor frequency of the nucleus and lead to a *chemical shift* (δ). In addition to the shielding offered by the electrons to the nucleus of an atom, other atoms in the vicinity exhibit similar fields towards the nucleus. The effective magnetic field experienced by a nucleus can be expressed as:

$$B_{eff} = B_0 - B_{loc} \quad (4.8)$$

The change in B_0 observed in the value of B_{eff} is, practically, very small. As a result, chemical shift is expressed in parts per million (ppm) and the shift is measured with respect to a reference frequency (ω_{ref}), which corresponds to a molecule exhibiting low chemical shift-inducing distortions:

$$\delta = \frac{\omega_{\text{sample}} - \omega_{\text{ref}}}{\omega_{\text{ref}}} \quad (4.9)$$

In a solution-state experiment, the chemical shifts obtained for the positions of the peaks represent the isotropic average value (σ_{iso}) of the principal values of σ . In the solid-state, chemical shift is an orientation-dependent quantity. The local bonding environment is the primary cause of the chemical shifts. Secondary sources include intermolecular packing and molecular conformation (due to rotation of bonds), thus making their chemical shifts distinct. Due to the large ensemble of orientations, superposition of the chemical shifts occurs leading to the broadening of the NMR line in the form of a *powder spectrum*. Such a spectrum can be described using anisotropy and asymmetry tensors along with the isotropic value for the breadth, shape, and position of the center of mass of the signals, respectively [173, 174]. A method to achieve the isotropic limit in solids for high-resolution NMR spectra is described in Section 4.4.3.

4.2.2 Dipole–dipole coupling

Dipole–dipole or dipolar coupling is a direct, through-space interaction between magnetic moments of different spins in the vicinity of each other, in addition to B_0 . The dipolar coupling constant, D_{ij} (expressed in frequency units), between two magnetic moments ($\vec{\mu}_i$ and $\vec{\mu}_j$), separated by an internuclear distance, r_{ij} , is given by:

$$D_{ij} = \frac{\mu_0}{4\pi} \cdot \frac{\gamma_i \gamma_j}{r_{ij}^3} \cdot \hbar \quad (4.10)$$

The coupling constitutes the dipolar tensor (\mathbf{D}) and is a multiple of $-1/2$, $-1/2$, and 1 for the respective diagonal elements of the tensor. The axially symmetric interaction between the dipole moments is reminiscent of two interacting bar magnets held at a fixed distance to their centers and have fixed orientations (of their principal axes). A change in the orientation of one magnet would change the potential energy of the other. For example, when a magnet is turned by 180° , it would cause a change in sign of the potential energy of the other magnet. The orientation dependence of the dipolar coupling is described by the second Legendre polynomial: $P_2(\cos\theta_{ij}) = 0.5(3\cos^2\theta_{ij} - 1)$, where θ_{ij} is the angle the internuclear axis makes with the magnetic field. It should be acknowledged here that this relation is zero when the angle is 54.74° .

Dipolar coupling is a source of significant broadening in NMR peaks of solids. A proton bonded to an aromatic carbon (*heteronuclear coupling*) has a coupling constant of about 24 kHz. It is on the order of 20–30 kHz between neighboring protons (*homonuclear coupling*) of organic solids [175]. In a static powder sample, the splitting

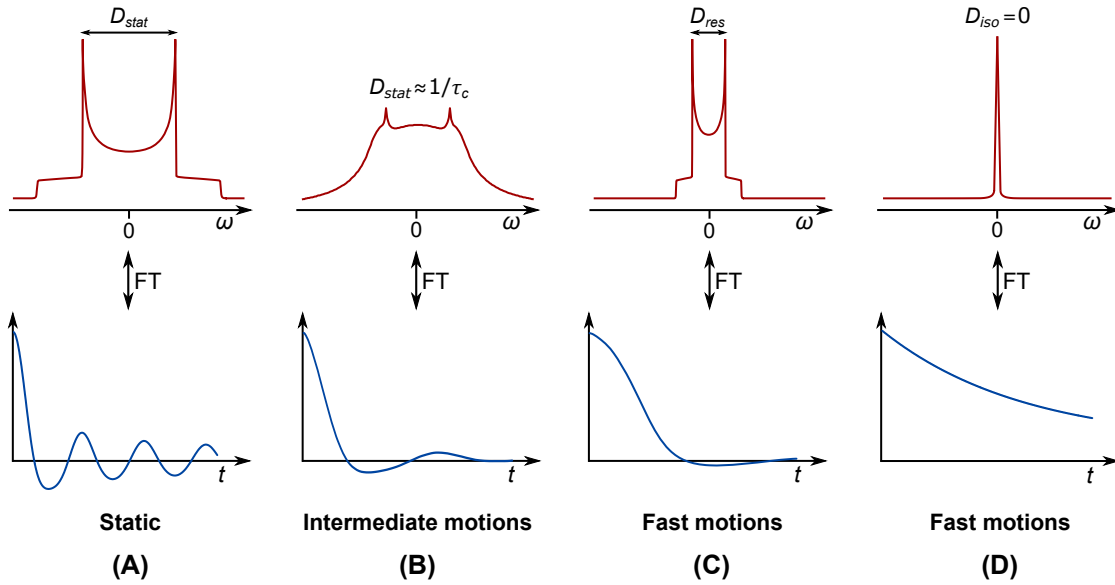


Figure 4.1: Effects of dynamic averaging on the spectral (top row) and the corresponding Fourier-transformed time-domain (bottom row) signals of an isolated spin pair. The width of the Pake doublet obtained in the static rigid limit (A) is equal to the strength of the dipolar coupling (D_{stat}). The spectrum undergoes shape transformation at the “NMR- T_g ” (see text) when the segmental correlation time is on the scale of $10\ \mu\text{s}$ (B). In the fast motional limit, anisotropic segmental motions due to constraints lead to the narrowing of the Pake to a width equal to the magnitude of the residual dipolar coupling, D_{res} (C). The dipolar coupling strength is zero when the segmental motions are isotropic (D).

due to orientation-dependence of an isolated pair of nuclear spins spanning all possible orientations is represented by a *Pake doublet* (Figure 4.1A, top row) [113]. The distance between the two horns of the spectrum is the static dipolar coupling constant (D_{stat}), from which the internuclear distance can be calculated. Such a spectrum and its corresponding time-domain signal (bottom row) can be approximated using a Gaussian distribution in a second-moment approximation [176]. While a Pake pattern is obtained for isolated spins, the presence of multiple spins in polymers causes splittings that lead to a broad and featureless, near-Gaussian line in the rigid limit. The decay intensity of the time-domain signal is defined by a time constant called the *spin-spin relaxation time* T_2 (see Section 4.3), which is shorter for strongly coupled spins and longer for weakly coupled spins.

Dynamic averaging changes the shape of the Pake and leads to its narrowing. At a temperature of 30–50 K above the T_g , called the “NMR- T_g ” [177], the segmental motions for typical polymeric (fragile) glass formers have a correlation time (τ_c) in the range of inverse D_{stat} ($\implies \approx 10\ \mu\text{s}$). In this intermediate motional limit, the Pake doublet is rather unresolved and lacks its typical features (Figure 4.1B). C and D in

Figure 4.1 represent the limit of fast motions. Here, two scenarios are possible: in the first situation (C), the width of the Pake spectrum decreases to a finite value. This width originates from molecular fractions that cannot undergo complete motional averaging and thus lead to the *residual dipolar coupling*, D_{res} (see Section 4.4.1). The other possibility (D) is associated with an isotropic value of the dipolar coupling ($D_{iso} = 0$) due to complete averaging by molecular tumbling, which gives an exponential decay of the time-domain signal. This is typically observed in solvents, despite dipolar coupling being the primary cause of relaxation.

The direct dependence of the magnitude of the coupling constant on the internuclear distance makes the measurement of dipolar interaction for geometrical and structural analysis of molecules in solid-state NMR possible.

4.3 Distinction of polymer fractions based on spin–spin relaxation

Relaxations of nuclei are central to an NMR experiment. They describe the molecular processes in a system. In materials with slowly moving molecules, and due to particular spin interactions (Section 4.2), line broadening occurs. The relaxation time T_2 accounts for the processes that lead to the loss of coherence. This is characterized by a decay of the magnetization (M_{xy}), caused by the dephasing of spins, perpendicular to the magnetic field in the transverse (x - y) plane, hence also known as *transverse relaxation*. It is affected by both slow and high-frequency processes. The width ($\Delta\omega_{1/2}$) of a spectral line at half-maximum intensity is related to T_2 by the equation:

$$\Delta\omega_{1/2} = 2/T_2 \quad (4.11)$$

The above equation describes the spectral line-width in a homogeneous field. The time-domain decay signal is mainly dominated by dipolar dephasing and the corresponding T_2 is inversely proportional to D_{res} . Thus, the decay time depends on the mobility of the molecules in the material. For example, uncross-linked rubber has a longer T_2 , whereas cross-linked rubber has a shorter T_2 . The T_2 also varies with the extent of cross-linking, or with the presence of crystallites or filler. A distinction of different fractions having unique T_2 within the same material is also possible.

For dominating (quasi-) static dipolar couplings, the decay signal has a Gaussian form that is $\sim \exp(-\frac{1}{2}M_2t^2)$, where $M_2 = \frac{9}{20}D^2$ is the second moment and D can assume the quantity D_{ref} or D_{res} (see Section 4.4.1). In the following subsections,

experiments to measure T_2 for the distinction of their respective fractions in a polymer are discussed.

4.3.1 Single-pulse free induction decay (FID)

An RF pulse with a flip angle of 90° from the x -axis flips the magnetization M_z from the z -axis to the transverse y -axis. Since the irradiation and detection are done by a coil in the transverse plane, the strength of the observed signal is determined by the magnitude of M_{xy} . This *free induction signal* is cosine in nature and precesses freely in the transverse plane until transverse relaxation occurs. Relaxation causes *decay* of the free induction signal as the magnetization regains its equilibrium position along z . This situation is described in Figure 4.2. In actuality, an FID signal is a superposition of cosine signals of all (interacting) nuclei present in the sample, each possibly oscillating at a different Larmor frequency. This means that the sum signal often decays non-exponentially, see below.

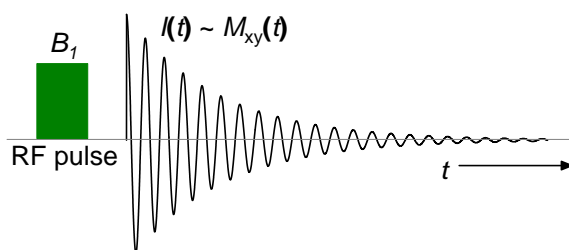


Figure 4.2: Free induction decay of the magnetization (M_{xy}) composed of non-interacting spins after a 90° RF pulse associated with a field B_1 , as observed in the lab frame. The decay is exponential, caused by transverse relaxation with the time constant T_2 .

Measuring the free induction decay signal following a single 90° pulse is the simplest of all NMR experiments. It is purely exponential for a single spin species in the presence of a perfectly homogeneous field and is characterized by T_2 . In reality, field inhomogeneity causes individual spins in different regions to go out of phase with each other faster. This results in a shorter, *apparent* (or *effective*) T_2 denoted as T_2^* (or T_2^{eff}). In solids, topological constraints to molecular motions lead to a fast decay of the free induction signal. In the rigid coupling limit, the T_2 is as low as $20 \mu\text{s}$ with a spectral line-width exceeding the condition given in Equation 4.11.

4.3.2 Spin-echo

The spin-echo pulse sequence is one of the many sequences that are used for overcoming the problem of B_0 inhomogeneity. Developed by Erwin Hahn [178], it is also commonly

referred to as Hahn-echo. It features a $90^\circ - \tau - 180^\circ - \tau$ pulse block with two incremental spin evolution delays (τ) before the read-out in the form of an *echo*.

In addition to the inhomogeneity of the field, resonance offsets, and chemical shift dispersion lead to the dephasing of the spin moments. With the flip angle of 180° , this distribution in frequencies is refocussed as a time-reversed echo, which forms at the end of the second τ . In successive experiments, the two delays are increased equally and the corresponding echo intensities are measured. The echo intensities decrease with every increment in delay time due to transverse relaxation and decay completely at sufficiently long delays. Thus, relaxations of fractions associated with different mobilities can be obtained.

4.3.3 Pulsed magic-sandwich echo (MSE)

Signals originating from crystallites of semi-crystalline polymers, highly crosslinked fractions of networks, or chains adsorbed on filler surfaces decay within 20 μs due to fast relaxation of the strongly dipolar-coupled spins. Due to an unavoidable delay between RF irradiation and signal acquisition by the coil called the *receiver dead time*, which can be as long as 12 μs in low-field spectrometers, the material-relevant information contained within this duration is lost from an FID signal. Pulsed magic-sandwich echo (MSE)-FID experiment [177] compensates for this loss in an FID signal by performing a time reversal of spin interactions, just like the Hahn-echo experiment [179, 180] but here adapted to dipolar couplings, which are not affected by a 180° pulse. Apart from resonance offsets and magnetic field inhomogeneities, it especially refocuses multi-spin dipolar couplings, which are the primary reasons for the short-time decay. In samples with regions of different molecular mobility, it is used as a dipolar filter with long echo times.

At the NMR- T_g , intermediate motions in the microsecond range cause changes in the strength of dipolar interactions that lead to a minimum in the MSE efficiency prefactor ($A_0^{MSE-FID}/A_0^{FID}$) by hindering full refocussing of the signal [175]. At temperatures higher than the NMR- T_g , molecular rearrangements can lead to a secondary minimum of the efficiency prefactor. Losses also occur at temperatures below the NMR- T_g , where dipolar interactions larger than the inverse pulse length dominate.

4.3.4 Distinction of polymer fractions

The various fractions in a polymer material exhibit specific T_2 times that describe their molecular motions. By combining the FID and Hahn-echo, the entire spectrum

of signal decay can be analyzed [181]. MSE-FID signal is plotted along with the FID and Hahn-echo to assess the amount of rigid components and to stabilize the fit within the short time window. Illustrations of this approach are shown in Chapters 5 and 7. The plots also emphasize the consequence of the presence of a long dead time.

The intensity (I) data can be fitted using a modified multi-exponential decay function as shown in the following equation:

$$I = \sum_{i=1}^n f_i \exp(-(t/T_{2,i}^*)^{\beta_i}) \quad (4.12)$$

where, f_i corresponds to the amount of any fraction, and $T_{2,i}^*$ and β_i are the corresponding apparent relaxation time and shape factor. The subscript i usually ranges from 2 to 4. A shape factor of 2 describes a Gaussian decay and indicates the presence of highly constrained molecular segments (dominating dipolar coupling), while a stretched exponential (β lower than 1) arises due to a distribution of relaxation times caused by inhomogeneous mobilities. This aspect is demonstrated by several examples in the following chapters.

4.4 Measurement of cross-link density by NMR

4.4.1 Connecting polymer chain dynamics and NMR observables

Cross-linked and/or entangled chains induce a semi-local anisotropy by hindering fast segmental motions such as Rouse modes and bring about long-lived orientation correlations and thus residual dipolar couplings whose magnitude depends on the cross-link density, the entanglement length, or the tube diameter [176]. Parameters like terminal relaxation time or the disengagement time of the tube/reptation model are related to the lifetime of these correlations.

As established earlier, dipolar interactions between nuclei are described by the second Legendre polynomial. A connection of this orientation dependence to the segmental dynamics of a polymer chain can be made through the angle θ the chain end-to-end vector makes with the magnetic field (B_0) and by introducing an NMR *submolecule* [176, 182, 183], which is described by a Kuhn chain segment of length l_K (Figure 4.3).

At temperatures far above the T_g , the traverse of a segment-based effective dipolar tensor (D_{ref}), encompassing local and fast intra-segmental motions, reflects the segmental dynamics. D_{ref} ($= D_{stat}/k$, where k is a constant) is a polymer-specific

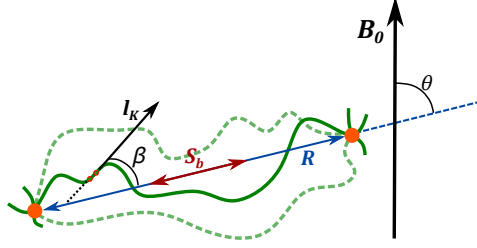


Figure 4.3: Orientation dependence of a polymer chain composed of Kuhn segments held between cross-links. The various conformations of the segments can be described by the second Legendre polynomial and its value is encoded in the order tensor (with the norm termed order parameter S_b), which lies parallel to the chain end-to-end vector. Adapted from references [175, 184].

and model-dependent quantity [185, 186], which can be considered to be along the polymer backbone and thus, reports on the backbone orientation fluctuations with a time-dependence, $\beta(t)$. Due to constraints such as cross-links, the tensorial NMR interactions are incompletely averaged by anisotropic segmental motions, thus resulting in *residual* quantities of the dipolar coupling (D_{res}). These quantities are related to the segmental dynamic order parameter (S_b) as:

$$S_b = \frac{D_{res}}{D_{ref}} = \frac{M_{2,res}}{M_{2,ref}} = \frac{1}{2} [3\langle \cos^2(\beta) \rangle - 1] = \frac{3}{5} \left(\frac{l_K R}{R_0^2} \right)^2 = \frac{3}{5N_K} \propto \frac{1}{M_c} \quad (4.13)$$

where, $\langle \dots \rangle$ and $[\dots]$ are the ensemble averages of conformation and segmental structure, respectively. R and R_0 are the instantaneous and unperturbed chain end-to-end distances, where the vector \vec{R} makes an angle θ with respect to B_0 . The ratio of the end-to-end distances for a bulk sample simplifies to the number of Kuhn segments between the cross-links (N_K) and is proportional to the molecular weight between the cross-links (M_c). The multi-pair couplings lead to all the protons in a monomer having the same D_{ref} value due to fast intra-segmental motions far above the T_g .

In soft materials like polymers, the residual interactions are lower due to the significant motional averaging by fast anisotropic dynamics. The dipolar interaction frequency of a segment is thus given by:

$$\omega_D(\beta) = \frac{3}{2} D_{ref} S_b P_2[\cos\theta] \quad (4.14)$$

The significance of cross-links and their impact on S_b can be appreciated in Figure 4.4, where an orientation autocorrelation function ($C(t)$) has been used to measure the probability of a chain segment that assumes the same orientation between times t_a and t_b . The correlation function thus describes the fluctuations in the orientation of the segments and is given by:

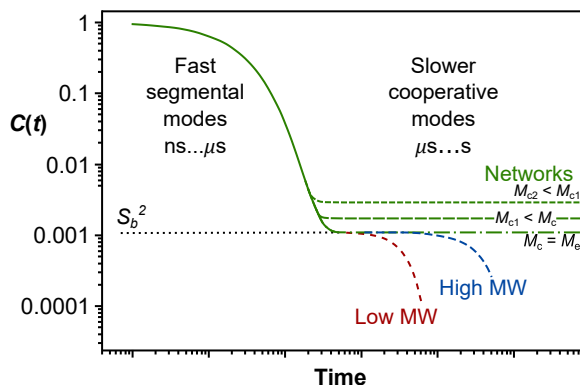


Figure 4.4: Schematic representation of the orientation autocorrelation function, $C(t)$, for entangled melt and elastomer chain segments far above T_g . Adapted from reference [174].

$$C(t) = C|t_a - t_b| = \langle P_2(\cos\theta_{t_a})P_2(\cos\theta_{t_b}) \rangle \quad (4.15)$$

Fast segmental motions such as Rouse modes contribute to the initial decay. Thereafter, a plateau is reached due to contributions from entanglements and cross-links. A further drop in the correlation times is observed for entangled polymers caused by reptation. Polymers with a higher molecular weight exhibit slow reptation and hence longer correlation times. In the presence of cross-links, the plateau is affected only marginally at longer correlation times due to slow motions. The height of the plateau (S_b^2) gives a measure of the magnitude of constraints, which increases as M_c gets shorter with respect to the entanglement molecular weight, M_e .

4.4.2 Proton multiple-quantum NMR spectroscopy

The coupling constant between two or more coupled spins can be measured through multiple-quantum (MQ) experiments, whereby excitations of higher-order coherences occur through which the presence of dipolar couplings can be probed quantitatively. An MQ pulse sequence that has achieved tremendous growth in the past two decades is based on the pulse sequence of Baum and Pines [125], which overcomes the limitations of T_2 -based experiments such as Hahn-echo and CPMG, also used for determining D_{res} [187]. Based on a pure DQ Hamiltonian, the pulse sequence excites all even quantum coherences, mostly double-quantum (DQ) as well as zero-quantum (ZQ) coherence that can be selected by use of phase cycling. The pulse sequence employing different phase cycles records two signals, viz., a DQ build-up signal (I_{DQ}) and a reference signal with decaying intensity (I_{ref}), as a function of the sequence duration, τ_{DQ} (Figure 4.5).

At short evolution times, the build-up is dominated by DQ coherences and reflects on the strongest residual couplings in the small subsystems of spins in the monomer

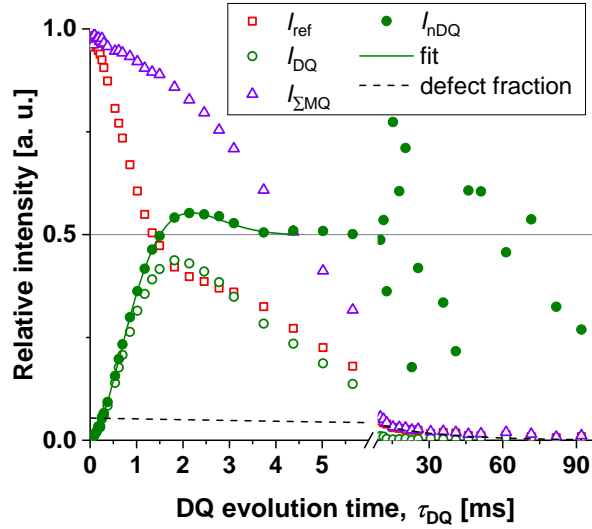


Figure 4.5: Representation of the various signals measured by and derived from the multiple-quantum (MQ) experiment discussed here. The I_{nDQ} signal is derived by subtracting the defects from the sum signal ($I_{\Sigma MQ}$) of the reference I_{ref} and double-quantum I_{DQ} signals. The normalized build-up curve is fitted using Equation 4.16.

units that dominate the signal intensity [188]. This makes extraction of very specific localized information of the polymer system possible. I_{ref} complements I_{DQ} wherein it contains all magnetization that has not evolved into DQ. For the quantum-mechanical background [188], and detailed discussions of the basic principles [176] and phase cycle [189] of the pulse sequence, readers are requested to refer to the cited literature. Further, a modified pulse sequence that uses a T_2 filter based on Magic And Polarization Echo (MAPE) for suppressing signals from crystal and crystal–amorphous interfaces in rubber/plastic blends has been published by Papon *et al.* [177]. Discussion pertaining to data interpretation will follow.

The intensity decay in both these signals, arising from relaxation effects (T_2 , T_1 , and $T_{1\rho}$), is found to be almost identical in networks (but not in reptating melts). This enables the removal of these molecular motions-related contributions by point-by-point division of the I_{DQ} intensity by the sum intensity, $I_{\Sigma MQ}$ ($= I_{DQ} + I_{ref}$). A further correction is necessary to account for the defects. In most cases, this is a single exponential decay that is subtracted from $I_{\Sigma MQ}$. Thus, the normalized DQ intensity, (I_{nDQ}) is a signal that approaches the 0.5 intensity limit due to equal distribution of excited coherences into all even quantum orders [125]. This procedure makes the data temperature-independent over a wide range [176, 188] and reports only on the network structure.

The structural information can be obtained by fitting the I_{nDQ} curve using a numerical integral that assumes a log-normal distribution of couplings, $\ln(D_{res})$:

$$I_{\text{nDQ}}(\tau_{\text{DQ}}) = \int P(\ln(D_{\text{res}})) I_{\text{nDQ}}(\tau_{\text{DQ}}, D_{\text{res}}) d\ln(D_{\text{res}}) \quad (4.16)$$

It is composed of two entities, one of which is an Abragam-like kernel function, which is suitable to describe, both, homogeneous and heterogeneous spin systems [190]:

$$I_{\text{nDQ}}(\tau_{\text{DQ}}, D_{\text{res}}) = 0.5[1 - \exp\{-(0.378\epsilon D_{\text{res}}\tau_{\text{DQ}})^{1.5}\} \times \cos(0.583\epsilon D_{\text{res}}\tau_{\text{DQ}})] \quad (4.17)$$

The efficiency factor, ϵ , takes a value of unity for the static Baum–Pines experiment. The other component of the integral is the *a priori* log–Gaussian distribution function to describe the distribution of couplings in the sample volume:

$$P(\ln(D_{\text{res}})) = \frac{1}{\sigma_{\ln}\sqrt{2\pi}} \exp\left[-\frac{\{\ln(D_{\text{res}}) - \ln(D_{\text{med}})\}^2}{2\sigma_{\ln}^2}\right] \quad (4.18)$$

In the case of a network having two distinct phases, such as in an elastomer blend, the fitting function can be accommodated to account for the two components in a bimodal fitting function. This has been demonstrated in the publications pertaining to this thesis.

4.4.3 Enhancement of spectral resolution for phase-resolved measurements

The second Legendre polynomial describes the orientation-dependence of internal NMR interactions. The value of the dipolar interaction is zero when the motion is isotropic (\implies complete averaging). The naturally occurring line broadening in solid samples can be removed by inducing such isotropic motions of chain segments by physically rotating the sample at a defined angle to B_0 , as demonstrated separately by Andrew and Lowe in the late 1950s [191, 192]. In an experiment known as magic-angle spinning (MAS) NMR spectroscopy, a ceramic rotor containing the sample is pneumatically spun rapidly at an angle of 54.74° , called the *magic angle*, to the static magnetic field. The anisotropic interactions are thus spatially averaged to zero to yield narrow, resolved resonance peaks. Thus, the approach is handy for picking resonance peaks in complicated polymeric systems like blends and copolymers. It must be noted that high spinning frequencies are necessary to average out proton–proton dipolar interactions in rigid organic solids. For achieving fully narrowed signals, the spinning rate must be significantly greater than the line-width from a static experiment (sidebands [112] are still broad in rigid ^1H solids!).

Figure 4.6 schematically shows the narrowing of NMR peaks upon spinning a sample

in a rotor at a sufficiently high frequency. For soft polymers like rubbers, however, one should exercise caution with the spinning rates, as very high spinning rates are not necessary and can deform the sample.

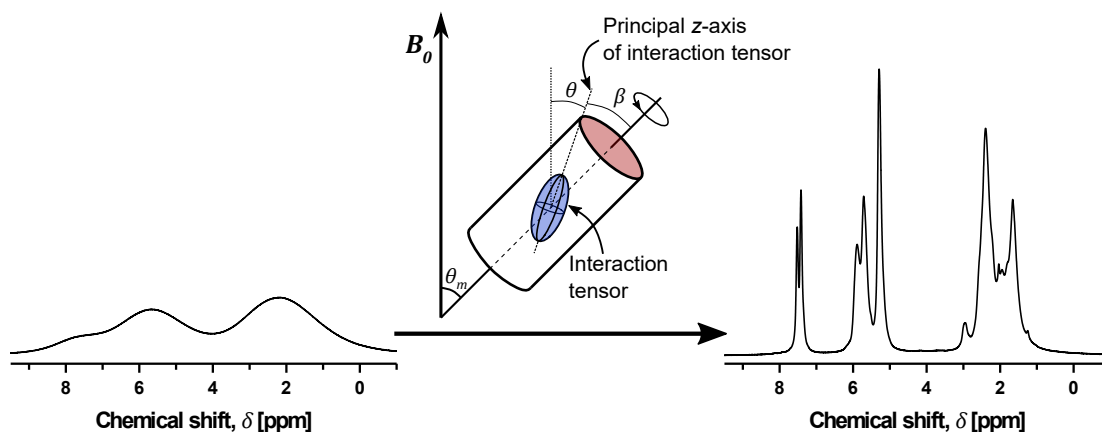


Figure 4.6: Relative intensities from a 90° -pulse experiment of a sulfur-cross-linked SBR measured in a static mode (left) and the resolved characteristic peaks obtained through magic-angle spinning at 10 kHz (right), both measured at 80°C . The image in the center (adapted from reference [112]) is a schematic representation of a MAS experiment (see text for details).

The descriptions of the angles in Figure 4.6 and their relationship are given in the following equation:

$$\left\langle \frac{1}{2}(3 \cos^2 \theta - 1) \right\rangle = \frac{1}{2}(3 \cos^2 \theta_m - 1) \times \frac{1}{2}(3 \cos^2 \beta - 1) \quad (4.19)$$

The angle between the spinning axis and a molecular direction is represented by β , and is fixed for a given nucleus. Depending upon the interaction in consideration, the latter can be regarded as the principal z -axis of a shielding tensor or the internuclear vector (and also the distance) of a dipolar interaction. For rubbers and polycrystalline samples, β takes all possible angles, as does θ . When the angle between B_0 and the spinning axis (θ_m) is 54.74° , the quantity in the corresponding bracket is zero, and thus the value of the quantity on the left-hand side of the equation is also zero when averaging θ by fast spinning takes place.

However, the high resolution comes at a cost; with the anisotropic broadening, MAS also suppresses dipole–dipole coupling information [193]. By a *dipolar recoupling* approach, dipolar information can be coherently and selectively reintroduced by the application of a carefully chosen sequence of RF pulses. The phase-resolved studies in this work are based on a homonuclear DQ recoupling pulse sequence known as the BaBa-xy16 [124].

The 2D pulse sequence is based on a popular Back-to-Back (BaBa) pulse sequence developed by Feike *et al.* [194], and uses xy16 phase cycling providing increment in DQ build-up points as low as 1 rotor period, τ_R (one data point for every rotation of the rotor). The experiment produces the same two sets of signals: I_{DQ} and I_{ref} , and conveniently demands the same data processing rigor of signal normalization, as demanded by the Baum–Pines pulse sequence. In relation to the Baum–Pines pulse sequence, BaBa–xy16 has a 78% efficiency. Thus ϵ is reduced to 0.78 in the kernel function in Equation 4.17. Although the Baum–Pines pulse sequence is a robust tool, as established by its usage in understanding different polymer material systems, it is not designed to be used in conjunction with MAS. Hence, the chemically-resolved studies presented in the following chapters use BaBa–xy16 pulse sequence.

5. NMR Studies on the Phase-Resolved Evolution of Cross-Link Densities in Thermo-Oxidatively Aged Elastomer Blends¹

Differences in cross-link densities within the phases of a rubber/rubber blend can arise due to their inherent chemical nature and their reactivity towards cross-linker such as sulfur. Factors such as polymer ratio, processing conditions, and morphology further influence polymer–cross-linker reactivity, leading to blends having phases that have cross-linked to various degrees. When such unequally cured phases are present, exposure of the material to high temperatures can exacerbate the cure properties due to oxidation reactions. Due to the lack of quantitative methods to detect these differences and changes in cross-link densities within the individual phases, a complete understanding of blend behavior is still missing.

In this paper, MAS NMR spectroscopy-based pulse sequence [124] is successfully used to differentiate the cross-link densities in the phases of an NR/SBR blend. The unique evolution of cross-link densities in the NR and SBR phases of the blend due to thermo-oxidative aging at 80 °C up to a duration of about 1000 h is also measured. The study is supplemented by results from a low-field NMR experiment for cross-link density measurement and by T_2 -distinguished polymer fractions.

Contributor Roles Taxonomy (CRediT) author statement²

Akshay Karekar: Conceptualization, methodology, validation, formal analysis, investigation, data curation, writing – original draft, visualization, project administration.

Katja Oßwald: Conceptualization, methodology, validation, resources, writing – review & editing, supervision.

Katrin Reincke: Conceptualization, methodology, validation, resources, writing – review & editing, supervision.

Beate Langer: Resources, writing – review & editing, supervision, funding acquisition.

Kay Saalwächter: Conceptualization, methodology, software, validation, resources, writing – review & editing, supervision, project administration, funding acquisition.

¹The associated open-access article is reprinted here under a Creative Commons Attribution 4.0 International Public License (CC BY-NC-ND 4.0). **Authors:** Akshay Karekar, Katja Oßwald, Katrin Reincke, Beate Lange, and Kay Saalwächter. **Source:** *Macromolecules*, **2020**, *53*, 11166–11177, DOI: 10.1021/acs.macromol.0c01614. **Website:** <https://pubs.acs.org/doi/full/10.1021/acs.macromol.0c01614#>. No changes were made to the article.

²L. Allen, A. O’Connell, V. Kiermer, “How Can We Ensure Visibility and Diversity in Research Contributions? How the Contributor Role Taxonomy (CRediT) is Helping the Shift from Authorship to Contributorship”, *Learned Publishing* **2019**, *32*, 71–74.

NMR Studies on the Phase-Resolved Evolution of Cross-Link Densities in Thermo-Oxidatively Aged Elastomer Blends

Akshay Karekar,* Katja Oßwald, Katrin Reincke, Beate Langer, and Kay Saalwächter*

Cite This: *Macromolecules* 2020, 53, 11166–11177

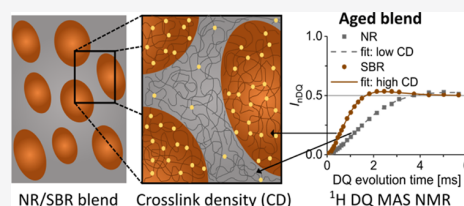
Read Online

ACCESS |

Metrics & More

Article Recommendations

ABSTRACT: A knowledge of the distribution of cross-link densities (CDs) in the constituent rubber phases of an elastomer blend is essential to understand its overall service properties, but phase-resolved CD estimations have so far been limited to qualitative assessments. In a first study of its kind, we demonstrate a phase-resolved quantification of the CDs in sulfur-cured blends of natural rubber (NR) and styrene–butadiene rubber (SBR) using solid-state ^1H homonuclear dipolar double-quantum (DQ) magic-angle spinning (MAS) NMR spectroscopy. The blends were also subjected to prolonged thermo-oxidative aging to monitor the chemical changes in the two phases. Analyses of the residual dipolar coupling constant (D_{res}), arising due to spatial restrictions by cross-links to molecular motions, as observed in MAS and static ^1H DQ experiments, suggest that unaged NR and SBR cross-link to similar extents. A minimum in D_{res} after around 500 h of aging duration is observed in NR, associated with the formation of highly mobile defect fractions, as seen from free induction decay (FID) combined with transverse relaxationometry, with further cross-linking up to 1000 h. SBR appears more stable, with a gradual increase in D_{res} over the aging duration. Phase-resolved experiments reveal a somewhat less cross-linked SBR phase in an unaged 50:50 blend. The phase-specific distribution of CDs in the blend phases becomes significant upon aging, which suggests that NR ages more strongly in the blend as compared to the aged single vulcanisates, thus dictating the blend properties.



1. INTRODUCTION

Blends of two or more polymers offer significant technological and economical opportunities for tailoring a wide spectrum of properties of the elastomers, making them suitable for a wider range of applications than the single vulcanisates of their constituent polymers.¹ However, controlling the effective performance of the individual blend phases can be tricky. In general, the blend properties are affected by the polymer component ratio; phase morphology; interfacial adhesion/cross-linking; and distribution of fillers, plasticizers, and cross-links between the elastomers, as summarized in the review by Chapman and Tinker.² Studying the distribution of cross-links is of importance as it gives a molecular-level understanding that can be correlated to the macroscopic properties of the blend. The extent of unsaturation in the participating rubbers and their solubility to the vulcanization reactants (sulfur, accelerator, and species derived from these during vulcanization process) that cause cross-linking, dictate the distribution of cross-links.³ Based on these factors, the reactants can distribute themselves preferentially in the rubber phases upon migration due to mixing and, thus, result in a corresponding distribution of properties upon curing.⁴

The cross-link density, which is proportional to the inverse of average molecular weight between cross-link junctions, is a largely empirical quantity that describes the constraints to the chain mobility post cross-linking, and this understanding can be translated to the macroscopic behavior. Experimental

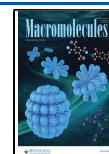
approaches involving equilibrium swelling of the vulcanisate (based on the Flory–Rehner equation),⁵ rheometry,⁶ rubber elasticity theory (based on the Mooney–Rivlin equation),⁷ and atomic force microscopy (AFM)⁸ have been exercised for determination of the cross-link densities of elastomer blends. However, a phase-resolved quantification of cross-link densities from these methods is not achieved. The first three approaches lack resolution as they cannot distinguish between the cross-link densities across the blend phases, but give an average value,⁹ whereas AFM gives only qualitative information based on image contrasts in the phases.

Nuclear magnetic resonance (NMR) spectroscopy has grown to be a viable tool for probing molecular structure and dynamics. However, a rather limited number of works is available concerning phase-resolved measurements. Early phase-specific studies have been performed using high-resolution static ^1H NMR spectroscopy by Tinker et al.^{10–12} Here, the linewidths of peaks in spectra of solvent-swollen samples were used as a measure for the cross-link densities.

Received: July 13, 2020

Revised: October 21, 2020

Published: December 3, 2020



This approach is qualitative at best, and one cannot be sure whether the resolved peaks may be dominated by mobile defects, whereas the actual network chain signals may be too broad to be resolved.

In a somewhat different yet complex system of dynamically cured polypropylene (PP)/ethylene propylene diene monomer (EPDM) thermoplastic vulcanisates, solid-state NMR has been used to resolve the overlap of PP signatures to identify the cross-link density using magic-angle spinning (MAS) techniques.^{13,14} In the former study, changes in cross-link density in the EPDM phase were only qualitatively discussed through line-width analyses of ¹H spectra from one-pulse experiments. In the latter, results from ¹H–¹³C cross-polarization (CP) technique under MAS were used in tandem with different models to qualitatively describe the extent of cross-linking by analyzing the CP curves.

In a relatively recent study,¹⁵ static proton multiple-quantum (MQ) technique was used to elucidate the cross-link density and the width of its distribution in polyisoprene/butadiene rubber blends. The approach did not yield phase-resolved results, and the components were found to be made up of comparable dipolar couplings. In a similar study using the MQ-NMR technique,¹⁶ no distinction between the phases of natural rubber (NR) and styrene–butadiene rubber (SBR) blends could be made as it was found that the distribution of dipolar couplings of NR and SBR overlaps to a high extent.

As can be seen, research concerning the quantification of cross-link densities in rubber blend components is still lacking. It will be the aim of this work to demonstrate a method based on a homonuclear dipolar double-quantum (DQ) recoupling sequence¹⁷ that effectively quantifies the distribution of cross-link densities in the blend phases. As in static ¹H MQ-NMR, an NMR measurable quantity called the residual dipolar coupling constant, D_{res} , can be obtained and used to quantify the cross-link density of the system.

Residual dipolar couplings arise due to only partial orientational averaging of proton dipole-dipole couplings caused by molecular motions constrained by cross-links, crystals, trapped entanglements, etc. The residual dipolar coupling can be used to measure the average molecular weight between cross-links through the chain dynamic order parameter, S_b , by the relation

$$S_b = \frac{D_{\text{res}}}{D_{\text{ref}}} = \frac{3}{5N} \propto \frac{1}{M_c} \quad (1)$$

where D_{ref} is the segmental reference coupling that takes into account preaveraging due to motions within a Kuhn segment,¹⁸ N is the number of segments between cross-links or topological constraints, and M_c is the network chain molecular weight. In this study, the cross-link densities will be reported in terms of the residual dipolar coupling constants, which have units in hertz.

The above method will be applied to blends of NR and SBR. NR/SBR blends are important from an industrial point of view. NR shows low hysteresis, high elasticity, and self-reinforcing property due to strain-induced crystallization. SBR shows excellent abrasion resistance and relatively good heat-properties. Hence, NR/SBR blends are used in technically demanding applications such as in tyres and conveyor belts. In tyres, their blends offer high abrasion resistance, wet-skid resistance, and lower rolling resistance.¹⁹

In view of these extreme applications, the phenomena of aging come into play. Aging is an important aspect of the engineering application of elastomers. Aging leads to changes in molecules over time, thus affecting the overall property of a product. NR and SBR are immiscible and react differently in the presence of heat and oxygen. In general, NR initially undergoes chain scission, while cross-linking reactions dominate upon progressive aging with excessive oxidation leaving NR hard and brittle, whereas SBR undergoes cyclization and cross-linking reactions upon aging leading to a hardening of the material.^{20–27} In particular, studies of the mechanical properties of short-term aged NR/SBR blends have broadly revealed that tensile strength and elongation-at-break reduce, with a simultaneous increase in hardness with the duration of aging.^{28–30} Additionally, a reduction in resistance to crack growth has been observed from fatigue crack growth analysis.³¹ A novel way of qualitatively predicting the different aging mechanisms leading to these properties can be achieved by plotting the extension ratio at break with respect to modulus at 100% strain.^{32,33} Such plots, applicable to non-strain-crystallizing rubbers at different cross-link densities due to aging, provide a broad indication of the aging mechanisms. However, such a classification depends on the ultimate properties, which are beyond the scope of this study.

The amount of polysulfidic bonds present in the blend as a result of the type of sulfur vulcanization system used will also be expected to affect the aging phenomenon dramatically, as it is known that polysulfidic bonds are rebuilt into disulfidic and monosulfidic in the presence of heat.²⁴ From an NMR perspective on aging, relaxation times have been the subject of study in a review by Asano,³⁴ and in understanding the effect of radiation-thermal aging on jacketing and insulation materials of cables used in nuclear power plant applications.³⁵ MQ (or more specifically DQ) NMR has also been used as a tool to study aging phenomena.^{36,37} However, studies in this direction for blend systems are still missing and attempts will be made in this work to open up new perspectives.

In this study, we highlight the great potential of ¹H DQ MAS NMR for characterizing and quantifying molecular-level modifications in complex elastomer systems in a phase-resolved fashion. To illustrate this, the effect of prolonged thermo-oxidative aging on the changes in molecular motions in the different components of the NR/SBR blends will be studied. The resulting degree and distribution of cross-linking will be first investigated by ¹H low-field MQ-NMR spectroscopy. The appearance of quasi-rigid components with a much-increased glass transition temperature, T_g , appearing upon aging will be further assessed through free induction decay (FID) and Hahn-echo T_2 relaxometry. Phase-resolved studies of the cross-link density will be made by high-field ¹H DQ MAS NMR spectroscopy.

2. EXPERIMENTAL SECTION

2.1. Materials and Preparation. Natural rubber (grade SMR10, $T_g = -60$ °C) was supplied by Weber and Schaefer GmbH & Co. KG (Hamburg, Germany), and solution-polymerized styrene–butadiene rubber (grade SPRINTAN SLR 4602-Schkopau, $T_g = -25$ °C), with a styrene content of 21.1% and a vinyl (1,2-polybutadiene) content of 62.1%, was supplied by Trinseo Deutschland GmbH (Schkopau, Germany). Formulations containing natural rubber were prepared after masticating the rubber for 3 min on a two-roll mill. All formulations were vulcanized based on a conventional vulcanization system composed of sulfur (2.5 phr), *n*-cyclohexylbenzothiazol-2-sulfenamide (CBS) accelerator (1.5 phr), and an activator system

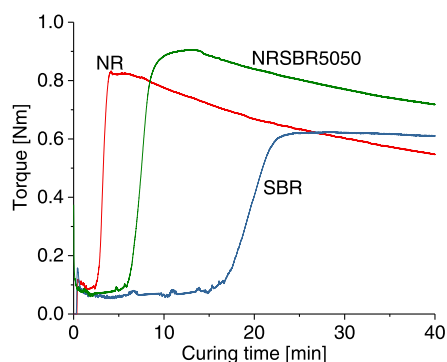


Figure 1. Vulcanization curves demonstrating the relative onset of cross-linking.

consisting of stearic acid (1 phr) and zinc oxide (3 phr). No stabilizing agents were added to the rubber mixtures. The ingredients were mixed in a Thermo Haake Rheomix 600p lab-scale internal mixer to a fill factor of 0.7, with a rotor speed of 50 rpm at a temperature of 50 °C for 10 min. Curing curves of the mixture were measured on a Göttfert Elastograph moving-die rheometer according to DIN53529. A curing (or a vulcanization) curve gives information about the curing kinetics, of cross-link formation and sometimes destruction, of a rubber recipe at the desired curing temperature.^{20,25} Curing curves for NR, SBR, and a 50:50 (by phr) blend of NR/SBR (NRSBR5050) are shown in Figure 1.

As can be seen, NR has a shorter scorch time (duration for the onset of vulcanization) due to a higher concentration of unsaturation compared to SBR. The t_{90} cure times, which correspond to 90% torque, were measured to be 4 min for NR and 22 min for SBR. Beyond the maximum torque, NR undergoes a “reversion” reaction when subjected to prolonged heating, resulting in a reduction in the torque that arises due to desulfuration and a dominant thermal decomposition with main chain modification in NR.^{38,39} The magnitude of this reduction is governed by the type of sulfur vulcanization system used. A conventional vulcanization system generates a high amount of di- and polysulfidic bonds.⁴⁰ Upon extended curing, these weak higher-order sulfidic bonds get converted to monosulfidic bonds.³⁹ The other types of sulfur vulcanization systems, viz., efficient and semiefficient vulcanization systems, have a lower amount of these thermally unstable sulfidic bonds and thus show lesser changes upon overcuring. In SBR, the irreversible binding of the accelerator to the rubber deactivates the activator complex thus preventing desulfuration and giving a broad plateau upon overcuring.³⁸ For the blend, the presence of a reversion behavior in the overcuring region that is characteristic of NR suggests that the overall blend curing property is dominated by the reactions within the NR phase. A rather shorter t_{90} curing time of 8 min than the weighted average suggests that SBR has a shorter scorch time in the blend. As was reported recently,⁴¹ this can be attributed to a higher reaction rate of SBR than that of NR in the blend, possibly due to π - π interactions between the aromatic rings of CBS accelerator and styrene in SBR rendering a preferential distribution of CBS in the SBR phase. A similar behavior in t_{90} cures times of 15 and 5 min was obtained for two more variants of the blend, 10:90 and 90:10 (by phr), respectively, of NR/SBR, thus emphasizing the enhanced reaction rate of SBR in the blends.

The different formulations were molded into sheets of 120 × 120 × 1 mm³ by compression molding at 160 °C for their respective t_{90} times. For thermo-oxidative aging, strips of 10 mm width and 80 mm length were punched out from the molded sheets and placed in an oven with a continuous flow of air at 80 °C for up to 1000 h.

2.2. Methods. **2.2.1. Static Low-Field Time-Domain ¹H MQ-NMR.** Time-domain static MQ experiments in the solid state were performed on a Bruker minispec mq20 benchtop spectrometer that operates at a 19.95 MHz ($B_0 \approx 0.5$ T) resonance frequency with a 90° pulse length of 1.6 and 15 μ s of receiver dead-time. Small disks of 8

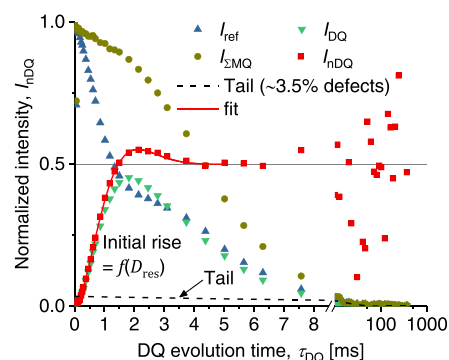


Figure 2. Experimental reference (I_{ref}) and double-quantum (I_{DQ}) signals and a normalized (I_{nDQ}) signal obtained after optimum tail subtraction from sum signal ($I_{\Sigma MQ}$) for NR.

mm diameter were punched out of the vulcanized rubber plates and stacked to a height of 4 mm inside a glass tube that was then placed in the spectrometer. Experiments were performed at 80 °C, controlled by a Bruker BVT 3000 temperature controller for all specimens, sufficiently above the glass transition temperatures of NR and SBR. A longer recycle delay (5 times the longitudinal relaxation time, T_1) was required for NR, owing to a higher temperature difference between its T_g and the test temperature, when compared to SBR. As will be apparent later, the recycle delay had to be further increased for the NR samples that had undergone chain-scission reactions due to thermo-oxidative aging.

An MQ pulse sequence featuring a pure DQ Hamiltonian,⁴² based on the works of Baum and Pines,⁴³ excites all even quantum coherences in a multispin system and gives two signals at variable DQ evolution duration, τ_{DQ} . A DQ signal (Figure 2), I_{DQ} arises due to contributions from $4n + 2$ quantum orders. At shorter times, the response is dominated by contributions from coupled spins to the second quantum order ($n = 0$). A decaying reference signal, I_{ref} contains contributions from $4n$ quantum orders and dipolar-encoded longitudinal magnetization (quantum order 0). A more detailed explanation of the pulse sequence can be found elsewhere.⁴⁴ Additionally, I_{ref} contains contributions from uncoupled spins that have isotropic mobility. In a rubber network, these are the molecular units associated with loops, dangling chains and sol that behave inelastically. The two signals eventually decay at longer evolution times due to transverse relaxation whose presence must be accounted for. A normalization via point-by-point division of I_{DQ} by a sum signal, $I_{\Sigma MQ} = I_{ref} + I_{DQ}$ after accounting for the defects by “tail subtraction” gives a normalized DQ (nDQ) build-up curve, I_{nDQ} based on the condition $I_{nDQ} = I_{DQ}/(I_{\Sigma MQ} - \text{tail})$, where I_{nDQ} reaches a plateau at 0.5 intensity based on a quantum-mechanical requirement⁴⁵ that makes the data temperature independent to a good degree.

The fitting function⁴⁶ to the build-up curve is based on an Abragam-like kernel function⁴⁵ (eq 2), which is suitable for homogeneous as well as inhomogeneous spin systems, of NR and SBR, respectively

$$I_{nDQ}(\tau_{DQ}, D_{res}) = 0.5[1 - \exp\{-0.378D_{res}\tau_{DQ}^{1.5}\}] \times \cos(0.583D_{res}\tau_{DQ}) \quad (2)$$

The probability distribution of residual couplings in the sample, $P(\ln(D_{res}))$, is assumed to be log-normal and depends on the median value of the distribution, represented as D_{med}

$$P(\ln(D_{res})) = \frac{1}{\sigma_{in}\sqrt{2\pi}} \exp\left[-\frac{\{\ln(D_{res}) - \ln(D_{med})\}^2}{2\sigma_{in}^2}\right] \quad (3)$$

The logarithmic standard deviation, σ_{in} , characterizes the width of the distribution. It is positive and dimensionless and represents the (in)homogeneity of the cross-link density in an elastomer system. The

fitting function is computed as a numerical integral over all coupling constants as shown below

$$I_{\text{nDQ}}(\tau_{\text{DQ}}) = \int P(\ln(D_{\text{res}})) I_{\text{nDQ}}(\tau_{\text{DQ}}, D_{\text{res}}) d\ln(D_{\text{res}}) \quad (4)$$

The cross-link density, now in the form of D_{med} , is qualitatively reflected in the initial rise of the build-up curve, which can be approximated by an inverted Gaussian for narrow distributions. The fitting function is modified for blends or other highly phase-separating samples to account for a potential bimodality in the distribution of the residual dipolar coupling constants.

2.2.2. Chemically Resolved High-Field ^1H DQ MAS NMR. MAS experiments provide high-resolution spectra by removing line broadening, arising from dipolar coupling or anisotropic chemical shifts, through spinning at high frequencies at the magic angle (54.74°).⁴⁷ Chemically and thus phase-resolved experiments were performed at high field on a Bruker Avance III, 400 MHz ($B_0 \approx 9.4$ T) spectrometer with a 4 mm triple-resonance MAS probe. A single rubber disk of 1 mm thickness, punched into a ring with an outer diameter of 3 mm and an inner diameter of 2 mm, was placed in a Zirconia rotor with a Vespel cap and held firmly in position by poly(tetrafluoroethylene) spacers on either side. The choice of using the specimen in a ring form is discussed in the Appendix. For a comparative study, high-field experiments were also performed at 80°C using a Bruker BVT 3000 temperature controller. A homonuclear dipolar recoupling pulse sequence, BaBa-xy16,¹⁷ provides DQ build-up curves as discussed above to enable phase-resolved coupling information. The rotor-synchronized pulse sequence consists of 32 90° pulses that correspond to eight rotor periods, τ_{R} , each for the excitation and reconversion blocks. They embody a virtual π pulse train that removes offset and chemical-shift effects to first order.

As examples, simple one-dimensional (1D) spectra of cross-linked NR and SBR samples obtained after a single 90° pulse of $2.5 \mu\text{s}$ pulse length under 10 kHz MAS frequency are shown in Figure 3a,b, respectively. The assignment of the spectral peaks in SBR can be found in Table 1. The random arrangement of comonomers in SBR leads to broadening of the peaks. The resolution can be marginally improved at higher temperatures and spinning frequencies, but this could lead to chemical changes in the polymers due to heating during the experiment time. More importantly, higher rotor frequencies deform the soft elastomer samples due to the high centrifugal forces and would introduce anisotropic effects in the samples that lead to distorted build-up curves that rise significantly beyond the 50% intensity limit. To avoid such deformations and yet meet the bandwidth requirements of BaBa-xy16, the rotors were spun at 10 kHz MAS frequency. Effects of spinning frequency on excitation of all proton spectral frequencies in a given spectral window are discussed in the Appendix. Here, it is acknowledged that the 10 kHz spinning frequency yields D_{med} values that complement results from the robust low-field measurements.

Reference decay and DQ signals with data points for even rotor cycles were obtained by taking 1D projections of the respective two-dimensional (2D) peaks and following the data treatment procedure as discussed for the static experiments. The family of nDQ build-up curves for the peaks in SBR is plotted in Figure 3c. The curves are decisively different, and the conclusions with regard to the heterogeneity of SBR are drawn and discussed below. Notably, as published already previously,¹⁷ the build-up curves of the three resonances in NR are virtually identical, corroborating the local and global homogeneity of this elastomer. The fitting function for the BaBa-xy16-based curves is modified with an efficiency factor of 0.78¹⁷ as compared to that of the Baum–Pines sequence and takes the form as given in eq 5. The obtained coupling constants are summarized in Table 1. Here, it is to be noted that no deconvolution of the peaks was performed and that the residual dipolar couplings have been presented as an integral over the groups of peaks in the different chemical shift ranges.

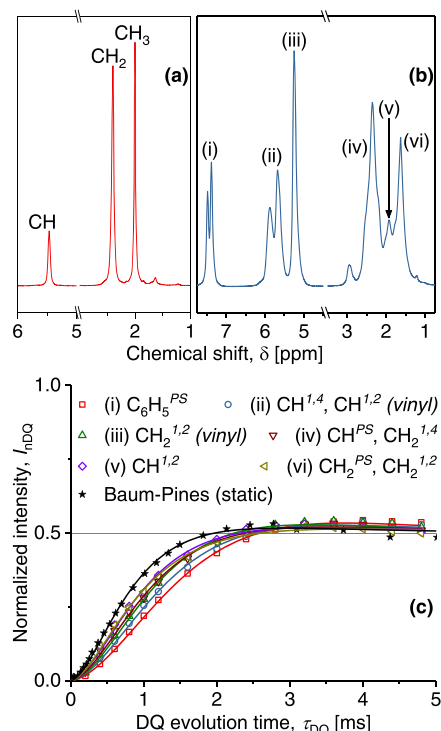


Figure 3. (a) One-dimensional (1D) spectrum of NR and (b) magnified 1D spectrum of cross-linked SBR. (c) nDQ build-up curves corresponding to the different spectral lines (designated by lowercase Roman numerals) of SBR in (b) obtained by BaBa-xy16. The solid lines represent the modified fits for BaBa-xy16 (see Table 1). The suffix “PS” corresponds to protons of polystyrene. Likewise, suffixes “1,4” and “1,2” refer to the respective variants of polybutadiene present in SBR. The “vinyl”, here, corresponds to the protons of the vinyl group only in 1,2-polybutadiene. A DQ build-up curve of SBR from a low-field experiment based on the Baum–Pines pulse sequence is plotted for comparison.

Table 1. Phase-Resolved Median Values of the Residual Dipolar Couplings and Their Distribution Widths for Vulcanized SBR

	chemical shift, δ (ppm)	unaged	
		$D_{\text{med}}/2\pi$ (kHz)	σ_{in}
$\text{C}_6\text{H}_5^{\text{PS}}$	7.2–7.7	0.233	0.278
$\text{CH}^{1,4}, \text{CH}^{1,2}$ (vinyl)	5.5–6.1	0.258	0.352
$\text{CH}_2^{1,2}$ (vinyl)	5.3	0.284	0.337
$\text{CH}^{\text{PS}}, \text{CH}_2^{1,4}$	2.1–2.8	0.292	0.420
$\text{CH}^{1,2}$	1.9	0.315	0.449
$\text{CH}_2^{\text{PS}}, \text{CH}_2^{1,2}$	1.2–1.8	0.313	0.518
spectral average		0.278	0.455
Baum–Pines (static)		0.297	0.470

$$I_{\text{nDQ}}(\tau_{\text{DQ}}, D_{\text{res}}) = 0.5[1 - \exp\{-0.295D_{\text{res}}\tau_{\text{DQ}}\}^{1.5}] \times \cos(0.455D_{\text{res}}\tau_{\text{DQ}}) \quad (5)$$

A build-up curve from a static Baum–Pines experiment with fit using eq 2 as a kernel function is also plotted in Figure 3c and listed in Table 1 for comparison and is a subject of discussion in the next section. The differences in scaling factor between BaBa-xy16 and Baum–Pines (for the static experiment) are evident from the slopes of the build-up curves. A relatively lower value of the weighted average of residual dipolar coupling constants, obtained from the

number of protons corresponding to each peak, can be attributed to experimental imperfections associated with pulse imperfections.

3. RESULTS AND DISCUSSION

3.1. Cross-Link Densities and Their Distributions in Unaged Vulcanisates. The (in)homogeneities in the single elastomers will be discussed first. Chemically resolved results for SBR are shown in Figure 3b and Table 1. A similar study was performed on vulcanized NR which has resonance peaks of CH, CH₂, and CH₃ at 5.5, 2.4, and 2.0 ppm, respectively, as shown in Figure 3a. The coupling strengths for each of these proton species are identical in magnitude⁴⁸ and gave a spectral average coupling strength of 0.287 kHz and $\sigma_{in} = 0.100$. This low-distribution width in NR comes about due to the homogeneous nature of the polymer and the resulting networks.

In contrast, previous low-field MQ-NMR studies⁴⁹ have revealed that SBR generally exhibits much broader D_{res} distributions than NR. This was attributed to “spin inhomogeneity” related to different behaviors of the different comonomers. We are now in a position to check this assumption.

Evidently, the D_{med} values in Table 1 vary across the different molecular moieties by about $\pm 15\%$. For instance, a relatively lower residual dipolar coupling constant of the protons on the phenyl ring can be attributed to the freedom in motion of the ring about its axis. A high 1,2-polybutadiene content along with styrene contributes to a high T_g in SBR.²⁴ This comes about due to the presence of vinyl substituted molecules that cause motional restrictions to the short main chain monomer units of 1,2-polybutadiene. Also, the bulky phenyl ring in styrene stiffens the polystyrene main chain. This results in higher values of D_{med} for the proton groups especially in the (v) and (vi) spectral positions. Notably, though, all of these structure-related differences are smaller than the variations in the logarithmic distribution widths σ_{in} (a value of 0.5 implies a variation over roughly half a decade). It can thus be concluded that SBR features intrinsically a more inhomogeneous cross-linked structure than NR, possibly due to an interplay of the copolymer structure and the vulcanization reactions. More insights into the origin of distribution widths can be found in the discussion related to Figure 5b.

The integral low-field DQ build-up curves in Figure 4 for unaged NR and SBR, obtained after the data processing as described in the previous section, feature the typical differences

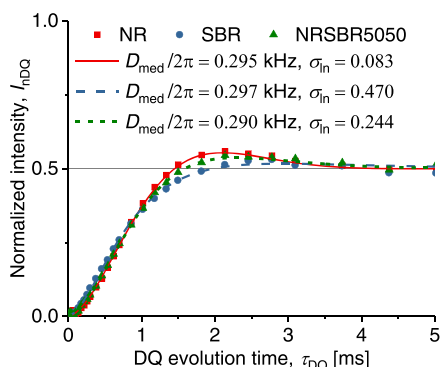


Figure 4. Fitted DQ build-up curves for unaged NR, SBR, and their 50:50 blend.

between the two materials. The presence of *cis*-1,4 polyisoprene in NR as the main component makes NR a very homogeneous polymer that has an approximate inverted Gaussian shape of the build-up curve. The homogeneity contributes to an overshoot of the build-up curve beyond the 0.5 intensity limit arising from a damped oscillation of quantum-mechanical origin. On the contrary, SBR shows a gradual rise to 0.5 intensity without a distinct overshoot. This is a characteristic of a more heterogeneous system, as discussed above. This difference in spin (in)homogeneity in NR and SBR is reflected in the distribution width σ_{in} . Despite these differences in their distribution widths, NR and SBR give a similar quantity for the D_{med} . This is probably a coincidence, as the reference couplings for NR and SBR to be used in eq 1 for conversion into cross-link density¹⁸ are likely different (it is unknown for SBR).

The fitting function in eq 4 was modified to a bimodal case to assess the possible occurrence of the distribution of cross-link densities in NRSBR5050. Higher vinyl content is known to increase the miscibility of NR with SBR.⁵⁰ Nevertheless, due to their different chemistries, they phase-separate on a molecular level in a blend and can be expected to exhibit different cross-link densities in their phases. However, the bimodal fitting function yielded a single value for the cross-link density that is analogous to the extent of cross-linking as observed in the single vulcanisates discussed above. Sulfur has a high solubility in polymers containing a diene or styrene group¹ and is, hence, expected to distribute homogeneously with no preference across the two blend phases. The distribution width of the blend takes a value that is approximately the weighted average of the widths of the single vulcanisates. The spread of cross-link densities can be visualized in the distributions plotted in Figure 5a. Such distribution plots can be obtained by subjecting the normalized build-up data to a regularization procedure of any ill-posed data⁴⁵ by a technique called ftikreg (Fast-Tikhonov regularization). The analyses reflect the trend of coupling distribution shapes observed through fitting of the build-up curves. NR has a symmetric and narrow distribution of coupling strengths pertaining to all of the proton environments as was mentioned earlier. Remarkably for the SBR sample, ftikreg gives a skewed distribution of coupling strengths arising from the different monomers and shows the fraction of relatively highly motion-restricted spins that could not be resolved by the regular fitting method. A detailed analysis of this will follow below. The 50:50 blend, as can be expected, features a distribution of the weighted average of the two blend components. Further, the bimodal fitting function did not indicate any bimodality in the distribution as both NR and SBR have an overlap of residual dipolar coupling constant distributions to a great extent.

Likewise, the distribution trends of NRSBR1090 and NRSBR9010 strongly follow the ratios of their constituent polymers, becoming narrower with an increase in NR. Direct fits of nDQ build-up data for these samples (not shown here) produced single values of D_{med} of identical magnitude as for the 50:50 blend, thus proving that sulfur has no preference of distribution in either phase when their ratios are changed in the samples discussed here. In line with the ratios of the constituent rubbers in a blend, σ_{in} varies as their weighted average, thus demonstrating the sensitivity of our experimental technique toward any changes in the microstructure.

Chemically resolved distributions of coupling constants in SBR obtained from MAS build-up curves in Figure 3b are

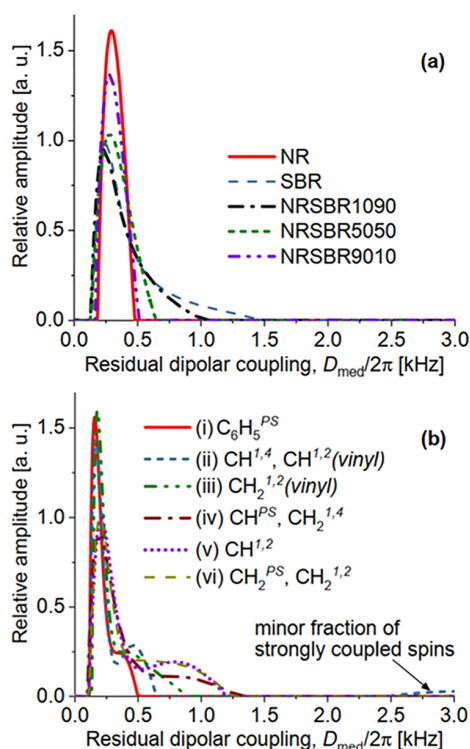


Figure 5. Residual dipolar coupling distributions obtained by fitkreg from normalized DQ build-up curves for (a) unaged samples at low fields and (b) different resonance peaks of SBR obtained at high fields.

plotted in Figure 5b. The distribution of coupling strengths corresponding to the spectral position (ii) gives a clear bimodal distribution with values presented earlier. The strongly coupled spins with a $D_{\text{med}} \approx 0.530$ kHz contribute to about 22% of the coupling fraction (from fitting) and could be stemming from the CH moiety on the vinyl side group. However, the exact molecular origin of this strong coupling cannot be ascertained. In addition to the bimodality, broad shoulders are observed for spectral positions (iii)–(vi), which could be mainly due to motional restrictions to the main chain protons of 1,2-polybutadiene and polystyrene posed by vinyl side group and the phenyl ring, respectively. These also contribute to an overall wide coupling distribution in SBR as was observed from the low-field measurements, all pointing to an overall rather inhomogeneously cross-linked structure of SBR.

3.2. Effect of Thermo-Oxidative Aging. **3.2.1. Evolution of Cross-Link Densities in Aged Samples.** Thermo-oxidative aging causes irreversible chemical changes in the architecture of the polymer chains and this can be readily detected through NMR spectroscopy. The 50:50 blend subjected to 1000 h of aging (see Figure 6a) shows a stark variation in its DQ build-up trend when compared with its unaged variant. The coupling constant has a reduced value that can be regarded as a result of chain scissions due to prolonged aging. A rather broad distribution of coupling constants indicates the modification of the chains to different lengths, thus contributing to different coupling strengths.

The evolution of cross-link densities in the NR, SBR, and their blend at various aging intervals is summarized in Figure 6b. The median value of the cross-link density remains

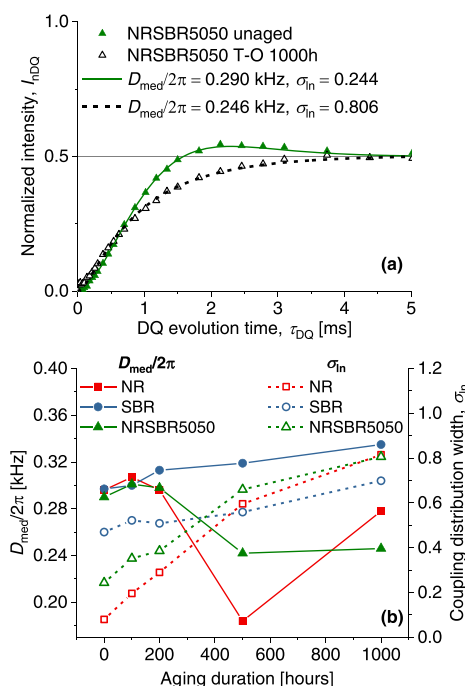


Figure 6. (a) DQ build-up curves of 1000 h thermo-oxidatively aged NRSBR5050 and unaged NRSBR5050 (replotted for comparison). (b) Plots of the evolution of residual dipolar couplings in NR, SBR, and their 50:50 blend at different aging intervals with their distributions.

relatively unchanged up to 200 h for all of the three compositions. However, a gradual increase in coupling distribution widths in NR and its blend with SBR at these aging durations reflects a modification of the network architecture. Upon further aging, NR demonstrates a sudden decrease in the cross-link density around 500 h, which accounts for a reduction in D_{med} by about 40% to its original value. Here, the exact aging duration at which the minimum is reached and how long it stays, before it increases due to cross-linking and oxidation leading up to 1000 h in the samples, cannot be ascertained. The heterogeneity increases further due to the different chemical modifications and localized motional restrictions. It is important to note here that the build-up curve for the 1000 h aged NR sample showed a sudden increase in intensity (about 10%) for data points approximately up to the 100 μs DQ evolution time and then continued with the expected trend. This jump is an indication of the presence of very strongly coupled components in the sample. The bimodal fitting function performed a fair fit to quantify the coupling constant of a motionally more constrained component (≈ 0.400 kHz). The value of the coupling constant shown in Figure 6a is obtained as a weighted average of the two components of different coupling strengths and is still a somewhat underestimated value as the function could not precisely take an actually constrained fraction (with significantly increased T_g) into consideration.

The coupling strength in SBR increases by about 40 Hz within 1000 h of aging. Thus, the chain lengths remain relatively unchanged with only a minor increase in the distribution width (≈ 0.70). The blend follows a similar trend to NR, albeit to a lesser extent, but suggests that NR is the dictating phase of the two. A proportionately lesser amount of

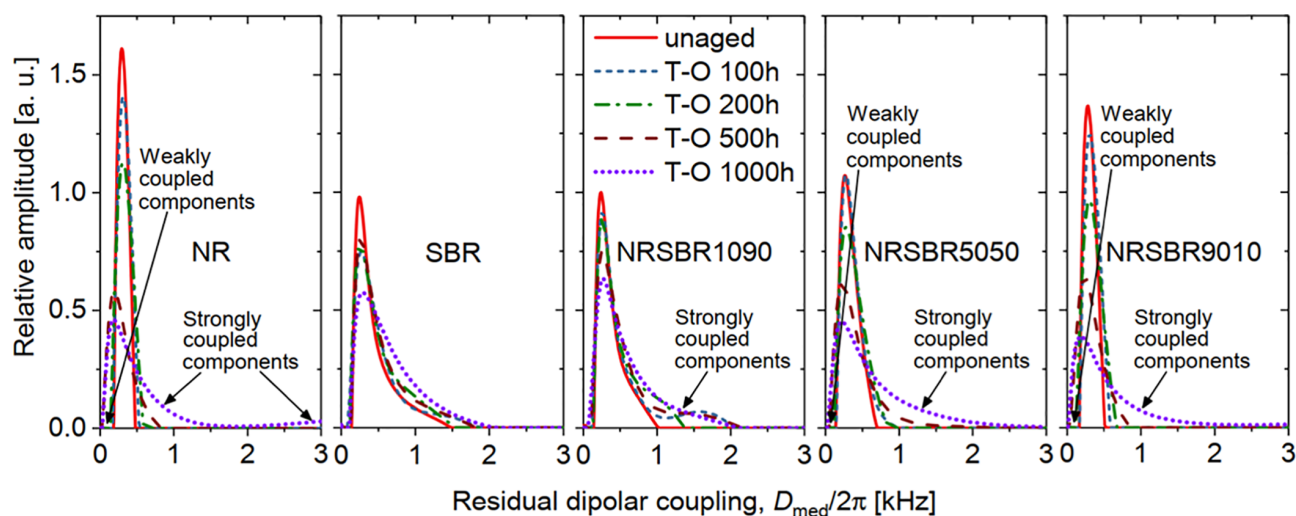


Figure 7. Distribution plots of residual couplings obtained by fitkreg show the formation of weakly and strongly coupled fractions in NR and NR-containing samples aged for prolonged durations. Only a minor increase in the coupling strength is observed for SBR T-O 1000 h.

constrained fraction relative to 1000 h aged NR can be expected for the blend. However, the bimodal fitting function could not quantify contributions from the rather lesser amount of constrained fraction (seen as a vertical jump in the data points in Figure 6a up to 100 μ s DQ evolution time), thus resulting in an underestimated D_{med} of 0.246 kHz that is dominated by contributions from weakly coupled components.

The defect fraction in SBR in its unaged form amounted to less than 1% and did not increase upon aging. On the contrary, the increase in the number of isotropic defects in NR and its blend was analogous to their increase in coupling distribution. The defects in NR was unchanged around 3% up to 200 h of aging and then grew to 9 and 10% for 500 and 1000 h of aging, respectively. The tail fraction in the blend was similar in magnitude to NR owing to the low-to-no tail fraction in SBR.

Clearly, NR and SBR demonstrate quite different trends in their aging characteristics. A higher degree of unsaturation in NR makes it susceptible to thermal and oxygen attack. The presence of the methyl group in NR as an electron donor reduces the stability of the polymer against oxygen attack.¹ The first 200 h can be associated to the maturation of polysulfidic bonds into mono- and disulfidic bonds. This leads to the shortening of the existing long sulfur bridges and formation of new short ones.³⁸ The median value of D_{res} remains relatively unchanged but has contributions arising from the newly formed sulfur bonds that increase the distribution widths. The lowering of cross-link density around 500 h of aging occurs due to chain scission reactions caused by oxidation. The cross-linking reaction then dominates leading to an increase in cross-link density up to 1000 h.²⁴ The deactivation of the activator complex in SBR prevents desulfuration, and the absence of a reaction-inducing methyl group in SBR makes it chemically less susceptible to chain scission reactions. Hence, cyclization reactions take place that increase chain restrictions.

An apparent increase in the coupling distribution width upon extended aging can be visualized by regularization, see Figure 7. The effect is particularly pronounced for NR and NR-containing blends. These results also reflect the formation of new weakly coupled segments in low coupling strength regions up to about 0.2 kHz that occur due to chain scission reactions and the breakdown of polysulfidic bonds. The strongly coupled

fractions of spins seen in aged NR and its blends are caused by a dominant cross-linking reaction upon extended aging. In addition to cross-linking, possible oxidation of the samples may have also occurred as the NR sample was found to be hard and brittle.²⁴ This increase in restriction to molecular motion is in fact at the origin of the small jump in intensity at short evolution times in the corresponding build-up curve discussed earlier that could not be completely quantified by the fitting function. These cumulative findings suggest a sample with a highly oxidized surface and a bulk with lowly cross-linked molecules. No weakly cross-linked chain fraction can be found in SBR. An increase in cross-link density due to different factors upon prolonged aging⁵¹ leads to broadening of the distribution at the higher end of the cross-link density spectrum.

At this point, the quantification of the fractions of strongly and weakly coupled segments observed above for 1000 h aged NR will be made based on T_2 (spin–spin or transverse relaxation) times. In such experiments, network components with D_{res} in the range of a few hundred hertz appear as components with T_2 in the millisecond range, but also more strongly coupled, more constrained, or even fully rigid segments with couplings approaching the rigid limit (~ 30 kHz), and thus T_2 in the 20 μ s range, are accessible. These are beyond the frequency/time resolution of the DQ experiments. Transverse relaxation-based studies⁵² were performed by analyzing free induction decays (FIDs), extended by a Hahn-echo T_2 decay. These decay curves were stabilized by a dead-time free magic sandwich echo FID (MSE-FID)⁵³ and fitted simultaneously (globally) by a multicomponent modified-exponential ($\propto e^{-(t/T_2^{eff})^\beta}$) decay fit with relevant shape parameters (the purely dipolar T_2^{eff} decay is Gaussian with $\beta = 2$, and lower values arise due to coupling distributions and actual relaxation effects). One such fit is demonstrated here for the case of 1000 h aged NR in Figure 8a.

Aging of sulfur-vulcanized NR brings about changes in its structure due to chain scission, decross-linking, postcuring, and oxidation, leading to a network with different local dynamics. In the presence of dipolar couplings, a modified “effective T_2 ”, (T_2^{eff}), is obtained for such components. These components are best described by a Gaussian function⁵⁴ and lack the

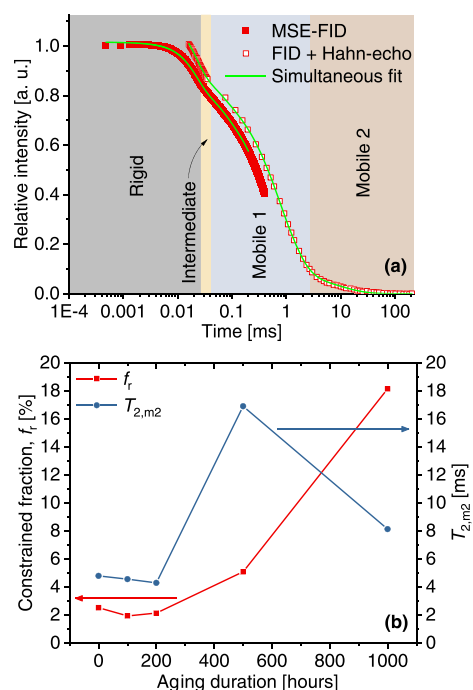


Figure 8. (a) Plot of MSE-FID and FID extended by Hahn-echo for 1000 h aged NR showing the different components corresponding to different spin–spin (transverse) relaxation times obtained by a four-component exponential decay simultaneous fit. (b) Evolution of the quantity of constrained components and the T_2 corresponding to the most mobile components (mobile 2 (m2)) as a function of the aging duration.

characteristic exponential decay typical of a pure T_2 relaxation. In a four-component exponential decay fit to 1000 h aged NR, T_2^{eff} values ranging from about 20 μs for constrained components to about 8 ms for the highly mobile defect components were obtained. The fit is stabilized by the large T_2^{eff} differences and simultaneous fitting. The fractions of the different components and their respective T_2^{eff} are given in Table 2 along with their decay shape parameters. On the

Table 2. Results from Simultaneous Fits to 1000 h aged NR

components	fraction, f	T_2^{eff} (ms)	β
constrained	0.181	0.021	2.00
intermediate	0.059	0.057	1.70
mobile 1	0.672	0.782	0.92
mobile 2	0.088	8.125	0.80

contrary, unaged NR and samples aged up to 500 h can be best described by a three-component exponential decay fit, where the second component is a mobile fraction (mobile 1) with T_2^{eff} increasing from 1.05 to 1.5 ms and the corresponding fraction reducing from 89 to 81% with the aging duration. The percentage of constrained fractions (corresponding to T_2^{eff} of about 20 μs) in NR aged for different durations is plotted in Figure 8b along with the T_2 of the third, highly mobile component (mobile 2), $T_{2,m2}$.

A proportionally lesser amount of the different fractions can be expected for the aged blends. No significant change in the relaxation time scales could be observed for SBR from FID and Hahn-echo measurements due to its higher temperature stability.

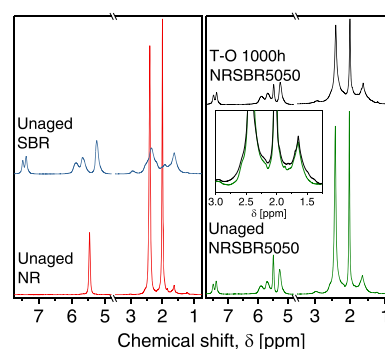


Figure 9. Proton spectra of the unaged and aged blend samples. See Figure 3 for the peak assignments. The spectrum of the thermo-oxidatively aged blend undergoes broadening (inset) of the peaks due to increasing dynamic heterogeneity.

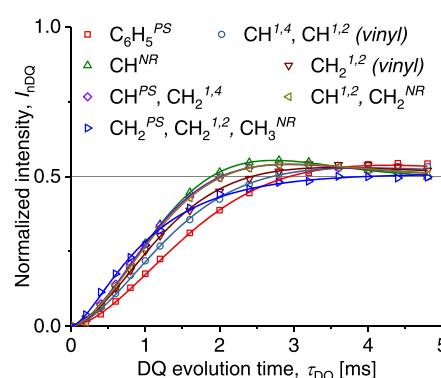


Figure 10. DQ build-up curves for unaged NRSBR5050 obtained by the BaBa-xy16 pulse sequence under MAS. The fits are represented as solid lines.

Similar yet more qualitative studies, based on component-decomposition by transverse relaxation time measurements using Hahn-echo (only), have been performed by Knörger et al.⁵⁴ and Somers et al.⁵⁵ Results from the latter study demonstrated a resemblance to the current study, wherein the transverse relaxation times showed a reducing trend in samples aged up to about 200 h. In the former study focussed on short-term aging, the transverse relaxation time showed a minimum after about 20 h of aging and increased again (but still shorter than an unaged sample) around 80 h of aging. However, the results are not directly comparable due to different aging durations. In a different study,⁵⁶ inference to motional restrictions in polymer chains has been made by studying ^{13}C NMR peak intensities, where a reduction in the peak intensity (or broadening of the NMR peak) was caused by an increase in constraints due to aging. The peak intensities reduced subsequently with the duration (14 days) of aging, in analogy to the results presented in this work.

From a mechanical property standpoint, the tensile strength in SBR was observed to show an initial decline and thereafter a continuous increase up to 2-folds when compared to its unaged sample, with the aging duration.²⁵ In contrast, NR demonstrated a significant loss in tensile strength upon aging relative to its original value.^{25,57} In both polymers, the strain-at-break continuously reduced due to stiffening related to aging. The respective trends of tensile strengths in these studies are largely analogous to those of the D_{res} in the present study. It may hence be expected that the formulations

Table 3. Summary of Phase-Resolved Residual Dipolar Couplings of Unaged and 1000 h Aged Samples

	chemical shift, δ (ppm)	NR		SBR		NRSBR5050			
		unaged	aged	unaged	aged	unaged		aged	
		$D_{\text{med}}/2\pi$ (kHz)	$D_{\text{med}}/2\pi$ (kHz)	$D_{\text{med}}/2\pi$ (kHz)	$D_{\text{med}}/2\pi$ (kHz)	$D_{\text{med}}/2\pi$ (kHz)	σ_{in}	$D_{\text{med}}/2\pi$ (kHz)	σ_{in}
$\text{C}_6\text{H}_5^{\text{PS}}$	7.2–7.7	-	-	0.233	0.261	0.200	0.236	0.225	0.643
$\text{CH}^{1,4}, \text{CH}^{1,2}$ (vinyl)	5.6–6.1	-	-	0.258	0.290	0.232	0.323	0.234	0.661
CH^{NR}	5.5	0.287	0.284	-	-	0.291	0.038	0.236	0.669
$\text{CH}_2^{1,2}$ (vinyl)	5.3	-	-	0.284	0.327	0.256	0.316	0.283	0.671
$\text{CH}^{\text{PS}}, \text{CH}_2^{1,4}, \text{CH}_2^{\text{NR}}$	2.1–2.8	0.293	0.276	0.292	0.333	0.287	0.215	0.307	0.749
$\text{CH}^{1,2}, \text{CH}_3^{\text{NR}}$	1.8–2.1	0.278	0.260	0.315	0.365	0.281	0.200	0.268	0.729
$\text{CH}_2^{\text{PS}}, \text{CH}_2^{1,2}$	1.2–1.8	-	-	0.313	0.364	0.282	0.669	0.292	0.671
spectral average		0.287	0.275	0.278	0.315	0.274	0.303	0.267	0.740
Baum–Pines (static)		0.295	0.278	0.297	0.335	0.290	0.244	0.246	0.806

discussed here behave similarly upon mechanical analysis, with the blends scaling proportionately.

3.2.2. Determination of Phase-Specific Cross-Link Densities in Blends. Phase-resolved studies were performed using the MAS parameters discussed above. For convenience, we show in Figure 9 again the 1D spectra of the pure compounds alongside spectra of an unaged and an aged 50:50 blend. To remind, unaged SBR demonstrates broader peaks due to comonomer inhomogeneity when compared with unaged NR.

The phase-resolved DQ build-up curves, for the unaged NRSBR5050 blend, are plotted in Figure 10. The curves enable a clear distinction due to different residual couplings. The methylene and methyl groups of NR overlap with the main chain proton resonances of SBR at the respective chemical shifts to give common residual dipolar couplings. Fitting results to DQ build-up curves of 1000 h aged NR and SBR along with their unaged variants obtained from the BaBa-xy16 pulse sequence are presented in Table 3. In general, the D_{res} values of the spectral average and coupling distribution width are in line with the results from the static experiment.

For highly aged SBR, an apparent increase in D_{med} is observed across all resonances. The average coupling constant of 0.315 kHz had a coupling distribution width of about 0.670, significantly wider than that for unaged SBR. The marginal increase in coupling constant values is found to be in good agreement with the values obtained from the low-field experiment. A tail fraction corresponding to about 2.5% was obtained for the build-up curve of the last resonance peak but was negligible for the others. In the case of 1000 h aged NR, the spectral average over all resonances is comparable in value to that from the low-field experiment. In the current experimental setup for elastomers, the shortest measurable DQ evolution time is 100 μs (when every integer rotor period is considered), which is longer than the $\approx 20 \mu\text{s}$ T_2^{eff} of the constrained components. Thus, the value of D_{med} obtained at the high field would also be somewhat underestimated since the contribution of strongly coupled segments cannot be captured. Shorter DQ evolution times for measurement can be achieved at much higher rotor frequencies, but this would deform the sample and induce anisotropy.

We are now in a position to provide a more accurate comparison of the individual coupling strengths in the unaged blend with the values of the individual vulcanisates discussed in the Section 2 (and reintroduced here). We now see that SBR has, in general, somewhat lower coupling constants in the blend, whereas the values corresponding to NR remain similar to those in the single vulcanisate. The reduction is on the order

of 10% and could be related to still slower curing of SBR in the blend, as discussed under the Section 2.

Changes in the intensities of the resonance peaks of the spectrum due to aging of the blend can be seen in Figure 9. Prominent changes can be observed in the form of peak broadening at chemical shifts of NR peaks. This broadening arises due to strongly coupled spins that are associated with a short T_2^{eff} and corresponds to the constrained fraction obtained from the time-domain FID fits in Figure 8. Compared to the unaged blend, the only-SBR resonances show a marginal increase in the cross-link densities and restrictions to motions that is analogous to the results from the static low-field experiments. Distinctly, the NR-containing resonances have lower values as compared to before aging, except for the methylene resonance of NR that is superimposed by contributions from the main chain protons of polystyrene and 1,4-polybutadiene. As discussed before, the lowering in the coupling strengths arises from chain scission reactions that give somewhat less cross-linked intermediates and mobile fractions that make up for the majority of the sample after aging for 1000 h. A proportionately lesser quantity of constrained components can be expected in the blend that unfortunately cannot be quantified due to restriction in using higher MAS frequencies for elastomer samples.

Nevertheless, the aged phases of SBR and NR in the blend showcase interesting trends. The changes in cross-link densities of these samples obtained from DQ experiments are analogous to the “marching modulus cure” and “reversion” phenomena observed in synthetic rubbers (SBR in this case) and NR, respectively, through the vulcanization curves. These trends clearly demonstrate the occurrence of an inhomogeneous distribution of cross-link densities in the two phases of the aged blend, thus validating our method. The reduction in the cross-link density in NR upon aging is analogous to the reduction in its torque over the short duration of “thermal aging” at 160 °C observed in Figure 1. Likewise, an increase in D_{res} upon aging in SBR is a testimony to its thermal stability, as observed from its curing curve. Since torque increases with the cross-link density, an approximate estimation of the change in cross-link densities can also be obtained from the vulcanization curves as a difference between the maximum torque, and the minimum torque during the scorch time. In retrospective, it may hence be deduced that in NR the cross-link density (corresponding to a maximum torque of 0.73 N m) reduces to that corresponding to 0.46 N m over the duration of thermal treatment, whereas it is relatively unchanged for SBR.

Surprisingly, the NR-methine resonance in the blend mirrors a significant reduction in the coupling strength, which is in stark contradiction to its behavior in the case of the single vulcanisate, where it remained relatively unchanged. On the other hand, SBR in the blend aged differently, where the coupling strengths of all moieties in the SBR phase were lower than those obtained from the aged single vulcanisate. This is perhaps due to the somewhat lower starting values of D_{med} in the unaged blend caused by a previously incomplete cross-linking of the SBR phase.

4. CONCLUSIONS

In this work, the distribution of cross-link densities in blends of unaged and thermo-oxidatively aged NR and SBR was studied by MQ-NMR experiments. Static low-field experiments did not reveal the presence of any multimodal distributions of cross-link densities in unaged blends, thus suggesting that sulfur distributes itself homogeneously across the two blend phases. In the 1000 h aged blend, a general widening of the coupling strength distribution was observed analogous to the single vulcanisates. A single distribution mode was obtained mainly due to a large overlap of dipolar coupling strengths of the constituent rubbers in their blend. Nevertheless, these studies clearly demonstrated the evolution of motional constraints in the samples upon aging by an increasingly wider distribution of coupling constants. FID analyses of 1000 h aged NR showed the formation of constrained components associated with very short spin–spin relaxation times.

The phase-resolved quantification of cross-link densities by DQ MAS experiments proved the nonpreferential distribution of sulfur in the blend phases. Encouragingly, the method was able to identify the distribution of cross-link densities that was present due to different rates of curing in the respective phases. Measurements of the effect of 1000 h of aging on the samples showed a reduced cross-link density in NR and a somewhat higher cross-link density in SBR when compared to their unaged states. Cross-link density measurements on the aged blend sample revealed trends analogous to reversion and marching modulus cure in NR and SBR phases as observed in their respective vulcanization curves. These distinctly different behaviors contributed to phase-specific distribution of cross-link densities in the aged blend. Another intriguing finding was that the magnitude of motional constraints across all SBR resonances in the blend upon aging was lesser than its aged single vulcanisate, thus suggesting that the SBR in the blend ages to a lesser extent and is generally softer, possibly owing to a preferential distribution of oxygen in, and thus comparably stronger aging of, the NR phase.

APPENDIX

In MAS experiments, possibilities of deformation³⁴ of soft materials like an elastomer due to high rotor frequencies must be considered. Additionally, softening due to higher temperature aids in deforming the sample. The force acting on a sample increases by 4 times when the rotor frequency is doubled. Hence, it is necessary to set a low rotor frequency and yet obtain good spectral resolution. A comparative study was performed on a 3 mm diameter disk of a model sulfur-vulcanized unaged natural rubber that has a characteristic high homogeneity, using the rotor-packing protocol explained in Section 2.2.2. Experiments (Figure 11) were performed at 80 °C at 5 and 10 kHz rotor spinning frequencies with a

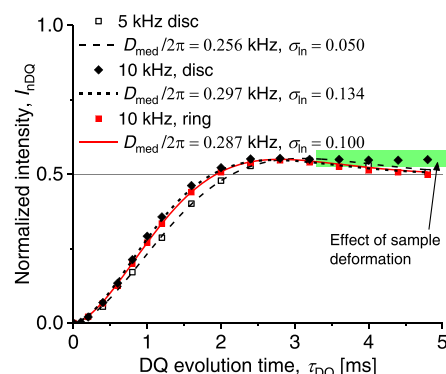


Figure 11. Effect of different MAS rotor frequencies on DQ build-up curves.

centrally positioned spectral offset frequency. The experiment with a 10 kHz MAS frequency yielded a spectral average D_{med} of 0.297 kHz. However, the experiment with a 5 kHz MAS frequency gave an underestimated value of 0.256 kHz for the residual dipolar coupling constant, which is about 40 Hz lower than the static low-field result of about 0.295 kHz. To check for the potential off-resonance effects, on-resonance measurements were performed at 5 kHz MAS frequency for the three aliphatic peaks in NR, viz., those corresponding to CH, CH₂, and CH₃, which still gave lower values of D_{med} .

The performance for a centrally positioned offset frequency was even poorer for unaged SBR that has a wide spectrum of resonances. For the case of SBR, the two extreme peaks are separated by about 6 ppm, which on a 400 MHz spectrometer corresponds to 2400 Hz, which is close to 2500 Hz (half the rotor frequency). While the BaBa-xy16 experiment is rather broadbanded at higher MAS frequencies,¹⁷ it is thus found that this is not the case for slower spinning.

The results from the 10 kHz rotor frequency were comparable with the results from the low field and hence were pursued. Unfortunately, visual inspection of the sample after experiment showed a depression around the center of the sample and a thin rubber layer protruding around the circumference could also be observed due to the high forces experienced by the rubber sample. A consequence of this is a DQ build-up curve that does not flatten at the 0.5 intensity limit at longer DQ evolution times but stays above and occurs due to a biased powder averaging in the deformed sample.⁵⁸ Such deformations were not observed for highly aged samples that had an increased rigidity. To minimize the effect of high deformation forces, 2 mm holes were punched in the center of the disks to form thin rings. As a result, no significant deformation of the rubber against the inner wall of the rotor was observed, leading to undistorted build-up curves (see Figure 11).

In summary, it can be concluded that the favorable offset performance of the BaBa-xy16 pulse sequence, initially tested only for high spinning frequencies,¹⁷ and also its overall performance deteriorate at low spinning frequencies. The use of other suitable recoupling sequences such as POST-C7⁵⁹ is advised in this limit.¹⁷

AUTHOR INFORMATION

Corresponding Authors

Akshay Karekar – Institut für Physik-NMR, Martin-Luther-Universität Halle-Wittenberg, 06120 Halle (Saale),

Germany; orcid.org/0000-0003-0476-1790;
Email: akshay.karekar@physik.uni-halle.de

Kay Saalwächter – Institut für Physik-NMR, Martin-Luther-Universität Halle-Wittenberg, 06120 Halle (Saale), Germany; orcid.org/0000-0002-6246-4770;
Email: kay.saalwaechter@physik.uni-halle.de

Authors

Katja Oßwald – Polymer Service GmbH Merseburg, 06217 Merseburg, Germany

Katrin Reincke – Polymer Service GmbH Merseburg, 06217 Merseburg, Germany

Beate Langer – Polymer Service GmbH Merseburg, 06217 Merseburg, Germany; Fachbereich Ingenieur- und Naturwissenschaften, Hochschule Merseburg University of Applied Sciences, 06217 Merseburg, Germany

Complete contact information is available at:
<https://pubs.acs.org/10.1021/acs.macromol.0c01614>

Funding

The authors thank the Land Sachsen-Anhalt and the Europäischer Sozialfond (ESF) for grant ZS/2016/08/80644.

Notes

The authors declare no competing financial interest.

REFERENCES

- (1) Mark, J. E.; Erman, B.; Eirich, F. R., Eds. *The Science and Technology of Rubber*, 3rd ed.; Elsevier Academic Press: San Diego, 2005.
- (2) Chapman, A. V.; Tinker, A. J. Vulcanization of blends – Crosslink distribution and its effect on properties. *KGK, Kautsch. Gummi Kunstst.* **2003**, *56*, 533–544.
- (3) Tinker, A. J.; Jones, K. P., Eds. *Blends of Natural Rubber—Novel Techniques for Blending with Speciality Polymers*, 1st ed.; Chapman & Hall: London, 1998.
- (4) Shershnev, V. A. Vulcanization of polydiene and other hydrocarbon elastomers. *Rubber Chem. Technol.* **1982**, *55*, 537–574.
- (5) Srithawatpong, R.; Peng, Z. L.; Olson, B. G.; Jamieson, A. M.; Simha, R.; McGervey, J. D.; Maier, T. R.; Halasa, A. F.; Ishida, H. Positron annihilation lifetime studies of changes in free volume on cross-linking cis-polyisoprene, high-vinyl polybutadiene, and their miscible blends. *J. Polym. Sci., Part B: Polym. Phys.* **1999**, *37*, 2754–2770.
- (6) Ismail, H.; Tan, S.; Poh, B. T. Curing and mechanical properties of nitrile and natural rubber blends. *J. Elastomers Plast.* **2001**, *33*, 251–262.
- (7) Dzulkifli, A. I.; Said, C. M. S.; Han, C. C. Determination of crosslink concentration by Mooney-Rivlin equation for vulcanized NR/SBR blend and its influence on mechanical properties. *Malaysian J. Anal. Sci.* **2015**, *19*, 1309–1317.
- (8) Galuska, A. A.; Poulter, R. R.; McElrath, K. O. Force modulation AFM of elastomer blends: Morphology, fillers and cross-linking. *Surf. Interface Anal.* **1997**, *25*, 418–429.
- (9) Honiball, D.; McGill, W. J. A technique for measuring the crosslink densities in both phases of a vulcanizate blend. *J. Polym. Sci., Part B: Polym. Phys.* **1988**, *26*, 1529–1537.
- (10) Loadman, M. J. R.; Tinker, A. J. The application of swollen-state CW-¹H NMR spectroscopy to the estimation of the extent of crosslinking in vulcanized polymer blends. *Rubber Chem. Technol.* **1989**, *62*, 234–245.
- (11) Brown, P. S.; Tinker, A. J. Factors affecting the NMR technique for estimation of crosslink density in rubber blends. *J. Nat. Rubber Res.* **1990**, *5*, 286–295.
- (12) Brown, P. S.; John, M.; Loadman, R.; Tinker, A. J. Applications of FT-NMR to crosslink density determinations in natural rubber blend vulcanizates. *Rubber Chem. Technol.* **1992**, *65*, 744–760.
- (13) Ellul, M. D.; Tsou, A. H.; Hu, W. Crosslink densities and phase morphologies in thermoplastic vulcanizates. *Polymer* **2004**, *45*, 3351–3358.
- (14) Aluas, M.; Filip, C. Solid-state NMR characterization of cross-linking in EPDM/PP blends from ¹H–¹³C polarization transfer dynamics. *Solid State Nucl. Magn. Reson.* **2005**, *27*, 165–173.
- (15) Dibbanti, M. K.; Mauri, M.; Mauri, L.; Medaglia, G.; Simonutti, R. Probing small network differences in sulfur-cured rubber compounds by combining nuclear magnetic resonance and swelling methods. *J. Appl. Polym. Sci.* **2015**, *132*, No. 42700.
- (16) Mansilla, M. A.; Valentin, J. L.; López-Manchado, M. A.; González-Jiménez, A.; Marzocca, A. J. Effect of entanglements in the microstructure of cured NR/SBR blends prepared by solution and mixing in a two-roll mill. *Eur. Polym. J.* **2016**, *81*, 365–375.
- (17) Saalwächter, K.; Lange, F.; Matyjaszewski, K.; Huang, C. F.; Graf, R. BaBa-xy16: Robust and broadband homonuclear DQ recoupling for applications in rigid and soft solids up to the highest MAS frequencies. *J. Magn. Reson.* **2011**, *212*, 204–215.
- (18) Saalwächter, K.; Herrero, B.; López-Manchado, M. A. Chain order and cross-link density of elastomers as investigated by proton multiple-quantum NMR. *Macromolecules* **2005**, *38*, 9650–9660.
- (19) Shan, C.; Gu, Z.; Wang, L.; Li, P.; Song, G.; Gao, Z.; Yang, X. Preparation, characterization, and application of NR/SBR/Organoclay nanocomposites in the tire industry. *J. Appl. Polym. Sci.* **2011**, *119*, 1185–2011.
- (20) Blackman, E. J.; McCall, E. B. Relationships between the structures of natural rubber vulcanizates and their thermal and oxidative aging. *Rubber Chem. Technol.* **1970**, *43*, 651–663.
- (21) Shelton, J. R. Review of basic oxidation processes in elastomers*. *Rubber Chem. Technol.* **1972**, 359–380.
- (22) Studebaker, M. L.; Beatty, J. R. Oxidative hardening of SBR*. *Rubber Chem. Technol.* **1972**, 450–466.
- (23) Shelton, J. R. Oxidation and stabilization of rubbers*. *Rubber Chem. Technol.* **1983**, *56*, 71–86.
- (24) Hofmann, W. *Rubber Technology Handbook*, 1st ed.; Hanser Publishers: Munich, 1989.
- (25) Hamed, G. R.; Zhao, J. Tensile behavior after oxidative aging of gum and black-filled vulcanizates of SBR and NR. *Rubber Chem. Technol.* **1999**, *72*, 721–730.
- (26) Datta, R. N.; Huntink, N. M.; Datta, S.; Talma, A. G. Rubber vulcanizates degradation and stabilization. *Rubber Chem. Technol.* **2007**, *80*, 436–480.
- (27) Xiang, K.; Wang, X.; Huang, G.; Zheng, J.; Huang, J.; Li, G. Thermal ageing behavior of styrene-butadiene random copolymer: A study on the ageing mechanism and relaxation properties. *Polym. Degrad. Stab.* **2012**, *97*, 1704–1715.
- (28) Thavamani, P.; Bhowmick, A. K.; Khastgir, D. Effect of ageing on strength and wear of tank track pad compounds. *Wear* **1993**, *170*, 25–32.
- (29) Jovanović, S.; Samaržija-Jovanović, S.; Marković, G.; Jovanović, V.; Adamović, T.; Marinović-Cincović, M. Mechanical properties and thermal aging behaviour of polyisoprene/polybutadiene/styrene-butadiene rubber ternary blend reinforced with carbon black. *Composites, Part B* **2016**, *98*, 126–133.
- (30) Jovanović, S.; Samaržija-Jovanović, S.; Marković, G.; Jovanović, V.; Adamović, T.; Marinović-Cincović, M. Ternary NR/BR/SBR rubber blend nanocomposites. *J. Thermoplast. Compos. Mater.* **2018**, *31*, 265–287.
- (31) Stoček, R.; Kratina, O.; Ghosh, P.; Maláč, J.; Mukhopadhyay, R. Influence of Thermal Ageing Process on the Crack Propagation of Rubber Used for Tire Application. In *Deformation and Fracture Behaviour of Polymer Materials*; Grellmann, W.; Langer, B., Eds.; Springer Series in Materials Science; Springer Verlag, 2017; Vol. 247, pp 351–364.
- (32) Ahagon, A.; Kida, M.; Kaidou, H. Aging of tire parts during service. I. Types of aging in heavy-duty tires. *Rubber Chem. Technol.* **1990**, *63*, 683–697.

- (33) Kaidou, H.; Ahagon, A. Aging of tire parts during service. II. Aging of belt-skim rubbers in passenger tires. *Rubber Chem. Technol.* **1990**, *63*, 698–712.
- (34) Asano, A. *NMR Relaxation Studies of Elastomers*, 1st ed.; Elsevier Ltd., 2015; Vol. 86.
- (35) Gillen, K. T.; Celina, M. Predicting polymer degradation and mechanical property changes for combined radiation-thermal aging environments. *Rubber Chem. Technol.* **2018**, *91*, 27–63.
- (36) Patel, M.; Chinn, S.; Maxwell, R. S.; Wilson, T. S.; Birdsell, S. A. Compression set in gas-blown condensation-cured polysiloxane elastomers. *Polym. Degrad. Stab.* **2010**, *95*, 2499–2507.
- (37) Howse, S.; Porter, C.; Mengistu, T.; Petrov, I.; Pazur, R. J. Experimental determination of the quantity and distribution of chemical crosslinks in unaged and aged natural rubber. II: A sulfur donor system. *Rubber Chem. Technol.* **2019**, *92*, 513–530.
- (38) Morrison, N. J.; Porter, M. Temperature effects on the stability of intermediates and crosslinks in sulfur vulcanization. *Rubber Chem. Technol.* **1984**, *57*, 63–85.
- (39) Boonkerd, K.; Deeprasertkul, C.; Boonsomwong, K. Effect of sulfur to accelerator ratio on crosslink structure, reversion, and strength in natural rubber. *Rubber Chem. Technol.* **2016**, *89*, 450–464.
- (40) Aprem, A. S.; Joseph, K.; Thomas, S. Recent developments in crosslinking of elastomers. *Rubber Chem. Technol.* **2005**, *78*, 458–488.
- (41) Dong, H.; Luo, Y.; Lin, J.; Bai, J.; Chen, Y.; Zhong, B.; Jia, D. Effects of modified silica on the co-vulcanization kinetics and mechanical performances of natural rubber/styrene–butadiene rubber blends. *J. Appl. Polym. Sci.* **2019**, No. 48838.
- (42) Saalwächter, K.; Ziegler, P.; Spyckerelle, O.; Haidar, B.; Vidal, A.; Sommer, J.-U. ^1H multiple-quantum nuclear magnetic resonance investigations of molecular order distributions in poly-(dimethylsiloxane) networks: Evidence for a linear mixing law in bimodal systems. *J. Chem. Phys.* **2003**, *119*, 3468–3482.
- (43) Baum, J.; Pines, A. NMR studies of clustering in solids. *J. Am. Chem. Soc.* **1986**, *108*, 7447–7454.
- (44) Saalwächter, K. Proton multiple-quantum NMR for the study of chain dynamics and structural constraints in polymeric soft materials. *Prog. Nucl. Magn. Reson. Spectrosc.* **2007**, *51*, 1–35.
- (45) Chassé, W.; Valentín, J. L.; Genesky, G. D.; Cohen, C.; Saalwächter, K. Precise dipolar coupling constant distribution analysis in proton multiple-quantum NMR of elastomers. *J. Chem. Phys.* **2011**, *134*, No. 044907.
- (46) Jakisch, L.; Garaleh, M.; Schäfer, M.; Mordvinkin, A.; Saalwächter, K.; Böhme, F. Synthesis and structural NMR characterization of novel PPG/PCL conetworks based upon heterocomplementary coupling reactions. *Macromol. Chem. Phys.* **2018**, *219*, No. 1700327.
- (47) Duer, M. J. *Introduction to Solid-State NMR Spectroscopy*, 1st ed.; Wiley: New Delhi, 2010.
- (48) Saalwächter, K.; Herrero, B.; López-Manchado, M. A. Chemical shift-related artifacts in NMR determinations of proton residual dipolar couplings in elastomers. *Macromolecules* **2005**, *38*, 4040–4042.
- (49) Valentín, J. L.; Mora-Barrantes, I.; Carretero-González, J.; López-Manchado, M. A.; Sotta, P.; Long, D. R.; Saalwächter, K. Novel experimental approach to evaluate filler-elastomer interactions. *Macromolecules* **2010**, *43*, 334–346.
- (50) Klat, D.; Karimi-Varzaneh, H. A.; Lacayo-Pineda, J. Phase morphology of NR/SBR blends: Effect of curing temperature and curing time. *Polymers* **2018**, *10*, No. 510.
- (51) Choi, S. S.; Kim, J. C. Lifetime prediction and thermal aging behaviors of SBR and nbr composites using crosslink density changes. *J. Ind. Eng. Chem.* **2012**, *18*, 1166–1170.
- (52) Wittmer, A.; Wellen, R.; Saalwächter, K.; Koschek, K. Moisture-mediated self-healing kinetics and molecular dynamics in modified polyurethane urea polymers. *Polymer* **2018**, *151*, 125–135.
- (53) Schäler, K.; Achilles, A.; Bärenwald, R.; Hackel, C.; Saalwächter, K. Dynamics in crystallites of poly(ϵ -caprolactone) as investigated by solid-state NMR. *Macromolecules* **2013**, *46*, 7818–7825.
- (54) Knörger, M.; Heuert, U.; Schneider, H.; Barth, P.; Kuhn, W. Spatially resolved and integral NMR investigation of the aging process of carbon black filled natural rubber. *Polym. Bull.* **1997**, *38*, 101–108.
- (55) Somers, A. E.; Bastow, T. J.; Burgar, M. I.; Forsyth, M.; Hill, A. J. Quantifying rubber degradation using NMR. *Polym. Degrad. Stab.* **2000**, *70*, 31–37.
- (56) Parker, D. D.; Koenig, J. L. Solid-state ^{13}C -NMR studies of changes in crosslinked carbon structure of natural rubber during heating under air and nitrogen environments. *J. Appl. Polym. Sci.* **1998**, *70*, 1371–1383.
- (57) Mott, P. H.; Roland, C. M. Aging of natural rubber in air and seawater. *Rubber Chem. Technol.* **2001**, *74*, 79–88.
- (58) Naumova, A.; Tschierske, C.; Saalwächter, K. Orientation-dependent proton double-quantum NMR build-up function for soft materials with anisotropic mobility. *Solid State Nucl. Magn. Reson.* **2017**, *82–83*, 22–28.
- (59) Hohwy, M.; Jakobsen, H. J.; Edén, M.; Levitt, M. H.; Nielsen, N. C. Broadband dipolar recoupling in the nuclear magnetic resonance of rotating solids: A compensated C7 pulse sequence. *J. Chem. Phys.* **1998**, *108*, 2686–2694.

6. Effects of Artificial Weathering in NR/SBR Elastomer Blends¹

Controlled accelerated weathering is a representative method for replicating the effects of long-term outdoor aging in a short time. The setup induces macroscopic and microscopic changes in the polymer through the action of UV radiation, oxygen, ozone, water, and heat.

This chapter is an extension of the previous paper on unaged samples. Weathering up to a duration of about 1000 h is performed and the molecular and bulk changes in NR, SBR, and NR/SBR blend are analyzed. The evolution of cross-link densities over the weathering duration is measured by low-field MQ NMR. The changes in D_{res} at two different weathering intervals with respect to the unaged samples are compared and discussed using results from MAS NMR, which concludes that the blend is better suited for long-term usage compared to individual vulcanizates of NR and SBR. This is supported by the results of the modulus measured by DMTA. IR spectroscopy and AFM show proof of the formation of a stiff surface formed by weathering. This region is categorized with short T_2 time of 20 μ s. The formation of mobile defects is also discussed.

Contributor Roles Taxonomy (CRediT) author statement

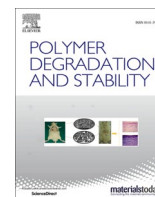
Akshay Karekar: Conceptualization, methodology, validation, formal analysis, investigation, data curation, writing – original draft, visualization, project administration. **Carsten Schicktanz:** Investigation, visualization. **Muhammad Tariq:** Investigation, writing – original draft, visualization. **Katja Oßwald:** Conceptualization, methodology, validation, resources, supervision. **Katrin Reincke:** Conceptualization, methodology, validation, resources, writing – review & editing, supervision. **Valentin Cepus:** Validation, investigation, resources, writing – original draft, writing – review & editing, visualization. **Beate Langer:** Resources, writing – review & editing, supervision, funding acquisition. **Kay Saalwächter:** Conceptualization, methodology, software, validation, resources, writing – review & editing, supervision, project administration, funding acquisition.

¹The associated open-access article and the supporting information are reprinted here under a Creative Commons Attribution 4.0 International Public License (CC BY 4.0). **Authors:** Akshay Karekar, Carsten Schicktanz, Muhammad Tariq, Katja Oßwald, Katrin Reincke, Valentin Cepus, Beate Lange, and Kay Saalwächter. **Source:** *Polym. Degrad. Stab.*, **2023**, *208*, 110267, DOI: 10.1016/j.polymdegradstab.2023.110267. **Website:** <https://www.sciencedirect.com/science/article/pii/S0141391023000198?v=s5#ecom0001>. No changes were made to the article and the supporting information.



Contents lists available at ScienceDirect

Polymer Degradation and Stability

journal homepage: www.journals.elsevier.com/polymer-degradation-and-stability

Effects of artificial weathering in NR/SBR elastomer blends

Akshay Karekar^{a,*}, Carsten Schick Tanz^{b,1}, Muhammad Tariq^{c,2}, Katja Obwald^d,
Katrin Reincke^d, Valentin Cepus^{b,d}, Beate Langer^b, Kay Saalwächter^{a,*}

^a Institut für Physik, Martin-Luther-Universität Halle-Wittenberg, Betty-Heimann-Str. 7, Halle (Saale) 06120, Germany

^b Fachbereich Ingenieur- und Naturwissenschaften, Hochschule Merseburg – University of Applied Sciences, Eberhard-Leibnitz-Str. 2, Merseburg 06217, Germany

^c Institut für Physik, Martin-Luther-Universität Halle-Wittenberg, Von-Danckelmann-Platz 3, Halle (Saale) 06120, Germany

^d Polymer Service GmbH Merseburg, Geusaer Str. 81f, Merseburg 06217, Germany

ARTICLE INFO

Keywords:

Elastomer blend
Cross-link density
Nuclear magnetic resonance
Residual dipolar coupling
Weathering
Degradation

ABSTRACT

Degradation of polymer blends occurs by the constituent phases undergoing distinct chemical changes that depend on their unique chemical structures. This makes predicting and establishing a structure-property relationship for each phase necessary as well as challenging. In this work, the molecular and physical changes occurring in sulfur-cross-linked natural rubber (NR), styrene–butadiene rubber (SBR), and their 50/50 blend subjected to accelerated weathering are analyzed by ¹H nuclear magnetic resonance (NMR) spectroscopy, Fourier-transform infrared (FTIR) spectroscopy, atomic-force microscopy (AFM), and dynamic mechanical thermal analysis (DMTA). NMR transverse relaxation time (T_2) studies suggest the formation of rigid components due to weathering. FTIR and AFM reveal that this is related to the formation of a stiff surface due to chemical modifications, which shows up as an additional thermal transition in the DMTA curves. Low-field double-quantum (DQ) NMR studies of the cross-link density, by the residual dipolar coupling constant (D_{res}), of SBR show a continuous increase in its cross-link density over the weathering duration (988 h). In contrast, NR exhibits dominant chain scission reactions resulting in defects, with both materials demonstrating the formation of different chain lengths. During the first 168 h, NR also undergoes modification of sulfur bond lengths, which is also observed in the blend. The blend largely follows an intermediate trend of cross-link densities compared to the two polymers but shows signs of lesser chain modifications than a weighted average of the two polymers. This is confirmed by phase-resolved DQ magic-angle spinning (MAS) NMR experiments whereby the peak-specific D_{res} of the blend was measured to be less modified than that of the individual vulcanizates, thus proving that the blend is more resistant to weathering than its constituent elastomers.

1. Introduction

In a natural setting, chemical and physical changes of polymeric materials occur due to various environmental stresses like heat, humidity, solar radiation (UV), atmosphere, etc., in a process referred to as weathering [1]. These detrimental factors eventually cause an early failure due to cracking, surface erosion, loss of flexibility, change in color, and breakdown of the chains. In elastomers, the unsaturated bonds are especially prone to these attacks. The susceptibility of aromatic rings to UV has been known, too [2]. The temperature dependence, characterized by an Arrhenius or slightly non-Arrhenius behavior, yields activation energy (E_a) of photodegradation values

around 12–20 kJ/mol for aromatic thermoplastics [3] and 27–50 kJ/mol for aliphatic thermoplastics. As much as the extent of weathering a polymer can undergo depends on its chemical structure, the constituent additives present in a polymer composition and the associated thermal history of the polymer system regulate its longevity [1].

The micro- and macrostructural integrity of cross-linked elastomers are directly linked to the density of cross-linking. Generally, a continuous rise in elastic recovery and stiffness is obtained with increasing cross-link density. Properties like tensile and tear strength, toughness, and resistance to fatigue increase up to a particular loading of the cross-linker and reduce gradually thereafter. Studying the network density becomes all the more necessary but tricky when dealing with

* Corresponding authors.

E-mail addresses: akshay.karekar@physik.uni-halle.de (A. Karekar), kay.saalwaechter@physik.uni-halle.de (K. Saalwächter).

¹ This paper is dedicated to the memory of Mr. Carsten Schick Tanz, who passed away unexpectedly during the preparation of this work.

² Present address: Basic Science Department, University of Engineering and Technology Taxila, Taxila 47040, Pakistan.

<https://doi.org/10.1016/j.polymdegradstab.2023.110267>

Received 4 November 2022; Received in revised form 6 January 2023; Accepted 10 January 2023

Available online 13 January 2023

0141-3910/© 2023 The Authors. Published by Elsevier Ltd. This is an open access article under the CC BY license (<http://creativecommons.org/licenses/by/4.0/>).

technologically and commercially viable polymer systems like elastomer blends. In elastomer blends, differences in the phase-specific cross-link densities can occur by a preferential distribution of the cross-linker in either polymer phase, where migration of the cross-linker across the interfaces can occur. Apart from the extent of reactivity between a curative and an elastomer phase, blend properties such as polymer component ratio, viscosities of the constituent polymers, etc., as well as the mixing procedure, dictate the migration of the additives [4–7]. In blends with phases having largely different curing rates, depletion of cross-linker due to its uptake in the phase with the higher curing rate can induce migration of cross-linker from the other phase, thus depriving the other phase. This results in a cure imbalance and expectedly large differences in the performance of the blend phases and the blend itself. Processes like weathering intensify these differences. All these factors warrant a phase-specific elucidation of cross-link densities for establishing structure–property relationships, and for product development.

The conventional methods of evaluating cross-link density of elastomers by tensile testing (using the Mooney-Rivlin phenomenological equation) [8,9], equilibrium swelling (using the Flory-Rehner equation) [10], and rheology [11] are limited in their applicability when the system involves an elastomer blend. The use of atomic force microscopy (AFM) has also been reported [12] but it lacks a quantitative assessment of the cross-link density.

Perhaps the most important technique for the elucidation of structure and chain dynamics in polymers is nuclear magnetic resonance (NMR) spectroscopy, which has thus been employed for cross-link density measurements in blends. Early phase-resolved studies using NMR involved the measurement of proton line-widths in solvent-swollen blend specimens [13–16]. This approach is qualitative at best, as discussed in recent work by this group [17], in which use of a quantitative alternative was made, as explained below. Using a more direct method, proof of curative migration due to diffusion and solubility in natural rubber and polybutadiene blends has been demonstrated by Klei and Koenig by NMR imaging based upon a Carr-Purcell spin-echo pulse sequence with a gradient magnetic field [18]. The curatives had a higher solubility in polybutadiene and thus resulted in a heterogeneous network.

Cross-link densities in dynamically cured thermoplastic vulcanizates of polypropylene and ethylene–propylene–diene rubber (EPDM) were studied by analyzing the line broadening in single 90° pulse ¹H magic-angle spinning (MAS) experiments [19]. In a similar system, qualitative assessments of the cross-link density were made by using different models along with cross-polarization (CP) curves obtained from ¹H–¹³C CP-MAS experiments [20].

In all these latter approaches, the measured results depend upon the through-space orientation-dependent ¹H–¹H (or ¹H–¹³C) dipole–dipole interaction, which reports on the cross-link density specifically. In a polymer, the spins exhibit a residual dipolar coupling (D_{res}) due to the presence of constraints like entanglements, cross-links, crystallites, etc. that cause incomplete averaging of segmental motions. D_{res} of protons measured under low-resolution conditions has been long used as a measure of cross-link density [21–23], and is connected to the dynamic order parameter (S_b) of the polymer backbone as:

$$S_b = \frac{D_{res}}{D_{ref}} = \frac{3}{5N} \frac{1}{M_c} \quad (1)$$

D_{ref} is polymer-specific coupling whose values for a variety of systems have been reported [24,25], and takes pre-averaging due to fast chain modes within a Kuhn segment into consideration. The equation is a measure of the average molecular weight (M_c , in units of mol/kg) of chains in terms of the number of segments (N) between cross-links or other topological constraints. Through the measurement of D_{res} via a multiple-quantum (MQ) pulse sequence [26], based on the pulse sequence of Baum and Pines [27], this approach has been applied for the measurement of cross-link density and its distribution in complex materials like polyisoprene/polybutadiene (IR/BR) blends [28] and natural

rubber/styrene–butadiene rubber (NR/SBR) blends [29]. Though quantitative, a complete distinction of phase-specific cross-link densities could not be established for these systems as the components were made of similar dipolar couplings. This method has also been extended to elastomer/plastic blends of EPDM and ultralow-density polyethylene (ULDPE) blends [30], where a spin–spin relaxation time (T_2) filter was used to suppress the signals arising from crystalline and crystalline–amorphous interface fractions of the ULDPE phase and to obtain cross-link density of the EPDM phase.

In our recent paper [17], a ¹H NMR methodology to quantitatively measure the cross-linked density in the individual phases of NR/SBR blends subjected to thermo-oxidative aging was demonstrated. Phase-distinction was achieved by spinning the sample at the magic-angle and using a homonuclear double-quantum (DQ) dipolar recoupling pulse sequence [31].

In the present paper, the role of artificial weathering in the dissimilar aging of NR and SBR phases in their blend is addressed. NR and SBR react differently to oxygen and ozone. SBR itself is composed of randomly bonded aromatic and aliphatic segments. Brown et al. have conducted extensive studies by thermo-oxidative aging and weathering, which show different effects with respect to the aging of NR and SBR in the blend [32,33]. During weathering the high energy UV radiation has been recognized to promote various reactions [34]. Thus, due to their markedly different characteristics, one may expect unique changes in the blend phases that could lead to a distribution of cross-link densities.

The cross-link densities in NR, SBR, and their blend subjected to prolonged weathering are first investigated by a ¹H low-field MQ NMR spectroscopy based on the robust pulse sequence introduced earlier. The evolution of cross-link densities of NR and SBR within the blends at different intervals of weathering is quantified through phase-specific studies by ¹H DQ MAS NMR spectroscopy using the BaBa-xy16 pulse sequence [31]. The formation of highly constrained fractions due to weathering is evaluated by free induction decay (FID) combined with magic-sandwich echo (MSE)–FID and Hahn-echo T_2 relaxometry, which is suitable to quantify solid-like components with dipolar couplings too strong for the above-mentioned technique. Further, the changes in the materials are chemically investigated by Fourier-transform infrared (FTIR) spectroscopy. Lastly, to get a physical perspective, dynamic mechanical thermal analysis (DMTA) and atomic force microscopy (AFM) are employed for probing the macroscopic and microscopic moduli, respectively.

2. Experimental section

2.1. Sample preparation

2.1.1. Materials

Compounds of NR, SBR, and NR/SBR blend (50/50 ratio by parts per hundred rubber, phr) were prepared using the composition reported in a previous work [17]. Solution-polymerized styrene–butadiene rubber (grade SPRINTAN SLR 4602-Schkopau, $T_g = -25$ °C) was supplied by Trinseo Deutschland GmbH (now Synthos Schkopau GmbH, Schkopau, Germany). This is composed of 21.1 % styrene and 62.1 % of the vinyl copolymer 1,2-polybutadiene. Thus, 1,4-polybutadiene constitutes 16.8 % of the rubber. Natural rubber (grade SMR10, $T_g = -60$ °C) was supplied by Weber and Schaer GmbH & Co. KG (Hamburg, Germany). NR was masticated by 10 passes over a two-roll mill before use in formulations.

The three compounds were formulated based on a conventional vulcanization system consisting of 2.5 phr sulfur (Carl Roth GmbH, Germany) and 1.5 phr n-cyclohexyl-2-benzothiazole sulfenamide (CBS) accelerator (TCI Deutschland GmbH, Germany), along with 1 phr stearic acid (Carl Roth GmbH, Germany) and 3 phr zinc oxide (Carl Roth GmbH, Germany) activators. The raw materials were mixed for 10 min at 50 °C and a rotor speed of 50 rpm in a Haake Rheomix 600p (Thermo Scientific, Germany) lab-scale internal mixer to a fill factor of 0.7. The mixed

compounds were cross-linked into 2 mm thick plates on a hydraulic press based on their 90 % curing times (t_{90}) of 4, 8, and 22 min for NR, SBR, and the blend, respectively, obtained according to DIN 53529 on an Elastograph MDR (Göttfert, Germany) moving-die rheometer. For comparative studies, pristine polymers with similar thermal histories were also prepared.

2.1.2. Weathering

Accelerated weathering was performed according to ISO 4892-2 (2013) Method A, Cycle 1 in a Q-SUN Xe-2 rotating rack xenon arc test chamber (Q-Lab Corporation, USA) equipped with a Xenon arc lamp emitting light equivalent to direct sunlight (Daylight-Q) using a silica glass filter. Rectangular specimens ($100 \times 10 \times 2 \text{ mm}^3$) were fixed on specimen holders by clamping the ends. These holders were then mounted on the rotary rack and subjected to an irradiation of $60 \pm 2 \text{ W/m}^2$ in the range of 300 nm and 400 nm. The radiation exposure corresponded to an energy of about 213 MJ/m^2 .

The specimens were subjected cyclically to light for 102 min followed by a spray cycle of 18 min by reverse-osmosis deionized water for a total exposure duration of 988 h. The chamber was maintained at a temperature of $38 \pm 3 \text{ }^\circ\text{C}$ and a relative humidity of $50 \pm 10 \%$, with the black-standard temperature at $65 \pm 3 \text{ }^\circ\text{C}$. Samples were picked at durations of 72, 168, 504, and 988 h of weathering for analyses.

2.2. Methods

2.2.1. Dynamic mechanical thermal analysis (DMTA)

Dynamic mechanical properties were measured in air in the torsion mode on an ARES-G2 (TA Instruments, USA). Specimens with a width of 10 mm and a thickness of 2 mm were mounted. The specimens were pre-stretched by an axial force of 0.2 N before cooling down to $-80 \text{ }^\circ\text{C}$ using a chiller. Following a soaking time of 5 min, a temperature ramp was performed up to $100 \text{ }^\circ\text{C}$ at a ramp rate of 5 K/min. Strain amplitude and frequency were set to 1 % and 1 Hz, respectively.

2.2.2. AFM nanoindentation measurements

For AFM nanoindentation experiments, the atomic force microscope NanoWizard 4 from JPK instruments (Germany) was used. Measurements were performed in contact mode using NSC 15 cantilevers, purchased from Mikromasch, with a nominal spring constant of 40 N/m and resonance frequency of 325 kHz, and a silicon tip with a radius of 8 nm, full tip cone angle of 40° , and tip height 12–18 μm (manufacturer's data). The employed cantilevers were calibrated using the contact-free method.

In AFM indentation, the tip of the AFM cantilever is brought into contact with the sample surface using a z-piezoscanner and pressed into the surface. The corresponding applied force is measured as a function of tip displacement, thus generating a force-distance curve. After the approach cycle, the tip is retracted back to its rest position. The indentation depth can be calculated as the z-piezoscanner displacement minus the cantilever deflection [35]. For all the measurements, a constant tip speed of 2 $\mu\text{m/s}$ was set. More than 50 indentation measurements were performed at different spots of the core region as well as of the skin region across the cut surface of the weathered sample. A similar number of measurements was also carried out on an unexposed sample. The suitable spots for the measurements were selected by first imaging the surface of the sample in the tapping mode of AFM operation. Selected spots were lying on locally flat areas and far from any grooves or adjacent walls/structures.

Samples for AFM measurements were prepared by microtomy using liquid nitrogen. Slices (size $\approx 2 \times 2 \text{ mm}^2$) of the samples were obtained by cutting a thin cross-section from the center of the sample bar ($80 \times 10 \times 2 \text{ mm}^3$). The obtained slices were then placed on freshly cleaned silicon (Si/SiO₂) substrates. Measurements on the skin region were performed within about 30 μm from the directly exposed face, whereas the measurements on the core region were performed at the central part

of the slice.

2.2.3. FTIR spectroscopy

The FTIR spectroscopic investigations were conducted on a Bruker Vertex 70 FTIR spectrometer (Germany) equipped with a Platinum ATR cell and connected to a Hyperion 2000 IR microscope with a 15 X Cassegrain objective. IR spectra of the skin and the core of the specimens were recorded at a resolution of 4 cm^{-1} from 4000 to 600 cm^{-1} using the ATR cell. IR microscopic mappings were recorded in the same spectral range in reflectance mode, processed with Kramers-Kronig transformation to extract absorbance information, and represented as Gram-Schmidt integral in a pseudo-color representation.

The sample stripes were fixed in Micro Vice Clamps equipped with SliceIR Clamps (both S.T. Japan) and were cut with a fresh razor blade at an angle of 90° for IR microscopy.

2.2.4. Static low-field time-domain ^1H NMR spectroscopy

Experiments were performed on a Bruker minispec mq20 (Germany) benchtop spectrometer having a magnetic field strength of approximately 0.5 T, which corresponds to a resonance frequency of 19.95 MHz. Small discs were punched from the weathered specimens and stacked in a 10 mm NMR tube up to a height of 6 mm. A Bruker BVT 3000 temperature controller was used to maintain a constant measurement temperature of $80 \pm 0.1 \text{ }^\circ\text{C}$. The 90° pulse length and receiver dead time corresponded to 2.6 μs and 11 μs , respectively. The recycle delay ($5T_1$) for the pristine, unexposed, and weathered samples were determined to be about 0.6 s for NR and 0.2 s for SBR.

2.2.5. High-field ^1H DQ MAS NMR spectroscopy

Chemically (phase-resolved) measurements were performed on a Bruker Avance III (Germany) spectrometer with a magnetic field strength of 9.4 T, which corresponds to a resonance frequency of 400 MHz. A 1 mm thick rubber ring (3 mm outer diameter and 2 mm inner diameter) was packed at the center of a 4 mm zirconia rotor with a Vespel® rotor cap. The sample was held in position by polytetrafluoroethylene spacers on either side. A Bruker BVT 3000 temperature controller was used for measurements at $80 \pm 0.1 \text{ }^\circ\text{C}$. The 90° pulse corresponded to a length of 2.5 μs at a pulse power of 54 W.

3. NMR theory

3.1. Spin-spin relaxation time (T_2) measurements

Also known as the transverse relaxation time, T_2 can be used to quantitatively distinguish the amounts of different fractions based on the ease of their segmental mobility within a specimen. In a weathered specimen, the stiff, tightly cross-linked, and/or oxidized fractions can be separated from the moderately cross-linked mobile regions and the fast-moving defects (in cross-linked rubbers these are the loops, dangling chain-ends, and sol fractions that are mechanically inelastic). In a T_2 sense, rigid (possibly glassy) fractions formed due to shorter chain segments have a faster relaxation decay (shorter T_2), whereas the others have slower relaxation decay (longer T_2). The most constrained fractions, in this case, the regions closer to the irradiated surface, are associated with a rigid-limit coupling between the protons as high as about 30 kHz. This translates to a T_2^{eff} (effective T_2) of about 20 μs for the stiff/rigid components of the surface and underneath. The corresponding shape parameter (β_r) of the rigid fractions in a multicomponent modified-exponential decay fitting function ($\propto f_x \exp[-(t/T_{2,x}^{\text{eff}})^{\beta_x}]$) takes a value of 2 (Gaussian decay) in this case. Measuring the rigid fraction (f_r) by an FID experiment (by a single 90° pulse) alone leads to underestimated results due to a loss in the initial decay signal owing to a longer receiver dead time (RDT, see Fig. S1 in Supporting Information). It is 11 μs for the low-field spectrometer used in these studies. The loss in the initial part of the signal can be compensated by performing the

pulsed version of the magic-sandwich echo (MSE) experiment that performs a time-reversal by refocusing multispin dipolar interactions of the decay signal [36]. The signals from both these experiments can be simultaneously fitted to obtain the relevant fractions and their respective transverse relaxation times [37]. Slowly decaying components having relatively larger mobility are also probed by stitching a Hahn-echo signal to the FID. Fig. S1 in the Supporting Information illustrates this and the role of MSE-FID for NR and SBR weathered up to 988 h.

A three-component fitting function is required to completely gage these samples. Due to the higher number of data points obtained in an FID experiment, a 10 % weighting is applied. The three fractions obtained are: a rigid fraction due to tightly cross-linked or oxidized (due to weathering) regions, a second fraction that is representative of the majority of the vulcanizate's volume composed of relatively softer components of moderate cross-linking, and a third fraction consisting of the (mobile) defect fraction. A detailed discussion can be found in Section 4.3.2.

3.2. Static low-field time-domain ^1H MQ-NMR

As introduced earlier, cross-link densities on a low-field spectrometer are measured using an MQ pulse sequence [26]. The method has been detailed elsewhere [38] and is therefore described here only very shortly. The experiment yields two signals as a function of pulse sequence duration, τ_{DQ} : a double quantum signal (I_{DQ}) and a decaying reference signal (I_{ref}). I_{DQ} results from contributions of coupled spins at shorter times. I_{ref} also contains a contribution from uncoupled spins (defects) that behave isotropically. A sum MQ signal ($I_{\Sigma\text{MQ}} = I_{\text{ref}} + I_{\text{DQ}}$) is a fully dipolar refocused signal that decays due to molecular motions. In networks, this decay is found to be nearly equal to that of an I_{DQ} signal. This enables the removal of the effects of molecular motions from I_{DQ} through normalization by a point-by-point division, satisfying the condition: $I_{\text{nDQ}} = I_{\text{DQ}}/(I_{\Sigma\text{MQ}} - \text{defects})$. The resulting normalized DQ (nDQ) signal, I_{nDQ} , is an inverted dephasing curve that reaches a 0.5 intensity limit upon optimum removal of the defect fraction. The defect fraction can be normally described using a single- or bi-exponential decay function [39]. The resulting nDQ build-up curve is a network-structure-only quantity and is independent of temperature, as long as it is measured far above T_g .

The fitting function to this build-up curve is a numerical integral assuming a log-normal distribution of coupling constants ($\ln(D_{\text{res}})$) [40]. The Abragam-like kernel function [41], shown in Eq. (2), is suitable to describe data taken on homogeneous rubbers based upon homopolymers without long side chains.

$$I_{\text{nDQ}}(\tau_{\text{DQ}}, D_{\text{res}}) = 0.5 \left[1 - \exp \left\{ - (0.378 \epsilon D_{\text{res}} \tau_{\text{DQ}})^{1.5} \right\} \right] \times \cos(0.583 \epsilon D_{\text{res}} \tau_{\text{DQ}}) \quad (2)$$

For this static experiment, the efficiency factor $\epsilon = 1$. τ_{DQ} is the instantaneous DQ evolution time for the respective point in the I_{ref} and I_{DQ} signals, both of which decay at longer τ_{DQ} . The log-normal probability distribution function of residual couplings, $P(\ln(D_{\text{res}}))$ reads:

$$P(\ln(D_{\text{res}})) = \frac{1}{\sigma_{\ln} \sqrt{2\pi}} \exp \left[- \frac{\{\ln(D_{\text{res}}) - \ln(D_{\text{med}})\}^2}{2\sigma_{\ln}^2} \right] \quad (3)$$

It provides the average D_{res} as a median value (D_{med}) and a logarithmic distribution width (σ_{\ln}). The standard deviation is a positive and dimensionless quantity, where $\sigma_{\ln} = 0.5$ corresponds roughly to a half-decade-wide distribution. For narrow distributions, the build-up curve can be approximated by an inverted Gaussian, and the cross-link density (D_{med}) is encoded in its initial slope.

3.3. Phase-resolved high-field ^1H DQ MAS NMR

The broad and featureless spectrum of a solid sample in a static

experiment can be improved by spinning it at moderately high frequencies in a MAS experiment. A demonstration of this can be seen in Fig. 1 for the three unaged samples of cross-linked NR, SBR, and the 50/50 blend, one-dimensional spectra of which are obtained after Fourier transformation of the respective FIDs following a 90° pulse. Thus, MAS yields high-resolution spectra for phase-specific studies.

The cross-link densities in this case can be measured by obtaining build-up curves in a 2D fashion using the BaBa-xy16 pulse sequence. Like the static MQ experiment discussed earlier, this DQ MAS experiment yields the typical I_{DQ} and I_{ref} signals, which can be obtained by taking one-dimensional projections of every two-dimensional resonance peak of interest. The rotor-synchronized pulse sequence facilitates obtaining points at every rotor period. However, for these studies, signals at every even multiple of the rotor period were measured.

The fitting function is based on that used for the static measurements. The quantum mechanical treatment of this experiment gives the efficiency factor in the kernel function (Eq. (2)) that is reduced to $\epsilon = 0.78$ [31].

4. Results and discussion

4.1. Macroscopic moduli

Weathering brings about physical and chemical changes in the exposed specimens. The cyclic water sprays cause cooling and shrinking of the specimen, whereas UV irradiation leads to heating and expansion. The resulting expansion and contraction lead to specimen deformation and cracks formation and their propagation. This aspect is discussed in more detail in Section 4.3.1.

The DMTA experiments give a first indication of the bulk changes occurring in the weathered samples. The storage and loss modulus (G' and G'' , respectively) obtained from temperature ramps of NR and SBR samples subjected to various durations of weathering are shown in Fig. 2. Below T_g , NR reveals a reduction in modulus with the exposure duration. With an increase in the temperature, the 72 and 168 h weathered specimens demonstrate identically marginal retention of G' , indicating hardening compared to the unaged specimen. Thus, a

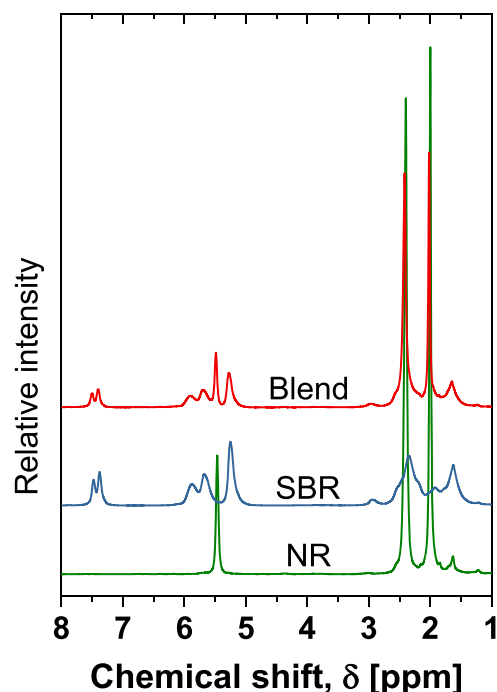


Fig. 1. Chemically resolved peaks in ^1H spectrum of cross-linked NR, SBR, and the blend. (Adapted from Ref. [17]).

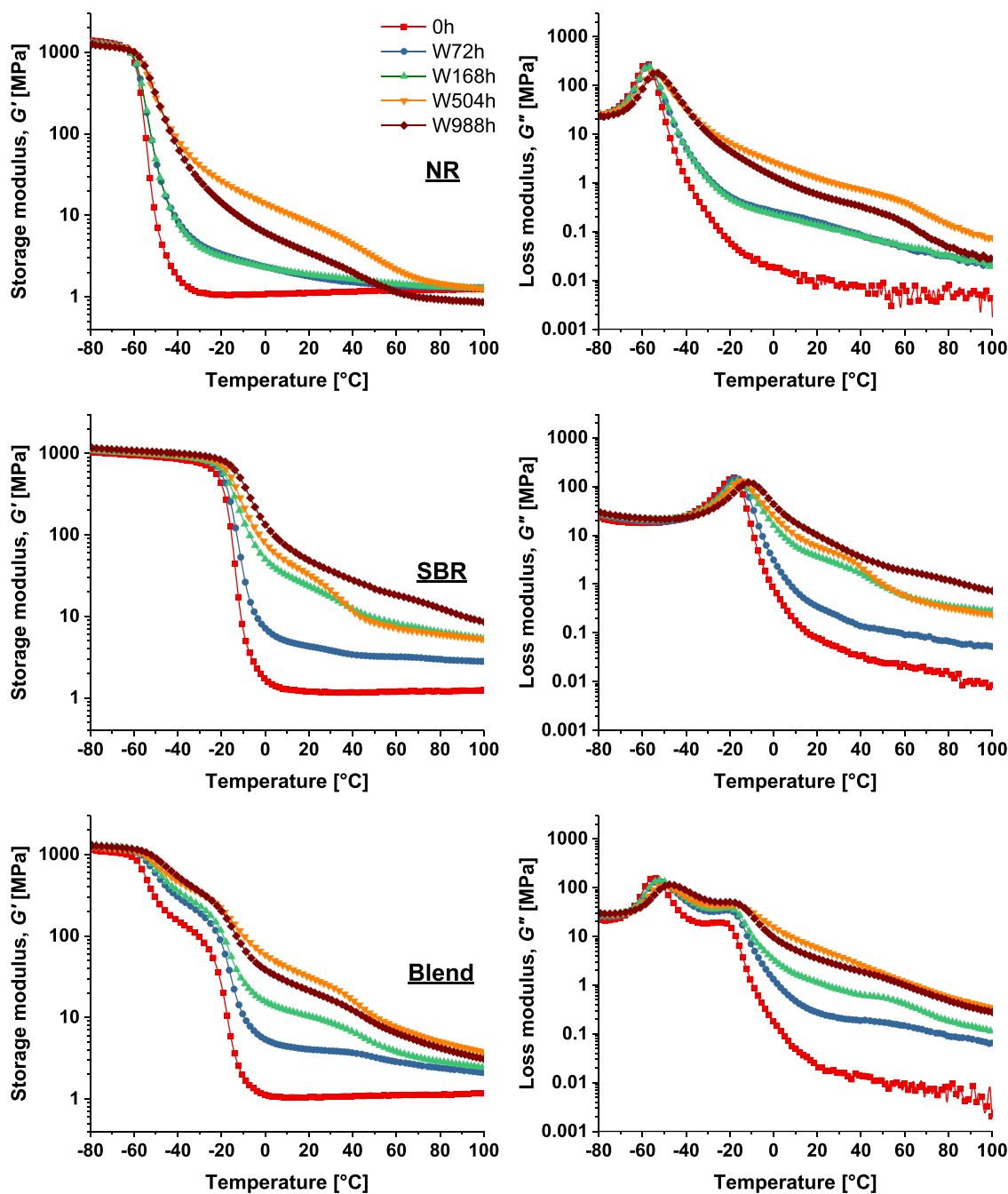


Fig. 2. DMTA temperature ramps of the storage (left) and loss (right) moduli of NR, SBR, and a 50/50 blend of NR and SBR after various weathering (W) durations.

marginal increase in the T_g from the unaged sample is also observable. Distinct changes occur around 500 h of weathering, where stiffening of the sample due to weathering leads to a significant increase in modulus. In addition, a broad second transition around 60 °C can also be seen, which probably is an indication of a second glass transition corresponding to over cross-linked regions of the specimen. With further weathering, stiffness drops below that of the 504 h weathered sample. At higher temperatures, the specimen undergoes softening, well below the plateau modulus of 0 h specimen, due to softening of the hardened regions and the possible presence of decomposed chains.

In the case of SBR, the rubber continuously stiffens in both temperature regions due to weathering-induced hardening. The additional transition appearing upon 500 h of weathering seems to be due to differently aged regions within the sample volume. One may expect that the surface is more aged than the core, thus creating regions of different

stiffness [42]. This difference seems to be lost after further weathering. The additional transition observed in the previous weathering interval probably is masked due to the stiffening of the overall sample. The relative stiffening in SBR is higher than NR and remains a decade stiffer even at 100 °C.

The temperature ramps of the blends provide some important insight into the performance of the material in relation to NR and SBR single vulcanizates. Unlike NR, the modulus in the lowest temperature region increases with the weathering duration as observed in SBR. At higher, yet sub-zero temperatures, the 72 and 168 h specimens almost overlap as in the case of NR but diverge somewhat after the SBR T_g . The most significant distinct observation in the blend in comparison to the single vulcanizates is after weathering up to 504 and 988 h. While both NR and SBR respectively demonstrate a decrease and an increase in their moduli beyond their glass transition temperatures at the two weathering

durations, the blend shows almost no deviation in the moduli at these weathering intervals. Fig. S2 in the Supporting Information emphasizes these observations through an overlay of DMTA curves for the three materials at the two weathering durations. A key takeaway message from these arguments is that the cross-link density, which imparts the modulus in the material compositions considered here, is probably identical at the two weathering durations. This aspect will be discussed in detail in Section 4.4.

4.2. Chemical modifications due to weathering as studied by FTIR spectroscopy

Weathering is a depth-dependent phenomenon, where it starts at the exposed surface of the material and then proceeds into the bulk, thus creating a gradient of changes. It is important to note here that the specimen mounting setup in the weatherometer led to one face of the specimen always being hidden from direct irradiation and water sprinkles. One can hence hypothesize that chemical differences between the directly irradiated surface and the other regions, such as the core, would widen with continuous exposure. These chemical modifications are analyzed here by IR spectroscopy.

In a preparatory step, the cross-section of the prepared specimens was first observed in an IR microscope. Pseudo-color Gram-Schmidt plots of IR maps in reflectance mode were generated to provide a visual representation of the chemically modified/unmodified regions within the cross-section of the specimens. The Gram-Schmidt signal provides the integral IR reflectance intensity over all wavenumbers in the spectral range of the experiment. However, it must be considered that the surface quality will also interfere with the scattering intensities.

The warmer colors, i.e., higher Gram-Schmidt signals (higher total integral for all wavenumbers), within the bulk of SBR W168h in Fig. 3 are interpreted as the presence of higher amounts of hydrocarbon structures. In contrast, the cooler colors in the heat map, near the surface (UV irradiated side), are indicative of chemical changes, i.e., modification due to weathering, caused mainly by reaction with oxygen. This also serves as a first proof of the formation of 'skin' and 'core' regions across the sample thickness, due to distinct chemical and, possibly, physical differences. From the microscopic image in the background, a thick skin region for this specimen is observed to be up to about 95 μm from the surface. This demarcation is noted as the moderately modified yellow-green separation line in the Gram-Schmidt plot. Of course, a much more modified, thinner skin can be present immediately at the surface due to the gradient, but analyses of these regions are excluded here. The yellow-green blob on the right-end could be resulting from the topography effects of the surface and highlights the after all qualitative nature of the observation of the skin with this method. Microscopic

images of NR weathered up to the same duration demonstrated a skin thickness of about 60 to 80 μm .

The IR microscopy measurements were used as a control to probe the desired regions ('skin' and 'core') through ATR FTIR measurements. Overlays of absorption spectra for NR and SBR weathered to various durations can be found in Fig. 4. A general trend of peak broadening with the weathering duration can be observed in the core-specific spectra of both, NR and SBR.

In both NR and SBR, a broad $-\text{OH}$ stretching band is observed between 3660 and 3125 cm^{-1} in the unaged material due to hydroxyl groups present in CBS [2]. The signal intensity increases up to 168 h, possibly due to oxidation or hydration, but reduces thereafter as the additives are consumed [43]. A direct result of weathering in both materials is the occurrence of a carbonyl band at about 1713 cm^{-1} (see * in Fig. 4) after 168 h of weathering and is prominently present in the skin at 504 h but disappears in the core [44].

In NR, the asymmetric $=\text{C}-\text{H}$ stretching band at 3035 cm^{-1} (i) decreases from 0 h to 504 h [45], while the skin shows its complete loss at 504 h. Likewise, the asymmetric $-\text{CH}_3$ stretching (2959 cm^{-1} , ii) and asymmetric $-\text{CH}_2-$ stretching (2918 cm^{-1} , iii) bands also reduce with weathering. Further, the symmetric $-\text{CH}_3$ stretching and symmetric $-\text{CH}_2-$ stretching bands are seen as a single peak at 2849 cm^{-1} (iv) [45], which shows a decrease in intensity and suppression in the skin region at extended weathering.

To put this into context, in a thermo-oxidatively aged NR study [46], the $-\text{CH}_2-$ stretching vibration demonstrated peak retention, contrary to the observation made in the present work. Using only UV radiation, dos Santos et al. summarize the formation of different groups in polyisoprene (*cis*, *trans*, and NR) subjected to various wavelengths [45]. It was concluded that apart from the wavelength, the type of isomer and the pre-condition (presence of groups characteristic of partial oxidation) of the polymer dictate the effects of UV.

The $-\text{C}=\text{C}-$ stretching vibration occurs at 1662 cm^{-1} (v), whose intensity decreases with weathering. In the fingerprint region, the IR spectra are dominated by $-\text{CH}_3$ and $-\text{CH}_2-$ bending vibrations at 1452 cm^{-1} (vi) and 1375 cm^{-1} (vii), respectively, and the rocking vibration of $-\text{CH}_2-$ at 724 cm^{-1} . As stated before, these peaks also decrease upon increasing the time of weathering, representing a likely explanation for the appearance of the skin in the Gram-Schmidt maps (Fig. 3).

In SBR, the $-\text{C}=\text{C}-$ stretching of the vinyl group at 1640 cm^{-1} (a) [2] tends to become stronger with successive weathering due to cross-linking. The aromatic $-\text{C}=\text{C}-$ stretching vibration peak occurs at 1601 cm^{-1} (b) [47] and its contribution is masked by the presence of the $-\text{C}=\text{C}-$ vinyl stretching. It has been noted that an increase in the intensity of the $-\text{COO}-$ stretching vibration at 1541 cm^{-1} (c) in thermo-oxidatively aged SBR is an indication of the carboxylate

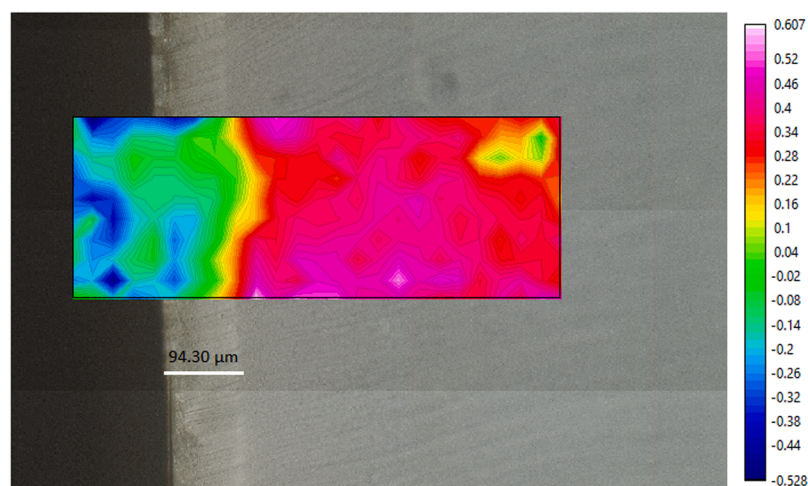


Fig. 3. Gram-Schmidt plot generated using IR microscopy mapping in reflectance mode to assess the chemical modifications across the specimen (SBR W168h) thickness. The blue color end indicates higher weathering-induced modifications, whereas the warmer colors indicate lesser weathering-induced changes. A moderately modified (yellow-green) region is obtained about 95 μm from the sample surface highlighting a distinction between the highly modified 'skin' and the lowly modified 'core'.

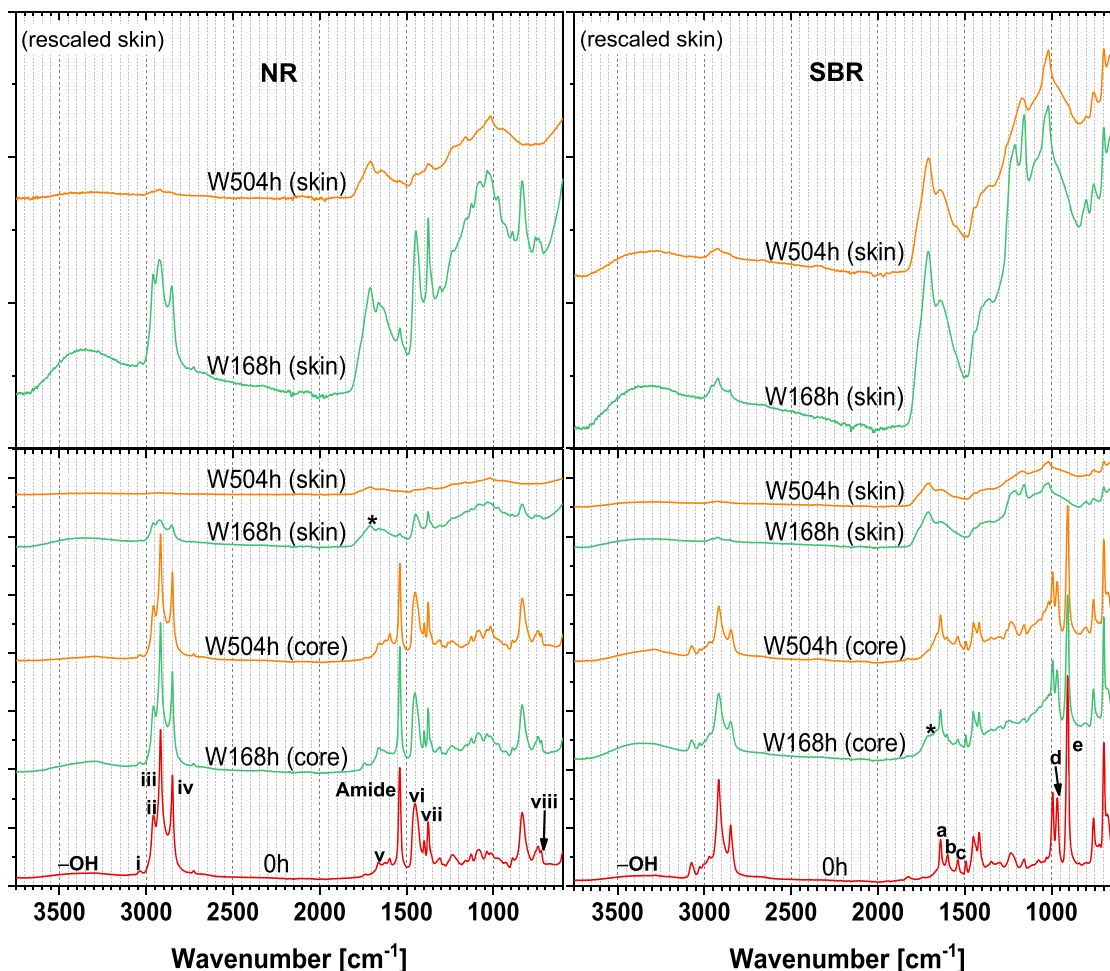


Fig. 4. ATR FTIR absorption spectra for NR (left) and SBR (right) weathered for various durations (bottom boxes). Both the sample series are relatively scaled. The top boxes contain skin-specific spectra rescaled vertically (and equally). The labeled vibration bands are described in the text.

formation as the main product on the material surface [48]. However, such a conclusion cannot be drawn in this study due to the broadening of the $-C=C-$ stretching.

Lastly, the $-C=C-$ vibrations of butadiene at 966 cm^{-1} (d) and 909 cm^{-1} (e) present in the unaged sample disappeared completely after weathering. This is in line with the gas chromatography flame ionization detector (GC/FID) studies on similar samples by Kano *et al.*, which revealed that the relative amount of butadiene with respect to the pristine sample completely disappeared after 100 h of accelerated weathering [44].

From these observations, it can be appreciated that the reactions caused by weathering, mainly involving oxygen, lead to chemical modifications that affect the surface preferentially. Nevertheless, several changes occurring within the core lead to unique physical properties that affect the macroscopic moduli as observed in the previous section.

4.3. Assessment of skin and core regions

4.3.1. AFM nanoindentation measurements

Results from vibrational spectroscopy highlight the formation of chemically different regions upon weathering. One may hence hypothesize that the mechanical properties of these regions would be correspondingly different. To confirm this aspect, AFM nanoindentation experiments were performed at room temperature on SBR W504h, as well as on unexposed SBR (0 h) for comparison. SBR W504h was chosen for its remarkable thermal behavior under dynamic load. The AFM measurements on the skin region of SBR W504h were performed within

approximately $30\text{ }\mu\text{m}$ from the directly exposed surface, whereas the measurements on the core region were performed in the central part of the specimen (around 1 mm from the exposed surface). The results are shown in Fig. 5, which displays a plot of cantilever force as a function of indentation depth obtained from the force-distance measurements of the two samples. These indentation curves are indicative of different mechanical properties of the skin and core regions of the weathered SBR.

As can be seen, an increase in applied force causes a larger indentation in the sample. To produce a certain indentation, a significantly different force is needed for all three specimens due to their different mechanical response. Although the correlation between force and indentation depth is nonlinear as described by various nanomechanical models [35,49] and depends on the cantilever's tip radius and shape, the different slopes of indentation curves can be considered to be reflecting the differences in the local stiffness of the material [50,51]. Here, to exclude any effects arising from different tip radii or shapes, and for direct comparison of the data, the same cantilever has been used for the indentation measurements on all three samples. As apparent from Fig. 5, the slope of the indentation curve for the skin region is larger than that for the core region of SBR W504h. This result indicates that the skin region is stiffer compared to the core of weathered SBR. Thus, Fig. 5 clearly illustrates the difference in the stiffness of the two regions of the weathered specimen.

Moreover, the slopes of the curves for the weathered SBR are also remarkably large compared with the unexposed sample. The marked increase in stiffness of the core compared to the unexposed sample indicates a region that has undergone higher cross-linking due to

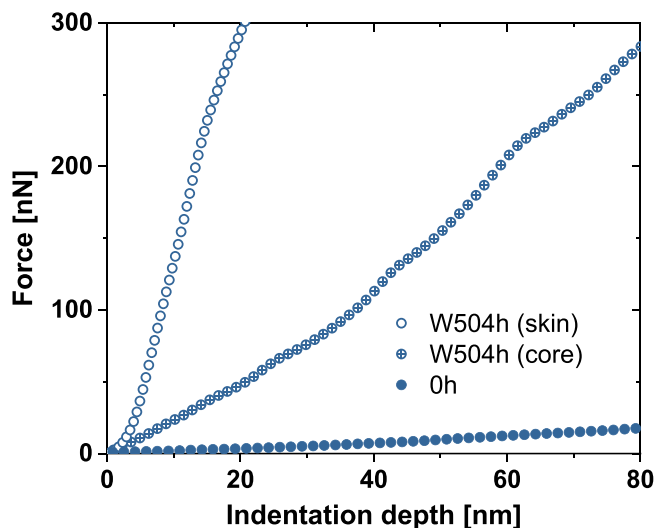


Fig. 5. Representative AFM force vs. indentation depth curves (during approach) for an unexposed (0 h) SBR specimen, and for the ‘skin’ and ‘core’ regions of SBR subjected to 504 h of weathering. The skin region is measured within approximately 30 μm from the directly exposed surface. For a direct comparison, all measurements were performed with the same cantilever and experimental parameters.

weathering and corroborates with the shift in T_g observed in the DMTA trends. The second modulus transition observed in the DMTA plot of SBR W504h is, thus, resulting from the even stiffer skin region, as confirmed here by AFM. As such, from the AFM results and the concepts of diffusion of oxygen [42,52], it can be concluded that the moduli of the samples presented in Fig. 2 are, in fact, an outcome of a gradient of depth-specific moduli.

From a physical point of view, due to the intermittent water sprays, associated expansion and shrinkage of the sample may occur due to the associated temperature changes. These effects in the core region will be somewhat reduced and delayed. Eventually, this results in the formation of distinct stiff skin and soft core that develop different linear coefficients of expansion. For up to 100 h of weathering of SBR Kano, *et al.* observed a 0.5 % volume change due to temperature increase during photo irradiation and temperature decrease during water sprays [44]. This periodic thermal treatment leads to differential expansion and contraction of the skin and the core. In the present study, the long-term weathering of SBR for 504 and 988 h caused a visual caving-in of the specimen towards the irradiated surface due to contraction and stretching of the rear surface due to expansion. Naturally, the clamped ends did not demonstrate this deformation, leaving the unclamped region to appear like a shallow boat.

As another consequence, successive heating/cooling has been observed to cause crazing (or elephant skin formation) on the sample surface, which also propagate to the depth of the specimen. Although these small unoriented connected cracks are typical of an unstressed vulcanizate, the difference in shrinkage leads to the build-up of stresses and the development and propagation of microcracks. The possibility of surface erosion due to spraying cycles cannot be ruled out.

Understandably, this phenomenon would be amplified when weathering up to 988 h as in the case of the present study. These cracks act as a pathway to the leaching of water and more chemical attacks into the bulk of the specimen [34]. The intensity of cracks in SBR is aligned with its poor resistance to crack growth despite having a strong resistance to crack formation. In the case of NR, cracks are formed relatively quickly but grow rather slowly [53]. This can be confirmed from the seemingly protected core of NR vulcanizates as seen in FTIR results.

From these collective arguments it may perhaps be hypothesized that once the integrity of the stiff skin is destroyed, such as by a pre-

stretching to a moderately larger strain, the G' of SBR associated with the skin (in Fig. 2) will be effectively reduced. Thus, an ‘as-is’ interpretation of bulk mechanical results is difficult if not impossible in such materials. More detailed mechanical experiments along these lines were unfortunately beyond our present scope.

4.3.2. Quantification of skin and core regions by T_2 analyzes

As introduced in Section 3.1, the different fractions in a rubber vulcanizate (detected in terms of their proton fractions) can be distinguished based on their respective T_2 times, which makes quantifying the skin and core regions possible. To emphasize the effects of the stiff skin and the soft core, the hardened surface of the 504 h weathered SBR was shaved off using a blade to a depth of roughly 200 μm for separate measurements.

Firstly, the results of a three-component modified exponential decay fit to NR and SBR vulcanizates at different weathering durations are partially presented in Fig. 6A. To recall, the rigid-limit coupling corresponds to a $T_{2,r}^{eff}$ of about 20 μs , which can be assigned to the highly constrained fraction. With a shape parameter (β_r) fixed to 2, the amount of this rigid fraction (f_r) was almost negligible in SBR and about 1.5 % in NR at 0 h. The latter is likely associated with the presence of proteins.

As is shown in Fig. 6A, with weathering the rigid fraction in NR increases, the addition being the oxidized surface, which stabilizes at about 4 % between 504 and 988 h. On the contrary, in SBR, a continuous increase in rigid fraction up to about 7 % occurs due to oxidation of the surface and the underlying layers. The larger amount of rigid components in SBR compared to NR corroborates with the observation made by DMTA towards high temperatures.

The second fitting fraction, regarded as the mobile 1 fraction (f_{m1}) (not shown in Figure) with apparent transverse relaxation time $T_{2,m1}^{eff}$ (Fig. 6A), corresponds to the component that mainly represents the cross-linked bulk. The third fraction composed of defects is represented as the mobile 2 fraction (f_{m2}). These two fractions can be better characterized by MQ measurements and hence, are deferred to Section 4.4.1. Nevertheless, for completeness, the fitting yielded a negligible amount of defect fraction in all SBR samples. NR weathered up to 988 h contained up to about 9 % defects with a $T_{2,m2}^{eff}$ of about 12 ms. The corresponding shape parameter β_{m2} was force-fitted to a limiting minimum value of 0.8 (stretched exponential), meaning that the mobile 1 and 2 fractions cannot be reliably separated in all cases. $T_{2,m1}^{eff}$ (also, in Fig. 6A) corresponding to the majority bulk remains relatively unchanged in NR, whereas a gradual decrease is observed in SBR due to an increase in cross-link density with the weathering duration. An increasing f_r and decreasing $T_{2,m1}^{eff}$ in SBR suggests the presence of a gradient of stiffness due to weathering. In NR, the skin and core could be somewhat distinct. These aspects would become clearer when discussing the cross-link densities in Section 4.4.

For the depth-specific studies, the separated skin and core of 504 h weathered SBR were compared with an intact sample. As an illustration, MSE-FIDs (only) for the two regions and an intact SBR weathered up to 504 h are shown in Fig. 6B. A two-component fitting yielded about 8 % rigid fraction for the skin sample, and as expected, 0 % for the core sample. The second fitting component produced a $T_{2,m1}^{eff}$ of 45 μs and 80 μs , respectively, thus emphasizing gradient stiffening below a relatively hard surface in SBR.

4.4. Changes in network density by weathering

4.4.1. Low-resolution NMR studies

The efficiency of cross-linking, apart from the choice of cross-linker system and the processing conditions, is governed mainly by the extent of unsaturation present in the polymer chain. The higher unsaturation in NR provides a potential for a higher number of cross-links. It also aids in faster cross-link formation, which is confirmed by the shorter curing

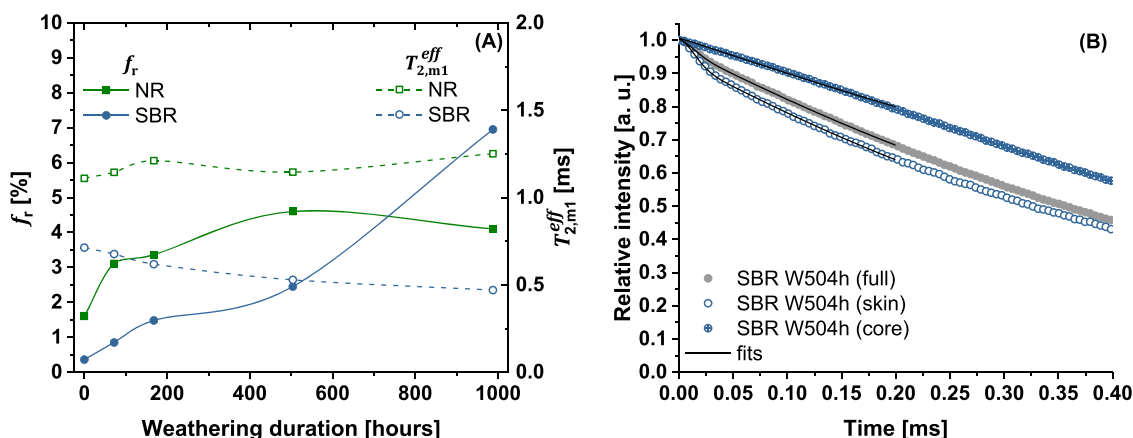


Fig. 6. (A) The variation of weathering-induced rigid fractions (f_r) that correspond to a transverse relaxation time of 20 μ s for NR and SBR at different weathering intervals. The right y-scale shows relaxation times of a comparatively slowly decaying softer, mobile majority fraction (f_{m1}). See Section 4.4.1 for a discussion of a much more slowly decaying defect fraction. (B) MSE-FID decays of the skin and core regions of the SBR W504h specimen obtained after crudely slicing the exposed layer (thickness of roughly 200 μ m). MSE-FID of an intact sample is plotted for reference.

time. The effect of sulfur cross-linking in NR and SBR, in addition to the effect of entanglements, can be ascertained from the values of D_{res} in Fig. 7A corresponding to 0 h. Interestingly, due to differences in the density of unsaturation between them, NR and SBR, upon vulcanization, produce identical D_{res} despite their largely different starting values of about 70 Hz and 135 Hz, respectively in the uncross-linked (pristine) state (not shown in Figure). This is for sure coincidental, as both M_e (entanglement molecular weight) and the reference coupling of the monomer units (D_{ref} in Eq. (1)) are different. The distribution widths of these samples are also similar to the values before cross-linking. Thus, it can be deduced that sulfur does not affect the inherent distribution of these constraints within the sample volume, or sulfur characteristically leads to a narrow distribution of cross-links. Analogous to the single vulcanizates, the 50/50 blend also cross-links to a similar extent. The experimentally measured coupling width is also identical to the weighted average of σ_{in} of the two constituent vulcanizates, thus indicating that sulfur distributes itself non-preferentially within the phases of the blend.

Distinct variations occur in the samples when exposed to the aging elements in the weatherometer as seen from the evolution of cross-link density in Fig. 7A. The biggest change can be seen in SBR, where degradation generally occurs through cyclic cross-linking, which leads to an increase in stiffness (embrittlement). The corresponding coupling distribution width complements the formation of different chain lengths between cross-links.

As established earlier, the regions closer to the surface undergo stiffening due to direct exposure to irradiation, oxygen, water, and heat. Like in the T_2 measurements, the constrained fractions also show up in the I_{nDQ} signal. This can be seen as a step-up in the I_{nDQ} curve at the short evolution times of up to 100 μ s (probing lower values is not feasible due to the pulse sequence length). The build-up curve in Fig. 7B represents this feature for SBR weathered up to 504 h.

A modified bimodal fitting function [17] can be used to separately fit these hardened surface fractions and those that lie beneath that are comparatively less aged. The input parameters to the fitting function are a fixed coupling value $D_{med,2}/2\pi = 12$ kHz, and distribution value $\sigma_{in,2} = 0.01$, where 12 kHz is sufficiently high to have a constant intensity contribution in the plateau region of the respective build-up curve. The constrained fraction is around 2.5 %, which is lower than the actual value because the pulse sequence is inefficient for these components.

The other mode ($D_{med,1}$), represented in Fig. 7A is obtained as a fitting result to the data points of the build-up curve after those that correspond to the highly cross-linked regions (step-up), and thus represent the bulk of the sample. In SBR, prolonged exposure leads to

further stiffening with a net $D_{med,1}$ gain of about 33 %. Likewise, $\sigma_{in,1}$ shows an increase in the coupling distribution due to chain modifications.

Interestingly, this increase in cross-link density of SBR is rather marginal compared to the (approximately) 15-fold increase in the slope of the core region of SBR W504h with respect to the unexposed sample, as observed from AFM. This can be explained by the temperature-dependent gain in modulus of aged SBR with respect to that of unaged SBR. The gain in G' for the 504 h aged SBR is higher at 25 $^{\circ}$ C (23-fold) than at 80 $^{\circ}$ C (5-fold), the two temperatures being the measurement temperatures for AFM and NMR, respectively. This is, of course, without denying that the modulus in DMTA is a combined effect of, both, the skin and core regions. Another factor for the observed (apparent) inconsistency in property change is a systematic error originating from the choice of the cantilever in the AFM experiment. The cantilever used in the AFM experiments was chosen in accordance with the stiffness of SBR weathered for 504 h. The same cantilever was used to probe the rather soft unaged SBR, which could have led to penetration of the cantilever tip into the specimen.

In the case of NR, contrary to SBR, the D_{res} appears to remain unchanged upon weathering up to 168 h. However, the broadening of coupling distribution suggests the modification of covalent bonds. The conventional sulfur-vulcanization system is known to majorly produce polysulfidic bonds [54]. The broadening of coupling distribution is thus suggestive of the reformation of polysulfidic bonds into shorter variants like the mono- and disulfidic bonds [55]. The same observation has been made earlier with NR exposed to thermo-oxidative aging at 80 $^{\circ}$ C [17]. Oxidation-induced chain scission is another contributing factor to the broadening of the coupling distribution. Upon continued weathering, the bulk of NR undergoes a reduction in cross-link density due to the extensive decomposition of main chains. These changes are also evident in the distribution width.

In the blend, until 168 h, D_{res} varies only moderately and produces values that are similar to those of NR. The corresponding changes in $\sigma_{in,1}$, however, suggest distinct chemical changes within the sample volume which are again indicative of the maturation of sulfur bonds as seen in NR. A standout observation here is that the blend ages less in comparison to its expected value (wtd. blend), plotted for reference. This is a numerically measured weighted average of NR and SBR single vulcanizates. By acknowledging the similarity in D_{res} of NR and the blend up to 168 h, one can infer that the bulk of the SBR phase experiences lesser chemical changes in the blend than when it is a pure vulcanizate.

At the extended weathering durations, the coupling strengths of the

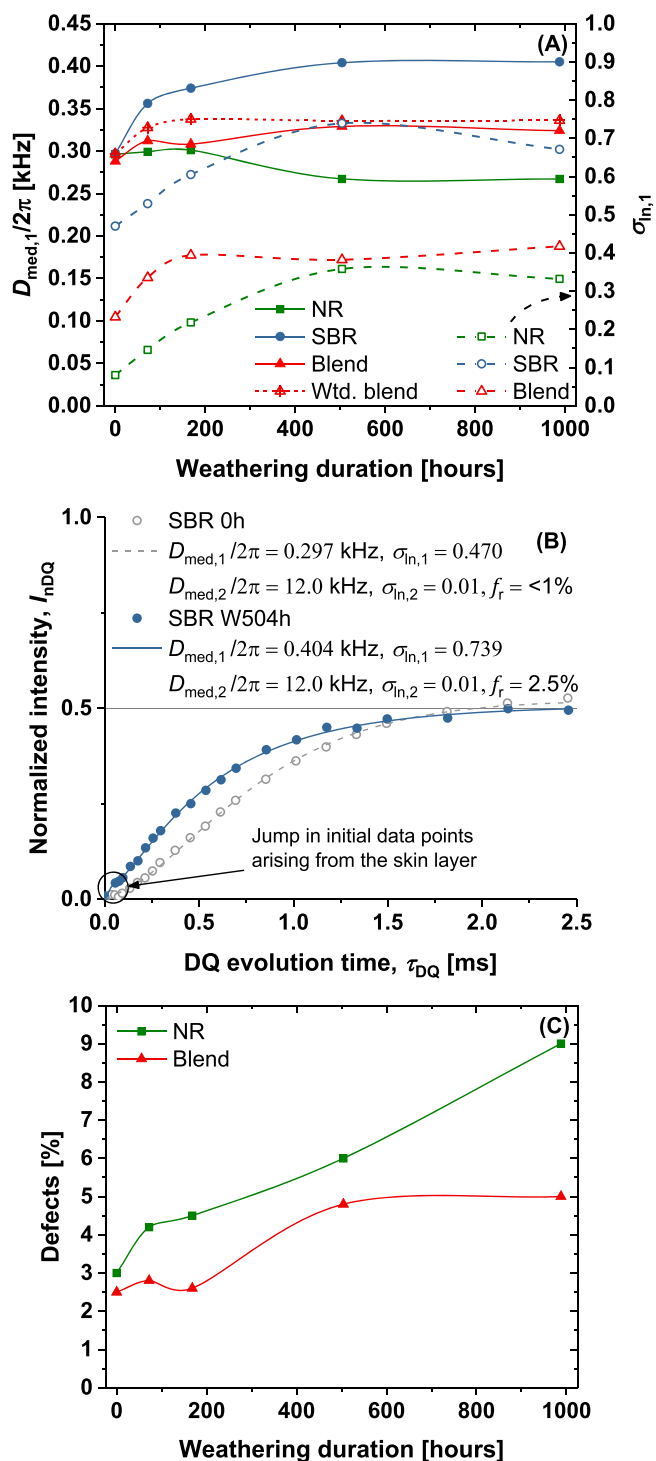


Fig. 7. Results of MQ NMR measurements for NR, SBR, and their 50/50 blend. (A) Cross-link densities (solid lines) and their distributions (dashed lines) within the polymer bulk. The weighted (wtd.) average of D_{med} for the blend (short-dashed line), based on the D_{med} of NR and SBR, is shown for comparison (see text). An additional fitting mode was used to account for surface-stiffening observed in the samples due to weathering based on the rigid fractions in Fig. 6A. (B) Demonstration of the rigid fraction as a step-up in the I_{nDQ} signal at shorter DQ evolution times for SBR W504h. Its coupling is set to a fit-adequate value of 12 kHz (see discussion). (C) The defect fraction obtained from normalization. No defects are detected in SBR.

blend are intermediate to those of NR and SBR. Interestingly, no significant variation of $D_{med,1}$ can be observed for the three materials between 504 and 988 h. Also, the invariance of the corresponding coupling widths suggests no significant chemical modifications in the samples beyond 500 h. In comparison to the previous work [17], these trends highlight that sulfur-cross-linked NR is chemically unstable at higher temperatures (thermo-oxidative aging at 80 °C), whereas sulfur-cross-linked SBR is more susceptible to artificial weathering.

The defect fraction (in Fig. 7C) obtained by an exponential decay fit to $I_{\Sigma MQ}$ during normalization is analogous to the third fraction obtained through T_2 analyses in Section 4.3.2. The amount of defect fraction in NR, corresponding to a T_2 relaxation time of about 15 ms, changed from about 3 % for the unaged sample to 9 % for the most weathered sample. In the case of SBR, as expected, no presence of defects was detected. This confirms the complete cross-linking in SBR due to weathering. For the blend, surprisingly, the amount of defect fraction varied from about 2.5 % to only 5 %. Assuming that the defect amount of the SBR phase remains negligible also in the blend, the lower amount of overall defects in the blend is an unexpected finding and probably suggests that NR is also protected from weathering when it is a part of the blend.

More coupling information can be obtained by Fast-Tikhonov regularization (*ftikreg*) of the normalized build-up data [41]. This procedure yields a visual representation of the distribution of D_{res} within the samples (Fig. 8). The median value of D_{res} (D_{med}) corresponds to the value at which the normalized integral of these curves is 0.5. The inherent (in)homogeneity of spins in uncross-linked (pristine) NR and SBR remains relatively unchanged upon vulcanization (0 h) but increases due to weathering. Already upon 72 h of weathering of SBR, the formation of a small amount of rigid fraction can be observed towards the higher coupling end of the distribution. In addition to this, SBR at 504 and 988 h of weathering contains small amounts of cross-linking-induced, newly formed constrained fractions that are ubiquitous in the coupling distribution graphs. In the case of the blend, proportional changes can be observed.

To summarize the low-field results, SBR undergoes perfectioning of cross-links leading to stiffening, whereas NR demonstrates both cross-linking and chain scission that lead to stiffening and softening processes, with chain scission eventually dominating. Interestingly, measurements of the blend material reveal that the NR and SBR phases are protected when they are a part of the blend in contrast to the respective single vulcanizates.

4.4.2. Phase-resolved studies of the evolution of cross-link densities

MAS NMR experiments benefit from the resolution of a spectrum into defined peaks. This enables phase-specific studies in polymer mixtures. With every integer rotor period and a rotor frequency of 10 kHz, the shortest DQ evolution time achievable in the current setup is 100 μ s. Hence, the DQ signals obtained here are free of contributions from the rigid fractions.

The three proton resonances in NR corresponding to CH, CH₂, and CH₃, as has been previously demonstrated [31], and adapted in Table 1 yield identical coupling, and the spectral average is similar in magnitude to the low-field experiment value.

Unexposed SBR yields a spectral average coupling value of about 0.280 kHz. The lowest value is attributed to the phenyl ring due to its motional freedom about the main-chain CH bond. The highest coupling corresponds to the groups at chemical shifts of 1.9 ppm and 1.2–1.8 ppm, coming majorly from the main chain protons of vinyl polybutadiene. This copolymer is also responsible for the spin heterogeneity in the SBR grade considered in this study.

The changes occurring in the samples due to weathering are represented as a ratio of coupling constants and their distribution after 504 and 988 h of weathering to their corresponding values at 0 h in Fig. 9. The chemical groups have been arranged from left to right in the sequence of resonances as NR-only \rightarrow mixed \rightarrow SBR-only. In the case of NR (Fig. 9B), one can observe that the polymer cross-link density

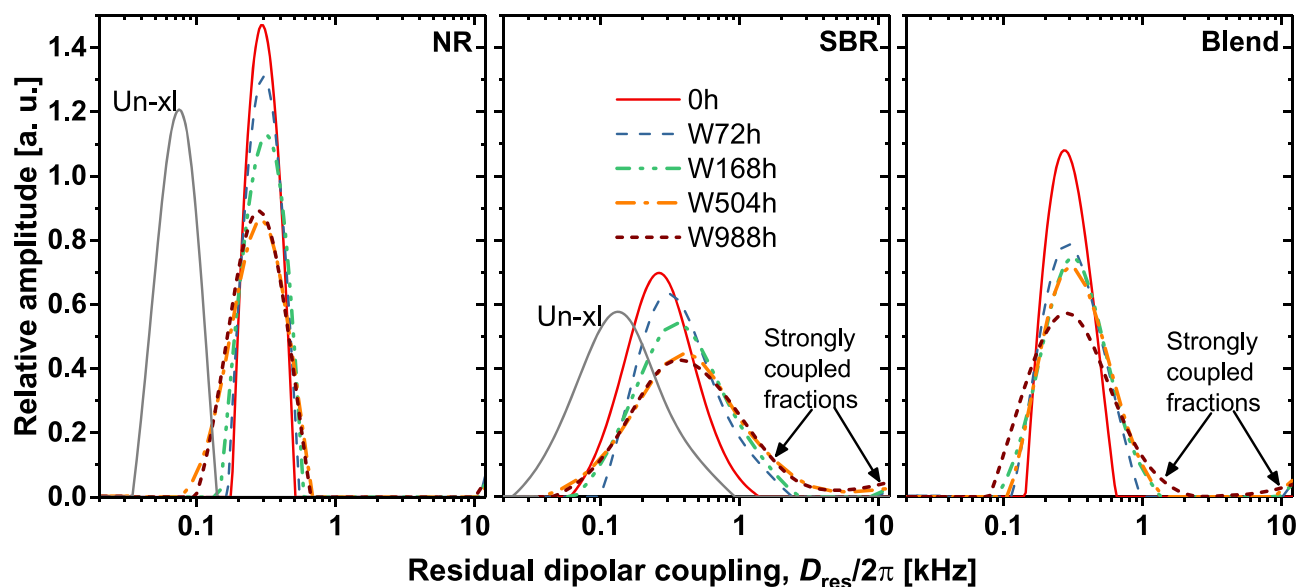


Fig. 8. Changes in the distribution of cross-links due to weathering. These are obtained by regularization of the normalized DQ data. The presence of strongly coupled fractions can be seen in SBR and the blend. The inherent coupling distributions of uncross-linked (Un-xl) NR and SBR are plotted for reference.

Table 1
Phase-resolved D_{med} and respective σ_{in} for the unexposed materials. (Adapted from Ref. [17]).

Chemical group/s	Chemical shift, δ [ppm]	NR		SBR		Blend	
		$D_{\text{med},2/2\pi}$ [kHz]	σ_{in}	$D_{\text{med},2/2\pi}$ [kHz]	σ_{in}	$D_{\text{med},2/2\pi}$ [kHz]	σ_{in}
$\text{C}_6\text{H}_5^{\text{PS}}$	7.2 – 7.7	–	–	0.233	0.278	0.200	0.236
$\text{CH}^{1,4}, \text{CH}^{1,2}$ (vinyl)	5.5 – 6.1	–	–	0.258	0.352	0.232	0.323
CH^{NR}	5.5	0.287	<0.01	–	–	0.291	0.038
$\text{CH}_2^{1,2}$ (vinyl)	5.3	–	–	0.284	0.337	0.256	0.316
$\text{CH}_2^{\text{NR}}, \text{CH}^{\text{PS}}, \text{CH}_2^{1,4}$	2.1 – 2.8	0.293	0.044	0.292	0.420	0.287	0.215
$\text{CH}_3^{\text{NR}}, \text{CH}^{1,2}$	1.9	0.278	0.112	0.315	0.449	0.281	0.200
$\text{CH}_2^{\text{PS}}, \text{CH}_2^{1,2}$	1.2 – 1.8	–	–	0.313	0.518	0.282	0.669
Spectral average	–	0.287	0.104	0.278	0.455	0.274	0.303

reduces after weathering to 504 h, and is analogous to the observations made using the low-field experiment. The increase in its coupling width is an indication of the increasing cross-linking inhomogeneity. This aspect is pronounced in the CH and CH_2 moieties, as these sites are directly affected by the various reactions (S-modification, chain scission, cross-linking, etc.) occurring in the vicinity. Here it is important to note that despite the observed widening, the average absolute value of σ_{in} after 504 h of weathering is about 0.410.

Weathering SBR to 504 h leads to an average increase of about 35 % in D_{med} across all chemical environments of the rubber (Fig. 9C) and complements the results of the low-field. Unlike in NR, the change in coupling distribution width is almost identical for all the proton environments.

Upon 988 h of weathering, NR undergoes a further reduction in its cross-link density. This finding is different from the low-field measurement where the D_{med} seemed to have stabilized at extended exposure durations. The corresponding distribution appears to have slightly narrowed down upon extended weathering. This is consistent with the low-field results and could be due to the recross-linking of some weakly coupled segments that are present after 504 h of weathering, thus leading to uniformity of chain lengths between cross-links.

Perhaps the most important observation in NR from the high-field and low-field measurements is that as the surface stiffens, the core softens. This behavior suggests that the hardened surface acts as a barrier to layers underneath wherein chain scission dominates.

With SBR, weathering to 988 h shows a reversal of the cross-linking trend. The average coupling strength reduced from 0.377 kHz (after 504 h) by about 50 to 0.326 kHz (after 988 h). This is a rather surprising

finding that was not observed in the low-field experiment. Variations can be observed at resonances ii, iii, and vii (see Fig. 9C), which correspond to the main chain protons of the three monomers in SBR, suggesting changes in the bonding situation in due to weathering. But the cross-link distribution remains almost unaffected by weathering.

NR and SBR have similar solubility parameters of about $16.7 \text{ MPa}^{1/2}$ and $17.5 \text{ MPa}^{1/2}$, respectively [56], making their blends technologically relevant due to macroscopic miscibility as a result of low interfacial tension. Nevertheless, they tend to exhibit phase separation on a microscopic scale due to their molecular incompatibility and thus provide scope for potential variations in the blend phases. The low-field measurements discussed earlier suggest that NR and SBR cross-link to similar extents in the blend, as do their corresponding single vulcanizates. However, MAS experiments reveal some inconsistencies in SBR. The SBR phase cross-links to a lesser extent in the blend compared to its single vulcanizate. This is despite its preferential and faster reaction rate with CBS accelerator than that of NR [17,57]. Thus, a relatively softer SBR phase is present in relation to an NR phase which yields identical D_{res} as its single vulcanizate.

The changes arising in the blend upon weathering are evident in Fig. 9A. Upon 504 h of weathering, the extent of changes in the NR-containing resonances is minimal, especially the D_{res} of CH resonance appears unchanged, albeit with a small broadening of the coupling constant. On the other hand, a distinct increase in D_{res} can be observed for the pure SBR resonances. The corresponding coupling distribution widths across the various resonances are largely similar to those obtained from the single vulcanizates. Despite the finite increase, the increase in D_{res} of SBR-phase resonances is, on average, still lower than the

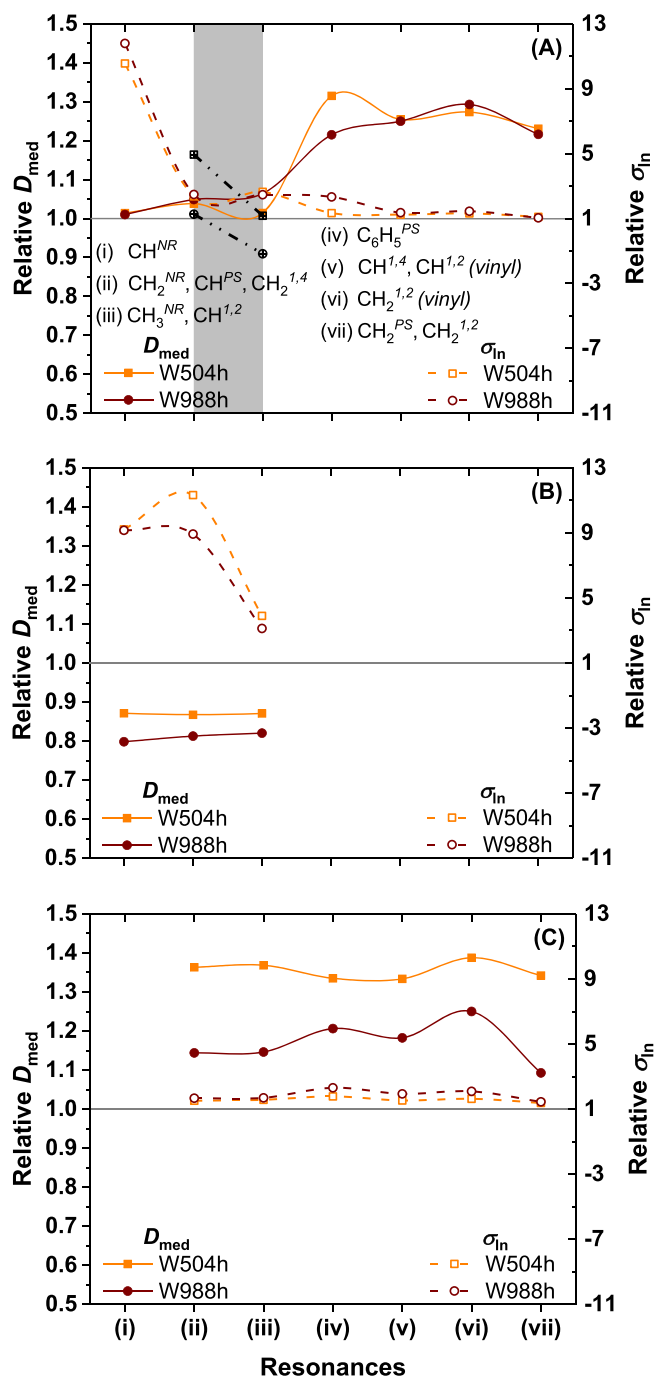


Fig. 9. Relative changes in cross-link densities and their distribution described as a ratio of coupling parameters at 504 and 988 h weathering to those at 0 h for (A) blend, (B) NR, and (C) SBR. “Vinyl” in parentheses refers to the vinyl part of 1,2-polybutadiene. The lines are a guide to the eye only. The gray shaded area in (A) highlights the overlapped resonances in the blend. The crossed open symbols (square: 504 h, circle: 988 h) represent the proton-weighted averages of D_{med} of the mixed resonances obtained from the correspondingly weathered single vulcanizates and thus highlight the “protective” nature of the blend.

single vulcanizate. This is probably due to a lowly cross-linked SBR phase before weathering.

Upon further weathering to 988 h, the distribution of cross-links in both phases almost overlaps with the values obtained after 504 h, thus suggesting that the chain lengths remain virtually unaffected. This is confirmed by the comparably similar changes in D_{res} even after almost doubling the weathering duration and explains the reason for the

almost-identical moduli of the blend at the two durations. This is a rather astonishing behavior of the blend compared to the single vulcanizates, where NR underwent continuous softening over the two weathering intervals, and SBR demonstrated a stiffening and then softening property at 504 and 988 h, respectively.

To emphasize this experimental finding, Fig. 9A also compares the ‘expected’ values of changes in D_{res} of the blend based on proton-weighted averages from the single vulcanizates at the two intervals for the mixed resonances (gray shaded area) at resonance locations ii and iii (see Fig. 9A). Thus, this highlights the effects of softening and stiffening that should have been observed in the blend but are rather weak. These observations made through MAS also corroborate with the lower defect fraction in the blend observed through the low-resolution experiment. These arguments collectively demonstrate that the two polymers are protected in the blend even at prolonged weathering durations. In other words, under the experimental conditions discussed here, the blend lasts longer and is hence technologically better suitable than the constituent single vulcanizates.

5. Conclusion

In this study, the molecular and bulk changes in sulfur-cross-linked NR, SBR, and their blend (50/50 ratio by phr) subjected to artificial weathering were monitored by various techniques. At longer weathering durations, DMTA measurements revealed stiffening in NR that softened almost entirely at higher temperatures. The stiffening was pronounced in SBR. This contributed to an additional softening transition which showed significant modulus even at 100 °C. The chemical origins of these were evaluated by FTIR, which revealed modification of the surface layer into a stiff skin due to oxidation processes aided by various weathering parameters. The regions below this skin layer oxidized to a lesser extent due to the barrier-like behavior of the skin. AFM nano-indentation measurements at various depths of SBR weathered up to 504 h confirmed the oxidation-induced stiffening that imparted an additional transition in DMTA experiments.

Further analyses of the skin and core by NMR T_2 studies suggested a continuous increase in the skin fractions in SBR up to about 7 % for 988 h of weathering. In NR, the stiff fraction stabilized between 504 and 988 h at about 4 %. It was also indicated that the bulk of NR probably remained unchanged due to prolonged weathering, whereas in SBR a gradient of stiffness existed beneath the stiff skin due to continuous cross-linking.

The cross-link density measurements by an MQ pulse sequence on a low-field spectrometer highlighted an increase in the cross-linked density of SBR up to 504 h by 33 %, which remained unchanged up to 988 h. In contrast, NR had the same cross-link density up to 168 h, which then dropped by 10 % approaching 504 h. The stagnation in cross-link density up to 168 h was attributed to a modification of polysulfidic bonds to the lower, disulfidic and monosulfidic variants and due to oxidation-induced chain scission.

In the blend, cross-link density varied only moderately, which was lower than a calculated average obtained by weighting D_{res} of NR and SBR single vulcanizates, thus showing that blends age lesser compared to their single vulcanizates. The cross-link distribution values indicated the formation of different chain lengths between cross-links due to weathering in all samples. Further, it was observed that weathering caused the formation of defects in NR and the blend but was non-existent in SBR due to complete cross-linking. Thus, the MQ experiments prove the existence of a stiff skin but a soft core, where chain scission reactions dominate. In SBR, a stiff skin is obtained with a core that is still generally harder than the unaged sample.

Phase-resolved studies by 1H DQ MAS NMR provided some additional insights into the weathered samples. In NR, unlike the low-field measurements, the cross-link density reduced continuously between 504 and 988 h. In the case of SBR, the cross-link density increased up to 504 h but then reduced after extended weathering with no change in the

distribution of cross-links. The most fascinating outcome of the high-field experiments was the formation of a distribution of cross-links in the blend phases, where a soft NR phase varied insignificantly in its cross-link density for the entire weathering duration. A strongly cross-linked hard SBR phase remained invariant to weathering between 504 and 988 h. These observations are supported by the similarity in the dynamic moduli of the blend at the two durations. Via the inherent proton counting feature of NMR, it was established that the blend was relatively resistant to weathering compared to its single vulcanizates, thus making the blend an ideal choice for long-term applications.

CRedit authorship contribution statement

Akshay Karekar: Conceptualization, Methodology, Validation, Formal analysis, Investigation, Data curation, Writing – original draft, Visualization, Project administration. **Carsten Schickanz:** Investigation, Visualization. **Muhammad Tariq:** Investigation, Writing – original draft, Visualization. **Katja Obwald:** Conceptualization, Methodology, Validation, Resources, Supervision. **Katrin Reincke:** Conceptualization, Methodology, Validation, Resources, Writing – review & editing, Supervision. **Valentin Cepus:** Validation, Investigation, Resources, Writing – original draft, Writing – review & editing, Visualization. **Beate Langer:** Resources, Writing – review & editing, Supervision, Funding acquisition. **Kay Saalwächter:** Conceptualization, Methodology, Software, Validation, Resources, Writing – review & editing, Supervision, Project administration, Funding acquisition.

Declaration of Competing Interest

The authors declare that they have no known competing financial interests or personal relationships that could have appeared to influence the work reported in this paper.

Data availability

Data will be made available on request.

Acknowledgments

The authors thank the Land Sachsen-Anhalt and the European Social Fund (ESF) [grant number ZS/2016/08/80644]. M.T. acknowledges funding from the Deutsche Forschungsgemeinschaft (DFG, German Research Foundation)—Project-ID 189853844—TRR 102. M.T. also thanks Mr. Qiang Yu for assistance in microtomy. A.K. thanks Dr. Marcus Schoßig at Polymer Service GmbH Merseburg for facilitating weathering of the specimens, and Prof. Thomas Thurn-Albrecht for access to ARES G2 and his insights on AFM.

Supplementary materials

Supplementary material associated with this article can be found, in the online version, at doi:10.1016/j.polymdegradstab.2023.110267.

References

- J.E. Pickett, Introduction to polymer weathering, stabilization, and testing. Service Life Prediction of Polymers and Coatings, Elsevier, 2020, pp. 1–18, <https://doi.org/10.1016/b978-0-12-818367-0.00001-1>.
- N. Rezig, T. Bellahcene, M. Aberkane, N. Abdelaziz, M. Thermo-Oxidative, Ageing of a SBR rubber: effects on mechanical and chemical properties, J. Polym. Res. 27 (11) (2020) 1–13, <https://doi.org/10.1007/S10965-020-02330-Y>.
- J.E. Pickett, D.A. Gibson, S.T. Rice, M.M. Gardner, Effects of temperature on the weathering of engineering thermoplastics, Polym. Degrad. Stab. 93 (3) (2008) 684–691, <https://doi.org/10.1016/J.POLYMEDEGRADSTAB.2007.12.013>.
- Tinker, A. J. A.J. Tinker, K.P. Jones, Introduction — the book and rubber blends. Blends of Natural Rubber, Springer, Dordrecht, 1998, <https://doi.org/10.1007/978-94-011-4922-8>. Tinker, A. J.
- C.M. Roland, A.K. Bhowmick, H.L. Stephens, Rubber-rubber blends: part I. Handbook of Elastomers, Marcel Dekker, New York, 2001, pp. 197–225.
- A.V. Chapman, A.J. Tinker, Vulcanization of blends – crosslink distribution and its effect on properties, Kautsch. Gummi Kunstst. 56 (10) (2003) 533–544.
- C.M. Roland Immiscible rubber blends. In advances in elastomers I, P.M. Visakh, S. Thomas, A.K. Chandra, A.P. Mathew, eds., Advanced Structured Materials, Springer Berlin Heidelberg: Berlin, Heidelberg, 2013, Vol. 11. 10.1007/978-3-64-2-20925-3.
- S. Schlögl, M.L. Trutschel, W. Chassé, G. Riess, K. Saalwächter, Entanglement effects in elastomers: macroscopic vs microscopic properties, Macromolecules 47 (9) (2014) 2759–2773, <https://doi.org/10.1021/MA4026064>.
- A.I. Dzulkifli, C.M.S. Said, C.C. Han, Determination of crosslink concentration by mooney-rivlin equation for vulcanized NR/SBR blend and its influence on mechanical properties, Malays. J. Anal. Sci. 19 (6) (2015) 1309–1317.
- R. Srithawatpong, Z.L. Peng, B.G. Olson, A.M. Jamieson, R. Simha, J.D. McGervey, T.R. Maier, A.F. Halasa, H. Ishida, Positron annihilation lifetime studies of changes in free volume on cross-linking cis-polyisoprene, high-vinyl polybutadiene, and their miscible blends, J. Polym. Sci. Part B Polym. Phys. 37 (1999) 2754–2770, [https://doi.org/10.1002/\(SICI\)1099-0488\(19991001\)37](https://doi.org/10.1002/(SICI)1099-0488(19991001)37).
- H. Ismail, S. Tan, B.T. Poh, Curing and mechanical properties of nitrile and natural rubber blends, J. Elastomers Plast. 33 (4) (2001) 251–262, <https://doi.org/10.1106/DQNG-QXA0-UC3W-U45H>.
- A.A. Galuska, R.R. Poulter, K.O. McElrath, Force modulation AFM of elastomer blends: morphology, fillers and cross-linking, Surf. Interface Anal. 25 (6) (1997) 418–429, [https://doi.org/10.1002/\(SICI\)1096-9918\(199706\)25:6<418::AID-SIA253>3.0.CO;2-P](https://doi.org/10.1002/(SICI)1096-9918(199706)25:6<418::AID-SIA253>3.0.CO;2-P).
- M.J.R. Loadman, A.J. Tinker, The application of swollen-state CW-1H NMR spectroscopy to the estimation of the extent of crosslinking in vulcanized polymer blends, Rubber Chem. Technol. 62 (2) (1989) 234–245, <https://doi.org/10.5254/1.3536242>.
- P.S. Brown, A.J. Tinker, Factors affecting the NMR technique for estimation of crosslink density in rubber blends, J. Nat. Rubber Res. 5 (4) (1990) 286–295.
- P.S. Brown, M. John, R. Loadman, A.J. Tinker, Applications of FT-NMR to crosslink density determinations in natural rubber blend vulcanizates, Rubber Chem. Technol. 65 (4) (1992) 744–760, <https://doi.org/10.5254/1.3538639>.
- A.J. Tinker, Distribution of Crosslinks in Vulcanized Blends, Rubber Chem. Technol. 68 (3) (1995) 461–480, <https://doi.org/10.5254/1.3538751>.
- A. Karekar, K. Obwald, K. Reincke, B. Langer, K. Saalwächter, NMR studies on the phase-resolved evolution of cross-link densities in thermo-oxidatively aged elastomer blends, Macromolecules 53 (24) (2020) 11166–11177, <https://doi.org/10.1021/acs.macromol.0c01614>.
- B. Klei, J.L. Koenig, NMR imaging of the competitive vulcanization of natural rubber and polybutadiene blends, Acta Polym. 48 (5–6) (1997) 199–207, <https://doi.org/10.1002/actp.1997.010480505>.
- M.D. Ellul, A.H. Tsou, W. Hu, Crosslink densities and phase morphologies in thermoplastic vulcanizates, Polymer 45 (10) (2004) 3351–3358, <https://doi.org/10.1016/j.polymer.2004.03.029> (Guilfd).
- M. Aluas, C. Filip, Solid-state NMR characterization of cross-linking in EPDM/PP blends from 1H –13C polarization transfer dynamics, Solid State Nucl. Magn. Reson. 27 (2005) 165–173, <https://doi.org/10.1016/j.snmr.2004.10.001>.
- P. Sotta, C. Fülber, D.E. Demco, B. Blümich, H.W. Spiess, Effect of residual dipolar interactions on the NMR relaxation in cross-linked elastomers, Macromolecules 29 (19) (1996) 6222–6230, <https://doi.org/10.1021/ma960141e>.
- M. Schneider, L. Gasper, D.E. Demco, B. Blümich, Residual dipolar couplings by 1H dipolar-encoded longitudinal magnetization, double- and triple-quantum nuclear magnetic resonance in cross-linked elastomers, J. Chem. Phys. 111 (1) (1999) 402, <https://doi.org/10.1063/1.479291>.
- T. Dollase, R. Graf, A. Heuer, H.W. Spiess, Local order and chain dynamics in molten polymer blocks revealed by proton double-quantum NMR, Macromolecules 34 (2) (2001) 298–309, <https://doi.org/10.1021/MA0013915>.
- K. Saalwächter, B. Herrero, M.A. López-Manchado, Chain order and cross-link density of elastomers as investigated by proton multiple-quantum NMR, Macromolecules 38 (23) (2005) 9650–9660, <https://doi.org/10.1021/ma051238g>.
- I. Syed, G. Hempel, K. Saalwächter, P. Stratmann, M. Klüppel, Entanglements, defects, and Inhomogeneities in nitrile butadiene rubbers: macroscopic versus microscopic properties, Macromolecules 49 (23) (2016) 9004–9016, <https://doi.org/10.1021/acs.macromol.6b01802>.
- K. Saalwächter, P. Ziegler, O. Spycykerelle, W. Haidar, A. Vidal, J.U. Sommer, 1H Multiple-quantum nuclear magnetic resonance investigations of molecular order distributions in poly(Dimethylsiloxane) networks: evidence for a linear mixing law in bimodal systems, J. Chem. Phys. 119 (6) (2003) 3468–3482, <https://doi.org/10.1063/1.1589000>.
- J. Baum, A. Pines, NMR studies of clustering in solids, J. Am. Chem. Soc. 108 (24) (1986) 7447–7454, <https://doi.org/10.1021/ja00284a001>.
- M.K. Dibbanti, M. Mauri, L. Mauri, G. Medaglia, R. Simonutti, Probing small network differences in sulfur-cured rubber compounds by combining nuclear magnetic resonance and swelling methods, J. Appl. Polym. Sci. 132 (1–8) (2015) 42700, <https://doi.org/10.1002/app.42700>.
- M.A. Mansilla, J.L. Valentín, M.A. López-Manchado, A. González-Jiménez, A. J. Marzocca, Effect of entanglements in the microstructure of cured NR/SBR blends prepared by solution and mixing in a two-roll mill, Eur. Polym. J. 81 (2016) 365–375, <https://doi.org/10.1016/j.eurpolymj.2016.06.023>.
- A. Karekar, R. Pommer, B. Prem, C. Czubala, C. Teichert, G. Trimmel, K. Saalwächter, NMR-based cross-link densities in EPDM and EPDM/ULDPE blend materials and correlation with mechanical properties, Macromol. Mater. Eng. 307 (7) (2022), 2100968, <https://doi.org/10.1002/MAME.202100968>.

- [31] K. Saalwächter, F. Lange, K. Matyjaszewski, C.F. Huang, R. Graf, BaBa-Xy16: robust and broadband homonuclear DQ Recoupling for applications in rigid and soft solids up to the highest MAS frequencies, *J. Magn. Reson.* 212 (1) (2011) 204–215, <https://doi.org/10.1016/j.jmr.2011.07.001>.
- [32] R.P. Brown, T. Butler, S.W. Hawley, *Ageing of Rubber - Accelerated Heat Ageing Test Results*, Smithers Rapra Technology, 2001.
- [33] R.P. Brown, T. Butler, S.W. Hawley, *Ageing of Rubber - Accelerated Weathering and Ozone Test Results*, Smithers Rapra Technology, 2001.
- [34] J. Crabtree, A.R. Kemp, Weathering of soft vulcanized rubber, *Rubber Chem. Technol.* 19 (3) (1946), <https://doi.org/10.5254/1.3557514>.
- [35] M. Chyasnachyus, S.L. Young, V.V. Tsukruk, Probing of polymer surfaces in the viscoelastic regime, *Langmuir* 30 (35) (2014) 10566–10582, <https://doi.org/10.1021/LA404925H>.
- [36] A. Maus, C. Hertlein, K. Saalwächter, A robust proton NMR method to investigate hard/soft ratios, crystallinity, and component mobility in polymers, *Macromol. Chem. Phys.* 207 (13) (2006) 1150–1158, <https://doi.org/10.1002/MACP.200600169>.
- [37] A. Wittmer, R. Wellen, K. Saalwächter, K. Koschek, Moisture-mediated self-healing kinetics and molecular dynamics in modified polyurethane urea polymers, *Polymer* 151 (2018) 125–135, <https://doi.org/10.1016/j.polymer.2018.07.059> (Guildf).
- [38] K. Saalwächter, Proton multiple-quantum NMR for the study of chain dynamics and structural constraints in polymeric soft materials, *Prog. Nucl. Magn. Reson. Spectrosc.* 51 (1) (2007) 1–35, <https://doi.org/10.1016/j.pnmrs.2007.01.001>.
- [39] K. Saalwächter, M. Klüppel, H. Luo, H. Schneider, Chain order in filled SBR elastomers: a proton multiple-quantum NMR study, *Appl. Magn. Reson.* 27 (3–4) (2004) 401–417, <https://doi.org/10.1007/BF03166740>.
- [40] L. Jakisch, M. Garaleh, M. Schäfer, A. Mordvinkin, K. Saalwächter, F. Böhme, Synthesis and structural NMR characterization of novel PPG/PCL conetworks based upon heterocomplementary coupling reactions, *Macromol. Chem. Phys.* 219 (3) (2018) 1–9, <https://doi.org/10.1002/macp.201700327>.
- [41] W. Chassé, J.L. Valentín, G.D. Genesky, C. Cohen, K. Saalwächter, Precise dipolar coupling constant distribution analysis in proton multiple-quantum NMR of elastomers, *J. Chem. Phys.* 134 (4) (2011), <https://doi.org/10.1063/1.3534856>.
- [42] L. Audouin, V. Langlois, J. Verdu, J.C.M. de Bruijn, Role of oxygen diffusion in polymer ageing: kinetic and mechanical aspects, *J. Mater. Sci.* 29 (3) (1994) 569–583, <https://doi.org/10.1007/BF00445968>.
- [43] J. Zhi, Q. Wang, M. Zhang, Z. Zhou, A. Liu, Y. Jia, Coupled analysis on hyper-viscoelastic mechanical behavior and macromolecular network alteration of rubber during thermo-oxidative aging process, *Polymer* 171 (2019) 15–24, <https://doi.org/10.1016/j.polymer.2019.03.029> (Guildf).
- [44] M. Kano, Y. Ohtake, T. Yamanobe, H. Uehara, Effect of water spray on degradation of styrene-butadiene-rubber during accelerated weathering tests, *Polym. Degrad. Stab.* 182 (2020), 109379, <https://doi.org/10.1016/j.polyimdegradstab.2020.109379>.
- [45] K.A.M. Dos Santos, P.A.Z. Suarez, J.C. Rubim, Photo-degradation of synthetic and natural polyisoprenes at specific UV radiations, *Polym. Degrad. Stab.* 90 (1) (2005) 34–43, <https://doi.org/10.1016/j.polyimdegradstab.2005.01.038>.
- [46] G.Y. Li, J.L. Koenig, FT-IR Imaging of the thermal oxidation of polyisoprene (PI) rubber at high temperature, *Appl. Spectrosc.* 56 (11) (2002) 1390–1396, <https://doi.org/10.1366/00037020260377670>.
- [47] G. Martínez-Barrera, H. López, V.M. Castaño, R. Rodríguez, Studies on the rubber phase stability in gamma irradiated polystyrene-SBR blends by using FT-IR and Raman spectroscopy, *Radiat. Phys. Chem.* 69 (2) (2004) 155–162, [https://doi.org/10.1016/S0969-806X\(03\)00452-3](https://doi.org/10.1016/S0969-806X(03)00452-3).
- [48] A. Zanchet, L.N. Carli, M. Giovanela, R.N. Brandalise, J.S. Crespo, Use of styrene butadiene rubber industrial waste devulcanized by microwave in rubber composites for automotive application, *Mater. Des.* 39 (2012) 437–443, <https://doi.org/10.1016/J.MATDES.2012.03.014>.
- [49] H.J. Butt, B. Cappella, M. Kappl Force measurements with the atomic force microscope: technique, interpretation and applications, North-Holland, 2005, Vol. 59. <https://doi.org/10.1016/J.SURFREP.2005.08.003>.
- [50] B. Cappella, D. Silbernagl, Nanomechanical properties of polymer thin films measured by force–distance curves, *Thin Solid Films* 516 (8) (2008) 1952–1960, <https://doi.org/10.1016/J.TSF.2007.09.042>.
- [51] W. Wang, T. Peijs, A.H. Barber, Indentation induced solid state ordering of electrospun polyethylene oxide fibres, *Nanotechnology* 21 (3) (2009), 035705, <https://doi.org/10.1088/0957-4484/21/3/035705>.
- [52] K.T. Gillen, R.L. Clough, Rigorous experimental confirmation of a theoretical model for diffusion-limited oxidation, *Polymer* 33 (20) (1992) 4358–4365, [https://doi.org/10.1016/0032-3861\(92\)90280-A](https://doi.org/10.1016/0032-3861(92)90280-A) (Guildf).
- [53] W. Hofmann, *Rubber Technology Handbook*, Hanser Publishers, Munich, 1989, 1st.
- [54] A.S. Aprem, K. Joseph, S. Thomas, Recent developments in crosslinking of elastomers, *Rubber Chem. Technol.* 78 (3) (2005) 458–488, <https://doi.org/10.5254/1.3547892>.
- [55] N.J. Morrison, M. Porter, Temperature effects on the stability of intermediates and crosslinks in sulfur vulcanization, *Rubber Chem. Technol.* 57 (1) (1984) 63–85, <https://doi.org/10.5254/1.3536002>.
- [56] 1st A.J. Tinker, K.P. Jones, *Blends of Natural Rubber Novel Techniques for Blending with Speciality Polymers*, Chapman & Hall, London, 1998, 1st.
- [57] H. Dong, Y. Luo, J. Lin, J. Bai, Y. Chen, B. Zhong, D. Jia, Effects of modified silica on the Co-vulcanization kinetics and mechanical performances of natural rubber/styrene-butadiene rubber blends, *J. Appl. Polym. Sci.* 48838 (2019) 1–9, <https://doi.org/10.1002/app.48838>.

Supporting Information

Effects of artificial weathering in NR/SBR elastomer blends

Akshay Karekar*, Carsten Schickanz, Muhammad Tariq, Katja Oßwald, Katrin Reincke,
Valentin Cepus, Beate Langer, Kay Saalwächter*

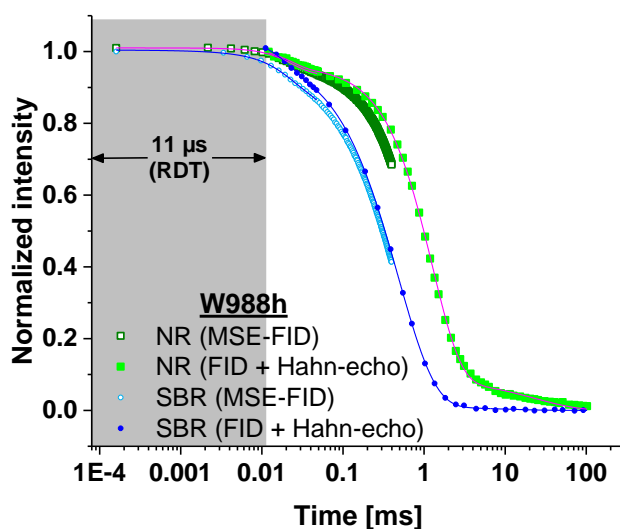


Figure S1. Overlays of MSE-FID, and FID extended with Hahn-echo decay signal for NR and SBR weathered up to 988 h. A three-component modified-exponential decay fitting function (represented by lines) is used to simultaneously fit the data from the two experiments. The number of data points has been reduced and the NR signals have been vertically offset by 0.01 units for visual clarity.

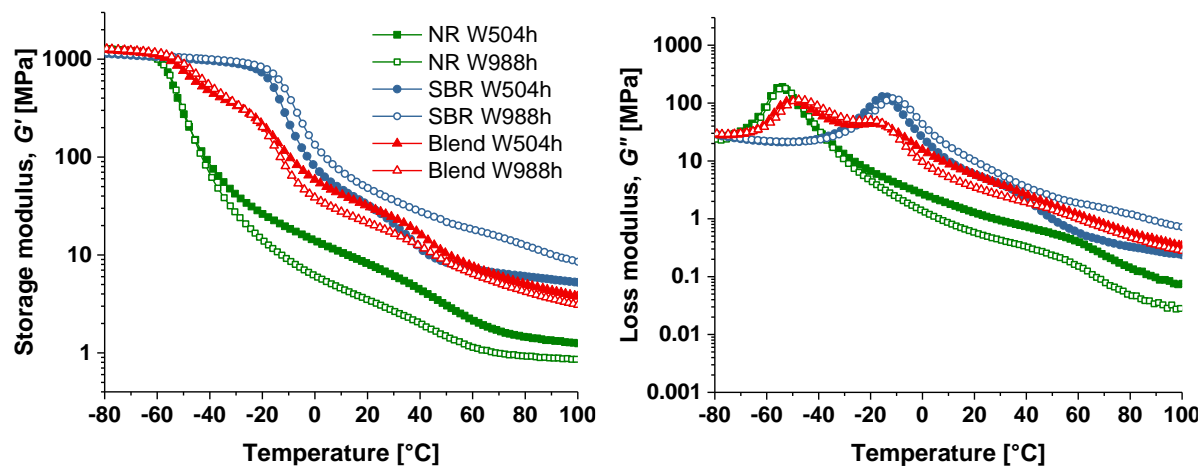


Figure S2. Overlays of DMTA temperature ramps of the storage (left) and loss (right) moduli of NR, SBR, and a 50/50 blend of NR and SBR after various weathering (W) durations.

7. NMR-Based Cross-Link Densities in EPDM and EPDM/ULDPE Blend Materials and Correlation with Mechanical Properties¹

Blends of PE with EPDM open opportunities for exploring a broad range of properties, enabled by the plastic semi-crystalline and amorphous rubber phases. On a microscopic level, possible co-crystallization between the two polymers and the presence of entanglements and cross-links at the interface influence blend behavior. Apart from processing, the ratio of the comonomers within EPDM plays a crucial role.

Here, blends of EPDM with long-branched ULDPE are prepared by cross-linking the EPDM phase with sulfur. The cross-link densities in the blends and an identically cross-linked series of EPDM are measured by the low-field MQ experiment. In the case of blends, the pulse sequence is modified to suppress contributions from the crystalline and crystalline–amorphous fractions to measure only the pure amorphous regions of ULDPE and the EPDM phase. Transverse relaxation experiments are also performed to distinguish the different fractions in ULDPE and EPDM and are used to explain the surprisingly superior tensile properties at higher extents of cross-linking.

Contributor Roles Taxonomy (CRediT) author statement

Akshay Karekar: Conceptualization, formal analysis, investigation, methodology, project administration, visualization, writing – original draft, writing – review & editing. **Reinhold Pommer:** Conceptualization, formal analysis, investigation, methodology, project administration, visualization, writing – original draft, writing – review & editing. **Bianca Prem:** Conceptualization, investigation, methodology. **Caterina Czubala:** Formal analysis, investigation, methodology, visualization, writing – original draft, writing – review & editing. **Christian Teichert:** Formal analysis, investigation, methodology, resources, writing – original draft, writing – review & editing. **Gregor Trimmel:** Funding acquisition, investigation, methodology, project administration, resources, supervision, writing – original draft, writing – review & editing. **Kay Saalwächter:** Project administration, resources, supervision, writing – original draft, writing – review & editing.

¹The associated open-access article and the supporting information are reprinted here under a Creative Commons Attribution 4.0 International Public License (CC BY-NC 4.0). **Authors:** Akshay Karekar, Reinhold Pommer, Bianca Prem, Caterina Czubala, Christian Teichert, Gregor Trimmel, and Kay Saalwächter. **Source:** *Macromol. Mater. Eng.*, **2022**, *307*, 2100968, DOI: 10.1002/mame.202100968. **Website:** <https://onlinelibrary.wiley.com/doi/full/10.1002/mame.202100968>. No changes were made to the article and the supporting information.

NMR-Based Cross-Link Densities in EPDM and EPDM/ULDPE Blend Materials and Correlation with Mechanical Properties

Akshay Karekar,* Reinhold Pommer, Bianca Prem, Caterina Czibula, Christian Teichert, Gregor Trimmel, and Kay Saalwächter*

The role of cross-linking in dictating the microstructural and mechanical properties in ethylene-propylene-diene-monomer rubber (EPDM) and EPDM/ULDPE blends cross-linked by different sulfur amounts is investigated by solid-state ^1H time-domain NMR spectroscopy and tensile-tests. Analyses of spin-spin relaxation time (T_2), by combining free-induction decay (FID), magic-sandwich echo-FID, and Hahn-echo experiments demonstrate a reduction in crystal-amorphous interface regions of pure ultralow-density polyethylene (ULDPE) upon curative addition. The blends demonstrate a complete loss of these fractions due to curative-induced plasticization and solvation by polyethylene segments of EPDM. Cross-link densities, quantified by the magnitude of residual dipolar coupling constant (D_{res}), arising from topological restrictions to segmental motions, are measured by multiple-quantum experiments. The entanglement-dominated EPDMs demonstrate a significant reduction in ultimate tensile properties with increasing D_{res} . The analogous blends yield similar D_{res} values up to 0.36 phr of free sulfur. Thereafter, a deviation from the cross-linking trend of the EPDMs is observed with the blends approaching a cross-linking limit, thus emphasizing the migration of additives to the amorphous phase of the ULDPE. From the additional contributions of solvation and complex entanglement scenarios in the blends, restoration and even significant enhancement in ultimate tensile strength are achieved. Limitations in applying the popular Mooney–Rivlin analysis are also briefly discussed.

1. Introduction

Vulcanized goods based on natural and synthetic rubbers have an enormous technological and economic importance in a range of industries.^[1–4] Considering the growing diversity of applications, however, single-component materials do not often meet the various requirements. In that respect, blending of raw polymeric components has become an established and versatile method to customize material properties. Polymer blending conveniently allows the favorable features of at least two constituents to be combined and balanced. Rather than a focus on inherent properties, their synergistic effects can be used.^[2,5,6] Further benefits arise from the possibility to utilize inexpensive components while maintaining a certain property profile and therefore the reduction of manufacturing costs, as well as the potential optimization of processability.^[7,8]

The sustained growth and significant market share of polymer blends have been comprehensively discussed in literature.^[9,10] Within these multicomponent systems, blends and composites of

A. Karekar, K. Saalwächter
 Institut für Physik-NMR
 Martin-Luther-Universität Halle-Wittenberg, Halle
 Betty-Heimann-Strasse 7, Halle (Saale) 06120, Germany
 E-mail: akshay.karekar@physik.uni-halle.de;
 kay.saalwaechter@physik.uni-halle.de

R. Pommer, B. Prem
 Polymer Competence Center Leoben GmbH
 Roseggerstrasse 12, Leoben 8700, Austria
 R. Pommer, B. Prem, G. Trimmel
 Institute for Chemistry and Technology of Materials
 Graz University of Technology
 Stremayrgasse 9, Graz 8010, Austria
 C. Czibula
 Institute of Bioproducts and Paper Technology
 Graz University of Technology
 Inffeldgasse 23, Graz 8010, Austria
 C. Czibula, C. Teichert
 Institute of Physics
 Montanuniversitaet Leoben
 Franz-Josef-Strasse 18, Leoben 8700, Austria

 The ORCID identification number(s) for the author(s) of this article can be found under <https://doi.org/10.1002/mame.202100968>

© 2022 The Authors. Macromolecular Materials and Engineering published by Wiley-VCH GmbH. This is an open access article under the terms of the Creative Commons Attribution-NonCommercial License, which permits use, distribution and reproduction in any medium, provided the original work is properly cited and is not used for commercial purposes.

DOI: 10.1002/mame.202100968

synthetic rubbers and thermoplastic polyolefins are commonly used. Combinations of ethylene-propylene-diene-monomer rubber (EPDM), an amorphous elastomer of major industrial importance, with different types of semicrystalline thermoplastics, that is, polypropylene or polyethylene, have been investigated and applied for decades.^[11–14] Overall physico-mechanical properties of polymer blends are evidently dependent on the chemical and structural properties of the raw components, their blending ratio, manufacturing methods, and effectively on their morphology and thermodynamic compatibility, which dictates how the components form into a fully miscible, partially miscible, or immiscible system. Here, EPDM/thermoplastic blends are typically assigned to the latter, despite some minor degree of compatibility.^[6,15–17]

The macroscopic performance of the resulting materials can be conveniently evaluated by mechanical testing, by the determination of thermal properties, chemical resistance, and solubility, as well as by the measurements of electrical or optical properties by different means.^[18,19] The typical rubber-elastic properties of EPDM and elastomers in general are attributed to moderate cross-linking of the soft polymer chains, which generates an insoluble network. Introducing a non-cross-linked, reinforcing and weldable thermoplastic constituent allows for a variety of improvements.^[4,5,18] Explaining the origin of the synergistic effects in the polymer blend is not a trivial task, and determining its macroscopic properties only do not usually provide sufficient information. Along with the abovementioned properties, another crucial aspect lies in the type of chemical cross-linking of the material, which is sulfur-, peroxide-based, or radiation promoted, as well as in an understanding of the density and distribution of cross-links within the blend system on a molecular level.^[20–22] Conventional methods to assess the segmental molecular weight include equilibrium swelling or diffusion experiments, rheological measurements, or by derivation from elasticity theory using mechanical data, such as stress-strain or dynamic-mechanical analysis.^[20,23–26] All of these methods reach their limits when it comes down to a true quantification of cross-linking densities or elucidation of a phase-resolved distribution thereof.

Nuclear magnetic resonance (NMR) spectroscopy has evolved as a popular technique for elucidation of molecular information, be it structure or dynamics. The dependence of the macromolecular behavior on these molecular and microscopic origins can thus be understood using NMR techniques. Cross-link density in EPDM using different cross-linker systems has already been studied by solid-state NMR, and the role of entanglements in network properties has been established, too.^[27–32]

Inclusion of thermoplastic polyolefins introduces synergistic effects now arising from the elements of crystallinity and molecular entanglements. Using NMR spectroscopy, the effects of these parameters in cross-linked EPDM/polyolefin blends have been investigated by ¹H lineshape analyses by spinning the blends at the magic-angle (MAS),^[33] and ¹H-¹³C cross polarization-MAS experiments.^[34] In a time-domain study, cross-link densities have been qualitatively analyzed by combining spin-spin relaxation time (T_2), obtained by a free induction decay (FID), with a double-quantum (DQ) filtered Hahn-echo.^[35] Despite the abundant molecular information obtained through these diverse NMR methodologies, they lack a direct quantification of the network density in the blends.

In the past couple of decades, a rather robust time-domain multiple-quantum (MQ) experiment has been used to unravel molecular details in a wide range of polymeric materials,^[36] such as swollen gels,^[37] nanocomposites,^[38] polymer melts,^[39] and rubber blends.^[40] Topological constraints such as cross-links and entanglements cause a non-isotropic averaging of segmental fluctuations of the polymer chains, which leads to a residual value of the dipole-dipole interaction constant, D_{res} , among the protons on the monomers. D_{res} is an appropriate and quantitative measure of the constraint density as it has an inverse proportionality with the number of Kuhn segments between the constraints. In addition to this, the distributions of these constraints across the volume of a sample, and the amount of defects (uncoupled fractions) can also be quantified. Thus, a realistic picture of the nature of a polymer sample can be obtained.

Subject of this study is the elucidation of relative cross-linking densities in sulfur-cured EPDM samples, as well as in binary EPDM/ultralow-density polyethylene (ULDPE) blends, and to reveal the correlation of these findings with macroscopic properties. EPDM and EPDM/ULDPE blends at a fixed weight ratio of 60/40 were processed by means of a standard mixing procedure and subsequent curing by hot-press molding, using gradually increasing amounts of a sulfur-based cross-linking system. Vulcanization characteristics and mechanical properties of the obtained materials were investigated by rheological measurements and uniaxial tensile testing, respectively. Differential scanning calorimetry (DSC) was performed to investigate miscibility and thermal properties of the materials. The blend morphology was further studied by atomic force microscopy (AFM). Weakening of mechanical properties for pure EPDM samples with an increasing sulfur content can be observed, whilst surprisingly, the immiscible EPDM/ULDPE blends benefit from a rising degree of cross-linking in the rubber phase and yield significantly improved mechanical properties. Extensive studies by solid-state ¹H NMR experiments provide information on the phase composition of the materials, the effect of additives on the respective phases as well as the preferential distribution in those. Herein, relative cross-linking densities as function of the sulfur content in the pure elastomer samples and elastomer/thermoplastic blends are determined and the relationship with the mechanical properties is discussed.

2. Experimental Section

2.1. Materials and Sample Preparation

Amorphous EPDM (grade Keltan 6950C) with a specified ethylene content of 44 ± 2.1 wt% and an ENB (ethylidene-norbornene) content of 9.0 ± 0.8 wt% was supplied by LANXESS (Germany), and ultralow-density polyethylene-hexene copolymer (ULDPE, grade Attane 4607GC) was obtained by Dow Chemical Company (Midland, USA). Ground sulfur was provided by Solvay (Germany), and accelerators *N*-cyclohexyl-2-benzothiazole sulfenamide, tetramethyl thiuram disulfide (TMTD), and diphenyl guanidine were supplied by Lions Industries (Slovakia). All chemicals were used without further purification. Samples of EPDM and EPDM/ULDPE (60/40 weight ratio) were prepared by mastication and melt-blending utilizing a Plasti-Corder internal mixer (Brabender, Germany) at a mixing temperature of

140 °C and a rotor speed of 75 rpm for 5 min each. Sulfur-based cross-linking formulations with varied quantities of S (0, 0.36, 0.72, and 1.44 parts per hundred rubber, “phr”) and the accelerator mixture at a consistent quantity of 4 phr were applied to EPDM. In the EPDM/ULDPE blends, the same proportions of additives with respect to the EPDM amount were applied. Following an overnight storage of the compounds, curing agents were subsequently added to the polymer compounds on a two-roll mill (Servitec, Germany) at room temperature. Vulcanization characteristics of the prepared mixtures after overnight storage were measured using a Rheoline Multifunction moving-die rheometer (Prescott Instruments, UK) at 190 °C (timed test at constant frequency of 1.67 Hz and amplitude of 0.50° arc). The compounded rubber sheets were thereafter vulcanized at 190 °C using an electrical press (Collin, Germany). For comparative purposes, pristine EPDM (without additives, named hereafter as “E-pure”), pristine ULDPPE (without additives, named hereafter as “U-pure”), and ULDPPE with a quantity of curing agents corresponding to an EPDM/ULDPE (20/80) formulation (referred to as U-20/80) were prepared analogously by subjecting them to the same thermal history as the EPDMs and the blends.

2.2. Characterization Methods

2.2.1. Mechanical Testing

Mechanical characteristics, that is, tensile strength (TS), ultimate elongation, and moduli of rubber samples and blends were investigated using an Autograph AGS-X universal tensile tester (Shimadzu, Japan). Tests were performed on dumbbell-shaped specimens (total length = 100 mm, clamping length = 75 mm, width = 3 mm) at a tensile rate of 500 mm min⁻¹ without preload. Sample thickness was determined by means of a Digimatic Micrometer (Mitutoyo, Japan).

2.2.2. Differential Scanning Calorimetry

DSC measurements were performed utilizing a DSC 214 Polyma (Netzsch, Germany). Heat flow curves were recorded from -120 to 300 °C at a heating rate of 10 K min⁻¹ in N₂ atmosphere. Glass transition and melting temperatures were defined by inflection and peak point values, respectively.

2.2.3. Atomic Force Microscopy

AFM was applied to study the morphology and phase separation of the samples. For this purpose, cross-sectional samples of cross-linked EPDM and EPDM/ULDPE blends were prepared by cryo-microtomy cutting. All AFM measurements were recorded in tapping mode using an Asylum Research MFP-3D AFM (Santa Barbara, CA, USA). The instrument was equipped with a closed-loop planar x - y -scanner with a scanning range of 85 × 85 μm² and a z -range of 15 μm. As AFM probes, standard silicon probes (Olympus AC160TS, Japan) were employed which had a cantilever spring constant of about 30 N m⁻¹ and a tip radius of about 15 nm. The measurements were obtained in intermittent

contact mode under ambient conditions at 46 ± 9% relative humidity and a temperature of 23 ± 1 °C. Topography and phase images were recorded at three independent positions for each sample. Phase imaging can be used to obtain a qualitative material contrast.^[41,42] The data was processed in the open-source software Gwyddion.^[43]

2.2.4. Solid-State Time-Domain ¹H NMR Spectroscopy

¹H NMR measurements of the cured series of EPDM and EPDM/ULDPE blends were performed on a Bruker minispec mq 20 benchtop spectrometer (20 MHz proton resonance frequency) having a 90° pulse length of 2.6 μs and a dead time of 12 μs. The samples, stacked to a height of 6 mm in an NMR tube having a diameter of 10 mm, were measured under air at 70 °C using a BVT 3000 temperature controller.

2.3. NMR Theory

2.3.1. Decomposition of Polymer Fractions by T₂ Relaxometry

Study of transverse magnetization decay by an FID gives information on polymer relaxation at short evolution times. Depending on the nature of the decay and by using a suitable fitting function,^[44–52] fractions associated with different T₂ relaxation times in the polymer can be classified. In the current setup, fractions with relaxation time scales up to 0.2 ms can be easily classified, beyond which magnetic field heterogeneities dominate. To probe somewhat mobile fractions (associated with longer relaxation time scales), Hahn-echo T₂ relaxometry is used. Thus, by stitching data obtained from FID and Hahn-echo, the gamut of different relaxation time scales and the corresponding quantities of the fractions can be extracted.^[53] In NMR phenomenology, protons in shorter chain segments (higher cross-linking) relax faster (⇒ shorter T₂) than segments in longer network chains (⇒ longer T₂).

Limitations arise when probing rigid fractions, such as chain segments that are part of the crystallites, as in the case of ULDPPE. These correspond to a rigid limit coupling constant of about 30 kHz, with time scale of relaxation of about 20 μs. Due to the inevitable receiver dead time, precious information is lost in the early part of an FID decay. To compensate for this signal loss in the short-time limit, an echo experiment like the pulsed version of the magic-sandwich echo (MSE) is used.^[54] MSE performs a time-reversal of the decay signal by refocusing multispin dipolar interactions. Figure A (see Appendix) gives a perspective highlighting the loss of initial signal in an FID due to the highly constrained fractions in pure ULDPPE. Also demonstrated is the signal compensation achieved by an MSE using a short interpulse delay ($\tau_{\phi, \text{MSE}}$) of 2 μs. Hence, by simultaneous fitting of the Hahn-echo-extended FID with MSE-FID using a multicomponent modified-exponential decay function ($\propto f_s \exp[-(t/T_{2,x}^{\text{eff}})^{\beta}]$), a complete description of polymer relaxation can be obtained.^[53] An effective T₂ (T₂^{eff}) is obtained in the presence of dipolar couplings. The rigid crystallites are described by a shape parameter, $\beta = 2$ (Gaussian decay), and lower values of β are obtained due to coupling distributions and relaxation

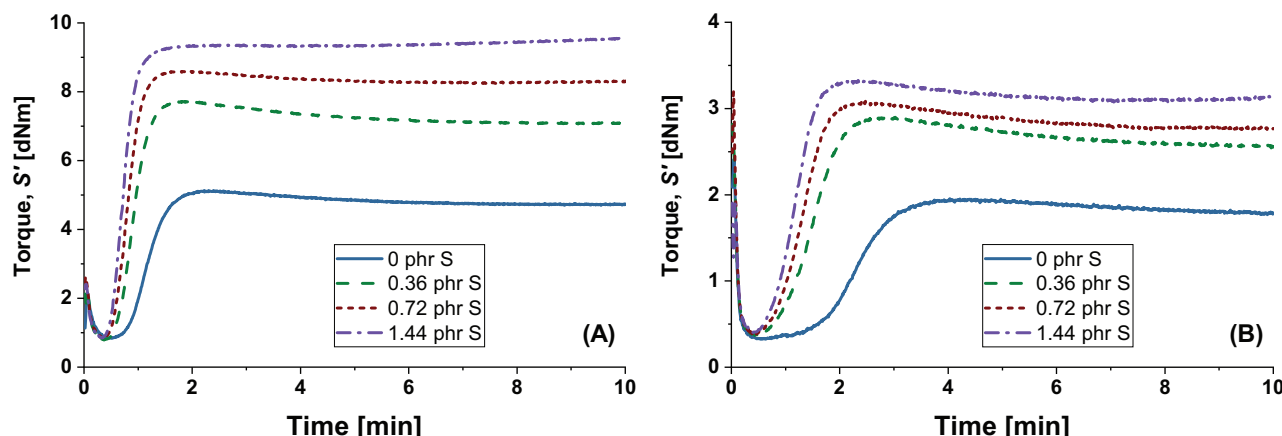


Figure 1. Vulcanization curves at a curing temperature of 190 °C for A) EPDM compounds, and B) EPDM/ULDPE blends, both with varied concentrations of elemental sulfur (0, 0.36, 0.72, and 1.44 phr S).

effects. The different fractions, f_x , corresponding to the different relaxation times can be thus obtained from such a fit.

2.3.2. Time-Domain MQ NMR Measurements for Elucidation of Cross-Link Densities

As for the degree of cross-linking, it is reflected in the residual dipolar coupling constant extracted from the MQ NMR data introduced earlier. It is directly proportional to the segmental dynamic order parameter, S_b , and thus inversely proportional to the Kuhn segments of the polymer chains. To obtain an absolute value of the cross-link density, certain model considerations are necessary for the polymer of interest.^[55] Since this value is unknown for EPDM, a relative D_{res} description would suffice.

The used MQ pulse sequence,^[36] based on the works of Baum and Pines,^[56] gives a DQ build-up signal (I_{DQ}) arising due to contributions from coupled spins, which decays at longer DQ evolution times. Additionally, a decaying reference signal (I_{ref}), comprising of contributions from coupled and also uncoupled spins (defects) is used for normalization by point-by-point division of the DQ signal. Presence of isotropically active mobile defects (consisting of mechanically irrelevant fractions of chain ends, loops and sol) are accounted for by subtracting them during normalizations. An adequate subtraction of the decay “tail” results in the normalized DQ signal, I_{nDQ} , reaching a 0.5 intensity limit. The I_{nDQ} signal can be fitted using a fitting function that uses an Abragam-like kernel function, which describes the rise of the nDQ intensity in terms of D_{res} ,^[57] combined with a numerically calculated integral over a log-normal coupling distribution:^[58]

$$P(\ln(D_{\text{res}})) = \frac{1}{\sigma_{\ln} \sqrt{2\pi}} \exp\left[-\frac{\{\ln(D_{\text{res}}) - \ln(D_{\text{med}})\}^2}{2\sigma_{\ln}^2}\right] \quad (1)$$

The fitting parameters are thus the median value D_{med} as well as the logarithmic standard deviation σ_{\ln} . The latter is positive and dimensionless and reflects the distribution full width at half maximum roughly in the unit of decades (e.g., $\sigma_{\ln} = 0.5$ corresponds

to a half-decade wide distribution). For an entanglement-rich polymer such as EPDM, the total measured coupling strength,

$$D_{\text{res}} \propto \frac{1}{M_{c, \text{EPDM}}} + \frac{1}{M_{e, \text{EPDM}}} \quad (2)$$

wherein M_c is the average molecular weight between cross-links and M_e is the average entanglement molecular weight.

3. Results and Discussion

3.1. Curing Characteristics

First, the vulcanization behaviors of the compounds were studied using a moving-die rheometer. Rheological curves at 190 °C for EPDM and EPDM/ULDPE (60/40) compounds with four different quantities of elemental sulfur recorded at preset strain and frequency are shown in **Figure 1**. It must be noted that all formulations contain equal amounts of sulfur-donating accelerator components (TMTD). This method allows to follow the progress of the vulcanization process by measuring the elastic torque (S'), as the material's resistance to shear deformation increases with the formation of cross-links in the system. EPDM compounds with free sulfur (0.36 to 1.44 phr S) exhibit very similar and sharp vulcanization onset times and subsequently reach plateaus, which expectedly show higher maximum torques for higher sulfur contents. Increasing torques can therefore be used as indication for an increase of the relative cross-linking densities in the system.^[24–26,59] Comparable observations regarding the vulcanization onset can be made for EPDM/ULDPE blends. Owing to the thermoplastic content in the mixture, the measured torque is significantly lower, and the curing period appears slightly broadened. Again, the steadily growing peak torque values in dependence on the sulfur loading indicate a higher degree of vulcanization. This applied curing formulation in combination with extended vulcanization times generally creates a network with predominantly short cross-links (esp. mono- and di-sulfide linkages) and a comparably low portion of polysulfide links.^[60,61]

Regarding the formulations without free sulfur (0 phr S), which essentially rely on the sulfur released from the donating

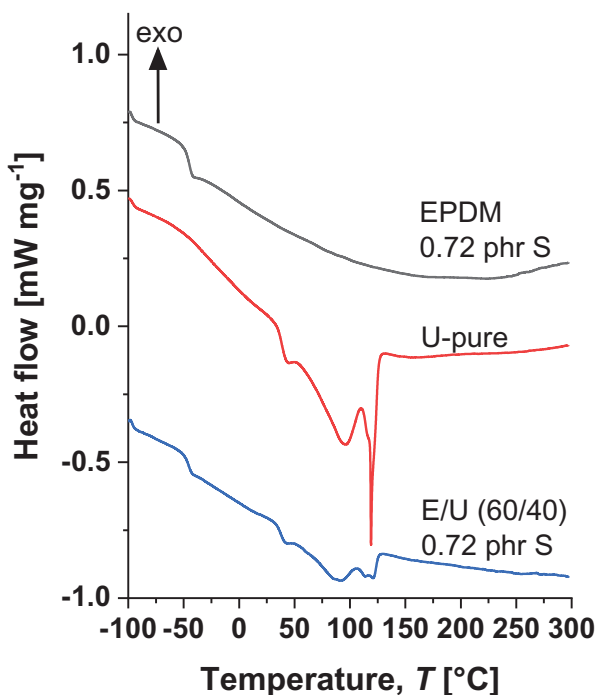


Figure 2. DSC curves for pure ULDPE (U-pure), and cross-linked EPDM and EPDM/ULDPE blend with 0.72 phr sulfur. Shown here are the first melting cycles measured at a temperature ramp rate of 10 K min⁻¹.

vulcanization agent TMTD, a prolonged scorch time is evident for both, the rubber and the rubber/thermoplastic blend systems. This is attributed to the delayed availability of sulfur provided by the decomposition process of the thiuram compound. In this case, using sulfur-donating agents only, a stable vulcanization network with a comparably very high content of mono- and di-sulfide links is formed.^[61,62] All samples were consistently prepared by hot press molding for 10 min at 190 °C.

3.2. Semicrystalline Morphology

DSC and AFM were used to analyze the effect of blending on the semicrystalline properties of the blends. DSC was on the one hand performed to investigate the thermal properties of the single materials, and on the other hand, to obtain information on the thermodynamic compatibility or miscibility of polymers in the blend system. Representative DSC curves for molded samples during the first heating cycle at a temperature ramp rate of 10 K min⁻¹ are presented in **Figure 2**. The glass transition temperature T_g of the vulcanized EPDM (0.72 phr S) compound was found to be -44 °C. The pure ULDPE shows a T_g at 38 °C and a rather broad melting range T_m with two distinct peaks at 96 °C and 119 °C. As for the EPDM/ULDPE (60/40) blend (0.72 phr S), a $T_{g,1}$ is measured at -46 °C which is assigned to the rubber phase. A further $T_{g,2}$ of 39 °C along with the broad melting range (with considerably less distinct, yet recognizable peaks at $\approx 92^\circ\text{C}$ and a double peak at 114–121 °C) are attributed to the ULDPE phase. Comparing the thermal transition temperatures in the blend and the respective single materials, only a negligible shift of the values can be observed. This suggests that the

EPDM/ULDPE blend represents an immiscible system at lower temperatures.

To get a better insight on the phase separation and illustrate its complexity, AFM topography scans with corresponding phase images have been obtained on microtomed cross sections of cross-linked EPDM and the EPDM/ULDPE (60/40) blend, both containing 0.72 phr free sulfur (**Figure 3**). In Figures 3A and 3B, topography images (acquired in intermittent contact mode) of the EPDM sample and the blend are presented, respectively. The corresponding phase images have been recorded for the EPDM sample (Figure 3C) in attractive mode with a phase angle larger than 90° and for the EPDM/ULDPE (60/40) blend in repulsive mode with phase angle <90° (see Figure 3D). Since EPDM is softer than ULDPE, the phase contrast between both materials is quite strong in Figure 3D. The darker color corresponds to a low phase angle and indicates the ULDPE domains, whereas the brighter color corresponds to a high phase angle and characterizes the softer EPDM matrix. The phases are rather randomly distributed in the EPDM/ULDPE blend and the phase separation length between the individual phases is roughly in the range of 0.1–0.5 μm . The ULDPE phase is characterized by spherical structures with about 0.1–0.2 μm diameter, which frequently coalesce to larger regions of 0.5 μm . Sometimes, even continuous random networks of connected ULDPE areas are observed. However, possible influences from sample preparation and migration effects cannot be completely excluded. Therefore, one should be careful to directly relate the AFM information to the actual bulk morphology.

3.3. Mechanical Properties

Improving the mechanical properties is one of the key reasons for blending elastomeric and thermoplastic materials. Systems combining rubbers and different grades of polyethylene have reportedly shown benefits for tensile, ageing, or abrasion properties.^[5,63,64] As already stated, within this study the effect of different quantities of vulcanization agents was investigated.

By standardized uniaxial tensile testing, the TS and elongation at break (EB) of the samples were determined, which constitute essential material characteristics. **Figure 4A** compares the TS and EB for cross-linked EPDM samples. Here, the sample cured with 0 phr elemental sulfur demonstrates superior TS and EB of ≈ 9 MPa and >1000%, respectively. A significant drop of both TS and elongation can be observed by introducing free sulfur (specimen with 0.36 phr S) as a vulcanization agent and therefore creating a denser cross-linking network with greater rigidity. A higher sulfur content leads to a subsequent but comparably less rapid decrease, effectively yielding a TS of 1.9 MPa and an EB of 240% at a sulfur loading of 1.44 phr S. The mechanical properties are apparently strongly dependent upon the distribution, density, and length of the sulfur cross-links, which reportedly can be varied by means of the sulfur quantity added to the rubber compounds.^[2,20,22] EPDM/ULDPE (60/40) samples, which are presented in **Figure 4B** demonstrate a contrary effect, which reveals superior tensile properties of the elastomer/thermoplastic blends and the reinforcing nature of the ULDPE component. By a stepwise increase of the sulfur content, the system shows an improved TS of up to 24 MPa, along with rather comparable

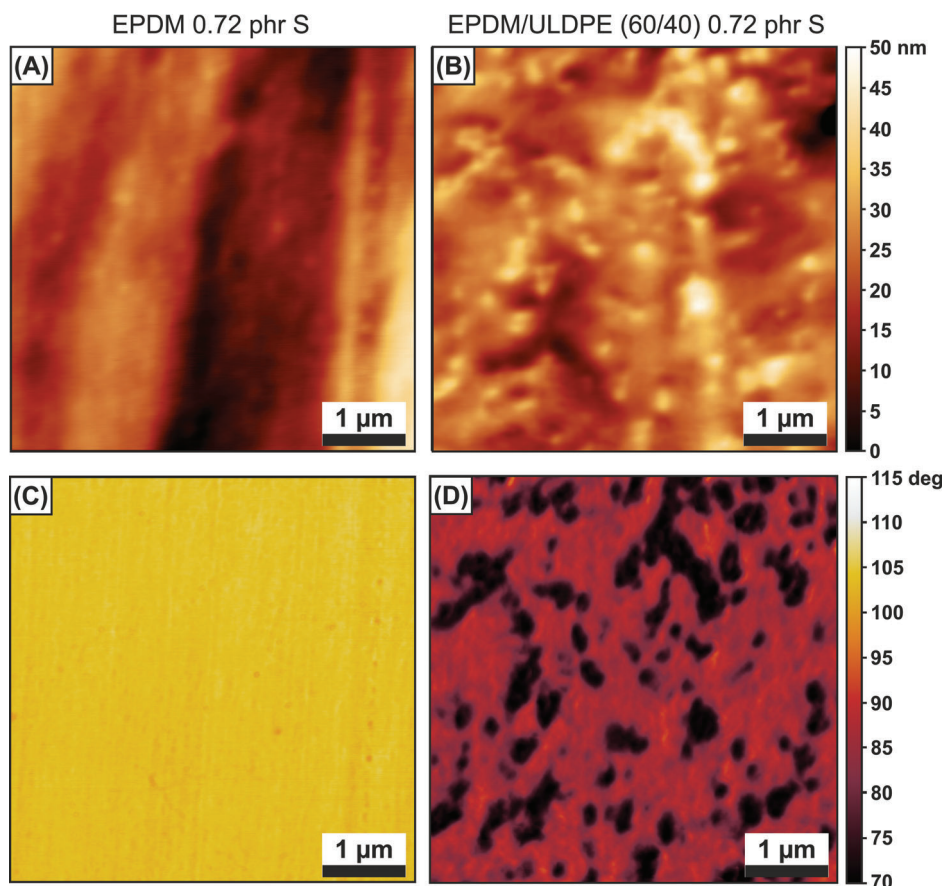


Figure 3. $5 \times 5 \mu\text{m}^2$ A,B) AFM topography images and C,D) corresponding phase images for A,C) cross-linked EPDM, and B,D) cross-linked EPDM/ULDPE (60/40) blend, both containing 0.72 phr free sulfur. The dark areas in (D) indicate the harder ULDPE phase.

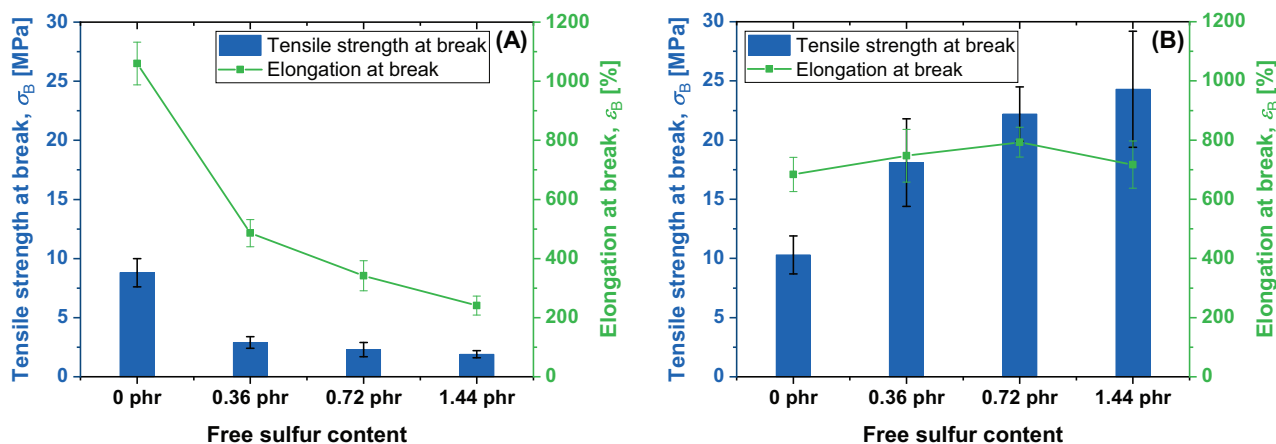


Figure 4. Comparison of tensile strength at break and elongation at break for A) EPDM compounds, and B) EPDM/ULDPE blends, both with varied concentrations of elemental sulfur (0, 0.36, 0.72, and 1.44 phr S).

mean elongations at break between about 700% and 800%. **Table 1** summarizes the results of the tensile tests. For reference, pure ULDPE (U-pure) was processed and tested analogously. Additionally, a sample of ULDPE containing vulcanization agents (U-20/80) was analyzed in order to see a potential influence of the vulcanization agents on the mechanical properties, as well as

on the phase composition determined via NMR characterization. Mechanical properties of these samples are also included in **Table 1**.

The reinforcing role of ULDPE within the rubber/thermoplastic system is further emphasized by comparing the stress–strain curves of the EPDM/ULDPE blend with

Table 1. Summary of tensile strength (TS) and elongation at break (EB) values for all investigated samples with varied formulations.

EPDM	TS [MPa]	EB [%]
0 phr S	8.8 ± 1.2	1060 ± 72
0.36 phr S	2.9 ± 0.5	486 ± 46
0.72 phr S	2.3 ± 0.6	342 ± 51
1.44 phr S	1.9 ± 0.3	241 ± 32
EPDM/ULDPE (60/40)	TS [MPa]	EB [%]
0 phr S	10.3 ± 1.6	684 ± 58
0.36 phr S	18.1 ± 3.7	747 ± 89
0.72 phr S	22.2 ± 2.3	793 ± 50
1.44 phr S	24.3 ± 4.9	717 ± 80
ULDPE	TS [MPa]	EB [%]
U-pure ^{a)}	27.8 ± 1.8	602 ± 20
U-20/80 ^{b)}	27.6 ± 2.0	610 ± 24

^{a)} ULDPE without any additives; ^{b)} ULDPE processed with a quantity of cross-linking agents corresponding to an EPDM/ULDPE (20/80) blend formulation.

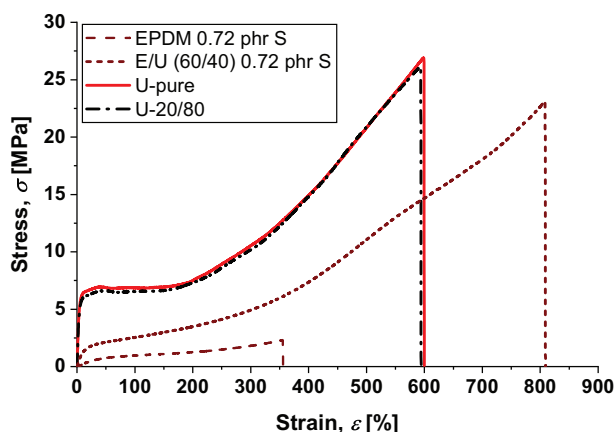


Figure 5. Representative stress–strain curves of EPDM as well as EPDM/ULDPE (60/40) cured with 0.72 phr S, and processed U-pure and U-20/80.

the respective single materials (Figure 5). Herein, the blend (0.72 phr S) does not only show superior mechanical features when compared to EPDM (0.72 phr S), but also clearly improved values of EB relative to pure ULDPE samples which were processed in the same way. The addition of vulcanization agents to ULDPE has no obvious impact on the macroscopic mechanical properties, neither on TS, EB, nor on the progression of the stress–strain curve. Likewise, the linear-regime modulus is also identical (≈ 150 MPa) for both the ULDPE variants. In case of the blends, the Young’s modulus is obtained to be about 10.5 MPa across all the sulfur compositions. It is hence remarkable to note that despite being much softer, at high cross-linking, the blend has virtually the same ultimate properties as pure ULDPE.

In order to correlate mechanical properties with results from cross-linking density determination, measured stress–strain curve relations were further used to calculate moduli of the

materials. Whilst for EPDM/ULDPE samples the distinct linear elastic region allowed for the direct determination of the Young’s modulus, this method appeared inadequate for the EPDM samples. Therefore, an evaluation based on the Mooney–Rivlin (MR) model was chosen.^[65,66] For assessment of the apparent Mooney–Rivlin constants ($2C_1$ and $2C_2$), which are assigned to the cross-link modulus (G_c) and entanglement modulus (G_e), respectively, the reduced stress (σ_{red}) is plotted against the reciprocal deformation (λ^{-1}), according to Equation (3).

$$\sigma_{\text{red}} = \frac{\sigma}{\lambda - \lambda^{-2}} = 2C_1 + \frac{2C_2}{\lambda} \quad (3)$$

where σ_{red} is the reduced stress or Mooney stress, λ is the deformation (L/L_0), and $2C_1$ and $2C_2$ are the MR constants.

Such a plot is shown in Figure 6A for an EPDM sample at 0.72 phr loading of sulfur. However, to fit such a plot it is optimum to account for errors related to the testing itself. Thus, a small correction to the deformation component as $\lambda \pm \Delta\lambda$ can yield a linearized “corrected” reduced stress ($\sigma_{\text{red,corr}}$) curve in the limit up to $1/\lambda_{\text{corr}} = 1$.^[65] Applying a linear fitting function in the range of $1.25 < \lambda \pm \Delta\lambda < 2.5$ ($0.8 > \lambda \pm \Delta\lambda^{-1} > 0.4$), which also avoids the upturn due to finite extensibility at large strains, numerical values for $2C_1$ and $2C_2$ are thus determined, which are tabulated in Table 2.

The measure of cross-link density from the intercept ($2C_1$) shows an expected increase in values with an increase in sulfur, as seen from G_c for the EPDMs. Contrary to the G_c trend, the apparent entanglement modulus is found to decrease slightly with increasing sulfur. Consequently, this results in the total modulus ($G_c + G_e$) varying insignificantly with respect to the added free sulfur. This behavior of the entanglement modulus is an unusual finding which requires molecular-level investigations and is thus deferred to the end of the paper.

In contrast to a characteristic neo-Hookean behavior demonstrated by the EPDMs, pure ULDPE and the representative blend in Figure 6B show a deviation from this behavior. The sharp departure from linearity in the quick rise for $1/\lambda \rightarrow 1$ even upon $\Delta\lambda$ -correction is due to yielding in polyethylene. The retention of higher strength even after breakdown of the crystalline framework in ULDPE appears to be delayed in the blend, which probably leads to larger break-stress upon cross-linker increment even at larger strains. This could be due to a non-trivial interaction of ULDPE with the other phase (EPDM), and probably also the additives which appear to enhance the ultimate properties by dilution (discussed later).

3.4. Distinction of Crystalline, Amorphous, and Crystalline-Amorphous Interface Fractions in EPDM/ULDPE Blends by T_2 Relaxation Analyses

FID and Hahn-echo experiments serve as good tools for distinguishing the different T_2 -related fractions in a polymer sample. Owing to their compositions, one can expect different relaxation patterns for the samples under study. Typical FIDs extended by respective Hahn-echo decay curves for pure EPDM, pure ULDPE, and their 60/40 blend at 0.72 phr sulfur loading are represented in Figure 7 (open symbols). The trends of these curves thus highlight their different relaxation behaviors. Also

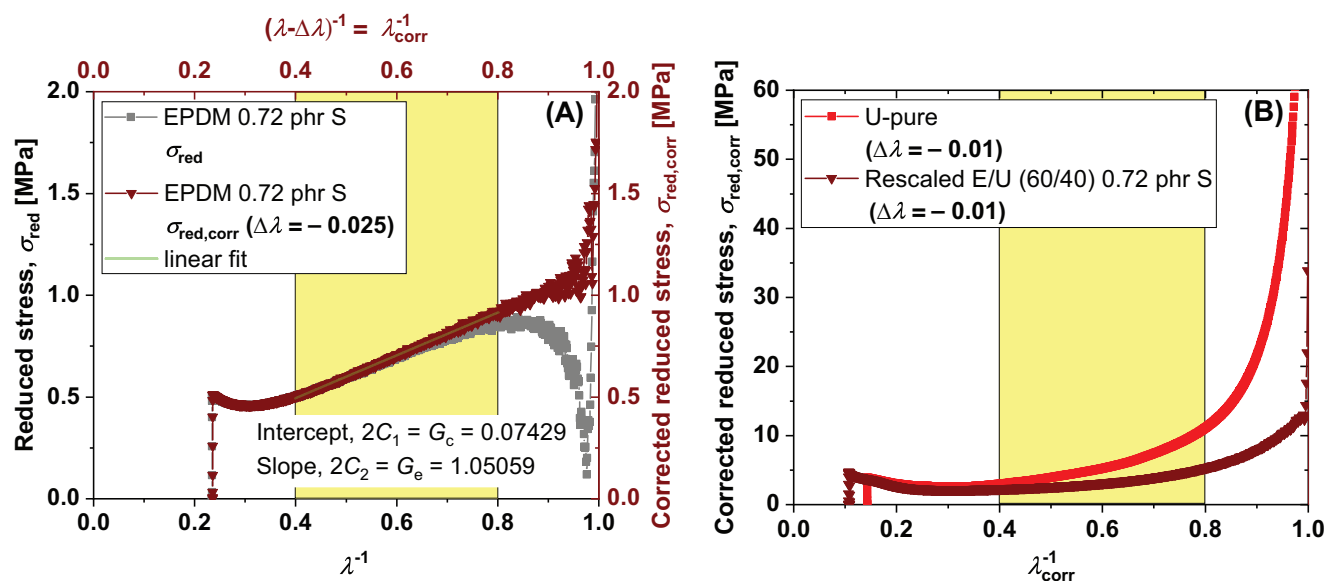


Figure 6. A) Exemplary plot of reduced stress against the reciprocal deformation, and the corrected reduced stress against the reciprocal corrected deformation, with a linear fit in the limits $1.25 < \lambda - \Delta\lambda < 2.5$ ($\Delta\lambda = -0.025$) according to the Mooney–Rivlin model. B) Corrected reduced stress plots of pure ULDPE and a (vertically rescaled) blend (0.72 phr S). Delayed strain-softening in the blend probably leads to enhanced strain-at-break. The sharp upturn (sharp decrease for $1/\lambda_{corr} < 1$) due to yielding in polyethylene renders MR fits unusable for such materials.

Table 2. Young's moduli as well as results from the Mooney–Rivlin hyperelastic model for cross-linked EPDMs.

EPDM	Young's modulus [MPa]	G_c^a [MPa]	G_e^b [MPa]	$(G_c + G_e)$ [MPa]
0 phr S	2.5 ± 0.1	-0.08	1.14	1.06
0.36 phr S	2.3 ± 0.1	-0.02	1.10	1.08
0.72 phr S	2.2 ± 0.1	0.07	1.04	1.11
1.44 phr S	2.3 ± 0.1	0.19	0.90	1.09

^{a)} Cross-link modulus; ^{b)} Entanglement modulus.

shown are the MSE-FIDs (solid symbols) to probe the fractions associated with very short transverse relaxation times. Simultaneous fits to the two data sets were first performed for pure EPDM (without cross-linker) using a three-component fitting function. A weighting of 10% was applied to the FID part due to the higher number of data points. The shape parameters (β_r and β_{m2}) for the most rigid fraction (f_r) and the most mobile fraction (f_{m2}) were fixed to 2 and 0.8 (stretched exponential), respectively. This yielded a $T_{2,m2}^{eff} = 1.6$ ms with the corresponding fraction, $f_{m2} = 37\%$. From the fit, a major fraction ($f_{m1} \approx 63\%$) with $T_{2,m1}^{eff}$ of about 0.8 ms and the corresponding value of the shape parameter ($\beta_{m1} = 1.3$) were also obtained. Due to the absence of any motion-constrained components in the sample, the fit showed no indications of the presence of a rigid fraction. Here, it must be emphasized that the two mobile fractions cannot be objectively distinguished due to the rather small separation in their relaxation times. They thus represent the more or less constrained ends of a broader distribution. Due to the negligible amount of rigid fraction, a two-component fit including a built-in distribution would suffice for this particular polymer. Nevertheless, a

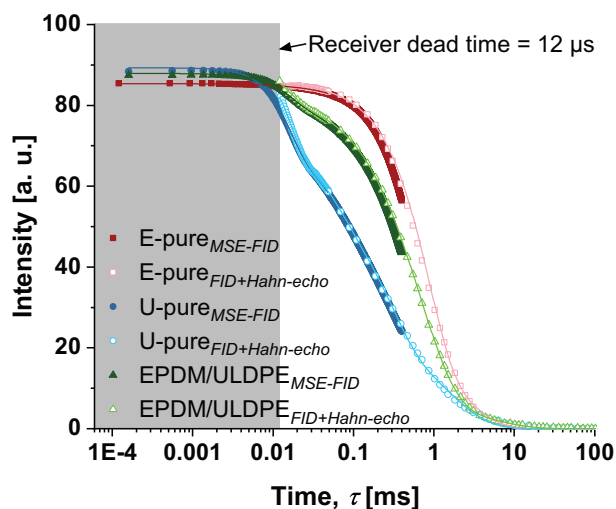


Figure 7. Simultaneous fits to MSE-FID with Hahn-echo-extended FID distinguishing the different relaxation patterns in various compositions. The fits are represented as solid lines for pure EPDM (three-component), pure ULDPE (four-component), and EPDM/ULDPE blend with 0.72 phr sulfur (four-component). The MSE-FIDs are fitted only until the corresponding evolution times of the FIDs (≈ 40 μ s).

three-component fitting function (consisting of $\beta_r = 2$) is essential to account for the fast relaxations of segments in crystal lamellae of ULDPE in the blends and to distinguish the contributions of EPDM fractions in the blends. Further, due to the presence of a distribution of spin–spin relaxation time constants, β_{m2} is restricted to a minimal value of 0.8 to avoid the ambiguity that a too-stretched exponential “steals away” amplitude from a close by T_2 component. Note that the two components used to describe the

Table 3. Rigid fractions in the polyethylene homopolymer variants and EPDM/ULDPE blends.

	U-pure	U-20/80	Blends
f_c [%]	24.0	24.0	9.5
f_{ci} [%]	14.0	9.0	0

long-time contribution do not correspond to physically distinguishable components; rather, the two-component fit just serves to parameterize the data and allow for a comparison among the samples.

Unlike the amorphous EPDM, the presence of crystalline regions in ULDPE contributes also to shorter relaxation times. Thus, a four-component fitting function is suitable to probe pure ULDPE and the blends. For pure ULDPE, the fit yielded a rigid fraction amounting to 24% of the sample. This fraction, having a Gaussian decay ($\beta = 2.0$) with a T_2^{eff} of about 16 μs , can be attributed to the crystalline lamellae (f_c). A second fraction of 14%, associated with a transverse relaxation time of 65 μs and $\beta = 1.5$, was also obtained. Fractions with these relaxation times are associated with semirigid regions of intermediate motions, which in a semicrystalline polymer are the interfaces between crystalline lamellae and the amorphous regions (hence referred as f_{ci}).^[35] In comparison, U-20/80 (not shown in the figure) has a similar quantity of f_c , suggesting that the amount of crystalline regions remain unchanged (Table 3). Fascinatingly though, the intermediate regions dropped down to about 9%. This is a rather surprising outcome, and could probably be due to a plasticizing effect of the additives included in the polymer which seem to interfere at the crystallite-amorphous interface regions. An account of the fitting uncertainty in these systems by multicomponent modified-exponential decay function is given in the Supporting Information.

To have a comparative consistency between the samples, the shape parameters and the T_2^{eff} relaxation times of f_c and f_{ci} for U-20/80 were kept consistent with the values obtained through fitting pure ULDPE. The same protocol was employed for the blends too. The representative plot in Figure 7 demonstrates the changes arising in the sample due to blending. Figure 8 provides an overview of the soft EPDM-related fit fractions (\Rightarrow m1 and m2) in the blends. These are compared with the fit components having similar spin-spin relaxation times in the polyethylene variants. The loss in the intermediate fractions of U-20/80 reflects as a gain in its amorphous f_{m1} fraction. However, no evidence of these microscopic changes can be inferred in the stress-strain curve in Figure 5.

In the blend, upon addition of the accelerator mixture, a jump of 30% in f_{m1} can be seen which can be attributed to the formation of cross-links in the EPDM phases. Here, it is important to note that f_{m1} also contains polyethylene segments constrained by entanglements and linkage to the crystals in the amorphous regions of ULDPE. Upon addition of free sulfur to the subsequent blends, one may expect a measurable change in the fit components related to m1 fractions. Surprisingly though, no apparent change in f_{m1} can be observed, but only a small decrease in the subsequent $T_{2,m1}^{eff}$. This probably suggests that the blends are approaching a cross-linking limit. The most mobile frac-

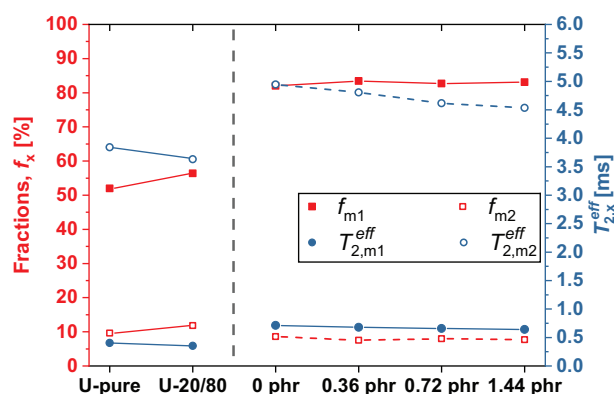


Figure 8. EPDM-related fit components in the blends compared with fit components of similar T_2 in pure ULDPE (U-pure) obtained from a four-component fit. Also shown is U-20/80 for comparison. The lines are a guide to the eye only. For discussion pertaining to crystalline and intermediate fractions, see text.

tion (f_{m2}) has low-to-no change between the polyethylenes and the blends, suggesting that these fractions are unaffected by the cross-links.

Table 3 contains a summary of the results from the crystalline and intermediate fractions. The crystalline fractions remained constant at about 9.5% for all the blends, which scales with the weighted amount of ULDPE in the blends. Interestingly though, no evidence of fractions with intermediate motions can be observed in the blends, either due to the additives interfering with the crystal-amorphous interfaces (as witnessed in U-20/80) or polyethylene regions of EPDM interacting with the ULDPE phases or both. The latter factor may be supported by the finding that largely similar relaxation times are obtained for the amorphous regions of ULDPE and EPDM pertaining fractions in the blends (f_{m1} and f_{m2}) at any given cross-linker amount (Figure 8). Thus, one may expect a miscibility of amorphous ULDPE with the chemically similar EPDM phase. Elsewhere, X-ray studies have demonstrated the solvation of LDPE by ethylene termonomers present in EPDM in peroxide vulcanized EPDM/LDPE blends.^[67] The solvation has been attributed to interfere with the crystalline phases in LDPE. In a follow-up research, the blend composition has been observed to affect the overall degree of crystallinity and the morphology of the crystalline phases too.^[68] However, in the present study, the most constrained fractions (crystalline phases, f_c) have been measured to be almost equal to the weighted average of the rigid fraction in pure ULDPE. It may thus be deduced that the solvation, in the samples discussed here, does not interfere with the crystallization and hence, occurs only at the interfaces.

The changes in EPDM upon cross-linking are better understood through D_{res} studies. Hence, these samples will be dealt in the next section with MQ experiments.

3.5. Cross-Linking in EPDM and EPDM/ULDPE Blends

Cross-linking leads to restrictions in chain motions due to the arising constraints. Additionally, depending on various factors like cross-linker system, processing conditions, presence of

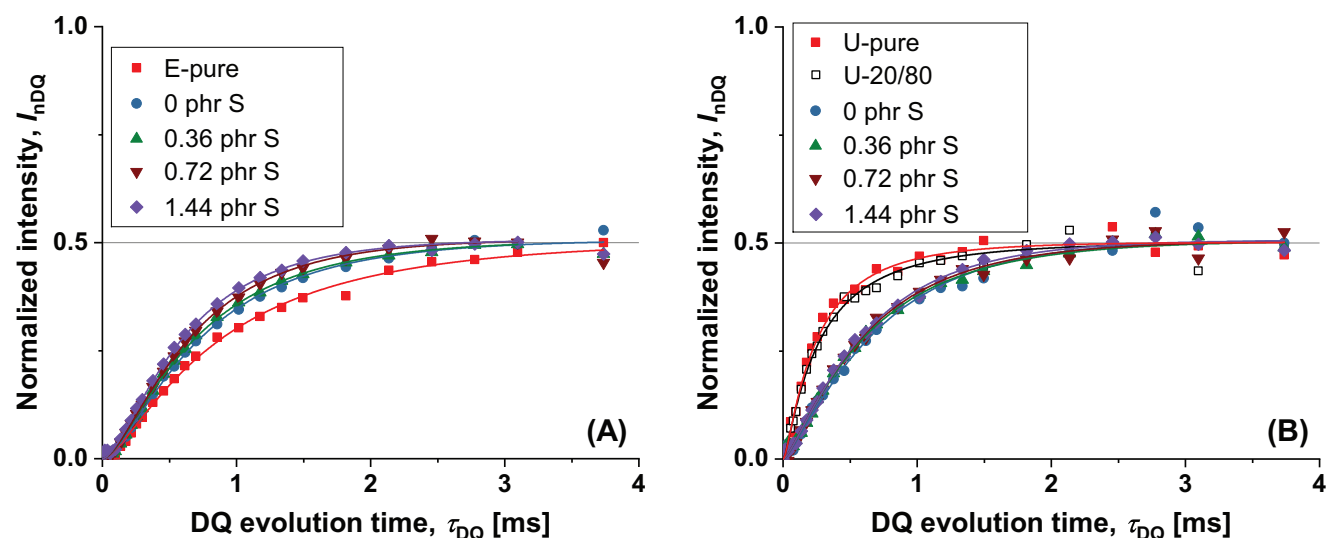


Figure 9. Normalized DQ build-up curves for A) EPDM, and B) EPDM/ULDPE (60/40) blends at different cross-linker levels. DQ curves of E-pure, U-pure, and U-20/80 are plotted for comparison. A bimodal fitting function is used for the blends to separately account for ULDPPE and EPDM phases (see text for explanation), whereas a single-mode fitting function is sufficient for the EPDMs. The fits are represented as solid lines, while the fit results are summarized in Figure 10.

fillers, and the polymer itself, finite amounts of isotropically relaxing defects are also generated due to imperfect cross-linking reactions. These were quantified by fitting an exponential decay fitting function to the difference signal ($I_{\text{ref}} - I_{\text{DQ}}$) to achieve an optimum normalized DQ build-up signal. The cross-linked EPDMs possess a single defect fraction (average $T_2 \approx 5.5$ ms), which amounted to $\approx 7\%$ in the lowly cross-linked sample and reduced to $\approx 3\%$ in the sample with 1.44 phr sulfur. In the blends, in addition to the defects from EPDM, a rather slowly relaxing defect component (average $T_2 \approx 13.5$ ms) was also obtained. The total defect fraction in the blends reduced from $\approx 18\%$ for the blend without free sulfur to $\approx 10\%$ in the highly cross-linked sample, the additional defect fraction coming from the unconstrained chain segments in ULDPPE phase.

The normalized DQ build-up curves obtained after the normalization for the different EPDM samples are plotted in **Figure 9A**. The D_{res} is reflected in the slope of the curves in the initial region. A somewhat high D_{res} value of 0.240 kHz for uncross-linked EPDM suggests the presence of strong entanglement-related effects in the terpolymer. It thus becomes apparent that in this case $D_{\text{res}} \approx 1/M_{\text{e,EPDM}}$ only. A comparably wide D_{res} distribution ($\sigma_{\text{in}} = 0.862$) is obtained for uncross-linked EPDM, which is a manifestation of the inherent spin-heterogeneity due to the different constituent monomers. In the cross-linked samples, as can be expected, the cross-link density increases with the addition of the fixed amount of accelerator mixture and the increasing free sulfur, and thus follows the D_{res} description given in Equation (2). It may be necessary to remind oneself that the trends of build-up curves seen here are originating only due to the modifications of unsaturations present in the ENB fractions of the terpolymer. The ethylene and propylene segments would remain chemically inert. Additionally, the inherently present entanglements can also get trapped upon cross-linking and contribute to the overall D_{res} .^[31] This effect can

become profound when norbornene rings are trapped at such junctions.

MQ experiments on samples with ULDPPE (**Figure 9B**) were performed by applying a MAPE (Magic And Polarization Echo) filter to the Baum–Pines pulse sequence discussed above.^[69] Such a T_2^{eff} -filter, effectively an “artificially ineffective” MSE sequence, can be used to remove contributions from highly coupled spins, like those coming from the crystallites. This, thus, enables probing only the signals from cross-linked and entangled chains. For the samples discussed here, the MAPE interpulse delay ($\tau_{\varphi, \text{MAPE}}$) was set to 50 μs , just sufficient to remove the effects of the crystalline regions (see **Figure A** for a qualitative description of an FID with a MAPE filter at different interpulse delays). Thus, the obtained signals will be a sum of the intermediate and amorphous regions. After such a procedure, pure ULDPPE yielded a D_{med} of 0.840 kHz and a coupling distribution width of 1.01. Analogous to the reduced intermediate fractions (f_{ci}) in U-20/80, a reduced D_{med} of about 0.760 kHz, and a comparable σ_{in} of 1.08 were obtained, further highlighting plasticization in ULDPPE due to the additives (see Section 2.3.2 for details on the fitting parameters).

To separately account for the ULDPPE and EPDM phases in the blends, the fitting function was modified to a bimodal type. Here, the values of D_{res} and its distribution obtained from pure ULDPPE were attributed to the first mode in the new fit. To this, a weighting factor corresponding to the amount of ULDPPE in the blends, and the exact quantity of active regions in ULDPPE contributing to D_{res} was also applied during fitting. Here, the active regions are those that are remaining after subtracting the fractions lost to the interpulse delay of 50 μs ($\approx 40\%$) and defect fraction ($\approx 10\%$). Thus, the resulting values of D_{res} and the distribution for the second mode will be those coming from the cross-links and entanglements in EPDM, and tie molecules and entanglements from amorphous (am) regions in ULDPPE, thus modifying

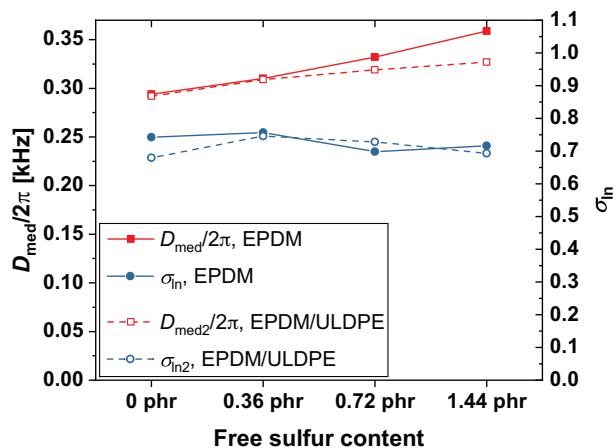


Figure 10. Residual dipolar coupling constants and their distributions at different sulfur concentrations for the second fitting mode (D_{med2} and σ_{in2}) in blends. Discussions pertaining to the first mode can be found in the text. The results of EPDM at different sulfur concentrations have been juxtaposed here for comparison.

Equation (2) to:

$$D_{res} \propto f_{EPDM} \left(\frac{1}{M_{c, EPDM}} + \frac{1}{M_{e, EPDM}} \right) + f_{ULDPE, am} \left(\frac{1}{M_{tie, ULDPE}} + \frac{1}{M_{e, ULDPE}} \right) \quad (4)$$

where $f_{EPDM} = 1 - f_{ULDPE, am}$ are the fractions of the detected signal. **Figure 10** summarizes and emphasizes the trends of residual dipolar coupling constants and their distributions in cross-linked EPDMs and the blends, obtained by fits to the build-up curves depicted in Figure 9. First, from the coupling distribution widths in the cross-linked EPDMs, it can be inferred that the accelerator mixture and sulfur concentration do not affect the distribution of cross-links in comparison to the inherent heterogeneity of the spin system in the EPDM terpolymer. The same observation has been made in EPDM cured by peroxides,^[31] where side reactions are known to increase the overall cross-linking distribution. Approximately similar distributions are obtained in the blends too, which is an outcome of the same monomer (ethylene) being present in both the phases.

The residual dipolar coupling constants and the coupling distributions corresponding to the second mode (D_{med2} and σ_{in2} , respectively) are plotted in Figure 10 for the blends. As can be expected, the D_{res} gradually increases with the amount of cross-linker in the samples. The same magnitude of cross-link density is obtained for the blend and EPDM at 0 and 0.36 phr of free sulfur. However, upon further sulfur addition, a distinct deviation in the trends of cross-link densities is observed. A noticeable increase is obtained for EPDMs whereas the blends appear to approach a plateau. This complements the stagnating trend of f_{m1} discussed for the blends above. Given that the corresponding EPDM-to-curative ratios in the single vulcanizates and the blends remain the same, the flattening may again indicate migration of the curatives to the ULDPE phases of the blends, thus limiting the cross-linking in EPDM phases. Additionally, the significant role of entanglements in the blends (as a contributing factor in

Equation (4)) cannot be discounted, which probably dominates the bulk properties.

3.6. Facets of Reinforcement in EPDM/ULDPE Blends

Entanglements certainly appear to play a dominating role in dictating the mechanical performance in EPDM. The presence of these entanglements complements the larger strain-at-break values for the lower cross-linked variants observed in Figure 4A. The chains undergo stretching to a higher degree due to the presence of lesser permanent junctions and more mobile entanglements. As more cross-links are formed, the reduced stretchability leads to insufficient load transfers across the network and, hence, to an early failure. Thus, the sulfur bonds form the weak links.

The observed migration of curatives that lead to a decrease in crystal-amorphous interfaces in U-20/80 and a complete loss in the blends indicates a plasticization of the semicrystalline structure, thus improving their resistance to deformation by strain-hardening (See Table 1 and Figure 5). The effects of entanglements appear to be compounded in the blends, as seen in Figure 4B. An increase in tensile stress by more than twofold between 0 and 1.44 phr free sulfur appears to be a synergistic outcome of several microstructural factors. First, apart from the characteristic load-bearing by a partly continuous rigid thermoplastic embedded in the rubber matrix that leads to retention of properties to a greater extent, the hardness of the largely continuous EPDM matrix possibly dictates the efficiency of load distributions. The mechanical superiority of the blend might come into its own when ULDPE is part of a harder EPDM matrix. Interfacial failures may occur if the EPDM is too soft.

Second, the solvation of ULDPE at the crystal interface by EPDM, as remarked earlier, is another major factor in determining the blends' properties. The dedicated mixing step at 140 °C enhances homopolymer-terpolymer blending, whereby complex interactions of the highly branched ULDPE with EPDM at the thermoplastic-rubber phase boundaries can lead to different entanglement situations.

Apart from the already established dilution of the crystal-amorphous interface regions, curatives can also be localized in the blend interphases. With the addition of higher amounts of sulfur, the cross-linking at the phase boundaries can increase, and also eventually lead to improved mechanical properties. This complements the flattening of D_{med2} due to the migration of the additives away from the EPDM phase as seen in Figure 10. Lastly, the contributions of entanglement, wherein trapping of the long ULDPE branches, tie molecules, and norbornenes due to cross-linking is possible, cannot be downplayed for their role in improving the ultimate properties.

The role of entanglements, however, appears to be discounted from the empirical value of the slope ($2C_2$) in the Mooney-Rivlin equation for the systems considered here, where the entanglement modulus (G_e) shows a decreasing trend for the cross-linked EPDMs. This is in stark contrast to the NMR observations (MQ, as well as amorphous fractions in Figure 8) where the entanglements are expected to be constant, or even slightly increase with increasing cross-linker.^[65] A similar trend has been observed earlier in EPDM containing about 5% ENB cross-linked

by peroxide.^[31] In both instances, the decline in apparent entanglement contribution has been attributed to network inhomogeneities. This suggests that the MR approach to isolate the entanglement contribution simply fails qualitatively. Nevertheless, a direct correlation of the cross-link modulus (G_c) to the cross-link densities with the NMR measurements for EPDMs was still possible. But again, for obtaining G_c from the polyethylene variants and the blends considered herewith, a modification of the Mooney–Rivlin equation or development of new models seems necessary.

4. Conclusion

Despite decades of investigations on EPDM/polyethylene blends, the basis for certain material properties remains unclear and underappreciated. Through this study, the contrasting mechanical behaviors of sulfur cross-linked EPDM and EPDM/ULDPE blends were elucidated by solid-state ^1H NMR spectroscopy. MQ NMR and T_2 relaxometry studies of pure EPDM reveal the existence of a highly entanglement-dominated environment. Though cross-link density increased with the amount of cross-linker, as found qualitatively from the Mooney–Rivlin model and quantitatively by MQ NMR, it contributed only negatively toward the mechanical properties. While superior tensile stress and strain were obtained for lowly cross-linked EPDM, these properties reduced drastically with an increase in the number of cross-links, possibly due to weaker sulfur bonds.

Insights into ULDPE and EPDM/ULDPE blends proved to be particularly interesting. Where an accurate distinction and quantification of crystalline, amorphous, and crystal-amorphous regions in ULDPE was possible by NMR experiments, the crystal-amorphous regions appeared to be diluted by the inclusion of accelerator and sulfur in a ULDPE homopolymer sample. Fascinatingly, the blends demonstrated a near-complete loss of these regions, possibly also due to solvation of ULDPE by ethylene monomers present in EPDM, in addition to the already-observed dilution by additives. The amount of crystalline fractions, however, remained unchanged across these samples.

MQ measurements proved that EPDM/ULDPE blends cross-link to the same extent as EPDM up to 0.36 phr of free sulfur. Thereafter, a divergence in the cross-link density trends was observed, wherein the blends seemed to approach a constant value. A primary reason for this could be the tendency of the cross-linking system migrating to the ULDPE phase and the blend interphase, and thus starving the EPDM phase. The significant entanglement scenario in the blends from EPDM and ULDPE phases may also dominate with the addition of cross-linker.

Along with the load-bearing feature of ULDPE, inherently dominant entanglement density in the blends, solvation by EPDM, plasticization of the crystal-amorphous interface by the curatives, and possible cross-linking at the interphase leading to trapped entanglements, the samples demonstrated strain hardening. This resulted in successively improved ultimate TS in the blends, without compromising the ultimate strain across the samples. Contrary to NMR, the phenomenological Mooney–Rivlin model failed to provide a logical explanation for the role of entanglements in cross-linked EPDMs, and was also rendered unusable for ULDPE and the blends which are dominated by the modulus of the polyethylene crystallites and undergo yielding.

Appendix

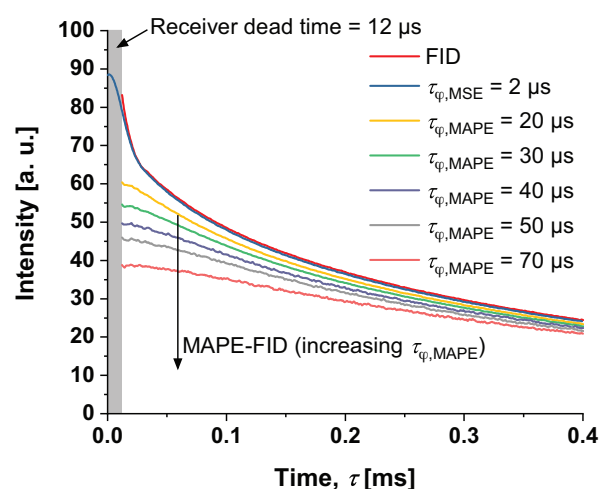


Figure A. An MSE-FID demonstrating signal refocusing in comparison to initial signal loss in an FID for pure ULDPE. The removal of the crystalline fractions-related signal using a MAPE filter at different interpulse delays is also demonstrated here for an FID.

Supporting Information

Supporting Information is available from the Wiley Online Library or from the author.

Acknowledgements

Parts of the research work were performed at the Polymer Competence Center Leoben GmbH (PCCL, Austria) within the framework of the COMET-program of the Federal Ministry for Climate Action, Environment, Energy, Mobility, Innovation and Technology and the Federal Ministry for Digital and Economic Affairs with contributions by Graz University of Technology, Austria (Institute of Chemistry and Technology of Materials). The PCCL is funded by the Austrian Government and the State Governments of Styria, Lower Austria and Upper Austria. A.K. thanks the Land Sachsen-Anhalt and the European Social Fund (ESF) for the grant ZS/2016/08/80644.

Open access funding enabled and organized by Projekt DEAL.

Conflict of Interest

The authors declare no conflict of interest.

Data Availability Statement

The data that support the findings of this study are available from the corresponding author upon reasonable request.

Keywords

cross-link densities, residual dipolar coupling constants, rubber/thermoplastic blends

Received: December 15, 2021

Revised: January 28, 2022

Published online: April 8, 2022

- [1] L. A. Utracki, P. Mukhopadhyay, R. K. Gupta, in *Polymer Blends Handbook*, Vol. 1, 2nd ed. (Eds: L. A. Utracki, C. A. Wilkie), Springer, Dordrecht **2014**, Ch. 1.
- [2] W. Hofmann, *Rubber Technology Handbook*, Hanser Publishers, Munich **1989**.
- [3] Y. Hirata, H. Kondo, Y. Ozawa, in *Chemistry, Manufacture and Applications of Natural Rubber* (Eds: S. Kohjiya, Y. Ikeda), Elsevier/Woodhead Publishing, Amsterdam **2014**, Ch. 12.
- [4] F. Röhthemeyer, F. Sommer, in *Kautschuk-Technologie: Werkstoffe – Verarbeitung – Produkte*, 3rd ed. (Eds: F. Röhthemeyer, F. Sommer), Hanser, Munich **2013**, Ch. 1.
- [5] S. F. Xavier, in *Polymer Blends Handbook*, Vol. 2, 2nd ed. (Eds: L. A. Utracki, C. A. Wilkie), Springer, Dordrecht **2014**, Ch. 10.
- [6] L. M. Robeson, *Polymer Blends: A Comprehensive Review*, Hanser, Munich **2007**.
- [7] L. A. Utracki, G. Z.-H. Shi, D. Rodrigue, R. Gonzalez-Núñez, in *Polymer Blends Handbook*, Vol. 1, 2nd ed. (Eds: L. A. Utracki, C. A. Wilkie), Springer, Dordrecht **2014**, Ch. 9.
- [8] M. N. Subramanian, *Polymer Blends and Composites: Chemistry and Technology*, 1st ed., Wiley-Scrivener, Hoboken, NJ **2017**.
- [9] L. A. Utracki, *Commercial Polymer Blends*, Springer US, Boston, MA **1998**.
- [10] L. Robeson, *Polymers* **2014**, 6, 1251.
- [11] I. Fortelný, J. Kovář, A. Sikora, D. Hlavatá, Z. Kruliš, Z. Nováková, Z. Pelzbauer, P. Čefelín, *Angew. Makromol. Chem.* **1985**, 132, 111.
- [12] C. S. Ha, D. J. Ihm, S. C. Kim, *J. Appl. Polym. Sci.* **1986**, 32, 6281.
- [13] Z. Bartczak, A. S. Argon, R. E. Cohen, M. Weinberg, *Polymer* **1999**, 40, 2331.
- [14] C. Cazan, A. Duta, in *Advances in Elastomers I*, Vol. 11 (Eds: P. M. Visakh, S. Thomas, A. K. Chandra, A. P. Mathew), Springer, Berlin, Heidelberg **2013**, Ch. 7.
- [15] C. M. Roland, in *Advances in Elastomers I*, Vol. 11 (Eds: P. M. Visakh, S. Thomas, A. K. Chandra, A. P. Mathew), Springer, Berlin, Heidelberg **2013**, Ch. 6.
- [16] H. Veenstra, P. C. Verkooyen, B. J. van Lent, J. van Dam, A. P. de Boer, A. P. H. Nijhof, *Polymer* **2000**, 41, 1817.
- [17] B. Pukánszky, F. Tüdös, *Makromol. Chem., Macromol. Symp.* **1990**, 38, 221.
- [18] D. Campbell, R. A. Pethrick, J. R. White, *Polymer Characterization: Physical Techniques*, 2nd ed., CRC Press, Cheltenham **2000**.
- [19] *Polymer Testing*, 2nd ed. (Eds: S. Seidler, V. Alstädt, W. Grellmann), Hanser, Munich **2013**.
- [20] O. Chaikumpollert, Y. Yamamoto, K. Suchiva, S. Kawahara, *Polym. J.* **2012**, 44, 772.
- [21] F. Zhao, W. Bi, S. Zhao, *J. Macromol. Sci., Part B: Phys.* **2011**, 50, 1460.
- [22] D. Y. Kim, J. W. Park, D. Y. Lee, K. H. Seo, *Polymers* **2020**, 12, 1.
- [23] Y. H. Zang, R. Muller, D. Froelich, *Polymer* **1989**, 30, 2060.
- [24] F. A.-E. Salam, M. H. A.-E. Salam, M. T. Mostafa, M. R. Nagy, M. I. Mohamed, *J. Appl. Polym. Sci.* **2003**, 90, 1539.
- [25] Y. Shangguan, J. Yang, Q. Zheng, *RSC Adv.* **2017**, 7, 15978.
- [26] W. Chassé, M. Lang, J.-U. Sommer, K. Saalwächter, *Macromolecules* **2011**, 45, 899.
- [27] V. M. Litvinov, W. Barendsward, M. Van Duin, *Rubber Chem. Technol.* **1998**, 71, 105.
- [28] R. A. Orza, P. C. M. M. Magusin, V. M. Litvinov, M. Van Duin, M. A. J. Michels, *Macromol. Symp.* **2005**, 230, 144.
- [29] R. A. Orza, P. C. M. M. Magusin, V. M. Litvinov, M. Van Duin, M. A. J. Michels, *Macromolecules* **2007**, 40, 8999.
- [30] P. C. M. M. Magusin, R. A. Orza, V. M. Litvinov, M. Van Duin, K. Saalwächter, *ACS Symp. Ser.* **2011**, 1077, 207.
- [31] T. Saleesung, D. Reichert, K. Saalwächter, C. Sirisinha, *Polymer* **2015**, 56, 309.
- [32] T. Saleesung, P. Saeoui, C. Sirisinha, *J. Appl. Polym. Sci.* **2017**, 134, 44523.
- [33] M. D. Ellul, A. H. Tsou, W. Hu, *Polymer* **2004**, 45, 3351.
- [34] M. Aluas, C. Filip, *Solid State Nucl. Magn. Reson.* **2005**, 27, 165.
- [35] V. M. Litvinov, *Macromolecules* **2006**, 39, 8727.
- [36] K. Saalwächter, P. Ziegler, O. Spycykerelle, B. Haidar, A. Vidal, J.-U. Sommer, *J. Chem. Phys.* **2003**, 119, 3468.
- [37] K. Saalwächter, *J. Am. Chem. Soc.* **2003**, 125, 14684.
- [38] J. Carretero-González, J. L. Valentín, M. Arroyo, K. Saalwächter, M. A. Lopez-Manchado, *Eur. Polym. J.* **2008**, 44, 3493.
- [39] F. V. Chávez, K. Saalwächter, *Phys. Rev. Lett.* **2010**, 104, 198305.
- [40] M. K. Dibbanti, M. Mauri, L. Mauri, G. Medaglia, R. Simonutti, *J. Appl. Polym. Sci.* **2015**, 132, 42700.
- [41] R. García, R. Pérez, *Surf. Sci. Rep.* **2002**, 47, 197.
- [42] S. N. Magonov, V. Elings, M.-H. Whangbo, *Surf. Sci.* **1997**, 375, L385.
- [43] D. Nečas, P. Klapetek, *Cent. Eur. J. Phys.* **2012**, 10, 181.
- [44] J. P. Cohen-Addad, *Polymer* **1983**, 24, 1128.
- [45] H. Tanaka, Y. Inoue, *Polym. Int.* **1993**, 31, 9.
- [46] D. Dadayli, R. K. Harris, A. M. Kenwright, B. J. Say, M. M. Sünnetçioğlu, *Polymer* **1994**, 35, 4083.
- [47] M. Knörger, U. Heuert, H. Schneider, P. Barth, W. Kuhn, *Polym. Bull.* **1997**, 38, 101.
- [48] E. W. Hansen, P. E. Kristiansen, P. Bjørn, *J. Phys. Chem. B* **1998**, 102, 5444.
- [49] L. Dujourdy, J. P. Bazile, J. P. Cohen-Addad, *Polym. Int.* **1999**, 48, 558.
- [50] P. E. Kristiansen, E. W. Hansen, P. Bjørn, *J. Phys. Chem. B* **1999**, 103, 3552.
- [51] S. Schreurs, J.-P. François, P. Adriaensens, J. Gelan, *J. Phys. Chem. B* **1999**, 103, 1393.
- [52] M. Knörger, U. Heuert, H. Schneider, G. Heinrich, *J. Macromol. Sci., Part B: Phys.* **1999**, 38, 1009.
- [53] A. Wittmer, R. Wellen, K. Saalwächter, K. Koschek, *Polymer* **2018**, 151, 125.
- [54] A. Maus, C. Hertlein, K. Saalwächter, *Macromol. Chem. Phys.* **2006**, 207, 1150.
- [55] K. Saalwächter, *Prog. Nucl. Magn. Reson. Spectrosc.* **2007**, 51, 1.
- [56] J. Baum, A. Pines, *J. Am. Chem. Soc.* **1986**, 108, 7447.
- [57] W. Chassé, J. L. Valentín, G. D. Genesky, C. Cohen, K. Saalwächter, *J. Chem. Phys.* **2011**, 134, 044907.
- [58] L. Jakisch, M. Garaleh, M. Schäfer, A. Mordvinkin, K. Saalwächter, F. Böhme, *Macromol. Chem. Phys.* **2018**, 219, 1700327.
- [59] C. W. Macosko, *Rheology: Principles, Measurements, and Applications*, Wiley-VCH, New York **1994**.
- [60] J. Kruželák, R. Sýkora, I. Hudec, *Chem. Pap.* **2016**, 70, 1533.
- [61] S. Howse, C. Porter, T. Mengistu, I. Petrov, R. J. Pazur, *Rubber Chem. Technol.* **2019**, 92, 513.
- [62] M. H. S. Gradwell, D. Grooff, *J. Appl. Polym. Sci.* **2002**, 83, 1119.
- [63] V. Tanrattanakul, W. Udomkitchdecha, *J. Appl. Polym. Sci.* **2001**, 82, 650.
- [64] H. Yao, J. Niu, J. Zhang, N. Ning, X. Yang, M. Tian, X. Sun, L. Zhang, S. Yan, *Chin. J. Polym. Sci.* **2016**, 34, 820.
- [65] S. Schlögl, M.-L. Trutschel, W. Chassé, G. Riess, K. Saalwächter, *Macromolecules* **2014**, 47, 2759.
- [66] I. Syed, G. Hempel, K. Saalwächter, P. Stratmann, M. Klüppel, *Macromolecules* **2016**, 49, 9004.
- [67] L. Ślusarski, D. Bieliński, A. Włochowicz, C. Ślusarczyk, *Polym. Int.* **1995**, 36, 261.
- [68] D. Bieliński, A. Włochowicz, J. Dryzek, C. Ślusarczyk, *Compos. Interfaces* **2001**, 8, 1.
- [69] A. Papon, K. Saalwächter, K. Schäler, L. Guy, F. Lequeux, H. Montes, *Macromolecules* **2011**, 44, 913.

 **acro-
molecular**
Materials and Engineering

Supporting Information

for *Macromol. Mater. Eng.*, DOI 10.1002/mame.202100968

NMR-Based Cross-Link Densities in EPDM and EPDM/ULDPE Blend Materials and Correlation with Mechanical Properties

*Akshay Karekar**, *Reinhold Pommer*, *Bianca Prem*, *Caterina Czibula*, *Christian Teichert*, *Gregor Trimmel* and *Kay Saalwächter**

Supporting Information

NMR-based cross-link densities in EPDM and EPDM/ULDPE blend materials and correlation with mechanical properties

Akshay Karekar,* Reinhold Pommer, Bianca Prem, Caterina Czibula, Christian Teichert, Gregor Trimmel, Kay Saalwächter*

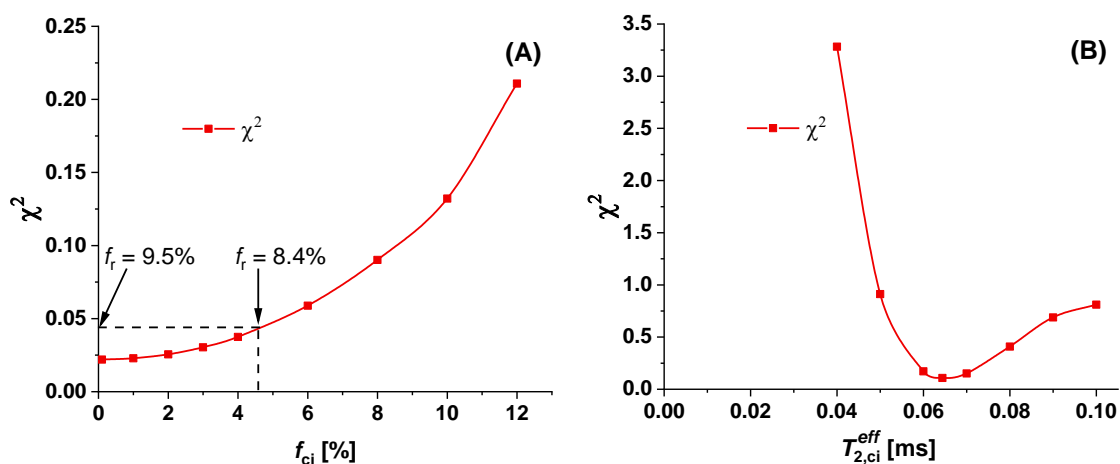


Figure S1. Exemplary χ^2 plots for a 4-component fit indicating the fitting uncertainty of (A) the crystal-amorphous interface fraction in an EPDM/ULDPE blend (0.72 phr S), and (B) the transverse relaxation time constant of the crystal-amorphous interface in U-pure. The height of the dash line in (A) corresponds to a width of $2\chi^2$. Within this χ^2 width the amount of rigid fraction corresponding to $f_{ci} = 0\%$ ($f_r = 9.5\%$, see Table 3 of the article) reduced by only about 1% after a calculated f_{ci} of 4.6%. The minima in (B) corresponds to a $T_{2,ci}^{eff}$ of about 65 μ s of the interface fraction ($f_{ci} = 14\%$).

8. Microstructure of Silica-Filled NR/SBR Blends

Reinforcing fillers are an essential component of elastomer materials for achieving an optimal balance of properties, especially mechanical ones. The inclusion of antiaging additives is also prudent to protect the material from early failure. This chapter extends the theme of thermo-oxidative aging in Chapter 5 to materials with added filler and an antioxidant. Here, only a limited account of the most important observations pertaining to unaged samples is given. A detailed report of the results and discussions, with findings of thermo-oxidative aging, will be made available as a journal article at a later date.

8.1 Materials, preparation, and exposure

The compounds were prepared based on the formulations discussed in Chapters 5 and 6. The ingredients consist of natural rubber (grade: SVR10), styrene-butadiene rubber (grade: SPRINTAN SLR 4602-Schkopau), zinc oxide and stearic acid as activators, sulfur as the cross-linker, and N-cyclohexyl-2-benzothiazole sulfenamide (CBS) accelerator. The filler system is composed of silica (grade: Ultrasil 7000 GR) and bis(triethoxysilylpropyl)disulfide (TESPD) silane coupling agent (grade: Si 75). The filler-to-rubber volume fraction is about 0.3. To study the role of antioxidant towards aging-related molecular changes in the polymers, N-Isopropyl-N'-phenyl-1,4-phenylenediamine (IPPD) was used. The raw materials were procured and compounded based on the recipe in Table 8.1 by Deutsches Institut für Kautschuktechnologie e. V., Hannover.

Mixing was carried out at a fill factor of 77 % in a two-step process in a GK 4N internal mixer with a tangential rotor system. The temperature was set to 40 °C and the rotor speed to 45 rpm. The first step comprised the addition of the ingredients (except sulfur and CBS) and silanization of the silica fillers at an average temperature of 150 °C for 4 min. Sulfur and CBS were added to this mixture in a separate step on the following day.

The mixtures were molded into plates of 120 x 120 x 2 mm³ at 160 °C on a compression molding machine for a duration corresponding to the time required for achieving 90 % cross-linking (t_{90}), also measured at 160 °C. The t_{90} times were calculated from the vulcanization curves measured at 1.67 Hz oscillation frequency and an oscillation amplitude of 6.98 % on a rubber process analyzer.

Table 8.1: Material compositions and their respective t_{90} times

Ingredients	1	2	3	4	5	6	7	8	9
NR [phr]	100	100	100	-	-	-	50	50	50
SBR [phr]	-	-	-	100	100	100	50	50	50
IPPD [phr]	5	-	5	5	-	5	5	-	5
Zinc oxide [phr]	3	3	3	3	3	3	3	3	3
Stearic acid [phr]	1	1	1	1	1	1	1	1	1
Silane [phr]	-	5.1	5.1	-	5.1	5.1	-	5.1	5.1
Silica [phr]	-	60	60	-	60	60	-	60	60
Sulfur [phr]	2.5	2.5	2.5	2.5	2.5	2.5	2.5	2.5	2.5
CBS [phr]	1.5	1.5	1.5	1.5	1.5	1.5	1.5	1.5	1.5
t_{90} [min]	6	13	9	16	34	30	9	28	19

8.2 Results and discussion

8.2.1 Curing kinetics

The curing curves provide an excellent insight into the kinetics of cross-linking of the different compounds over time. The corresponding curing curves are compared in Figure 8.1 and their respective t_{90} times are summarized in Table 8.1. For the unfilled samples (Figure 8.1A), the time corresponding to 90 % torque for NR, SBR, and the blend are about 6, 16, and 9 min, respectively. The reasons for the different natures of these curves have been discussed in Chapter 5 and also hold here. As noted there, the blend behavior here also appears to be dominated by the NR phase, where it demonstrates marginal reversion and a t_{90} that is relatively shorter compared to the weighted average of NR and SBR.

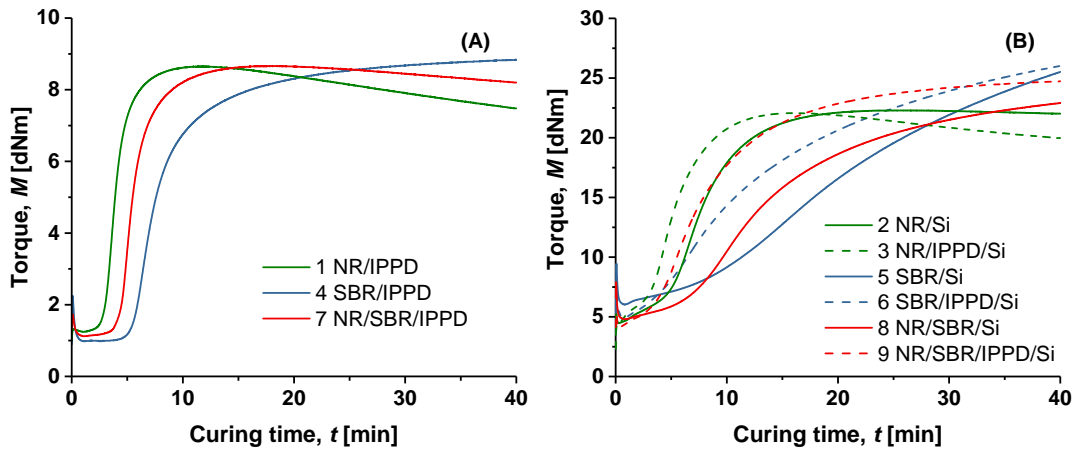


Figure 8.1: Curing curves of (A) unfilled materials, and (B) silica-filled compositions, both measured at 160 °C.

In the filled compositions, the presence of silica brings distinct variations relative to the unfilled materials and the antioxidant itself further contributes uniquely to the cross-linking. In general, the t_{90} times for the filled materials are longer than the unfilled ones. Moreover, the filled compositions with the antioxidant require a relatively shorter time to reach 90 % cross-link extent compared to their analogs without IPPD. In addition to the very strong behavior of “marching modulus” in the SBR samples, cross-linking reactions appear to dominate also in the blends, which are in contrast to the trend of the unfilled blend.

8.2.2 Phase-resolved cross-link densities

Figure 8.2 provides a summary of D_{med} for all resonant peaks of the unaged samples in Table 8.1. The unfilled blend in Figure 8.2C does not indicate any significant deviations from the corresponding values of the individual vulcanizates reported in Figure 8.2A and B. A spectral-average coupling value of about 0.250 was obtained for these three samples, which shows the similarity in the degree of motional constraints in the unfilled samples.

The inclusion of silica brings remarkable changes in NR, where the filled samples produce an average cross-link density of up to 90 Hz lower than that of the unfilled sample. Hasse *et al.* [195] have reported that in the presence of the silane TESPD sulfur inserts itself into the sulfide of the silane. Thus, the lower cross-link density of silica-filled NR here could only be a case of lower cross-linker availability in the matrix.

This argument, however, does not explain the (only) marginal decrease in the cross-link density of the filled samples of SBR in relation to the unfilled sample. The behavior observed here probably has its origin in the choice of SBR. The grade of SBR used in these studies is pre-functionalized to aid rubber–filler interactions. A consequence of this can be observed in the phase image of the blend NR/SBR/IPPD/Si (formulation 9) measured through AFM in the intermittent tapping mode (Figure 8.2 bottom-right). The bright silica fillers are preferentially localized in the SBR phase (lighter regions) than in the NR phase (darker regions). Hence, it can be concluded that SBR and silica present strong rubber–filler interactions. Thus, it can be deduced that the polymer chains get bound to the fillers. Such enhanced rubber–filler interactions have also been reported by Lee *et al.* for a similar end-functionalized SBR [196]. Hence, it can be concluded that SBR competes more favorably with the vulcanization system for adsorption to silica, which implies that more vulcanization agents are available eventually.

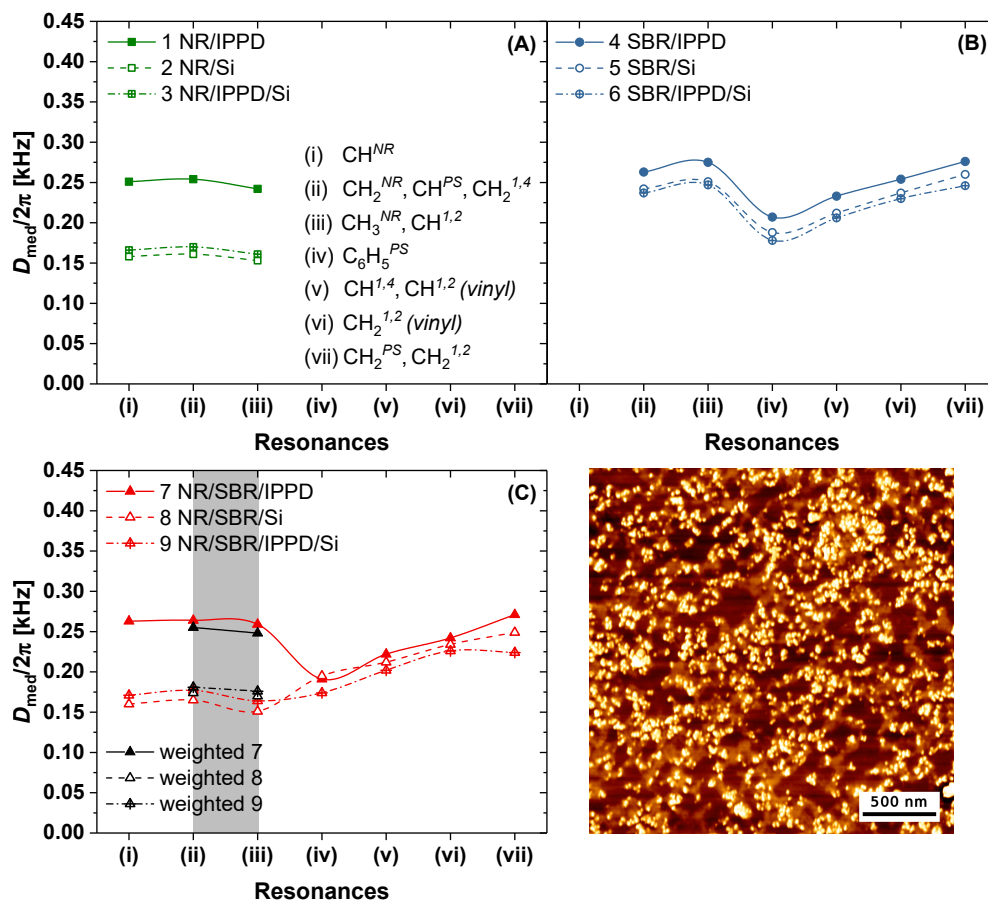


Figure 8.2: A, B, and C are the residual dipolar coupling strengths ($D_{med}/2\pi$) of unaged NR, SBR, and the blend, respectively, obtained by MAS using the protocol given in Chapters 5 and 6. The resonances are arranged in the sequence: NR-only \rightarrow mixed \rightarrow SBR-only. The symbols in black in C represent the ‘expected’ proton-weighted averages of D_{med} of the mixed resonances (gray shaded area) of NR and SBR, obtained from the corresponding resonance values in A and B. The lines are a guide to the eye only.

Bottom-right: AFM phase image of NR/SBR/IPPd/Si (formulation 9) measured in an intermittent contact mode. The darker phase is NR, while the lighter phase is SBR. The bright regions, corresponding to silica, are selectively incorporated in the SBR phase.

As in the unfilled blend, the filled blends in Figure 8.2C yield almost identical D_{med} values as their constituent filled polymers variants. Moreover, the two filled blends themselves are almost identical to each other, and to their corresponding numerically measured ‘expected’ weighted averages based on proton counting (shown in black in the gray shaded area) for the overlapping resonances of NR and SBR (ii and iii). The latter is true also for the unfilled blend. The relative difference between the unfilled blend and the filled variants at resonance positions i, ii, and iii is merely due to the lowly cross-linked NR phase as also seen in samples 2 and 3. Further discussion on these materials will be a part of a separate article.

9. Summary and Outlook

The full potential of polymer blends can be realized when molecular-level information about the phases within is accessible. These microscopic details are essential, in addition to the macroscopic results, for optimizing the choice of components, their ratio, and the processing conditions. In this research, rubber/rubber (NR/SBR) and rubber/plastic (EPDM/ULDPE) blends were considered to mainly measure the cross-link within the distinct rubber phases. The various approaches used by industry and academia to measure this lack a phase resolution, or where possible, quantification.

Through this research, a step was taken to address these shortcomings by employing MAS NMR in combination with a previously published NMR pulse sequence (BaBa-xy16) [124] to obtain chemically-resolved peaks in the spectra of blends and to extract the cross-link density, respectively. Here, the residual dipolar coupling constant is used as a measure of the cross-link density. A static, low-field analog for measuring the cross-link density was also used in tandem. Three papers were published to showcase the robustness of these methods in the elucidation of molecular structure and motions in polymer blends (two on NR/SBR and one on EPDM/ULDPE blends) and were presented as separate chapters in this dissertation. A short, unpublished chapter on silica-filled NR/SBR blends was also presented.

In the case of NR/SBR blends vulcanized to a duration corresponding to 90 % cross-linking, it was observed that the SBR phase does not cross-link to its full potential when it is a part of the blend because the cross-linking is mostly driven by the NR phase. This leads to a distribution of cross-link densities across the two phases. But, no such preferential distribution of the cross-link densities in the blend's phases was observed in the presence of an antioxidant. However, the addition of silica led to some variations in the extent to which NR and SBR are bound to the filler, thus affecting the degree of cross-linking in the bulk. These differences scaled proportionately in the filled blends with and without the antioxidant.

An important theme surrounding NR/SBR blends was studying their long-term applicability by measuring changes in their molecular properties when exposed to thermo-oxidative aging and accelerated weathering. In both cases, NR demonstrated dominant chain scission reactions while SBR underwent cross-linking. NR degradation was significant through thermo-oxidative aging while SBR was more affected by weathering. NR also lost about 10 % of its chains to defects in both cases, formed over 1000 h of exposure. Interestingly, no presence of defects was observed in SBR exposed to either condition. In weathered SBR, a stiff surface was formed, which exhibited unique chemical and physical/mechanical properties relative to its core, as measured by IR

spectroscopy, DMTA, and AFM. While a *gradient* of modulus was estimated for SBR, a formation of barrier-like skin was hypothesized for NR, which had stiff skin but a soft core. In both NR and SBR, T_2 measurements showed variations in the relaxation times of the respective fractions caused by modifications in the bonding situation of the chains. Fractions containing newly formed chains were found, especially in NR.

Cross-link densities of the blends measured at the low field reported values that were almost a weighted average of the values obtained individually for NR and SBR. Up to about 200 h of exposure, both NR and the blend had an invariant cross-link density but showed a broadening of its distribution. This was attributed to the modification of sulfur bonds in a system that mainly contained polysulfide linkages, and to the formation of newer chains upon scission reactions. Due to the unique routes of aging taken by NR and SBR, MAS studies of the 50/50 blend showed clear differences in the cross-link densities of the two phases in samples exposed to thermo-oxidative aging and weathering. A key finding of the weathered sample was that while the D_{res} of NR and SBR resonances in their single vulcanizates changed between 500 and 1000 h, it remained largely unchanged for the blend. This suggested that, compared to NR and SBR, their blend has a higher retention of properties and is hence, more durable.

In materials involving EPDM/ULDPE blends, the tensile properties of EPDM vulcanizates deteriorated with an increase in the quantity of sulfur, while that of the blends improved. Measurements of transverse relaxation times revealed that the amount of crystalline fractions in the blends, in comparison to a pristine ULDPE, stayed constant at all concentrations of sulfur. However, the crystal–amorphous interface regions demonstrated signs of plasticization, which led to an improvement in their tensile strengths. Low-field measurements of the cross-link density showed that EPDM and the blend have identical cross-link densities at lower concentrations of sulfur. The trends however diverge at higher sulfur concentrations: D_{res} of EPDM single vulcanizates increased continuously, while it increased only marginally for the blend. It was hence concluded that sulfur from the EPDM phase migrates to the crystalline–amorphous interfaces of the ULDPE phase, thus contributing to the improvement in the mechanical strength.

Outlook

The D_{res} -based NMR approaches for the measurement of cross-link densities have proven to be a great asset for gaining a deeper understanding of the different blends considered here. The time-domain-based Baum–Pines pulse sequence alone was valuable in uncovering the origin of reinforcement in EPDM/ULDPE blends. Its short

measurement time made it feasible for exploring a large collection of samples from the NR/SBR systems. The BaBa-xy16 pulse sequence, coupled with MAS helped delve into the individual phases.

The studies, thus far, reported on the cross-link density by a direct read-out of the fits to the build-up curves obtained from the respective peak projections. An aspect that was not duly addressed is cross-linking at the interfaces. It must be recognized that where a low interfacial tension between the different polymers in a blend exists, interfacial cross-links help retain the integrity of the blend and prevent premature failure caused by mechanical forces. Although a numerical measure of curing at the interface is difficult to obtain, qualitative assessments can be made by observing the interfaces through electron microscopy and measuring the nano-modulus in these regions by techniques like AFM.

A plausible next step for this research would be to apply the knowledge gathered through these methodologies to understanding industrially relevant materials. Practical compositions of rubbers contain a large number of different ingredients to make them suitable for the intended applications. These include polymer/s, cross-linker, accelerators, activators, fillers, plasticizers, processing aids, protective agents, etc. This would, of course, increase the analytical complexity due to the many ingredients present but can be promising from an industry point of view. An obvious material-related limitation here is the inclusion of carbon black. As the delocalized electrons in carbon black interfere with the magnetic field, spectral resolution suffers even at loading levels of 5 phr as found in a preliminary study.

Extending the scope of these NMR methodologies to other rubber blends would also be an interesting topic of research. Blends, especially those of butadiene rubber (BR) with NR and SBR are also technologically important for tire applications. BR has a low build-up of heat and is used in applications such as conveyor belts, cable insulation, and footwear. The blends of BR/SBR will be particularly challenging to decipher, given that monomers of polybutadiene are common in both phases. This will open up questions on the co-vulcanization of the phases.

For the rubber/plastic blends considered herein, factors such as crystallinity and entanglements played a vital role in determining the mechanical properties. These aspects must be further explored by varying the ratio of the monomers within EPDM and including polyolefins with relatively larger crystallinity such as HDPE and PP. An orthogonal series whereby the rubber-to-plastic ratio is varied can also be considered.

Bibliography

- [1] E. A. Grulke, *Polymer Process Engineering*, 1st ed., Prentice Hall, Englewood Cliffs, New Jersey, **1994**.
- [2] C. Koning, M. V. Duin, C. Pagnouille, R. Jerome, “Strategies for Compatibilization of Polymer Blends”, *Progress in Polymer Science* **1998**, *23*, 707–757.
- [3] A. J. Tinker, “Introduction – The Book and Rubber Blends” in *Blends of Natural Rubber*, (Eds.: A. J. Tinker, K. P. Jones), Springer, Dordrecht, **1998**.
- [4] C. M. Roland, “Rubber-Rubber Blends: Part I” in *Handbook of Elastomers*, (Eds.: A. K. Bhowmick, H. L. Stephens), Marcel Dekker, New York, **2001**, 197–225.
- [5] A. Chapman, A. J. Tinker, “Vulcanization of Blends – Crosslink Distribution and its Effect on Properties”, *KGK - Kautschuk Gummi Kunststoffe* **2003**, *56*, 533–544.
- [6] C. M. Roland, “Immiscible Rubber Blends” in *Advances in Elastomers I: Blends and Interpenetrating Networks, Vol. 11*, (Eds.: P. M. Visakh, S. Thomas, A. K. Chandra, A. P. Mathew), Springer, Berlin, Heidelberg, **2013**, 167–181.
- [7] J. L. Leblanc, “Interphase Distribution of Curatives in Natural Rubber/Polybutadiene Blends”, *Plastics and Rubber Processing and Applications* **1982**, *2*, 361–368.
- [8] W. M. Hess, C. R. Herd, P. C. Vegvari, “Characterization of Immiscible Elastomer Blends”, *Rubber Chemistry and Technology* **1993**, *66*, 329–375.
- [9] G. J. van Amerongen, “Diffusion in Elastomers”, *Rubber Chemistry and Technology* **1964**, *37*, 1065–1152.
- [10] S. Datta, “Elastomer Blends” in *The Science and Technology of Rubber*, (Eds.: J. E. Mark, B. Erman, C. M. Roland), Academic Press, Waltham, **2013**, 547–589.
- [11] J. B. Gardiner, “Curative Diffusion between Dissimilar Elastomers and its Influence on Adhesion”, *Rubber Chemistry and Technology* **1968**, *41*, 1312–1328.
- [12] R. Srithawatpong, Z. L. Peng, B. G. Olson, A. M. Jamieson, R. Simha, J. D. McGervey, T. R. Maier, A. F. Halasa, H. Ishida, “Positron Annihilation Lifetime Studies of Changes in Free Volume on Cross-linking cis-Polyisoprene, High-Vinyl Polybutadiene, and their Miscible Blends”, *Journal of Polymer Science Part B: Polymer Physics* **1999**, *37*, 2754–2770.

- [13] M. A. Mansilla, L. Silva, W. Salgueiro, A. J. Marzocca, A. Somoza, “A Study about the Structure of Vulcanized Natural Rubber/Styrene Butadiene Rubber Blends and the Glass Transition Behavior”, *Journal of Applied Polymer Science* **2012**, *125*, 992–999.
- [14] A. I. Dzulkifli, C. M. S. Said, C. C. Han, “Determination of Crosslink Concentration by Mooney-Rivlin Equation for Vulcanized NR/SBR Blend and its Influence on Mechanical Properties”, *Malaysian Journal of Analytical Sciences* **2015**, *19*, 1309–1317.
- [15] H. Ismail, S. Tan, B. T. Poh, “Curing and Mechanical Properties of Nitrile and Natural Rubber Blends”, *Journal of Elastomers and Plastics* **2001**, *33*, 251–262.
- [16] S. Cook, S. Groves, A. J. Tinker, “Investigating Crosslinking in Blends by Differential Scanning Calorimetry”, *Journal of Rubber Research* **2003**, *6*, 121–128.
- [17] A. Galuska, R. Poulter, K. McElrath, “Force Modulation AFM of Elastomer Blends: Morphology, Fillers and Cross-linking”, *Surface and Interface Analysis* **1997**, *25*, 418–429.
- [18] D. Honiball, W. J. McGill, “A technique for measuring the crosslink densities in both phases of a vulcanizate blend”, *Journal of Polymer Science Part B: Polymer Physics* **1988**, *26*, 1529–1537.
- [19] A. Karekar, K. Oßwald, K. Reincke, B. Langer, K. Saalwächter, “NMR Studies on the Phase-Resolved Evolution of Cross-Link Densities in Thermo-Oxidatively Aged Elastomer Blends”, *Macromolecules* **2020**, *53*, 11166–11177.
- [20] A. Karekar, C. Schicktanz, M. Tariq, K. Oßwald, K. Reincke, V. Cepus, B. Langer, K. Saalwächter, “Effects of Artificial Weathering in NR/SBR Elastomer Blends”, *Polymer Degradation and Stability* **2023**, *208*, 110267.
- [21] A. Karekar, R. Pommer, B. Prem, C. Czibula, C. Teichert, G. Trimmel, K. Saalwächter, “NMR-Based Cross-Link Densities in EPDM and EPDM/ULDPE Blend Materials and Correlation with Mechanical Properties”, *Macromolecular Materials and Engineering* **2022**, *307*, 2100968.
- [22] R. P. Patel, J. Shin, “Compounding and Processing of Plastic/Rubber Blends” in *Encyclopedia of Polymer Blends, Vol. 2*, (Ed.: A. I. Isayev), Wiley-VCH Verlag & Co. KGaA, Weinheim, **2011**, 109–162.
- [23] C. M. Roland, “Rubber Mixtures”, *Rubber Chemistry and Technology* **1989**, *62*, 456–497.

-
- [24] A. Ciesielski, *An Introduction to Rubber Technology*, 1st ed., Smithers Rapra Technology, Shawbury, **1999**, 1–173.
- [25] C. Goodyear, US000003633, **1844**.
- [26] J. A. Calzonetti, C. J. Laursen, “Patents of Charles Goodyear: His International Contributions to the Rubber Industry”, *Rubber Chemistry and Technology* **2010**, *83*, 303–321.
- [27] H. J. Stern, “History” in *Rubber Technology and Manufacture*, (Ed.: C. M. Blow), Butterworths, London, **1971**.
- [28] L. A. Utracki, “History of Commercial Polymer Alloys and Blends (from a Perspective of the Patent Literature)”, *Polymer Engineering & Science* **1995**, *35*, 2–17.
- [29] P. J. Corish, B. D. W. Powell, “Elastomer Blends”, *Rubber Chemistry and Technology* **1974**, *47*, 481–510.
- [30] P. J. Corish, “Elastomer Blends” in *Science & Technology of Rubber*, (Ed.: F. R. Eirich), Academic Press, New York, **1978**, 489–530.
- [31] P. J. Corish, “Rubber-Rubber Blends” in *Polymer Blends and Mixtures. NATO ASI Series, Series E: Applied Sciences, Vol. 89*, (Eds.: D. J. Walsh, J. S. Higgins, A. Maconnachie), Springer, Dordrecht, **1985**, 245–265.
- [32] K. Pal, V. Panwar, J. Bahadur, “Rubber Blend Nanocomposites” in *Progress in Rubber Nanocomposites*, (Eds.: S. Thomas, H. J. Maria), Woodhead Publishing, Duxford, **2017**, 319–348.
- [33] G. Kerrutt, H. Blumel, H. Weber, “Untersuchungen zur Covulkanisation”, *KGK - Kautschuk Gummi Kunststoffe* **1969**, *22*, 413–418.
- [34] T. Inoue, F. Shomura, T. Ougizawa, K. Miyasaka, “Covulcanization of Polymer Blends”, *Rubber Chemistry and Technology* **1985**, *58*, 873–884.
- [35] A. K. Bhowmick, S. K. De, “Effect of Curing Temperature and Curing System on Structure-Property Relations of Rubber Blends”, *Rubber Chemistry and Technology* **1980**, *53*, 960–974.
- [36] V. A. Shershnev, “Vulcanization of Polydiene and Other Hydrocarbon Elastomers”, *Rubber Chemistry and Technology* **1982**, *55*, 537–574.
- [37] M. G. Huson, W. J. McGill, R. D. Wiggett, “A Contribution to the Theory of Accelerated Sulphur Vulcanization of Natural Rubber and Polybutadiene BR with Tetramethyl Thiuram Disulphide and bis(2-benzothiazolyl) Disulphide”, *Journal of Polymer Science: Polymer Chemistry Edition* **1985**, *23*, 2833–2839.

- [38] K. Fujimoto, N. Yoshimiya, “Blends of cis-1,4-polybutadiene with Natural or Styrene Butadiene Rubber”, *Rubber Chemistry and Technology* **1968**, *41*, 669–677.
- [39] J. B. Gardiner, “Studies in the Morphology and Vulcanization of Gum Rubber Blends”, *Rubber Chemistry and Technology* **1970**, *43*, 370–399.
- [40] D. Mangaraj, “Elastomer Blends”, *Rubber Chemistry and Technology* **2002**, *75*, 365–427.
- [41] N. Yoshimura, K. Fujimoto, “Structure of Vulcanized and Unvulcanized SBR/BR Blends”, *Rubber Chemistry and Technology* **1969**, *42*, 1009–1013.
- [42] P. J. Corish, “Fundamental Studies of Rubber Blends”, *Rubber Chemistry and Technology* **1967**, *40*, 324–340.
- [43] W. Hofmann, *Rubber Technology Handbook*, 1st ed., Hanser Publishers, Munich, **1989**.
- [44] C. Shan, Z. Gu, L. Wang, P. Li, G. Song, Z. Gao, X. Yang, “Preparation, Characterization, and Application of NR/SBR/Organoclay Nanocomposites in the Tire Industry”, *Journal of Applied Polymer Science* **2011**, *119*, 1185–2011.
- [45] C. Fülber, B. Blümich, K. Unseld, V. Herrmann, “NMR Imaging of Thermal-Oxidative Aging in SBR”, *KGK - Kautschuk Gummi Kunststoffe* **1995**, *48*, 254–259.
- [46] B. Blümich, D. E. Demco, “NMR Imaging of Elastomers” in *Spectroscopy of Rubbers and Rubbery Materials*, (Eds.: V. M. Litvinov, P. P. De), Smithers Rapra Technology, Shawbury, **2002**, 247–290.
- [47] J. B. Gardiner, “Measurement of Curative Diffusion Between Rubbers by Microinterferometry”, *Rubber Chemistry and Technology* **1969**, *42*, 1058–1078.
- [48] E. M. Dannenberg, “Filler Choices in the Rubber Industry”, *Rubber Chemistry and Technology* **1982**, *55*, 860–880.
- [49] W. A. Wampler, T. F. Carlson, W. R. Jones, “Carbon Black” in *Rubber Compounding: Chemistry and Applications*, (Ed.: B. Rodgers), Marcel Dekker, New York, Basel, **2004**.
- [50] E. Princi, *Rubber: Science and Technology*, 1st ed., De Gruyter, Berlin, Boston, **2019**.
- [51] J. L. Leblanc, “Rubber–Filler Interactions and Rheological Properties in Filled Compounds”, *Progress in Polymer Science* **2002**, *27*, 627–687.

-
- [52] S. Kaufman, W. P. Slichter, D. D. Davis, “Nuclear Magnetic Resonance Study of Rubber–Carbon Black Interactions”, *Journal of Polymer Science Part A-2: Polymer Physics* **1971**, *9*, 829–839.
- [53] J. O’Brien, E. Cashell, G. E. Wardell, V. J. McBrierty, “An NMR Investigation of the Interaction between Carbon Black and cis-Polybutadiene”, *Macromolecules* **1976**, *9*, 653–660.
- [54] J. C. Kenny, V. J. McBrierty, Z. Rigbi, D. C. Douglass, “Carbon Black Filled Natural Rubber. 1. Structural Investigations”, *Macromolecules* **1991**, *24*, 436–443.
- [55] H. Lüchow, E. Breier, W. Gronski, “Characterization of Polymer Adsorption on Disordered Filler Surfaces by Transversal ^1H NMR Relaxation”, *Rubber Chemistry and Technology* **1997**, *70*, 747–758.
- [56] F. Yatsuyanagi, H. Kaidou, M. Ito, “Relationship between Viscoelastic Properties and Characteristics of Filler-Gel in Filled Rubber System”, *Rubber Chemistry and Technology* **1999**, *72*, 657–672.
- [57] V. M. Litvinov, P. A. Steeman, “EPDM-Carbon Black Interactions and the Reinforcement Mechanisms, as Studied by Low-Resolution ^1H NMR”, *Macromolecules* **1999**, *32*, 8476–8490.
- [58] S. Montes, J. L. White, N. Nakajima, “Rheological Behavior of Rubber Carbon Black Compounds in Various Shear Flow Histories”, *Journal of Non-Newtonian Fluid Mechanics* **1988**, *28*, 183–212.
- [59] C. M. Roland, “Reinforcement of Elastomers” in *Reference Module in Materials Science and Materials Engineering*, Elsevier, **2016**, 1–9.
- [60] H. H. Le, S. Ilisch, D. Heidenreich, A. Wutzler, H.-J. Radusch, “Kinetics of the Phase Selective Localization of Silica in Rubber Blends”, *Polymer Composites* **2010**, *31*, 1701–1711.
- [61] G. R. Cotten, L. J. Murphy, “Mixing of Carbon Black with Rubber. VI. Analysis of NR/SBR Blends”, *Rubber Chemistry and Technology* **1988**, *61*, 609–618.
- [62] H. H. Le, S. Ilisch, G. R. Kasaliwal, H. J. Radusch, “Filler Phase Distribution in Rubber Blends Characterized by Thermogravimetric Analysis of the Rubber-Filler Gel”, *Rubber Chemistry and Technology* **2008**, *81*, 767–781.
- [63] W. M. Hess, V. E. Chirico, “Elastomer Blend Properties — Influence of Carbon Black Type and Location”, *Rubber Chemistry and Technology* **1977**, *50*, 301–326.

- [64] W. Meon, A. Blume, H.-D. Luginsland, S. Uhrlandt, “Silica and Silanes” in *Rubber Compounding: Chemistry and Applications*, (Ed.: B. Rodgers), Marcel Dekker, New York, Basel, **2004**.
- [65] C. M. Blow, “Polymer/Particulate Filler Interaction – The Bound Rubber Phenomena”, *Polymer* **1973**, *14*, 309–323.
- [66] E. M. Dannenberg, “The Effects of Surface Chemical Interactions on the Properties of Filler-Reinforced Rubbers”, *Rubber Chemistry and Technology* **1975**, *48*, 410–444.
- [67] G. Kraus, “Reinforcement of Elastomers by Carbon Black”, *Rubber Chemistry and Technology* **1978**, *51*, 297–321.
- [68] S. Wolff, M.-J. Wang, “Carbon Black Reinforcement of Elastomers” in *Carbon Black: Science and Technology*, (Eds.: J.-B. Donnet, R. C. Bansal, M.-J. Wang), Routledge, New York, **1993**, 289–355.
- [69] H. Mouri, “Fillers” in *Rubber Technologist’s Handbook, Vol. 1*, (Eds.: S. K. De, J. R. White), Smithers Rapra Technology, Shawbury, **2001**.
- [70] C. M. Hill, J. L. Koenig, “Solid State Carbon-13 NMR Studies of Silica-Filled TBBS-Accelerated, Sulfur Vulcanized, cis-1,4 Polyisoprene”, *Polymer Bulletin* **1998**, *40:2*, 275–282.
- [71] M. L. Kravovich, J. L. Koenig, “The Effects of Polyethylene Glycol and the Coupling Agent bis-(γ -triethoxysilylpropyl)-tetrasulfide (Si-69) on the Interactions of Silica-Filled Natural Rubber”, *Composite Interfaces* **1997**, *5*, 125–135.
- [72] J. Ziegler, R. H. Schuster, “Influence of Silanisation of Precipitated Silica on Dynamic-Mechanical Properties and the Filler Partition in NBR/BR Blends”, *KGK - Kautschuk Gummi Kunststoffe* **2003**, *56*, 159–165.
- [73] H. H. Le, K. Reincke, A. Das, K. W. Stöckelhuber, S. Wiessner, T. Pham, Q. K. Do, X. T. Hoang, W. Grellmann, G. Heinrich, H. J. Radusch, “Filler Wetting in Miscible ESBR/SSBR Blends and Its Effect on Mechanical Properties”, *Macromolecular Materials and Engineering* **2016**, *301*, 414–422.
- [74] K. Pal, R. Rajasekar, T. Das, D. J. Kang, S. K. Pal, J. K. Kim, C. K. Das, “Effect of fillers on morphological properties in NR/SBR blends for OTR tyres”, *Plastics Rubber and Composites* **2009**, *38*, 302–308.
- [75] J. E. Pickett, “Introduction to Polymer Weathering, Stabilization, and Testing” in *Service Life Prediction of Polymers and Coatings*, (Eds.: C. C. White, M. E. Nichols, J. E. Pickett), William Andrew Publishing, **2020**, 1–18.

-
- [76] G. T. Kohman, “The Absorption of Oxygen by Rubber”, *Journal of Physical Chemistry* **1929**, *33*, 226–243.
- [77] J. R. Shelton, “Aging and Oxidation of Elastomers”, *Rubber Chemistry and Technology* **1957**, *30*, 1251–1290.
- [78] J. R. Shelton, “Review of Basic Oxidation Processes in Elastomers”, *Rubber Chemistry and Technology* **1972**, *45*, 359–380.
- [79] J. L. Morand, “Oxidation of Poly(isoprene)”, *Rubber Chemistry and Technology* **1974**, *47*, 1094–1115.
- [80] D. J. Carlsson, D. M. Wiles, “Importance of Singlet Oxygen in the Degradation of Rubbers and Plastics”, *Rubber Chemistry and Technology* **1974**, *47*, 991–1004.
- [81] J. R. Dunn, “Review of Unsolved Problems in the Protection of Rubber against Oxidative Degradation”, *Rubber Chemistry and Technology* **1974**, *47*, 960–975.
- [82] J. L. Morand, “Chain Scission in the Oxidation of Polyisoprene”, *Rubber Chemistry and Technology* **1977**, *50*, 373–396.
- [83] K. Ono, A. Kaeriyama, K. Murakami, “Effects of Diffusion in the Oxidative Degradation of Vulcanized Rubbers – 1. Rate of Chain Scission in the Steady State”, *Rubber Chemistry and Technology* **1977**, *50*, 43–48.
- [84] S. Yano, “Photo-Oxidation of an IR Vulcanizate”, *Rubber Chemistry and Technology* **1981**, *54*, 1–14.
- [85] J. R. Shelton, “Oxidation And Stabilization of Rubbers”, *Rubber Chemistry and Technology* **1983**, *56*, 71–86.
- [86] L. Audouin, V. Langlois, J. Verdu, J. C. M. de Bruijn, “Role of Oxygen Diffusion in Polymer Ageing: Kinetic and Mechanical Aspects”, *Journal of Materials Science* **1994**, *29*, 569–583.
- [87] G. Y. Li, J. L. Koenig, “A Review of Rubber Oxidation”, *Rubber Chemistry and Technology* **2005**, *78*, 355–390.
- [88] X. Colin, L. Audouin, J. Verdu, “Kinetic Modelling of the Thermal Oxidation of Polyisoprene Elastomers. Part 1: Unvulcanized Unstabilized Polyisoprene”, *Polymer Degradation and Stability* **2007**, *92*, 886–897.
- [89] X. Colin, L. Audouin, J. Verdu, M. L. Huy, “Kinetic Modelling of the Thermal Oxidation of Polyisoprene Elastomers. Part 2: Effect of Sulfur Vulcanization on Mass Changes and Thickness Distribution of Oxidation Products During Thermal Oxidation”, *Polymer Degradation and Stability* **2007**, *92*, 898–905.

- [90] X. Colin, L. Audouin, J. Verdu, “Kinetic Modelling of the Thermal Oxidation of Polyisoprene Elastomers. Part 3: Oxidation Induced Changes of Elastic Properties”, *Polymer Degradation and Stability* **2007**, *92*, 906–914.
- [91] J. Crabtree, A. R. Kemp, “Weathering of Soft Vulcanized Rubber”, *Rubber Chemistry and Technology* **1946**, *19*, 712–752.
- [92] R. P. Brown, T. Butler, *Natural Ageing of Rubber – Changes in Physical Properties Over 40 Years*, 1st ed., Smithers Rapra Technology, Shawbury, **2000**.
- [93] R. P. Brown, T. Butler, S. W. Hawley, *Ageing of Rubber – Accelerated Weathering and Ozone Test Results*, Smithers Rapra Technology, Shawbury, **2001**.
- [94] R. P. Brown, T. Butler, S. W. Hawley, *Ageing of Rubber – Accelerated Heat Ageing Test Results*, Smithers Rapra Technology, Shawbury, **2001**.
- [95] E. J. Blackman, E. B. McCall, “Relationships between the Structures of Natural Rubber Vulcanizates and their Thermal and Oxidative Aging”, *Rubber Chemistry and Technology* **1970**, *43*, 651–663.
- [96] M. L. Studebaker, J. R. Beatty, “Oxidative Hardening of SBR”, *Rubber Chemistry and Technology* **1972**, *45*, 450–466.
- [97] A. D. Jenkins, P. Kratochvíl, R. F. T. Stepto, U. W. Suter, “Glossary of Basic Terms in Polymer Science (IUPAC Recommendations 1996)”, *Pure and Applied Chemistry* **1996**, *68*, 2287–2311.
- [98] M. Morton, “Mechanisms of Reinforcement of Elastomers by Polymeric Fillers”, *Journal of Elastomers & Plastics* **1971**, *3*, 112–125.
- [99] A. B. Bhattacharya, T. Chatterjee, K. Naskar, “Automotive Applications of Thermoplastic Vulcanizates”, *Journal of Applied Polymer Science* **2020**, *137*, 49181.
- [100] H. W. Starkweather, “Cocrystallization and Polymer Miscibility”, *Journal of Applied Polymer Science* **1980**, *25*, 139–147.
- [101] W. K. Fischer, US3758643A, **1971**.
- [102] C. S. Ha, D. J. Ihm, S. C. Kim, “Structure and Properties of Dynamically Cured EPDM/PP blends”, *Journal of Applied Polymer Science* **1986**, *32*, 6281–6297.
- [103] V. Choudhary, H. S. Varma, I. K. Varma, “Polyolefin Blends: Effect of EPDM Rubber on Crystallization, Morphology and Mechanical Properties of Polypropylene/EPDM Blends. 1”, *Polymer* **1991**, *32*, 2534–2540.

-
- [104] V. M. Litvinov, “EPDM/PP Thermoplastic Vulcanizates as Studied by Proton NMR Relaxation: Phase Composition, Molecular Mobility, Network Structure in the Rubbery Phase, and Network Heterogeneity”, *Macromolecules* **2006**, *39*, 8727–8741.
- [105] M. Prillieux, P. Delbende, M. Moulin, FR1289580, **1962**.
- [106] G. A. Lindsay, C. J. Singleton, C. J. Carman, R. W. Smith, “Morphology of Low Density Polyethylene/EPDM Blends Having Tensile Strength Synergism” in *Multiphase Polymers, Vol. 176*, (Eds.: S. L. Cooper, G. M. Estes), American Chemical Society, Washington, **1979**, 367–379.
- [107] V. Choudhary, H. S. Varma, I. K. Varma, “Effects of EPDM Rubber on Crystallization Behaviour and Morphology of iPP/HDPE Blend”, *Journal of Thermal Analysis* **1987**, *32*, 579–593.
- [108] H. S. Varma, V. Choudhary, I. K. Varma, “Crystallisation Behaviour and Mechanical Properties of HDPE/EPDM Blends”, *Journal of Thermal Analysis* **1989**, *35*, 1257–1266.
- [109] A. K. Sen, B. Mukherjee, A. S. Bhattacharyya, L. K. Sanghi, P. P. De, A. K. Bhowmick, “Effect of Cross-linking on the Crystallization and Fusion Behaviour of Polyethylene-Ethylene Propylene Diene Terpolymer Blends”, *Thermochimica Acta* **1990**, *157*, 45–59.
- [110] A. Y. Coran, “Vulcanization” in *The Science and Technology of Rubber*, (Eds.: J. E. Mark, B. Erman, F. R. Eirich), Burlington, **2005**.
- [111] A. J. Tinker, “Distribution of Crosslinks in Vulcanized Blends”, *Rubber Chemistry and Technology* **1995**, *68*, 461–480.
- [112] M. J. Duer, *Introduction to Solid-State NMR Spectroscopy*, 1st ed., Wiley-Blackwell, Oxford, **2005**, 1–349.
- [113] D. C. Apperley, R. K. Harris, P. Hodgkinson, *Solid-State NMR: Basic Principles & Practice*, Momentum Press, New York, **2012**.
- [114] M. Loadman, A. Tinker, “The Application of Swollen-State CW-¹H NMR Spectroscopy to the Estimation of the Extent of Crosslinking in Vulcanized Polymer Blends”, *Rubber Chemistry and Technology* **1989**, *62*, 234–245.
- [115] P. S. Brown, A. J. Tinker, “Factors Affecting the NMR Technique for Estimation of Crosslink Density in Rubber Blends”, *Journal of Natural Rubber Research* **1990**, *5*, 286–295.

- [116] M. V. Duin, J. C. J. Krans, J. Smedinga, “Covulcanization and Ozone Resistance of NR/EPDM Blends”, *KGK - Kautschuk Gummi Kunststoffe* **1993**, *46*, 445–451.
- [117] P. S. Brown, M. John, R. Loadman, A. J. Tinker, “Applications of FT-NMR to Crosslink Density Determinations in Natural Rubber Blend Vulcanizates”, *Rubber Chemistry and Technology* **1992**, *65*, 744–760.
- [118] P. S. Brown, A. J. Tinker, “The Use of FT-NMR in the Analysis of Rubber Blends: Crosslink Distribution in Black Filled Blends of NR and cis-BR”, *KGK - Kautschuk Gummi Kunststoffe* **1995**, *48*, 606–610.
- [119] M. M. Abolhasani, V. Karimkhani, “Characterization of Polymer Blends with Solid-State NMR Spectroscopy” in *Characterization of Polymer Blends: Miscibility, Morphology and Interfaces, Vol. 1*, (Eds.: S. Thomas, Y. Grohens, P. Jyotishkumar), John Wiley & Sons, Ltd, Weinheim, **2015**, 679–704.
- [120] A. Asano, “NMR Relaxation Studies of Elastomers” in *Annual Reports on NMR Spectroscopy, Vol. 86*, (Ed.: G. A. Webb), Academic Press, Waltham, **2015**, 1–72.
- [121] A. Asano, “Polymer Blends and Composites” in *Modern Magnetic Resonance*, (Ed.: G. A. Webb), Springer International Publishing, Cham, **2018**, 793–807.
- [122] M. D. Ellul, A. H. Tsou, W. Hu, “Crosslink Densities and Phase Morphologies in Thermoplastic Vulcanizates”, *Polymer* **2004**, *45*, 3351–3358.
- [123] M. Aluas, C. Filip, “Solid-State NMR Characterization of Cross-Linking in EPDM/PP Blends from $^1\text{H} - ^{13}\text{C}$ Polarization Transfer Dynamics”, *Solid State Nuclear Magnetic Resonance* **2005**, *27*, 165–173.
- [124] K. Saalwächter, F. Lange, K. Matyjaszewski, C. F. Huang, R. Graf, “BaBaxy16: Robust and Broadband Homonuclear DQ Recoupling for Applications in Rigid and Soft Solids up to the Highest MAS Frequencies”, *Journal of Magnetic Resonance* **2011**, *212*, 204–215.
- [125] J. Baum, A. Pines, “NMR Studies of Clustering in Solids”, *Journal of the American Chemical Society* **1986**, *108*, 7447–7454.
- [126] M. K. Dibbanti, M. Mauri, L. Mauri, G. Medaglia, R. Simonutti, “Probing Small Network Differences in Sulfur-Cured Rubber Compounds by Combining Nuclear Magnetic Resonance and Swelling Methods”, *Journal of Applied Polymer Science* **2015**, *132*, 42700 (1–8).

-
- [127] M. A. Mansilla, J. L. Valentín, M. A. López-Manchado, A. González-Jiménez, A. J. Marzocca, “Effect of Entanglements in the Microstructure of Cured NR/SBR Blends Prepared by Solution and Mixing in a Two-Roll Mill”, *European Polymer Journal* **2016**, *81*, 365–375.
- [128] M. Rubinstein, R. H. Colby, *Polymer Physics*, 1st ed., Oxford University Press, Oxford, **2003**.
- [129] L. R. G. Treloar, *Physics of Rubber Elasticity*, 3rd ed., Oxford University Press, New York, **2005**, 1–310.
- [130] L. H. Sperling, *Introduction to Physical Polymer Science*, 4th ed., John Wiley & Sons, Inc., Hoboken, New Jersey, **2006**.
- [131] G. Strobl, *The Physics of Polymers: Concepts for Understanding Their Structures and Behavior*, 3rd ed., Springer, Berlin, **2007**.
- [132] I. Teraoka, *Polymer Solutions: An Introduction To Physical Properties*, 1st ed., John Wiley & Sons, Inc., New York, **2002**.
- [133] P. J. Flory, *Statistical Mechanics of Chain Molecules*, 1st ed., Hanser Publishers, Munich, **1989**.
- [134] D. Patterson, “Free Volume and Polymer Solubility. A Qualitative View”, *Macromolecules* **1969**, *2*, 672–677.
- [135] Z. Sary, “Thermodynamics and Morphology and Compatibilization of Polymer Blends” in *Characterization of Polymer Blends: Miscibility, Morphology and Interfaces, Vol. 1*, (Eds.: S. Thomas, Y. Grohens, P. Jyotishkumar), Wiley-VCH, Weinheim, **2015**, 93–132.
- [136] S. Kawahara, S. Akiyama, A. Ueda, “Miscibility and LCST Behavior of Polyisoprene/Poly(cis-butadiene-co-1,2-vinylbutadiene) Blends”, *Polymer Journal* **1989**, *21*, 221–229.
- [137] S. Kawahara, “Natural Rubber Based Non-Polar Synthetic Rubber Blends” in *Natural Rubber Materials: Volume 1: Blends and IPNs, Vol. 1*, (Eds.: S. Thomas, C. H. Chan, L. Pothen, R. K. R., H. Maria), The Royal Society of Chemistry, London, **2014**, 195–212.
- [138] D. Klat, H. A. Karimi-Varzaneh, J. Lacayo-Pineda, “Phase morphology of NR/SBR blends: Effect of curing temperature and curing time”, *Polymers* **2018**, *10*, 1–15.
- [139] B. Erman, J. E. Mark, “Rubber-Like Elasticity”, *Annual Review of Physical Chemistry* **1989**, *40*, 351–374.

- [140] P. J. Flory, “Effects of Molecular Structure on Physical Properties of Butyl Rubber”, *Industrial and Engineering Chemistry* **1946**, *38*, 417–436.
- [141] M. Doi, S. F. Edwards, “Dynamics of Concentrated Polymer Systems. Part 1.—Brownian Motion in the Equilibrium State”, *Journal of the Chemical Society Faraday Transactions 2: Molecular and Chemical Physics* **1978**, *74*, 1789–1801.
- [142] P. G. de Gennes, “Reptation of a Polymer Chain in the Presence of Fixed Obstacles”, *The Journal of Chemical Physics* **1971**, *55*, 579.
- [143] J. Klein, “Dynamics of Entangled Linear, Branched, and Cyclic Polymers”, *Macromolecules* **1986**, *19*, 105–118.
- [144] L. Mullins, “Determination of Degree of Crosslinking in Natural Rubber Vulcanizates. Part IV. Stress–Strain Behavior at Large Extensions”, *Journal of Applied Polymer Science* **1959**, *2*, 257–263.
- [145] T. C. Gruber, C. R. Herd, “Anisometry Measurements in Carbon Black Aggregate Populations”, *Rubber Chemistry and Technology* **1997**, *70*, 727–746.
- [146] J. Otegui, L. A. Miccio, A. Arbe, G. A. Schwartz, M. Meyer, S. Westermann, “Determination of Filler Structure in Silica-Filled SBR Compounds by means of SAXS and AFM”, *Rubber Chemistry and Technology* **2015**, *88*, 690–710.
- [147] K. Song, “Micro- and Nano-Fillers used in the Rubber Industry” in *Progress in Rubber Nanocomposites*, (Eds.: S. Thomas, H. J. Maria), Woodhead Publishing, Duxford, **2017**, 41–80.
- [148] C. G. Robertson, X. Wang, “Isoenergetic Jamming Transition in Particle-Filled Systems”, *Physical Review Letters* **2005**, *95*, 075703.
- [149] A. Einstein, “Eine neue Bestimmung der Moleküldimensionen”, *Annalen der Physik* **1906**, *324*, 289–306.
- [150] A. Einstein, “Berichtigung zu meiner Arbeit: “Eine neue Bestimmung der Moleküldimensionen””, *Annalen der Physik* **1911**, *339*, 591–592.
- [151] H. M. Smallwood, “Limiting Law of the Reinforcement of Rubber”, *Journal of Applied Physics* **2004**, *15*, 766.
- [152] G. Heinrich, M. Klüppel, T. A. Vilgis, “Reinforcement of elastomers”, *Current Opinion in Solid State and Materials Science* **2002**, *6*, 195–203.
- [153] J. Domurath, M. Saphiannikova, G. Heinrich, “The Concept of Hydrodynamic Amplification in Filled Elastomers”, *KGK - Kautschuk Gummi Kunststoffe* **2017**, *70*, 40–43.

-
- [154] J. L. White, J. W. Crowder, “The Influence of Carbon Black on the Extrusion Characteristics and Rheological Properties of Elastomers: Polybutadiene and Butadiene–Styrene Copolymer”, *Journal of Applied Polymer Science* **1974**, *18*, 1013–1038.
- [155] E. Guth, “Theory of Filler Reinforcement”, *Journal of Applied Physics* **1945**, *16*, 20–25.
- [156] G. K. Batchelor, J. T. Green, “The Determination of the Bulk Stress in a Suspension of Spherical Particles to Order C^2 ”, *Journal of Fluid Mechanics* **1972**, *56*, 401–427.
- [157] H.-S. Chen, A. Acrivos, “The Effective Elastic Moduli of Composite Materials Containing Spherical Inclusions at Non-Dilute Concentrations”, *International Journal of Solids and Structures* **1978**, *14*, 349–364.
- [158] J. Domurath, M. Saphiannikova, G. Ausias, G. Heinrich, “Modelling of Stress and Strain Amplification Effects in Filled Polymer Melts”, *Journal of Non-Newtonian Fluid Mechanics* **2012**, *171–172*, 8–16.
- [159] A. I. Medalia, “Elastic Modulus of Vulcanizates as Related to Carbon Black Structure”, *Rubber Chemistry and Technology* **1973**, *46*, 877–896.
- [160] G. Wypych, *Handbook of Fillers*, 4th ed., ChemTec Publishing, Toronto, **2016**.
- [161] J. W. M. Noordermeer, W. K. Dierkes, “Silica-Filled Rubber Compounds” in *Rubber Technologist’s Handbook Volume 2, Vol. 2*, (Eds.: J. White, S. K. De, K. Naskar), Smithers Rapra Technology, Shawbury, **2009**, 59–95.
- [162] A. R. Payne, “Nonlinearity in the Dynamic Properties of Rubber”, *Rubber Chemistry and Technology* **1957**, *30*, 218–241.
- [163] A. R. Payne, “The Dynamic Properties of Carbon Black-Loaded Natural Rubber Vulcanizates. Part I”, *Journal of Applied Polymer Science* **1962**, *6*, 57–63.
- [164] W. P. Fletcher, A. N. Gent, “Nonlinearity in the Dynamic Properties of Vulcanized Rubber Compounds”, *Transactions of the Institution of the Rubber Industry* **1953**, *29*, 226–280.
- [165] L. Mullins, “Effect of Stretching on the Properties of Rubber”, *Journal of Rubber Research* **1947**, *16*, 275–289.
- [166] J. A. Harwood, L. Mullins, A. R. Payne, “Stress Softening in Natural Rubber Vulcanizates. Part II. Stress Softening Effects in Pure Gum and Filler Loaded Rubbers”, *Journal of Applied Polymer Science* **1965**, *9*, 3011–3021.

- [167] H. Wan, K. Gao, S. Li, L. Zhang, X. Wu, X. Wang, J. Liu, “Chemical Bond Scission and Physical Slippage in the Mullins Effect and Fatigue Behavior of Elastomers”, *Macromolecules* **2019**, *52*, 4209–4221.
- [168] V. R. Gowariker, N. V. Viswanathan, J. Sreedhar, *Polymer Science*, 1st ed., New Age International Limited, New Delhi, **1986**.
- [169] R. Kurz, M. Schulz, F. Scheliga, Y. Men, A. Seidlitz, T. Thurn-Albrecht, K. Saalwächter, “Interplay between Crystallization and Entanglements in the Amorphous Phase of the Crystal-Fixed Polymer Poly(ϵ -caprolactone)”, *Macromolecules* **2018**, *51*, 5831–5841.
- [170] H. Friebolin, *Basic One- and Two-Dimensional NMR Spectroscopy*, 5th ed., Wiley-VCH, Weinheim, **2010**.
- [171] J. Keeler, *Understanding NMR Spectroscopy*, 2nd ed., John Wiley & Sons, Chichester, **2010**.
- [172] M. H. Levitt, *Spin Dynamics Basics of Nuclear Magnetic Resonance*, 2nd ed., John Wiley & Sons, Chichester, **2008**.
- [173] F. Nardelli, S. Borsacchi, L. Calucci, E. Carignani, F. Martini, M. Geppi, “Anisotropy and NMR spectroscopy”, *Rendiconti Lincei. Scienze Fisiche e Naturali* **2020**, *31*, 999–1010.
- [174] K. Saalwächter, H. W. Spiess, “Solid-State NMR of Polymers” in *Polymer Science: A Comprehensive Reference, Vol. 2*, (Eds.: K. Matyjaszewski, M. Möller), Elsevier, Amsterdam, **2012**, 185–219.
- [175] K. Saalwächter, “Microstructure and Molecular Dynamics of Elastomers as Studied by Advanced Low-Resolution Nuclear Magnetic Resonance Methods”, *Rubber Chemistry and Technology* **2012**, *85*, 350–386.
- [176] K. Saalwächter, “Proton Multiple-Quantum NMR for the Study of Chain Dynamics and Structural Constraints in Polymeric Soft Materials”, *Progress in Nuclear Magnetic Resonance Spectroscopy* **2007**, *51*, 1–35.
- [177] A. Papon, K. Saalwächter, K. Schäler, L. Guy, F. Lequeux, H. Montes, “Low-Field NMR Investigations of Nanocomposites: Polymer Dynamics and Network Effects”, *Macromolecules* **2011**, *44*, 913–922.
- [178] E. L. Hahn, “Spin Echoes”, *Physical Review* **1950**, *80*, 580–594.
- [179] A. Maus, C. Hertlein, K. Saalwächter, “A Robust Proton NMR Method to Investigate Hard/Soft Ratios, Crystallinity, and Component Mobility in Polymers”, *Macromolecular Chemistry and Physics* **2006**, *207*, 1150–1158.

-
- [180] M. Mauri, Y. Thomann, H. Schneider, K. Saalwächter, “Spin-Diffusion NMR at Low Field for the Study of Multiphase Solids”, *Solid State Nuclear Magnetic Resonance* **2008**, *34*, 125–141.
- [181] A. Wittmer, R. Wellen, K. Saalwächter, K. Koschek, “Moisture-Mediated Self-Healing Kinetics and Molecular Dynamics in Modified Polyurethane Urea Polymers”, *Polymer* **2018**, *151*, 125–135.
- [182] M. G. Brereton, “NMR Transverse Relaxation Function Calculated for the Rouse Model”, *Macromolecules* **1989**, *22*, 3667–3674.
- [183] M. G. Brereton, “NMR Transverse Relaxation Function Calculated for Constrained Polymer Chains: Application to Entanglements and Networks”, *Macromolecules* **1990**, *23*, 1119–1131.
- [184] K. Saalwächter, “Multiple-Quantum NMR Studies of Anisotropic Polymer Chain Dynamics” in *Modern Magnetic Resonance*, (Ed.: G. A. Webb), Springer International Publishing AG, Cham, **2017**, 1–28.
- [185] K. Saalwächter, B. Herrero, M. A. López-Manchado, “Chain Order and Cross-Link Density of Elastomers As Investigated by Proton Multiple-Quantum NMR”, *Macromolecules* **2005**, *38*, 9650–9660.
- [186] I. Syed, G. Hempel, K. Saalwächter, P. Stratmann, M. Klüppel, “Entanglements, Defects, and Inhomogeneities in Nitrile Butadiene Rubbers: Macroscopic versus Microscopic Properties”, *Macromolecules* **2016**, *49*, 9004–9016.
- [187] K. Saalwächter, B. Herrero, M. A. López-Manchado, “Chemical Shift-Related artifacts in NMR Determinations of Proton Residual Dipolar Couplings in Elastomers”, *Macromolecules* **2005**, *38*, 4040–4042.
- [188] K. Saalwächter, P. Ziegler, O. Spyckerelle, B. Haidar, A. Vidal, J.-U. Sommer, “¹H Multiple-Quantum Nuclear Magnetic Resonance Investigations of Molecular Order Distributions in Poly(dimethylsiloxane) Networks: Evidence for a Linear Mixing Law in Bimodal Systems”, *Journal of Chemical Physics* **2003**, *119*, 3468–3482.
- [189] A. Mordvinkin, “Mechanistic Investigations of Dynamics in Supramolecular Polymer Networks”, PhD Thesis, Martin-Luther-Universität Halle-Wittenberg, Halle (Saale), **2019**.
- [190] W. Chassé, J. L. Valentín, G. D. Genesky, C. Cohen, K. Saalwächter, “Precise Dipolar Coupling Constant Distribution Analysis in Proton Multiple-Quantum NMR of Elastomers”, *Journal of Chemical Physics* **2011**, *134*, 044907.

- [191] E. R. Andrew, A. Bradbury, R. G. Eades, “Nuclear Magnetic Resonance Spectra from a Crystal rotated at High Speed”, *Nature* **1958**, *182*, 1659–1659.
- [192] I. J. Lowe, “Free Induction Decays of Rotating Solids”, *Physical Review Letters* **1959**, *2*, 285–287.
- [193] G. D. Paëpe, “Dipolar Recoupling in Magic Angle Spinning Solid-State Nuclear Magnetic Resonance”, *Annual Review of Physical Chemistry* **2012**, *63*, 661–684.
- [194] M. Feike, D. E. Demco, R. Graf, J. Gottwald, S. Hafner, H. W. Spiess, “Broadband Multiple-Quantum NMR Spectroscopy”, *Journal of Magnetic Resonance Series A* **1996**, *122*, 214–221.
- [195] A. Hasse, O. Klockmann, A. Wehmeier, H. D. Luginsland, “Influence of the Amount of di- and polysulfane Silanes on the Crosslinking Density of Silica Filled Rubber Compounds”, *KGK - Kautschuk Gummi Kunststoffe* **2002**, *55*, 236–243.
- [196] J.-Y. Lee, N. Park, S. Lim, B. Ahn, W. Kim, H. Moon, H.-J. Paik, W. Kim, “Influence of the Silanes on the Crosslink Density and Crosslink Structure of Silica-Filled Solution Styrene Butadiene Rubber Compounds”, *Composite Interfaces* **2016**, *24*, 711–727.

Acknowledgements

My journey through these years of my Ph.D. life has been one of many teachings. Not only did I learn the nature of polymers on a deeper level but also about myself. This has helped me grow, both, professionally and personally, and there are many individuals and organizations to be thanked for it.

Foremost, I am indebted to Prof. Dr. Kay Saalwächter who trusted me in my capabilities and offered me this fulfilling opportunity when I was seeking an entry into natural sciences. His guidance and encouragement have helped me in pushing my boundaries as a researcher. The innumerable discussions we have had over the years have been enriching.

I would like to thank Prof. Dr. Beate Langer for co-securing the research fund and for her mentorship. Prof. Dr. Katrin Reincke and Dr. Katja Oßwald served as my go-to supervisors for rubber technology-related discussions. I am grateful to them for their insights and for providing resources for my experiments and access to their labs. For the latter, I am also thankful to Polymer Service GmbH Merseburg. I would also like to extend my gratitude to all my coauthors for their cooperation and for enabling the publishing of quality papers. DIK Hannover and Dr. Sven Henning at Fraunhofer IMWS in Halle are acknowledged for the samples and data used in Chapter 8.

Dr. Günter Hempel has played an important role in bringing me on board with the concepts of NMR spectroscopy during my early days with the NMR group. I am grateful to him for his time in educating me through his vast knowledge.

My work would not have seen the light of the day without the funding I received. I am thankful to Europäische Sozialfonds (ESF) for the monetary support towards the projects, conferences, and trainings. I am also thankful to the state of Sachsen-Anhalt and the graduate school AGRIPOLY for facilitating this. AGRIPOLY and InGrA have been instrumental in providing specialized technical trainings and sessions on soft skill development, which have helped me immensely in my overall professional development. The networking opportunities through the Ph.D. seminars and other social events organized by AGRIPOLY helped me make many new friends.

A seemingly trivial yet significant aspect of the life of an immigrant student is dealing with the occasional stress associated with their residence permit and related administrative concerns. Especially towards my closing months with the NMR group, our beloved Rositta Mothes was extremely helpful in dealing with the Ausländerbehörde, which eventually helped extend my stay in Germany. I thank her for alleviating the related stress.

The NMR/Biophysics group has been the community with which I spent a signifi-

cant amount of time. Apart from work, the barbeques, Christmas and dinner parties, outings, and cycling trips will be cherished. I thank Dr. Anton Mordvinkin, Dr. Anna Naumova, Dr. Mareen Schaller (Schäfer), Maria Camilles, Farhad Shahsavan, Afiq Anuar, Anika Wurl, Lucas Löser, David Haselberger, Mozhdeh Abbasi, Dr. Tiago Mendes Ferreira, Dr. Yury Golitsyn, Shubhra Sachan, Prof. Dr. Detlef Reichert, Pierre Seiboth, Stefan Gröger, and Kathrin Waldheim for creating the memories. Lastly, I thank Dr. Alexey Krushelnitsky and Assam Raja for being amazing office buddies. The political discussions with Alexey were particularly enjoyable.

I regard this fruition of my research as a collective effort of my family and myself. This would not have been achieved without their sacrifices and support. My wife, Sharvani Kommaraju, has been the pillar I could lean on during these challenging years. Thank you for keeping me strong and helping me persevere. I owe this thesis to her, my parents, and my brother.

Curriculum Vitae

Personal details

First name: Akshay
Family name: Karekar
Date of birth: 08.10.1987
Place of birth: Shimoga
Nationality: Indian

Education

09.2017 – *present* Doctoral Studies
Martin-Luther-Universität Halle-Wittenberg
Halle (Saale), Germany
10.2014 – 04.2017 Master of Science (in Polymer Materials Science)
Martin-Luther-Universität Halle-Wittenberg
Halle (Saale), Germany
09.2006 – 06.2010 Bachelor of Engineering (in Polymer Science and Technology)
Sri Jayachamarajendra College of Engineering
Mysore, India

Work experience

03.2023 – *present* Material Science Researcher
Braskem Europe GmbH
Wesseling Germany
10.2015 – 08.2017 Research Assistant
Fraunhofer - Institut für Mikrostruktur von Werkstoffen und
Systemen IMWS
Schkopau, Germany
03.2013 – 09.2014 Engineer
Saudi Basic Industries Corporation
Bangalore, India
05.2011 – 02.2013 Research Associate
11.2010 – 05.2011 Intern
General Electric
Bangalore, India

Halle (Saale), den 30. Mai 2023

Akshay Karekar

List of publications

1. A. Karekar, C. Schicktanz, M. Tariq, K. Oßwald, K. Reincke, V. Cepas, B. Langer, and K. Saalwächter, “Effects of Artificial Weathering in NR/SBR Elastomer Blends”, *Polym. Degrad. Stab.*, **2023**, *208*, 110267.
2. A. Karekar, R. Pommer, B. Prem, C. Czibula, C. Teichert, G. Trimmel, and K. Saalwächter. “NMR-Based Cross-Link Densities in EPDM and EPDM/ULDPE Blend Materials and Correlation with Mechanical Properties”, *Macromol. Mater. Eng.*, **2022**, *307*, 2100968.
3. A. Karekar, K. Oßwald, K. Reincke, B. Langer, and K. Saalwächter. “NMR Studies on the Phase-Resolved Evolution of Cross-Link Densities in Thermo-Oxidatively Aged Elastomer Blends”, *Macromolecules*, **2020**, *53*, 11166–11177.

Erklärung

Hiermit versichere ich, dass ich die vorliegende Arbeit selbständig und ohne fremde Hilfe verfasst und dabei nur die von mir angegebenen Quellen und Hilfsmittel benutzt habe. Die den benutzten Werken wörtlich oder inhaltlich entnommenen Stellen habe ich als solche kenntlich gemacht.

Ich erkläre, keine anderweitigen Promotionsversuche unternommen und die vorliegende Dissertation weder in der jetzigen noch in einer anderen Fassung einer anderen wissenschaftlichen Einrichtung vorgelegt zu haben.

Halle (Saale), den 30. Mai 2023

Akshay Karekar